UNIVERSITÀ DEGLI STUDI DI MILANO

PhD Course in Environmental Sciences

XXIX Cycle

# Exploring the potential of marine resources: echinoderms as valid models for regeneration studies and biotechnological applications

PhD Thesis

**Cinzia FERRARIO**

R10659

**Scientific tutor:** Prof. Maria Daniela CANDIA CARNEVALI

**Scientific co-tutor:** Dr. Michela SUGNI

Academic year: 2015-2016

SSD: BIO/05

Thesis performed at Department of Biosciences, University of Milan, Italy

*…to all my family with love and gratitude…*

*“The important thing is to never stop asking.*
*Curiosity has its own reason to exist.*
*One cannot help but be amazed when*
*contemplates the mysteries of eternity, of life,*
*of the marvellous structure of reality.*
*It is enough if one tries to understand only*
*a little of this mystery every day.*
*Never lose a holy curiosity.”*

*Albert Einstein*

## CONTENTS

**Page**

## LIST OF ABBREVIATIONS

a or ap-ampulla
acc-aboral coelomic cavity
*Afi-Amphiura filiformis*
AP-alkaline phosphatase buffer
as-aboral shield
ASW-artificial sea water
AV-aboral view
AW-aboral arm wall
BB-blocking buffer
BCIP-5-bromo-4-chloro-3-indolyl-phosphate
BCM-reassembled (fibrillar) bovine collagen membranes
BLAST-Basic Local Alignment Search Tool
bp-base pair
BSE-bovine spongiform encephalopathy
BW-whole body wall
c-collagen fibril
cc or c-coelomic cavity or coelom
cDART-conserved Domain Architecture Retrieval Tool
cDNA-copy DNA
CE-coelomic epithelium
ch-chamber
cl-cilia
CM-commercial membrane
CS-cross section
CSA-cross section area
ct or CT-connective tissue
cv-calcification vacuole
DAPI-4',6-diamidino-2-phenylindole
DCT-dense connective tissue
DEPC-diethylpyrocarbonate
d$H_2O$-distilled water
DIG-digoxigenin
DMF-dimethylformamide
DNA-deoxyribonucleic acid
dNTPs-deoxynucleotides
dpa-day(s) post-amputation
e-epithelium
ECM-extracellular matrix
ecn-ectoneural epithelium
EDC-1-ethyl-3-(3-dimethylaminopropyl)carbodiimide
EDCM-echinoderm-derived collagen membrane
EDTA-ethylenediaminetetraacetic acid
ep-epidermis
*Ese-Echinaster sepositus*
EtOH-ethanol
EX-external environment
f-myofilaments
fb-fibroblast

fb.z-fibrillar zone
FITC-fluorescein isothiocyanate
FS-frontal section
g or gl-mucous gland
GA-Golgi apparatus
GAG-glycosaminoglycan
GLM-Generalised Linear Model
Gly-glycine
GTR-Guided Tissue Regeneration
h p.a.-hour(s) post-amputation
HB-hybridisation buffer
HgfCOL-fibrous collagen (*Holothuria glaberrima*)
HMDS-hexamethyldisilazane
hn-hyponeural
hSDF-human skin-derived fibroblast
hy-hyaline layer
IF-immunofluorescence microscopy
If-intermediate filaments
IL-interleukin
IMTA-integrated multi-trophic aquacultures
ISH-*in situ* hybridisation
JLCs-juxta-ligamental cells
lac-lacunar area
lam-lower transverse ambulacral muscle
LCT-loose connective tissue
LM-light microscopy
ls-lateral shield
LV-lateral view
m-muscle
MABT-maleic acid buffer + Tween-20
MCT-mutable collagenous tissue
MES-2-(N-morpholino)ethanesulfonic acid
ml-myoepithelial layer
MOPS-3-(N-morpholino)propanesulfonic acid
MMP-metalloproteinase
n-nucleus
n-radial nerve cord
N-neuron
NBT-nitro blue tetrazolium
NCBI-National Center for Biotechnology Information
nch-niche
nCT-newly deposited collagen
ne-new epidermis
NF-$H_2O$-nuclease-free water
NHS-N-hydroxysuccinimide
NR-non-redundant
o-ossicle
oc-optic cushion
OCT-optimal cutting temperature
oe-oedematous area
os-oral shield

OV-oral view
P4H-prolyl-4-hydroxylase
p-podium
pa or p or pl-papula
p.a. or pa-post-amputation
pc-pyloric caeca
PBS-phosphate buffer saline
PBST-phosphate buffer saline + Tween-20
PBSTT-phosphate buffer saline + Tween-20 + Triton X-100
PBT-phosphate buffer saline + Tween-20
PCR-polymerase chain reaction
PEG-polyethylene glycol
PFA-paraformaldehyde
PG-proteoglycan
pl-papula lumen
PM-peristomial membrane
RER-rough endoplasmic reticulum
RNA-ribonucleic acid
RNC-radial nerve cord
RT-room temperature
RWC-radial water canal
sb-scleroblast
s or sp- spine
SC-supporting cell
SDS-sodium dodecyl sulphate
SEM-scanning electron microscopy
SLSs-spindle-like structures
sp-spicule
sp-septum
SPAFG-sucrose-picric acid-formaldehyde-glutaraldehyde
SPU-*Strongylocentrotus purpuratus*
SS-sagittal section
SSC-saline-sodium citrate
s.z-somatic zone
TBE-tris borate EDTA
TCA-trichloroacetic acid
te-tube foot epidermis
TE-tissue engineering
TEM-transmission electron microscopy
tf-tube foot or podium
TGF-β-transforming growth factor beta
TIMP-tissue inhibitor of metalloproteinase
tl-tube foot lumen
Tm-melting temperature
TNF-α-tumour necrosis factor alpha
TO-terminal ossicle
TRITC-tetramethylrhodamine
Tt or TP-terminal tube foot or podium
utam-upper transverse ambulacral muscle
v-vacuole
v-vertebra

w p.a. or wpa-week(s) post-amputation
WMISH-whole mount *in situ* hybridisation

## GENERAL NOTE

*The present research was carried out in collaboration with Dr. Paola Oliveri's group (Department of Genetics, Evolution and Environment, University College London, London, UK) for the molecular work (Chapter 3 and 4) and Prof. Caterina A. M. La Porta's group (Department of Biosciences, CC&B, University of Milan, Milan, Italy) for the cell culture work (Chapter 5). Animals were handled according to the Italian and English laws, i.e. no specific permits were required for the described studies since echinoderms are invertebrates and the employed species, namely Echinaster sepositus (Asteroidea), Amphiura filiformis (Ophiuroidea), Paracentrotus lividus (Echinoidea) and Holothuria tubulosa (Holothuroidea), are not endangered or protected. All efforts were made to minimise animal suffering during experimental procedures and, when possible, specimens were released into their natural environment once experimental procedures were completed.*

## ABSTRACT

The marine ecosystems have always been exploited by humans as source of food, inspiration, bioactive compounds and biomaterials. Marine invertebrates especially caught the interests of scientists for their potential in **basic research** and **applied biotechnology** studies displaying the most spectacular variety of morphological, physiological and behavioural adaptations to diverse environmental conditions. Among them, **echinoderms** are interesting models for three main reasons: 1) their **crucial phylogenetic position**, since they are the second largest group of deuterostomes after chordates, 2) their **striking regenerative abilities** and 3) their peculiar **dynamic connective tissues** (Mutable Collagenous Tissues or MCTs) capable of rapidly changing their mechanical properties. These last two features are strongly related: indeed, echinoderm connective tissues are considered one of the key characteristics that allows their effective regeneration phenomena. In particular, the extracellular matrix (ECM), with both its fibrous (mainly collagen) and cellular components, is primarily involved during regeneration and can be regarded as a promising source of biomaterial (collagen) for regenerative medicine applications.

Therefore, the present work followed two different but overlapping research lines whose **main aims** were to: **a)** describe echinoderm arm regeneration after traumatic amputation with a special focus on connective tissue and immune system in order to gain a better comprehension of this fundamental biological process and to compare it with other animals, especially with those with limited regenerative abilities (e.g. mammals), and **b)** explore the biotechnological potential of echinoderm connective tissues as source of fibrillar collagen to produce valuable tools for human biotechnological applications, such as regenerative medicine.

The starfish *Echinaster sepositus*, the brittle star *Amphiura filiformis*, the sea urchin *Paracentrotus lividus* and the sea cucumber *Holothuria tubulosa* were selected as experimental models. For both research lines a **multi-disciplinary approach** was employed mainly including microscopic anatomy, gene expression, immunohistochemistry, ultrastructural and biomechanical characterisation and *in vitro* tests.

Focusing on the **first research line**, starfish and brittle star were traumatically amputated and the regenerates at different time points were analysed with a specific focus on the ECM and immune system roles during the regenerative process. Our results showed that echinoderm emergency reaction and wound healing after injury are faster that those

described in mammals and ECM fibrillar organisation at the wound site is delayed in comparison to them. Absence of fibrosis (*i.e.* over-deposition of collagen) is shown as well. In general, all these evidences can be regarded as key features to ensure their subsequent effective regeneration. Gene expression analyses showed that the identified collagen-like and ECM-related molecule genes in brittle star are differentially expressed during regeneration, thus indicating that different tissues are involved in collagen and ECM production/remodelling. The expression pattern of the collagen biosynthesis enzyme gene here identified indicated that in both experimental models the regenerating epidermis is involved in collagen production. Preliminary analyses on immune system molecules showed that in brittle star TNF-α-like presence is comparable to that of mammals during wound healing. Overall, the regenerative process is faster in brittle star than in starfish, mainly due to smaller arm size, but in both models leads to the complete restoration and functionality of the lost structures following the distalisation-intercalation model and a proximal-distal gradient of differentiation.

Focusing on the **second research line**, echinoderm connective tissues can be regarded as eco-friendly sources of marine collagen since the starting material is coming e.g. from food industry wastes. Thanks to optimised extraction protocols we obtained fibrillar collagen suspensions used to produce two-dimensional collagen membranes (EDCMs) whose ultrastructural, biomechanical and biocompatibility features were characterised and compared to mammal-derived collagen membranes currently available in the market (commercial membranes or CMs) for biotechnological applications, e.g. Guided Tissue Regeneration (GTR). We showed that EDCMs are thinner, less porous and more resistant than CMs, all great advantages for GTR applications. *In vitro* tests using human skin-derived fibroblasts showed that cells seeded on EDCMs present an elongated shape and few and short filopodial processes at the sides of the cells and sea urchin-derived collagen membranes are the most promising in terms of cell number. Hence, EDCMs can be regarded as valuable marine-derived biomaterials for human applications.

Overall, the main outcome of this research was that echinoderms can be considered **valid models to explore both basic biological processes** (*i.e.* regeneration) and **biotechnological potential of marine-derived tissues**. Further analyses will be necessary to continue investigating both these intriguing aspects, including high-throughput molecular analyses (transcriptome) of regenerating tissues and *in vivo* tests for EDCMs.

## RIASSUNTO

Gli ecosistemi marini sono sempre stati sfruttati dagli uomini come fonte di cibo, ispirazione, composti bioattivi e biomateriali. Gli invertebrati marini specialmente hanno catturato l'interesse degli scienziati per il loro potenziale nella **ricerca di base** e negli studi di **biotecnologia applicata** mostrando la più spettacolare varietà di adattamenti morfologici, fisiologici e comportamentali alle diverse condizioni ambientali. Tra di loro, gli **echinodermi** sono modelli interessanti per tre ragioni principali: 1) la loro **cruciale posizione filogenetica**, essendo il secondo più grande gruppo di deuterostomi dopo i cordati, 2) le loro **straordinarie capacità rigenerative** e 3) i loro peculiari **tessuti connettivi dinamici** (Tessuti Connettivi Mutabili o MCTs) in grado di modificare rapidamente le loro proprietà meccaniche. Queste ultime due caratteristiche sono fortemente correlate: infatti, i tessuti connettivi degli echinodermi sono considerati uno dei caratteri chiave che permette i loro efficaci fenomeni rigenerativi. In particolare, la matrice extracellulare (ECM), con entrambe le sue componenti fibrosa (principalmente collagene) e cellulare, è coinvolta direttamente durante la rigenerazione e può essere considerata una promettente fonte di biomateriale (collagene) per applicazioni di medicina rigenerativa.

Pertanto, il presente lavoro ha seguito due linee di ricerca differenti, ma sovrapponibili i cui **scopi principali** erano di: **a)** descrivere la rigenerazione del braccio degli echinodermi dopo amputazione traumatica con una particolare attenzione al tessuto connettivo e al sistema immunitario per ottenere una miglior comprensione di questo fondamentale processo biologico e compararlo con altri animali, specialmente con quelli con limitate capacità rigenerative (per esempio i mammiferi), e **b)** esplorare il potenziale biotecnologico dei tessuti connettivi degli echinodermi come fonte di collagene fibrillare per produrre preziosi *tools* per applicazioni biotecnologiche umane come la medicina rigenerativa.

La stella di mare *Echinaster sepositus*, l'ofiura *Amphiura filiformis*, il riccio di mare *Paracentrotus lividus* e l'oloturia *Holothuria tubulosa* sono stati selezionati come modelli sperimentali. Per entrambe le linee di ricerca è stato utilizzato un **approccio multi-disciplinare** che comprendeva principalmente anatomia microscopica, espressione genica, immunoistochimica, caratterizzazione ultrastrutturale e biomeccanica e analisi *in vitro*.

Focalizzandosi sulla **prima linea di ricerca**, stella di mare e ofiura sono state amputate traumaticamente e i rigenerati a diversi stadi sono stati analizzati con una particolare

attenzione al ruolo della ECM e del sistema immunitario durante il processo rigenerativo. I nostri risultati hanno mostrato che negli echinodermi la reazione di emergenza e la chiusura della ferita dopo il danneggiamento sono più veloci degli stessi processi descritti nei mammiferi e l'organizzazione fibrillare della ECM nel sito della ferita è ritardata rispetto a loro. É evidente anche l'assenza di fibrosi (sovra-deposizione di collagene). In generale, tutte queste evidenze possono essere considerate come delle caratteristiche chiave per assicurare la loro successiva efficace rigenerazione. Le analisi di espressione genica hanno mostrato che i geni identificati nell'ofiura, geni collagene-*like* e geni di molecole correlate alla ECM, sono differenzialmente espressi durante la rigenerazione indicando così che diversi tessuti sono coinvolti nella produzione e nel rimodellamento di collagene ed ECM. Il pattern di espressione del gene che codifica per un enzima della biosintesi del collagene qui identificato ha indicato che in entrambi i modelli sperimentali l'epidermide rigenerante è coinvolta nella produzione di collagene. Analisi preliminari sulle molecole del sistema immunitario hanno mostrato che in ofiura la presenza di TNF-α-like è comparabile a quella dei mammiferi durante la riparazione della ferita. In generale, il processo rigenerativo nell'ofiura è più veloce che nella stella di mare, principalmente a causa della minore grandezza del braccio, ma in entrambi i modelli porta alla completa riformazione e funzionalità delle strutture perse seguendo il modello di distalizzazione-intercalazione e un gradiente prossimo-distale di differenziamento.

Focalizzandosi sulla **seconda linea di ricerca**, i tessuti connettivi degli echinodermi possono essere considerati delle fonti eco-sostenibili di collagene marino in quanto il materiale di partenza viene, per esempio, da scarti dell'industria alimentare. Grazie a protocolli di estrazione ottimizzati, è stato possibile ottenere sospensioni di collagene fibrillare da usare per la produzione di membrane bidimensionali di collagene (EDCMs) le cui proprietà ultrastrutturali, biomeccaniche e di biocompatibilità sono state caratterizzate e comparate con le membrane di collagene provenienti da mammiferi oggi disponibili sul mercato (membrane commerciali o CMs) per applicazioni biotecnologiche, per esempio la Rigenerazione Tissutale Guidata (GTR). Abbiamo mostrato che le EDCMs sono più sottili, meno porose e più resistenti delle CMs, tutti grossi vantaggi per applicazioni in GTR. Le analisi *in vitro* usando fibroblasti umani derivati dalla pelle hanno mostrato che le cellule piastrate sulle EDCMs presentano una forma allungata e pochi e corti processi fillopodiali alle estremità delle cellule e le membrane di collagene derivato dal riccio di mare sono le più promettenti in termini di numero di cellule. Perciò, le EDCMs

possono essere considerate come validi biomateriali di origine marina per applicazioni umane.

In generale, il principale risultato di questa ricerca è stato che gli echinodermi possono essere considerati **validi modelli per esplorare sia processi biologici di base** (cioè la rigenerazione) sia il **potenziale biotecnologico di tessuti di origine marina**. Ulteriori analisi saranno necessarie per continuare a investigare entrambi questi affascinanti aspetti, incluse analisi molecolari *high-throughput* (trascrittoma) dei tessuti rigeneranti e analisi *in vivo* per le EDCMs.

## GRAPHICAL ABSTRACT

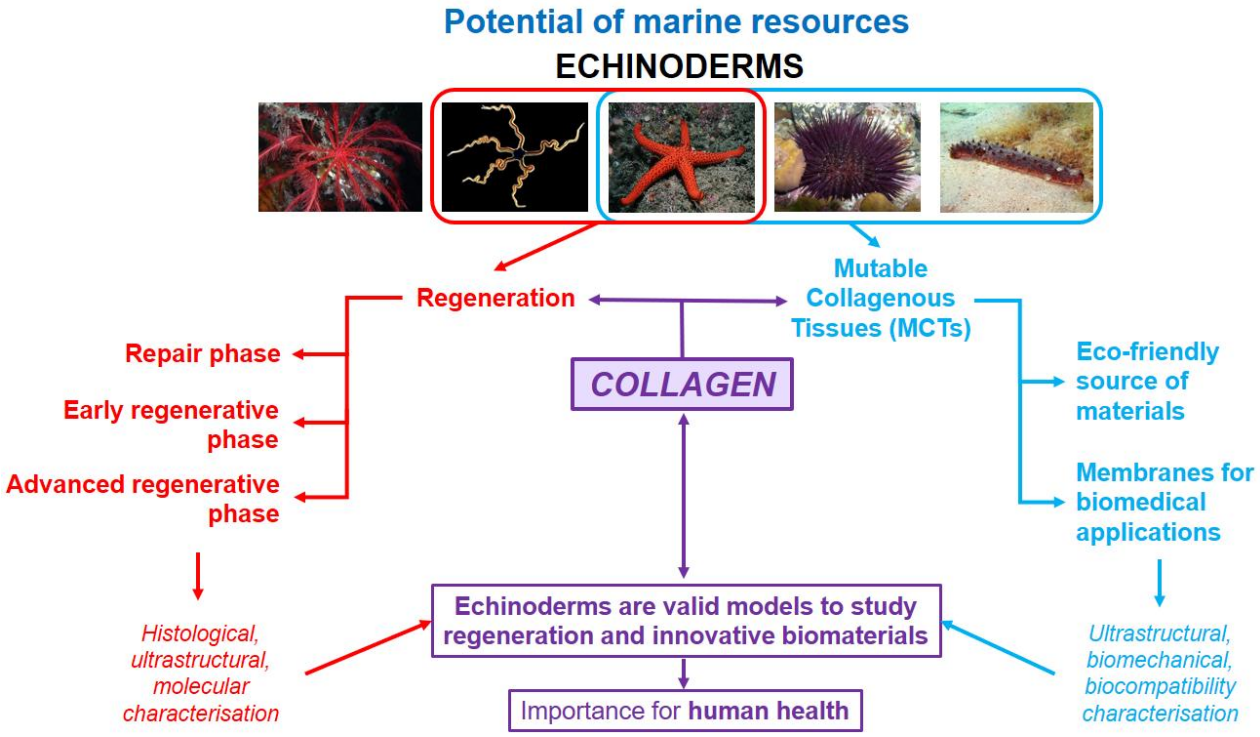

# 1) GENERAL INTRODUCTION

### *1.1. Marine ecosystems and their potential*

Seas and oceans cover three-fourths of the Earth's surface and contain 80% of the planet's biomass. They are considered the "cradle of life" and present a great variety of ecosystems and biodiversity, most of which is still largely unknown (Gray, 1997; Mora *et al.*, 2011). Both invertebrates and vertebrates inhabit from shallow to deep waters displaying amazing adaptations to face diverse environmental conditions. Morphological, physiological and behavioural differences showed by marine animals have always fascinated scientists, who have considered seas not as a simple source of food or means of travel (economic value) but mainly as source of knowledge, inspiration, compounds, bioactive molecules and materials (scientific value). Indeed, the study of marine life and biodiversity from different facets opens great possibilities in terms of **basic research** to understand fundamental biological phenomena and of **applied biotechnology** to develop innovative tools for human purposes. Under the name of "marine biodiversity" the large public often refers to vertebrate animals, such as fish or mammals, since they are more popular and linked to everyday life. However, marine invertebrates represent the highest percentage of animal life in terms not only of biomass but also of number of species (WoRMS Editorial Board, 2016). Moreover, biologists know that the study of invertebrate marine life led to some of the most interesting discoveries in terms of animal biology and applied biotechnologies e.g. the electrophysiology of axons using squids (Hodgkin and Katz, 1949), the processing of learning and memory using the gastropod *Aplysia californica* (Castellucci *et al.*, 1970), the symbiosis mechanisms using corals (Pearse and Muscatine, 1971), the regenerative events using planarians and echinoderms (Reddien and Sánchez Alvarado, 2004; Candia Carnevali, 2006), fertilisation and developmental biology using sea urchin gametes (Epel, 1978) and the characterisation of numerous natural compounds of sea water animal origin (Leal *et al.*, 2012). Therefore, marine invertebrates, that have been studied from centuries ago, are nowadays still actively used to understand important biological processes and as sources of inspiration and of biomaterials/compounds for innovative applications.

Among them, the phylum Echinodermata particularly caught the interests of biologists for their peculiar adaptations to environmental conditions that made and make them fascinating experimental models for basic research and biotechnological application

studies. Both these aspects are dealt in this study and detailed in the following paragraphs.

### *1.2. Echinoderms and their peculiarities/adaptations*

The phylum Echinodermata (the term means “spiny skin”) is composed of around 7000 extant species of deuterostome exclusively marine invertebrates divided into five classes (Fig. 1):

1) Crinoidea (sea lilies and feather stars);
2) Echinoidea (sea urchins and sand dollars);
3) Holothuroidea (sea cucumbers);
4) Ophiuroidea (brittle stars and basket stars);
5) Asteroidea (starfish or sea stars).

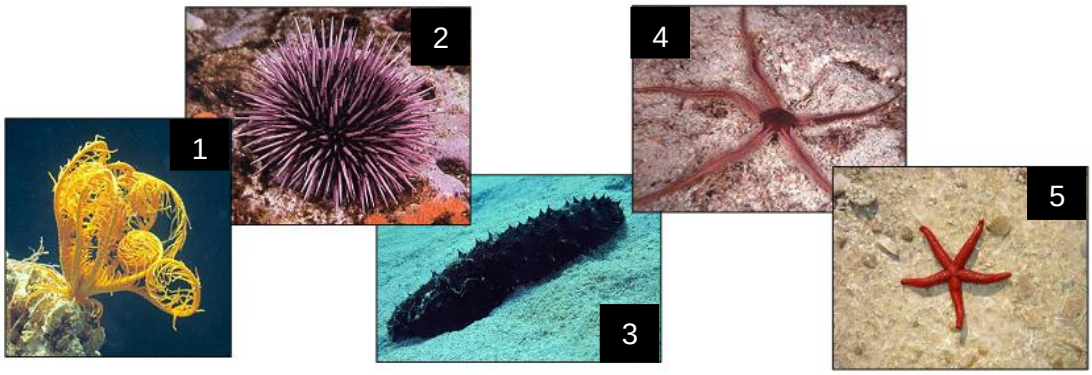


**Fig. 1.** *Diversity of extant echinoderms.* Representatives of: 1) Crinoidea; 2) Echinoidea; 3) Holothuroidea; 4) Ophiuroidea; 5) Asteroidea.

Echinoderms are generally quite small (around 10 cm in size) but can reach significant dimensions (e.g. 1-2 m for some sea cucumber and starfish species; Storer *et al.*, 1982). In their adult stage they usually possess a typical pentamerous symmetry, whereas a bilateral symmetry is usually shown at the larval stages (Riedl, 1991). They display a variety of body morphology and colours, from star-like to worm-like shapes, from dark brown/black to brilliant red/orange (Tortonese, 1965). Echinoderms present peculiar features, such as mesodermally-derived calcitic endoskeletal ossicles, a water vascular system with mainly locomotion, feeding, respiration and sensory functions (Barnes *et al.*, 1990), a complex tripartite nervous system and dynamic connective tissues, called Mutable Collagenous Tissues or MCTs (Wilkie, 2001). Table 1 briefly summarises the main peculiar characteristics of these animals.

**Table 1.** *Echinoderm general features.*

| | |
|---|---|
| ***Mode of life*** | Marine bottom-dwellers (only a few species tolerating even brackish water), free-living, mostly solitary and sedentary |
| ***Symmetry*** | Bilateral larvae, pentaradial (pentameral symmetry) adults |
| ***Enterocoelia*** | Triploblastic coelomates |
| ***Skeleton*** | Dermal skeleton (endoskeleton of bone-like plates called ossicles), calcium carbonate, mesodermal origin |
| ***External articulated appendages*** | Spines, tubercles, granules, pedicellariae |
| ***Water vascular system*** | Madreporite, stone canal, radial water canals, lateral canals, ampullae, tube feet or podia (with or without final suckers) |
| ***Nervous system*** | Separate sub-systems: ectoneural, hyponeural and entoneural systems |
| ***Mutable Collagenous Tissues*** | Connective tissues showing rapid, drastic, reversible/irreversible, modulable changes in mechanical properties (stiffness, etc.) |
| ***Locomotion*** | Sessile, tube feet, spines, peristaltic movements |
| ***Feeding*** | Passive filter-feeders, suspension feeders, grazers, deposite feeders, active hunters, detritivores |
| ***Reproduction*** | Sexual (with gametes) and asexual (fission) |
| ***Regeneration and autotomy*** | Epimorphosis and/or morphallaxis |
| ***Defence mechanisms*** | Spines, pedicellariae, toxins, mucus, autotomy |

Among marine invertebrates, echinoderms are well known for three main reasons:

- key phylogenetic position, being the second largest group of deuterostomes after chordates;
- striking regenerative abilities (Thouveny and Tassava, 1997; Candia Carnevali and Bonasoro, 2001a; Vickery *et al.*, 2001; Eaves and Palmer, 2003; Candia Carnevali, 2006);
- peculiar dynamic connective tissues, called Mutable Collagenous Tissues (MCTs; Wilkie, 2005).

Echinoderms are key animals in the marine ecosystems (Uthicke *et al.*, 2009). Moreover, as previously underlined, their phylogenetic position makes them key animals to study fundamental biological processes and compare them with those of vertebrates in a perspective of gaining a better understating of animal biology and evolution. Therefore, both regenerative capacities and presence of dynamic connective tissue are two of the most fascinating aspects to investigate to better understand different biological aspects and to develop bio-inspired technologies (Wilkie, 2005; Barbaglio *et al.*, 2012) of high relevance also for human life, e.g. regenerative medicine. Several authors hypothesise that the features of these particular connective tissues could be partially connected with the amazing regenerative abilities of these animals (Wilkie, 2001). They suggest that MCT

“mutability” and “plasticity” are responsible for rapid response to traumatic amputation or self-injury (autotomy) and partially also for easiness of regenerative events, ensuring a dynamic microenvironment for cell and tissue regeneration. Moreover, MCT potential as source of inspiration for human applications (biomimicry) and of marine-derived biomaterials is another aspect that deserves to be deepened mainly in view of possible applications for human biotechnologies (e.g. regenerative medicine or tissue engineering).

### *1.2.1. Regeneration*

Regeneration is defined as a complex post-embryonic developmental process during which a lost or severely injured body part is reformed (Candia Carnevali, 2006; Brockes and Kumar, 2008). It can occur at multiple levels of biological organisation (cells, tissues, organs, whole body parts), can be triggered by a variety of causes/insults/damages, can occur at different stages of the life cycle (*i.e.* embryos, larvae, juveniles, adults) and can produce structures of variable fidelity relative to the original (Bely and Nyberg, 2009). It is widespread in metazoan phylogeny, although it is not universal and both protostomes and deuterostomes possess regenerative capabilities. However, the degree of regeneration varies considerably among tissues within a body and among species and such differences are indicative of specific mechanisms that control the different types of regeneration (Tsonis, 2000). The evolution of regeneration is one of the most captivating issues in biology. From decades ago (Morgan, 1901) till now (Bely and Nyberg, 2009) biologists have studied this phenomenon using experimental models belonging to different animal kingdom classes (from invertebrates to vertebrates) in order to unlock its secrets. Indeed, the knowledge on regeneration will shed light on possible solutions to many different human clinical problems using innovative biotechnologies.

#### *1.2.1.1. Echinoderm regeneration*

Regenerative events are common in all the five classes of echinoderms, form an integral and fundamental part of their adaptive repertoire and involve both the larval and the adult stages (Hyman, 1955). Therefore, in view of their notable regenerative potential and their close phylogenetic relationship to vertebrates, these animals offer unique opportunities to study regenerative processes.

Echinoderms can regenerate not only damaged or lost external body parts, such as spines, tube feet and pedicellariae, but also internal organs (e.g. gonads, digestive tubes,

etc.) and whole arms following autotomy (self-induced mutilation) or traumatic amputations (Thorndyke *et al.*, 1999).

The ability to regenerate represents an obvious adaptive advantage for echinoderms because of:

- the replacement of tissues following predation or other traumatic events;
- the survival of detached body fragments for a long time and phenomena of partial or total regeneration independently of the donor animal (Candia Carnevali *et al.*, 1998);
- the asexual reproduction leading to the development of new individuals by specific fission mechanisms (Emson and Wilkie, 1980; Mladenov and Burke, 1994).

Echinoderm regenerative potential is extraordinarily high but it may vary according to life stage and age of the individual: in general, larval tissues and organs have a higher regenerative capacity compared to those of adults (Candia Carnevali, 2006).

Historically, two alternative mechanisms of regeneration have been described (Morgan, 1901): *epimorphosis* (blastemal regeneration) and *morphallaxis* (non-blastemal regeneration). The first process implies the development of new structures from presumptive and pre-existing stem (undifferentiated/dedifferentiated) cells which migrate and locally proliferate, forming a typical blastema (Candia Carnevali *et al.*, 1995). The second mechanism, slower and more complex than the first one, mainly consists in a rearrangement of the existing tissues through dedifferentiation, differentiation and/or migration of cells in order to regenerate the lost body structures, without a strong contribution of local proliferative events. Epimorphosis often follows autotomy, a widely predictable and effective phenomenon (Candia Carnevali and Bonasoro, 2001a), whereas morphallaxis often occurs after traumatic mutilations, which are non-predictable events (Mladenov *et al.*, 1989; Moss *et al.*, 1998). Although the differences between these two types of regenerative processes are quite well known, nowadays several studies suggest not only that cellular and tissue events are very flexible and widely overlapping but also that the same individual can employ both these mechanisms, modulating their different contributions according to its specific needs (Candia Carnevali and Bonasoro, 2001b).

### *1.2.2. Mutable Collagenous Tissues (MCTs)*

Mutable Collagenous Tissues (MCTs), also called “dynamic” or “catch” connective tissues, are, together with regeneration, one of the most intriguing characteristics of

echinoderms (Wilkie, 2001). These peculiar connective tissues are capable of changing their mechanical properties (e.g. stiffness and viscosity) within few seconds/minutes under the nervous system control in response to environmental and mechanical stimuli. Therefore, they play an important role in various vital functions such as locomotion, energy-sparing maintenance of posture, defence mechanisms and regeneration (Wilkie, 1996; Wilkie *et al.*, 2004; Wilkie, 2005), being fundamental for their success in different environmental conditions in terms of e.g. water depth, temperature, salinity and predation pressure. MCTs have been intensively investigated from ultrastructural, biochemical, physiological and biomechanical points of view (Tamori, 2006; Yamada *et al.*, 2010; Ribeiro *et al.*, 2011, 2012; Barbaglio *et al.*, 2012, 2015; Wilkie *et al.*, 2015; Mo *et al.*, 2016) but still several aspects need to be further detailed. The variable tensility ("mutability", *i.e.* softening and stiffening) displayed by MCTs relies on changes in the cohesive forces between adjacent collagen fibrils. Indeed, as all connective tissues, the main extracellular matrix component is collagen. Proteoglycans (PGs) are present on the surface of collagen fibrils and it has been suggested that they have a role in mutability by acting as binding sites for the effector molecules responsible for interfibrillar cohesion (Wilkie, 2005). Tensility variations are regulated by different effector molecules: proteins, such as tensilin and stiparin, have been suggested being "stiffening" factors (Koob *et al.*, 1999; Trotter *et al.*, 1999; Tipper *et al.*, 2003; Tamori, 2006), whereas softenin is thought to have a role as de-stiffening ("softening") factor (Takehana *et al.*, 2014). Few studies suggested that matrix metalloproteinases (MMPs) and their inhibitors (TIMPs) could be involved as well (Tipper *et al.*, 2003; Ribeiro *et al.*, 2012) or at least that the mechanisms of MCT mutability evolved from a MMP-TIMP system.

Besides their importance in echinoderms' biological processes and mode of life, these connective tissues can be valid source of inspiration (biomimicry) and biomaterials for human applications (Barbaglio *et al.*, 2012). When the "stiffening" and "softening" factors will be fully characterised and the physiological process underpinning mutability will be completely understood, this knowledge could be used for human biotechnological applications, e.g. where an *in loco* change of connective tissue mechanical conditions is needed due to specific pathology or where a biomaterial used for biomedical purposes has to be reversibly manipulated in its mechanical features *in situ*. So far, collagen in particular can be regarded as one of the most valuable echinoderm-derived product. Indeed, as recently suggested (Di Benedetto *et al.*, 2014), echinoderm-derived fibrillar collagen can be used as biomaterial to produce membranes useful in cell culture and

human health applications, such as tissue engineering, tissue regeneration, surgery and cosmetic surgery. Moreover, the possibility of obtaining fibrillar collagen in an eco-friendly way (e.g. from food industry wastes) is an added value to this promising echinoderm-derived biomaterial (Di Benedetto *et al.*, 2014).

### *1.3. The experimental models*

Among the great species variety of this phylum, four experimental models have been selected for this research: the starfish *Echinaster sepositus*, the brittle star *Amphiura filiformis*, the sea urchin *Paracentrotus lividus* and the sea cucumber *Holothuria tubulosa*. A brief description of these models is provided below. Starfish and brittle star will be described in more detail, with a specific focus on arm anatomy.

#### *1.3.1. The starfish Echinaster sepositus*

*E. sepositus* (Retzius, 1783; Fig. 3A) is a starfish belonging to the family Echinasteridae (order Spinulosa) and it is known as “red starfish”. Ranging between 10 and 30 cm, it is typically bright orange/red coloured. The distribution of this species is shown in Fig. 2. It can be found in many different benthic ecosystems: from shallow algal dominated rocky bottoms to *Posidonia oceanica* meadows, sandy bottoms or deep rodolith dominated bottoms (Villamor *et al.*, 2010). It is a carnivorous feeder and its predatory activity is mainly on several meiofaunal groups and detritus of animal origin (Villamor *et al.*, 2010). It moves on the oral surface which hosts the mouth and has a flattened (along the aboral-oral axis) and flexible body; this latter is in the form of a pentagonal central disc from which five long and slender arms radiate. Each arm is orally furrowed by an evident ambulacral groove housing the tube feet or podia equipped with final suckers (Hyman, 1955). The body cavity is occupied by a spacious coelom composed by three major components: the perivisceral coelom, consisting of large cavities surrounding the inner organs (digestive tract and gonads), the perihaemal system, closely associated to a system of lacunae (the haemal system) with lymphatic and transport functions, and the water vascular system (Hyman, 1955). This latter is the classic echinoderm hydraulic system made of a network of fluid-filled canals. Its function is related to locomotion, adhesion to the substrate (anchorage), food handling as well as respiration and excretion. Water “enters” from the madreporite (a porous, sieve-like ossicle), reaches the circumoral ring canal through the stone canal, arrives to the radial canals (one for each arm, running along the ambulacral groove) and, through the short lateral canals connecting the radial

canal and the ampullae, arrives at the two rows of tube feet. The last tube foot is the terminal tube foot (or terminal podium) which hosts the optic cushion, rich in photoreceptor structures called pigment-cup ocelli (Hyman, 1955). The digestive tract is straight and short (Hyman, 1955): the oral mouth leads into a short esophagus followed by the stomach to which the glandular appendages known as pyloric caeca are attached. From the pyloric stomach a short intestine ascends to the aboral anus.

The nervous system consists mainly of two components: the ectoneural system (motor and sensory components) and the hyponeural system (motor component). The first one, situated just beneath the epidermis, is composed of the circumoral nerve ring, the radial nerve cords, one for each arm, and the general sub-epidermal plexus, spreading throughout the entire body wall and innervating all the body wall appendages (Hyman, 1955). The radial nerve cords also include the hyponeural system with the hyponeural sinus which is immediately above the radial nerve cord and separated from the latter only by a thin layer of connective tissue. As all echinoderms, this starfish possesses an endoskeleton of calcitic ossicles embedded in the dermis and superficial epidermis-covered skeletal structures, such as spines, positioned in order to let emerge in regular groups of three-five elements the papulae (or gills), located only on the aboral surface. These are thin finger-like evaginations of the body wall, lined with coelomic myoepithelium, with mainly respiratory, transport and excretory functions (Hyman, 1955). In addition to the coelomic myoepithelium, in each arm there are different muscles articulating adjacent ossicles and operating the ambulacral groove in order to allow the movement of each arm in any direction (Hyman, 1955). From outside to inside, the body wall consists of a definite and thin cuticle covering the columnar epidermis, a thick dermis housing the ossicles and a thin coelomic myoepithelium. Indeed, a longitudinal smooth muscle layer is adjacent to the latter and separated from a further circular smooth muscle layer only through a thin layer of connective tissue. The dermis can be subdivided in two main layers, the outer loose connective tissue and the inner dense connective tissue, hosting the calcitic ossicles. The spiny body wall is characterised by the presence of large dermal glands opening onto the aboral surface and pouring out an abundant gelatinous secretion (mucus) in response to irritation (Hyman, 1955). Fig. 3B and 4 show schematic representations of the arm anatomy of this starfish with its main structures.

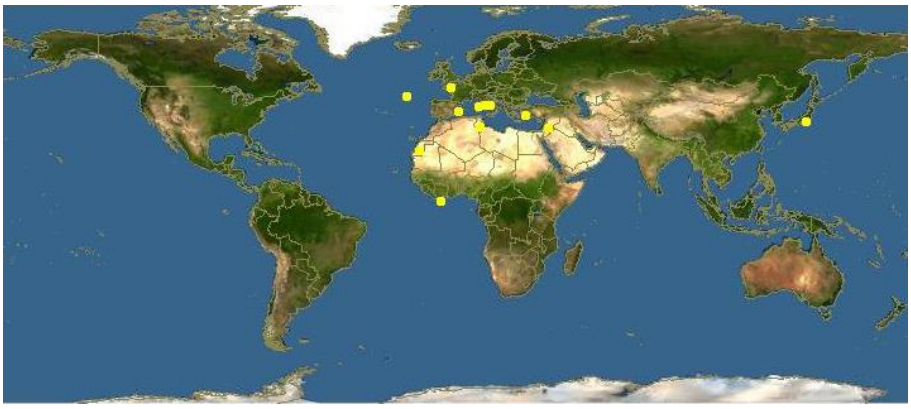

**Fig. 2.** *Worldwide distribution of E. sepositus (Encyclopaedia of Life).*

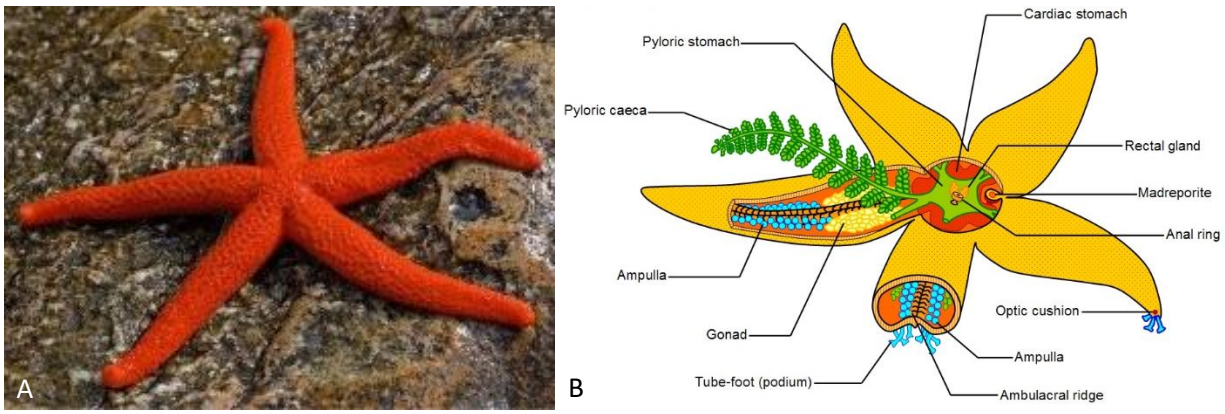


**Fig. 3.** *A) Adult specimen of E. sepositus (from http://www.treknature.com). B) Scheme of the gross anatomy of a generic starfish (from cronodon.com).*

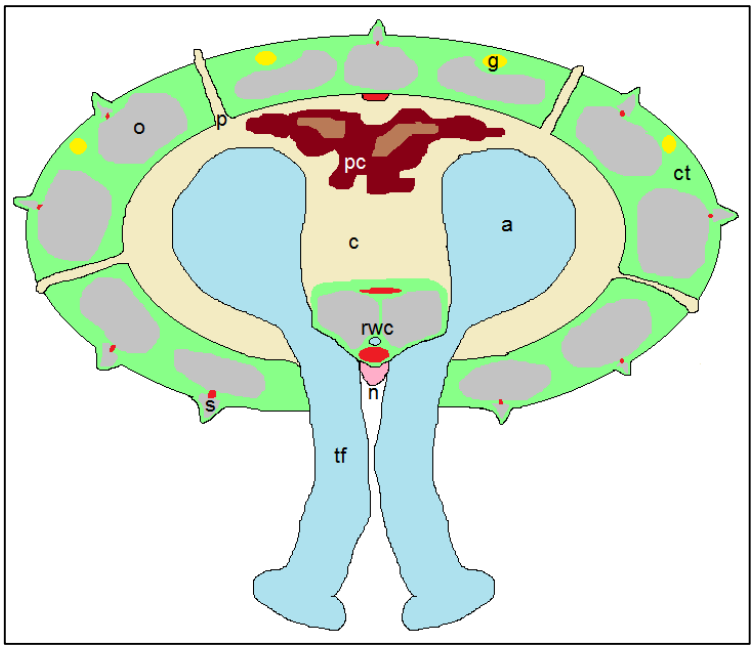


**Fig. 4.** *Scheme of a cross section of a starfish arm showing its main structures. Abbreviations*: a=ampulla; c=coelomic cavity; ct=connective tissue; g=mucous gland; n=radial nerve cord; p=papula; pc=pyloric caeca; o=ossicle; rwc=radial water canal; s=spine; tf=tube foot or podium. The main muscle bundles are showed in red.

*1.3.2. The brittle star Amphiura filiformis*

*A. filiformis* (O.F. Müller, 1776; Fig. 6A) is a brittle star belonging to the family Amphiuridae (order Ophiurida). Adult specimens have a central disc up to 1 cm in diameter and five slender arms which can reach 10 cm in length. In general, this brittle star presents a greyish-brownish-reddish colour, paler on the oral side facing the substrate (Hayward and Ryland, 1990). The distribution of this species is shown in Fig. 5. *A. filiformis* is found on the sea bed from 5 to 200 m depth. It usually burrows in sand or mud and alternately waves its arms in the water above to suspension feed on plankton and detritus as a typical infaunal suspension feeder (Gage, 1990). The arms are used also for ventilation and respiration, transport of sediment and waste materials out of the burrow (Ockelmann and Muus, 1978). As visible from Fig. 6B, the central disc is mainly filled by the viscera (from the oral mouth provided with five jaws at the centre of the peristomial membrane to the esophagus and large stomach), the gonads, and the haemal, vascular and nerve rings (Hyman, 1955). The arms do not host extension of the digestive tract as in starfish but present a reduced aboral coelomic cavity and an oral radial water canal with the corresponding couples of tube feet or podia running for the whole arm length. Podia do not possess final suckers and ampullae but pseudo-ampullae are periodically present at the level of the radial water canal in the aboral side and are hosted in the hole of the main skeletal piece, the central vertebra. The arm-tips bear a terminal tube foot or podium (Czarkwiani *et al.*, 2016). Orally to the radial water canal runs the radial nerve cord (ectoneural and hyponeural components), one for each arm, accompanied by the epineural sinus to its oral side and the hyponeural sinus to its aboral side (Hyman, 1955). This species presents a calcitic derma-skeleton with external appendages, such as spines, different in both number and shape depending on the position on the arm. The inner skeletal elements (repeated in each arm segment) are the more superficial aboral, oral and lateral shields or plates and the deeper vertebra also called vertebral ossicle (Hyman, 1955). Adjacent vertebrae are articulated through ligaments and two pairs of intervertebral aboral and oral muscle bundles, thus allowing this animal to move the arms in a typical snake-like mode, facilitating both feeding and respiration. Several other muscles are present along the arm and at the level of the disc. The body wall is covered by a cuticle, often housing bacteria, and the boundaries between epidermal cells are not well defined (Byrne, 1994). A well-defined basement membrane is apparently often lacking (Hyman, 1955). The dermal layer, composed of connective tissue, hosts the dermal plates described above. No muscle layer is detectable between the dermis and

the coelomic epithelium lining the coelomic cavities. Fig. 7 shows a cross section scheme of this brittle star arm anatomy with its main structures.

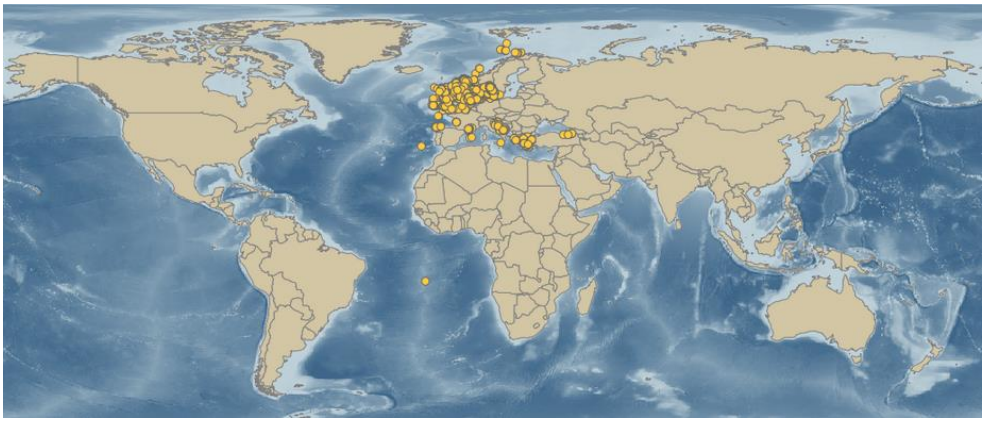

**Fig. 5.** *Worldwide distribution of A. filiformis (from iobis.org).*

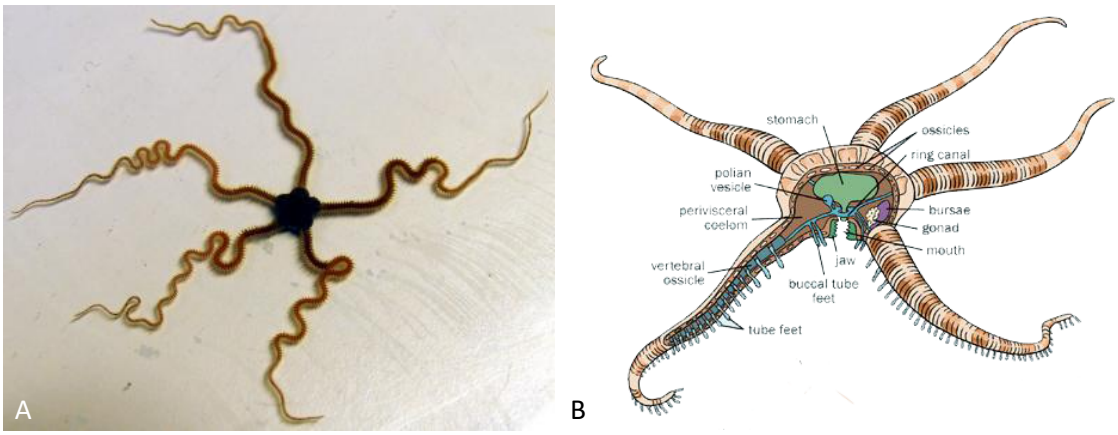


**Fig. 6.** *A) Adult specimen of A. filiformis (from www.eurekalert.org). B) Scheme of the gross anatomy of a generic brittle star (from studyblue.com).*

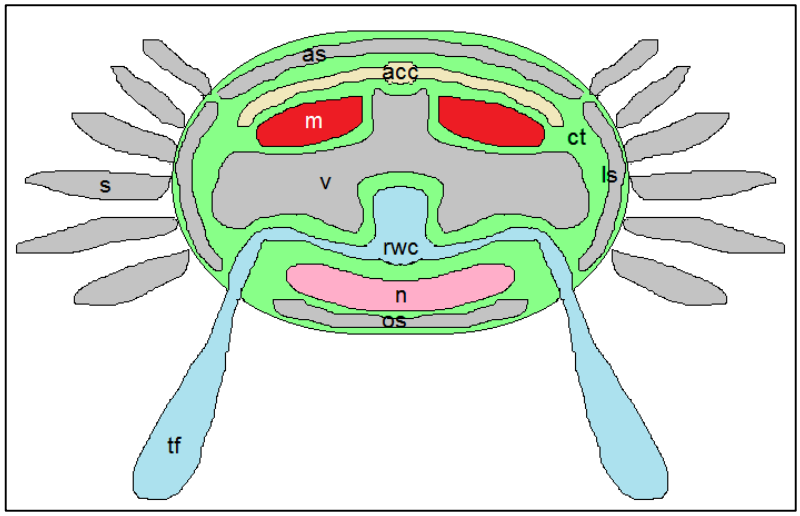


**Fig. 7.** *Scheme of a cross section of a brittle star arm showing its main structures. Abbreviations*: acc=aboral coelomic cavity; as=aboral shield; ct=connective tissue or

◀ dermal layer; ls=lateral shield; m=muscle; n=radial nerve cord; os=oral shield; rwc=radial water canal; s=spine; tf=tube foot or podium; v=vertebra.

*1.3.3. The sea urchin Paracentrotus lividus*

*P. lividus* (Lamarck, 1816; Fig. 9A) is a sea urchin belonging to the family Parechinidae (order Camarodonta). It has a diameter of up to 7 cm and it is covered by calcitic spines that are usually purple or brown-greenish. The distribution of *P. lividus* is shown in Fig. 8. This species is found up to 80 m of depth, usually on rocky bottoms and seagrass meadows of *Zostera marina* and *Posidonia oceanica*. It mainly eats algae, seagrass, small animals and sponges. It is sedentary but it can move on the substrate through its oral tube feet. As visible from Fig. 9B, this sea urchin possesses an almost circular test or theca with slightly flattened poles (along the aboral-oral axis) and its external surface is characterised by rows of tube feet or podia and spines of different length depending on their position. The body cavity is filled by a spacious coelom where the main organ systems are hosted. The water vascular system presents the usual organisation with a madreporite on the aboral side and the water canals along five main rows giving rise to the external tube feet (Hyman, 1955). The digestive tract starts from the mouth, facing the substrate and provided by a conspicuous masticatory apparatus, the Aristotle's lantern. This calcareous structure, composed by several skeletal elements (e.g. pyramids) joint together through muscles and ligaments, is mainly used to feed. The lantern is surrounded by the so called peristomial membrane (PM), a connective tissue layer mainly constituted of collagen and rare calcitic spicules lined by the epidermis at the external side and by the coelomic epithelium at the inner side. The PM is involved in lantern support and movements (Wilkie *et al.*, 1994; Bonasoro *et al.*, 1995). The mouth leads to a short esophagus, followed by the stomach and the intestine which opens on the aboral side through the anus (Hyman, 1955). The coelomic cavity hosts also the gonads which are considered a delicacy in several European countries, thus rendering this species highly valuable from an economic point of view. The nervous system is mainly composed of ectoneural and hyponeural systems organised in five radial nerve cords with corresponding sinuses, and the sub-epidermal nerve plexus. The main feature of this sea urchin, and of echinoid in general, is the presence of a body wall which is characterised by a quite thin dermis almost completely occupied by the preponderant derma-skeleton. The calcareous plates create the test or theca which is nearly completely rigid, providing an efficient defence against predator attacks. Each plate, depending on the position in the test, presents several holes corresponding to the tube feet emergence. On the plates

the spines are articulated through muscles and ligaments. On the surface pedicellariae are present as well. These are articulated skeletal elements with a defence/maintenance function, being mainly used to “clean” the test from epifauna. The inner side of the body wall is covered by the ciliated coelomic epithelium (Hyman, 1955).

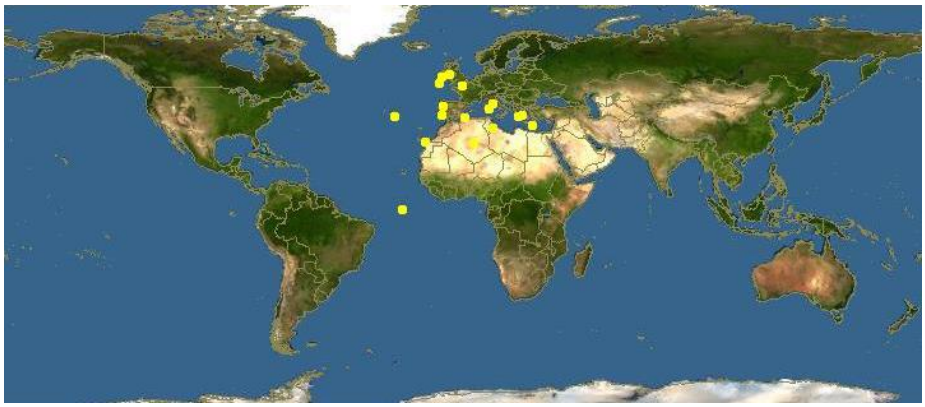

**Fig. 8.** *Worldwide distribution of P. lividus (Encyclopaedia of Life).*

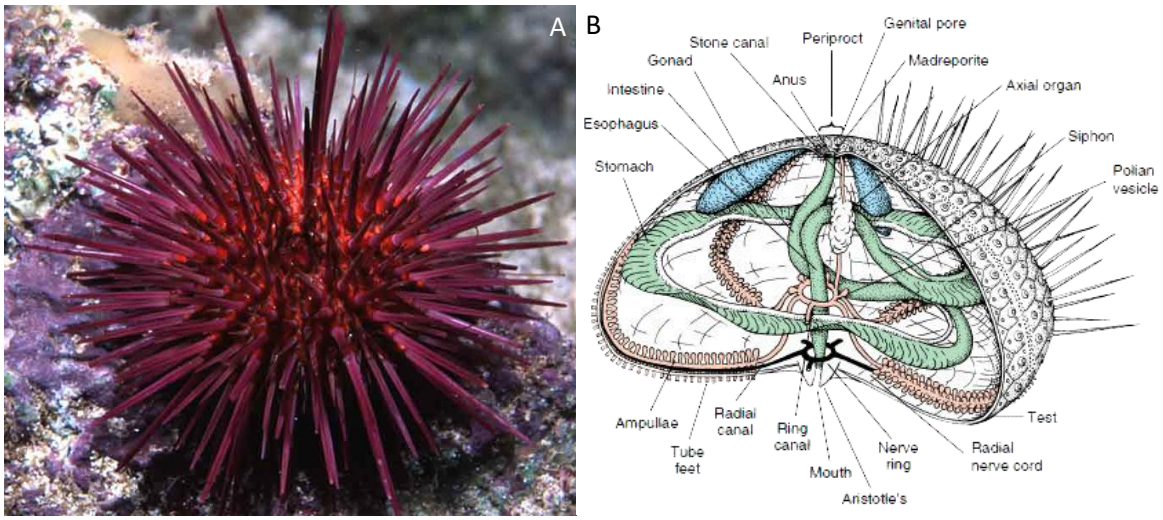


**Fig. 9.** *A) Adult specimen of P. lividus (from http://www.marlin.ac.uk). B) Scheme of the gross anatomy of a generic sea urchin (from studyblue.com).*

*1.3.4. The sea cucumber Holothuria tubulosa*

*H. tubulosa* (Gmelin, 1791; Fig. 11A) is a sea cucumber belonging to the family Holothuriidae (order Aspidochirotida). Ranging from 20 to 45 cm in length and around 6 cm in diameter, this animal usually presents a roughly cylindrical worm-shaped body with three longitudinal rows of tube feet (*trivium*) on the oral side facing the substrate and two drafted rows (*bivium*) of modified tube feet, called papillae, on the aboral side. It usually has a brownish-greyish body wall due to the presence of mucus (Hyman, 1955). The distribution of this species is shown in Fig. 10. It is usually found on sandy sea beds and

on muddy substrates up to a depth of about 100 m. It feeds on detritus, algae and plankton through its oral tentacles (modified tube feet) and it uses the ventral tube feet to move on the substrate. As visible in Fig. 11B, the body cavity is occupied by a spacious coelom between the body wall and the digestive tract which runs along the whole body from the mouth to the anus. The water vascular system, the haemal system, the radial nerve cords and the sinuses develop longitudinally along the body. In the body cavity are hosted the gonads as well (Hyman, 1955). The endoskeleton is highly reduced comparing with other echinoderms: indeed, only small calcitic spicules of microscopic size and of different shapes are widespread in the dermis. The body wall is covered by an epidermis provided with a thin cuticle and it is mainly composed of connective tissue, in particular of a thin loose outer layer with sparse collagen fibrils and a thick inner dense layer with highly packed collagen fibrils and fibres. The dermis is followed by circular and longitudinal muscle layers that permit animal movements and body size changes. The inner surface of the body wall is covered by a ciliated coelomic epithelium (Hyman, 1955).

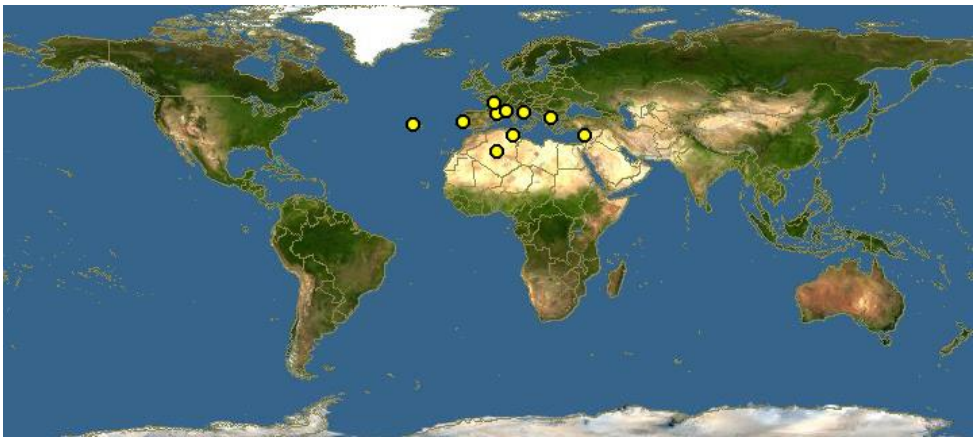

**Fig. 10.** *Worldwide distribution of H. tubulosa (Encyclopaedia of Life).*

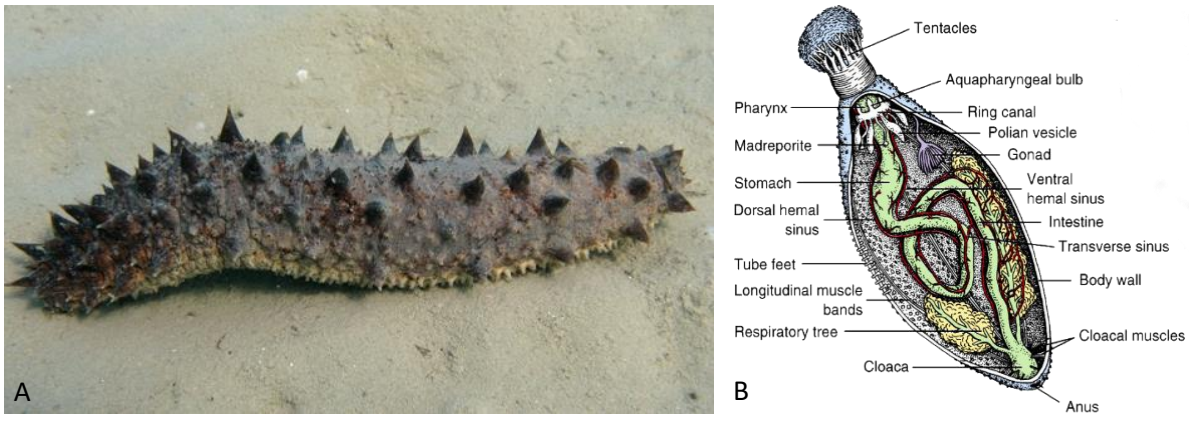


**Fig. 11.** *A) Adult specimen of H. tubulosa (from www.wikipedia.org). B) Scheme of the gross anatomy of a generic sea cucumber (from studyblue.com).*

### *1.4. Aims of this research*

Using as experimental models *E. sepositus* (Asteroidea) and *A. filiformis* (Ophiuroidea) for regeneration studies and *E. sepositus* (Asteroidea), *P. lividus* (Echinoidea) and *H. tubulosa* (Holothuroidea) for biotechnological application studies, the three main aims of this research are to:

1. describe the **arm regenerative process** after traumatic amputation, with a special focus on the connective tissue (especially collagen);
2. describe the **connective tissue** (especially collagen, extracellular matrix molecules and biosynthesis enzymes) and the **immune system** role during arm regeneration after traumatic amputation;
3. explore the **biotechnological potential** of echinoderm peculiar connective tissues (MCTs) as eco-friendly source of marine fibrillar collagen to produce **biomaterials** for human health applications (e.g. regenerative medicine or tissue engineering).

# 2) INTRODUCTION TO CHAPTERS 1, 2, 3 and 4

As previously mentioned, echinoderms are well known for their regenerative abilities and "armed" echinoderms (*i.e.* starfish, brittle stars and crinoids) are the most effective experimental models to study regeneration of whole body parts (*i.e.* arms) after both traumatic or self-induced amputation (Mladenov *et al.*, 1989; Candia Carnevali and Bonasoro, 2001a; Biressi *et al.*, 2010). The study of the regenerative phenomena in these deuterostomes will help shed light on vertebrate regenerative abilities, highlighting both similarities and differences between animals performing effective regeneration of whole body parts (*i.e.* echinoderms and some vertebrates as well) and animals with low regenerative abilities (*i.e.* most vertebrates, humans included). In this research, experimental models belonging to the classes Asteroidea and Ophiuroidea have been chosen and the state of the art on their regenerative events is detailed below.

### *2.1. Starfish regeneration*

Asteroids are famous for their striking regenerative abilities but they have not been extensively used as experimental model to study regeneration. Unlike other echinoderms, starfish have a single autotomic plane for each arm, at its base, close to the disc (Wilkie, 2001). In some species, isolated autotomized arms (called comets) can regenerate to produce a whole new adult (Emson and Wilkie, 1980; Mladenov and Burke, 1994). Both in post-traumatic and post-autotomic regenerative processes of starfish arms no discrete undifferentiated and proliferating blastema is usually evident. Therefore, typical morphallactic processes are apparently employed, although, in some cases, it is possible that a combined mechanism of epimorphosis and morphallaxis occurs during regeneration (Bonasoro *et al.*, 1998; Candia Carnevali, 2006).

In general, regenerative events include the following main steps (Candia Carnevali *et al.*, 1998; Moss *et al.*, 1998):

- repair phase: emergency reaction and wound healing;
- early regenerative phase: tissue reorganisation and first signs of tissue regenerative phenomena;
- advanced regenerative phase: cell proliferation, restoring and tissue re-growth with the formation of a new small regenerate with the same structures of the adult arm.

Starfish arm regeneration is a nerve-dependent process: in model species, such as *Asterina gibbosa*, arm regeneration cannot occur if the radial nerve has been removed and the neurotrophic action of the nervous system is needed throughout the whole course of regeneration (Huet, 1975; Huet and Franquinet, 1981; Thorndyke and Candia Carnevali, 2001).

Starfish larvae also undergo regeneration in case of loss of body parts after traumatic amputation and of clonal reproduction by fission. This latter situation is apparently very common: in fact, in samples of field-collected larvae up to 90% cloning has been recorded (Eaves and Palmer, 2003).

Among the different regenerative phases described above, little is known about the repair phase and the cicatrisation phenomenon after injury. The role of immune system during this first phase is not deeply described as well. It is known that the connective tissue plays an important role during the regenerative process in several echinoderm species (e.g. sea cucumbers; Quiñones *et al.*, 2002) but the role of connective tissue and especially of the extracellular matrix (ECM) has never been adequately investigated. It will be important to understand, from both a microscopic and a molecular point of view, the involvement of collagen and other ECM molecules during the repair phase in order to understand if the high efficiency and ability of regeneration displayed by starfish (and echinoderms in general) could be related to their peculiar connective tissues. Moreover, considering wound closure and cicatrisation, an interesting comparison with the same phenomena in mammals could be performed, shedding light on similarities and/or differences between these latter and echinoderms. Indeed, it is well known that mammals do not possess high regenerative abilities, especially in case of severe injuries and complete loss of body parts comparable to starfish arm amputation. Therefore, understanding the cellular and molecular basis of regeneration in echinoderms might be instrumental also for mammal regenerative studies. Briefly considering the immune system involvement after injury, few studies have suggested a role of coelomocytes and phagocytes in wound closure (Pinsino *et al.*, 2007; Gorshkov *et al.*, 2009; Ramírez-Gómez and García-Arrarás, 2010; Franco *et al.*, 2011) but deeper analyses are necessary. The comparison between echinoderm and mammal immune systems could be another key point to explore how to implement mammal regenerative potential.

In this research, adult specimens of *Echinaster sepositus* were chosen as experimental models for different reasons:

- *E. sepositus* is a very common starfish in the Mediterranean Sea, thus ecologically important for the Mediterranean ecosystem and fairly easily available;
- it is well adaptable to captivity: in fact, it can survive more than one year in artificial sea water and it is quite easy to maintain in laboratory conditions;
- considering its regenerative abilities, this species is still poorly studied: in fact, only few not definitive research works dating 1914 (Schapiro) and 1915 (Nusbaum and Oxner) were performed about this intriguing topic. Besides being quite dated, the authors have not investigated regenerative events following whole or partial arm loss, and, in particular, after traumatic arm amputation. Indeed, these conditions are typically found in nature and, therefore, deserve further investigations.

A histological, ultrastructural and molecular description of *E. sepositus* regenerative phases will help understanding the whole regeneration event and, in particular, the role of immune system and of connective tissue, especially collagen, during this complex process, offering also a valid comparison with other echinoderm, invertebrate and vertebrate regenerative mechanisms.

### *2.2. Brittle star regeneration*

Like asteroids, ophiuroids are well established experimental models to study regeneration (Dawydoff, 1901; Zeleny, 1903; Morgulis, 1909; Thorndyke *et al.*, 2003; Bannister *et al.*, 2005; Dupont and Thorndyke, 2006; Biressi *et al.*, 2010; Czarkwiani *et al.*, 2013, 2016). These animals are able to regenerate their arms after both self-induced or traumatic mutilations (Wilkie, 2001). Brittle star arm regeneration has always been described in literature as mainly an epimorphic process (Biressi *et al.*, 2010) but recent studies on *A. filiformis* (Czarkwiani *et al.*, 2016) have suggested the absence of a true blastema of undifferentiated cells, such as that described for crinoids (Candia Carnevali and Bonasoro, 2001b). The regenerative process has been subdivided into four main phases (Dupont and Thorndyke, 2006; Biressi *et al.*, 2010) characterised by similar processes already described for starfish regeneration: a repair phase, an early regenerative phase, an intermediate regenerative phase and an advanced regenerative phase. Czarkwiani and co-workers (2016) have recently proposed a slightly different staging system, especially for the initial phases, underlining the importance of a stage classification based on morphological hallmarks rather than time points since regeneration is a dynamic

process whose temporal progression can remarkably vary among individuals (Dupont and Thorndyke, 2006).

As for starfish, ophiuroid regeneration is a nerve-dependent process (Morgulis, 1909) and the neurotrophic role of the nervous system has been investigated by Thorndyke and co-workers (2001). Again similarly to starfish, ophiuroid larvae undergo regeneration too (Balser *et al.*, 1998; Vickery *et al.*, 2001). Also for brittle star regeneration several studies have been carried out on different species (Dawydoff, 1901; Zeleny, 1903; Morgulis, 1909; Thorndyke *et al.*, 2003; Bannister *et al.*, 2005; Dupont and Thorndyke, 2006; Biressi *et al.*, 2010; Czarkwiani *et al.*, 2013, 2016) but a focus on the role of the connective tissue and of the immune system during this process is still lacking.

In the present study, adult specimens of *Amphiura filiformis* were chosen as experimental models for the following main reasons:

- *A. filiformis* is of small dimensions and easy to handle in laboratory conditions;
- the regenerative process is relatively fast: indeed, in two-three weeks after traumatic amputation an almost complete and differentiated new arm is regenerated;
- the regenerating arms are almost transparent, making them suitable for molecular analysis e.g. whole mount *in situ* hybridisation;
- transcriptomes are available for this species (Purushothaman *et al.*, 2015; Dylus *et al.*, *submitted*), therefore, molecular analyses can be quite easily performed.

As for *E. sepositus*, both microscopy and molecular analyses are fundamental to gain a better understanding of the role of immune system and connective tissue, especially collagen, and other ECM molecules, during this complex process, and compare their involvement to that of other invertebrate and vertebrate regenerative mechanisms in view also of potential innovative applications for human health.

# CHAPTER 1

## Wound repair during arm regeneration in the red starfish *Echinaster sepositus*

Ben Khadra Yousra, Ferrario Cinzia, Di Benedetto Cristiano, Said Khaled, Bonasoro Francesco, Candia Carnevali Maria Daniela, Sugni Michela

Wound Repair and Regeneration (2015). 23: 611-622. doi: 10.1111/wrr.12333.

***Abstract***

Starfish can regenerate entire arms following their loss by both autotomic and traumatic amputation. Although the overall regenerative process has been studied several times in different asteroid species, there is still a considerable gap of knowledge as far as the detailed aspects of the repair phase at tissue and cellular level are concerned, particularly in post-traumatic regeneration. The present work is focused on the arm regeneration model in the Mediterranean red starfish *Echinaster sepositus*; in order to describe the early cellular mechanisms of arm regeneration following traumatic amputation, different microscopy techniques were employed. In *E. sepositus*, the repair phase was characterised by prompt wound healing by a syncytial network of phagocytes and re-epithelialisation followed by a localised sub-epidermal oedematous area formation. Scattered and apparently undifferentiated cells, intermixed with numerous phagocytes, were frequently found in the wound area during these first stages of regeneration and extensive dedifferentiation phenomena were seen at the level of the stump, particularly in the muscle bundles. A true localised blastema did not form. Our results confirm that regeneration in asteroids mainly relies on morphallactic processes, consisting in extensive rearrangement of the existing tissues which contribute to the new tissues through cell dedifferentiation, re-differentiation and/or migration.

### *1. Introduction*

According to Goss (1969) and Mattson (1976) regeneration is defined as the recovery process of lost or damaged tissues or organs due to injury. The regenerative capabilities vary a lot among phyla depending on their adaptive value in terms of evolutionary advantage (Brockes and Kumar, 2008), and are expressed to a different extent in the

diverse animal groups, independently of the phylogeny. The wide spectrum of regeneration processes in the diverse phyla is evident for the high adaptive value of this phenomenon. Although some vertebrates can display regeneration phenomena *i.e.* reptiles regenerate tails, amphibians lenses (Toshinori *et al.*, 2004) or limbs (Stocum, 2006) and mammals digits (Han *et al.*, 2008), these processes do not appear to be comparable to the amazing capacity of several invertebrates to repair and re-grow extensive body parts and organs. However, the highest potential of invertebrate regeneration is not related to primitive conditions and is not only found in the lower metazoans, such as *Hydra* and planarians (Tanaka and Reddien, 2011); many past and recent studies clearly demonstrated that extensive regeneration capabilities are displayed by highly evolved and complex animal groups, such as echinoderms and ascidians, both deuterostomes, which are excellent and promising experimental models for studies of regeneration (Candia Carnevali, 2006; Candia Carnevali and Burighel, 2010). Indeed, echinoderms are known to have the greatest capacity of regeneration among deuterostomes and the established gene conservation between echinoderms and vertebrates (the sea urchin genome, recently sequenced, shows 70% homologies with the human genome (Sea Urchin Genome Sequencing Consortium, 2006)) suggests that findings from these animal models might be relevant to research addressed to mammalian regeneration.

Amongst echinoderms, asteroids are well known to be able to undergo extensive regeneration of arms following their self-induced amputation (autotomy) or traumatic loss/damage due to predation, accidents, and so forth (Candia Carnevali, 2006). The histological and cellular aspects of the regenerative process have been described in detail in a few works using *Asterias rubens, Coscinasterias muricata* and *Leptasterias hexactis* as model species (Mladenov *et al.*, 1989; Moss *et al.*, 1998; Ducati *et al.*, 2004). According to these studies the overall regenerative process could be subdivided into three main phases: a repair phase, characterised by wound healing processes; an early regenerative phase, characterised by first differentiation phenomena; and an advanced regenerative phase, characterised by proper arm re-growth. Depending on the presence or absence of a localised blastema of undifferentiated and proliferating cells after wound healing, the regenerative events could be interpreted partly as epimorphic, partly as morphallactic processes, the borderline between these being apparently evident at macroscopical level but rather ambiguous and still not well defined at cellular level. Indeed, in echinoderm regeneration the different mechanisms co-exist and this ambiguity

is always present (Candia Carnevali, 2006). Epimorphic processes with blastema formation are usually found in those situations where regeneration is a widely predicted event implying a standardised sequence of developmental phases following auto-mutilations: this is the case of post-autotomic regeneration of arms in crinoids (Candia Carnevali and Bonasoro, 2001a) and some ophiuroids (Biressi *et al.*, 2010). In contrast, morphallactic regeneration seems to be a more complicated and slower process following accidental events whose extent is variable. This can be seen in post-traumatic arm-tip regeneration in asteroids and, more generally in all echinoderms, in all type of post-traumatic regeneration related to stress conditions (extreme mutilations, exposure to environmental pollution, etc.; Candia Carnevali, 2006; Sugni *et al.*, 2007). In all these cases, the mutilation impact can vary greatly and the lost tissues cannot be restored by following a standardised developmental model but they are re-grown starting from the rearrangement of the old structures of the stump (Candia Carnevali and Bonasoro, 2001b). With regard to the regenerative process of arm-tip in starfish, this is therefore considered mainly morphallactic: nevertheless, in terms of the cells that are involved, it can involve either pluripotent progenitor cells such as coelomocytes (Hernroth *et al.*, 2010) or/and differentiated cells, which may undergo dedifferentiation or transdifferentiation (Candia Carnevali, 2006).

Coelomocytes were found to be among the most actively involved elements during the repair phase of asteroid arm regeneration. In *Asterias rubens*, the aggregation of coelomocytes from adjacent tissues has been shown to significantly contribute to wound healing by clotting phenomena. The grouping of this non-proliferating cell type beneath the wound epidermis was considered also as the first line of defence following amputation (Holm *et al.*, 2008). These cells undergo phagocytosis of cell debris and of microorganisms penetrating the internal body fluids from the wound area (Mladenov *et al.*, 1989).

Although several previous studies have been focused on the early processes of arm regeneration in starfish, a comprehensive interpretation of the overall process is still missing and the cellular mechanisms and the origin of the involved cells are not yet well defined. For this reason, further studies are needed: moreover, the characteristic diversity existing among species (in terms of morphology, physiology, ecology, and susceptibility to autotomy/traumatic amputation) makes each model very different from the others and, therefore, a detailed comparative analysis of different models appears to be very appropriate.

In this study the common Mediterranean red starfish *Echinaster sepositus* has been selected as a suitable experimental model. The reasons for this choice are the following. First, regenerating specimens of *E. sepositus* are not frequently found in the wild, indeed, this species neither autotomizes easily (personal observations) nor is subjected to a high predation pressure; rather, it has maximised other defence strategies, such as the presence of sub-epidermal mucous glands containing toxic compounds (Hyman, 1955). Therefore, we assumed that a "forced and unpredicted regenerative process" induced in a species with a low regeneration incidence might differ from the regeneration response of species frequently undergoing traumatic amputations by predation or self-induced autotomies such as *A. rubens*. Second, *E. sepositus* has been recently used as model species to investigate molecular aspects (*homeobox* genes) of arm regeneration (Ben Khadra *et al.*, 2014) which need to be properly complemented by morphological investigations addressed to a detailed characterisation of the tissue and cellular pattern. Consequently, using different microscopy techniques (light and electron) we intend to provide basic essential information on the main anatomical and ultrastructural aspects of the regeneration process in this species. The present paper, besides facilitating any future research efforts in this field, will provide the basic knowledge of the main cellular mechanisms during the early stages of regeneration which are so critical for guaranteeing the correct fulfilment of the subsequent phenomena of growth, morphogenesis and differentiation.

## *2. Materials and Methods*

### *2.1. Ethics Statement*

All animal manipulations were performed according to the Italian law, *i.e.* no specific permits were required for the described studies since starfish are invertebrates. *Echinaster sepositus* is not an endangered or protected species. All efforts were made to minimise the animal suffering during experimental procedures. The specimens were released into their natural environment once the experimental procedures were completed.

### *2.2. Animal sampling and regeneration tests*

Adult (diameter ~ 12 cm) specimens of *Echinaster sepositus* were collected by scuba divers at depth of 5-8 m from the Marine Protected Area of Portofino (Paraggi, Ligurian Sea, Italy) between November 2012 and April 2013. They were left to acclimatise for two

weeks and maintained at 18°C in aerated aquaria filled with artificial sea water (Instant Ocean, 37‰) for the whole experimental period. Chemical-physical sea water parameters were checked daily (temperature and salinity) or weekly (concentrations of nitrites, nitrates, Ca, Mg, $PO_4$ and pH) and promptly adjusted if necessary. Specimens were fed with small pieces of cuttlefish twice a week. Traumatic amputation of the distal third of one arm for each specimen was performed by scalpel. Animals were then left to regenerate in the aquaria for pre-determined periods. The regeneration pattern was monitored at 1, 24 and 72 hour(s) post-amputation (p.a.) and was also compared with that of normal non-regenerating arms. Four-six samples/individuals were analysed for each stage. Regenerating arm tissues were removed including about 1 cm of the stump and were subsequently processed for the different microscopic analyses.

### *2.3. Microscopic analyses*

Non-regenerating and regenerating tissues collected at different time points were analysed by different microscopy techniques (light and electron, see below). Samples were initially observed and photographed under a LEICA MZ75 stereomicroscope provided with a Leica EC3 Camera and Leica Application Suite LAS EZ Software (Version 1.8.0).

#### *2.3.1. Light microscopy (LM)*

Both thick (paraffin) and semi-thin (resin) sections were prepared. Briefly, for thick sections three samples per stage were fixed in Bouin's fluid for about one month to allow decalcification, washed in tap water, dehydrated in an increasing ethanol series, cleared with xylene, washed in xylene:paraffin wax solution (1:1) and embedded in paraffin wax (56°-58°C). Sagittal (longitudinal-vertical) sections (5-7 µm) were cut and stained according to Milligan's trichrome technique (Milligan, 1946). For resin sections, three samples per stage were fixed in SPAFG fixative (3% glutaraldehyde, 1% para-formaldehyde, 7.5% picric acid saturated solution, 0.45 M sucrose, 70 mM cacodylate buffer) for one month to allow decalcification, washed in 0.15 M cacodylate buffer and post-fixed in 1% osmium tetroxide in the same buffer for 2 hours. Samples were rapidly washed in distilled water and then in 1% uranyl acetate in 25% ethanol (2 hours), dehydrated in an ethanol series, cleared in propylene oxide, washed in propylene oxide:Epon 812-Araldite solution (3:1 for 1 hour, 1:1 for 1 hour, 1:3 for 1 hour and 100% resin overnight) and embedded in Epon 812-Araldite. Samples were longitudinally

sectioned using a Reichert Ultracut E with glass knives. The semi-thin (1 µm) sections were stained with crystal violet and basic fuchsin. Thick and semi-thin sections were observed under a Jenaval light microscope provided with a DeltaPix Invenio 3S 3M CMOS Camera and DeltaPix Viewer LE Software.

*2.3.2. Scanning electron microscopy (SEM)*

After sagittal sectioning, the remaining paraffin embedded half-samples were also used for scanning electron microscopy (SEM) analyses. Samples were washed several times with xylene for five days in order to completely remove the paraffin wax. Then they were washed in absolute ethanol and subsequently in HMDS and ethanol (in the proportions: 1:3, 1:1, 3:1) for 15 minutes each wash, and then washed 3 times in 100% HMDS for 15 minutes. Finally, all the processed samples were mounted on stubs, covered by a thin layer of pure gold (Sputter Coater Nanotech) and observed under a scanning electron microscope (LEO-1430).

*2.3.3. Transmission electron microscopy (TEM)*

For transmission electron microscopy (TEM) analyses the same samples employed for semi-thin sections were cut with glass knives using the same Reichert Ultracut E. The obtained thin sections (0.07-0.1 µm) were collected on copper grids, stained with uranyl acetate followed by lead citrate and finally carbon coated with an EMITECH K400X Carbon Coater. The thin sections were observed and photographed using a Jeol 100SX transmission electron microscope.

## *3. Results*

### *3.1. Non-amputated arm: gross morphology and ultrastructure*

A histological cross section of an intact arm, showing the main anatomical features, is illustrated in Figure 1A (for a review of asteroid anatomy see Hyman, 1955). The arm body wall hosts a series of calcitic ossicles which are organised in the typical three-dimensional structure, the stereom, whose “cavities” are filled by cells and ECM (Fig. 1B, for a review see Smith, 1990). The ossicles are sandwiched between an inner and an outer dermis, formed by dense (DCT) and loose (LCT) connective tissue respectively. As reported in other starfish (Motokawa, 2011), most of the collagen fibres are arranged according to an orthogonal pattern. The body wall is internally completed by a coelomic myoepithelium (CE). In line with the literature (Chia and Koss, 1994), this consists of

apical peritoneocytes and basal longitudinal myocytes and nerve processes (Fig. 1C). Additionally, bands of transversal myoepithelial cells form rings of circular muscles, regularly distributed in the underlying connective tissue (Fig. 4C). A regular series of prominent papulae juts out from the external arm surface. Numerous large mucous glands, typical of some Echinasteridae (Hyman, 1955), are mainly present in the aboral dermis.

In the dermis several cells are distributed between collagen fibres. Besides the typical connective tissue cells (Fig. 2A), in our experimental model two other cytotypes could be frequently observed: myoepithelial cells and granulocytes (Fig. 2). Most often these two cell types were associated and enclosed together by a fibrous basal lamina, often in direct contact with collagen fibril bundles (Fig. 2A, C). Myoepithelial cells were scattered in the different dermis layers presumably organised in a loose network. They were characterised by a prominent euchromatic nucleus and their elongated cell processes were occupied mainly by bundles of myofilaments (Fig. 2B). The granulocytes were characterised by the presence of many circular and homogeneously electron-dense granules, approximately 1 µm in diameter (Fig. 2B, C). Their cell processes often formed a sort of “chamber” where microvilli and cilia could be observed (Fig. 2C, D). These morphological features resembled those of secretory cells observed in the CE (Chia and Koss, 1994). Additionally, neurosecretory-like cells containing small electron-dense and roundish/oval granules (approximately 300 nm in diameter) were occasionally present in association with the previously described cytotypes; their morphological features were similar to those of the juxta-ligamental cells (JLCs) or neurosecretory cells (Chia and Koss, 1994) described in the literature, which are considered to be distinctive elements of echinoderm mutable collagenous tissues (MCTs; Chia and Koss, 1994).

The main visible nervous component of the arm, the radial nerve cord (RNC), runs along the entire length of the ambulacral groove between the two rows of tube feet and ends into the optic cushion, the typical starfish photoreceptor structure. As in all asteroids, the RNC is typically V-shaped and continuous, in its lateral sides, with the epidermis (Fig. 1A, 3A). Indeed, the main nervous component of the RNC is the ectoneural system, showing the classic structure of a neuroepithelial plexus (Viehweg *et al.*, 1998): this is separated from the adjacent hyponeural sinus by a thin connective tissue layer and a coelothelium (Fig. 3A). On both sides (mainly in its apical part) the V-structure encloses layered aggregates of presumptive hyponeural somata. In sagittal sections the ectoneural epithelium of *E. sepositus* appeared to be composed of three distinct layers: (i) a thin

hyaline layer covering the surface of the cells and enclosing their cilia (Fig. 3B), (ii) a somatic zone (Fig. 3A), containing the nucleated portions of the epithelial supporting cells and neurons and (iii) a fibrillar zone (neuropile), made up of neurofibrillae intermixed with the axial parts of the supporting cells, containing intermediate filaments bundles (Fig. 3C).

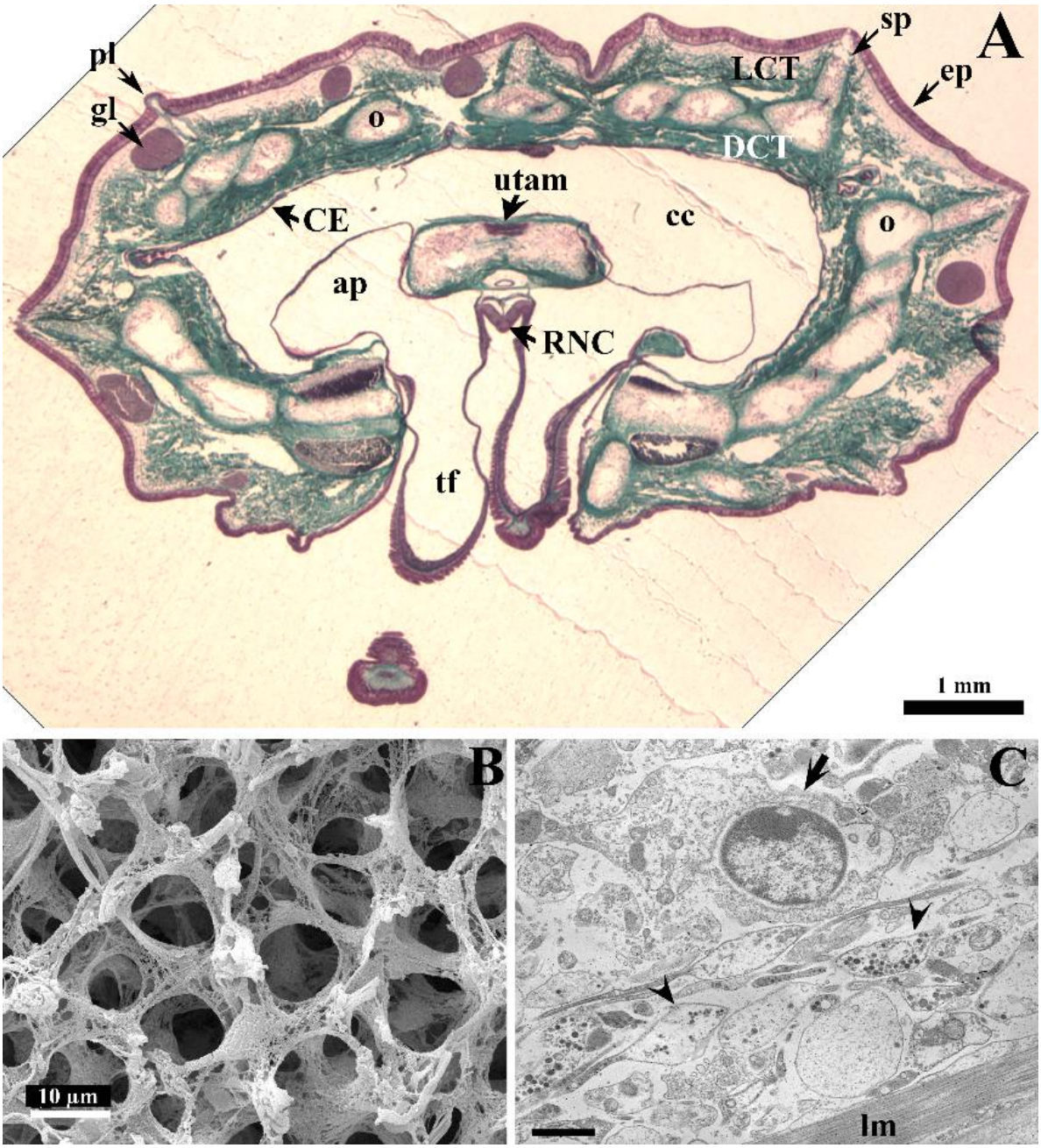


**Fig. 1.** *Main anatomical features of E. sepositus arm.* A) A transverse section of *E. sepositus* arm-tip (light microscopy (LM)). B) SEM photo of an ossicle. C) TEM micrograph of the basal part of the coelomic myoepithelium (CE) consisting of peritoneocytes (arrow) and longitudinal myocytes and nerve processes (arrowheads). *Abbreviations*: ap-ampulla, cc-coelomic cavity, CE-coelomic epithelium, DCT-dense connective tissue, ep-epidermis, gl-gland, LCT-loose connective tissue, lm-longitudinal myocyte, o-ossicle, pl-papulae, RNC-radial nerve cord, sp-spine, tf-tube foot, utam-upper transverse ambulacral muscle. Scale bar (C): 1 µm.

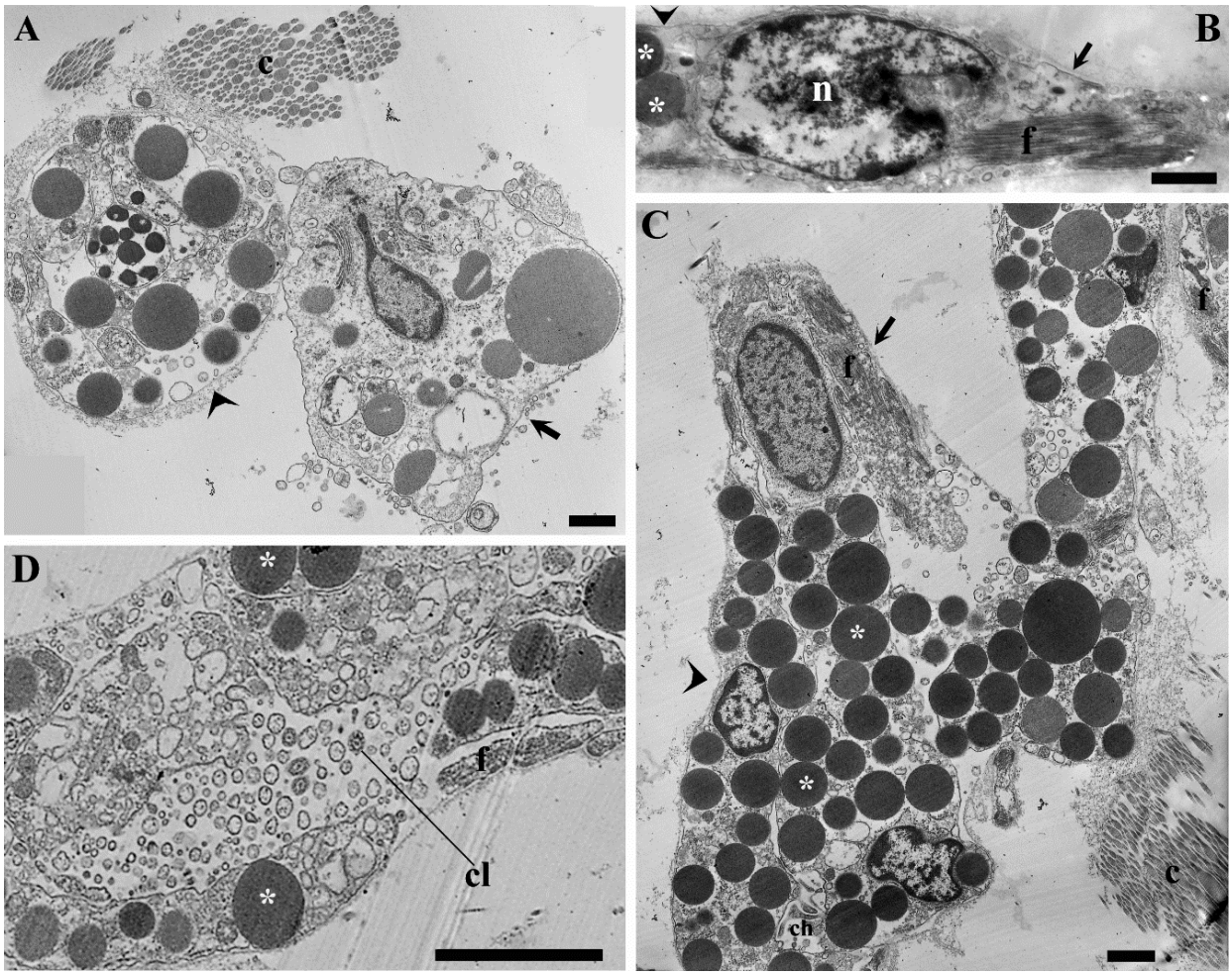


**Fig. 2.** *Ultrastructure of connective tissue cells.* A) TEM micrograph of a typical connective tissue cell (arrow), and myoepithelial cells and granulocytes enclosed by a basal lamina (arrowhead). B) TEM micrograph of a myoepithelial cell (arrow), characterised by a prominent euchromatic nucleus and a cytoplasm occupied by bundles of myofilaments, in strict association with a granulocyte (arrowhead) containing electron-dense granules (asterisks). C) TEM micrograph of myoepithelial cells (arrow) occupied by bundles of myofilaments and granulocytes (arrowhead) with a massive cytoplasmic presence of roundish and homogeneously electron-dense granules (asterisks). D) Detail of cell processes between myoepithelial cells and granulocytes (chamber) where microvilli and cilia are observed. *Abbreviations and symbols*: c-collagen fibrils, ch-chamber, cl-cilia, f-myofilaments, n-nucleus, *-electron-dense granule. Scale bars: 1 µm (A-C), 0.5 µm (D).

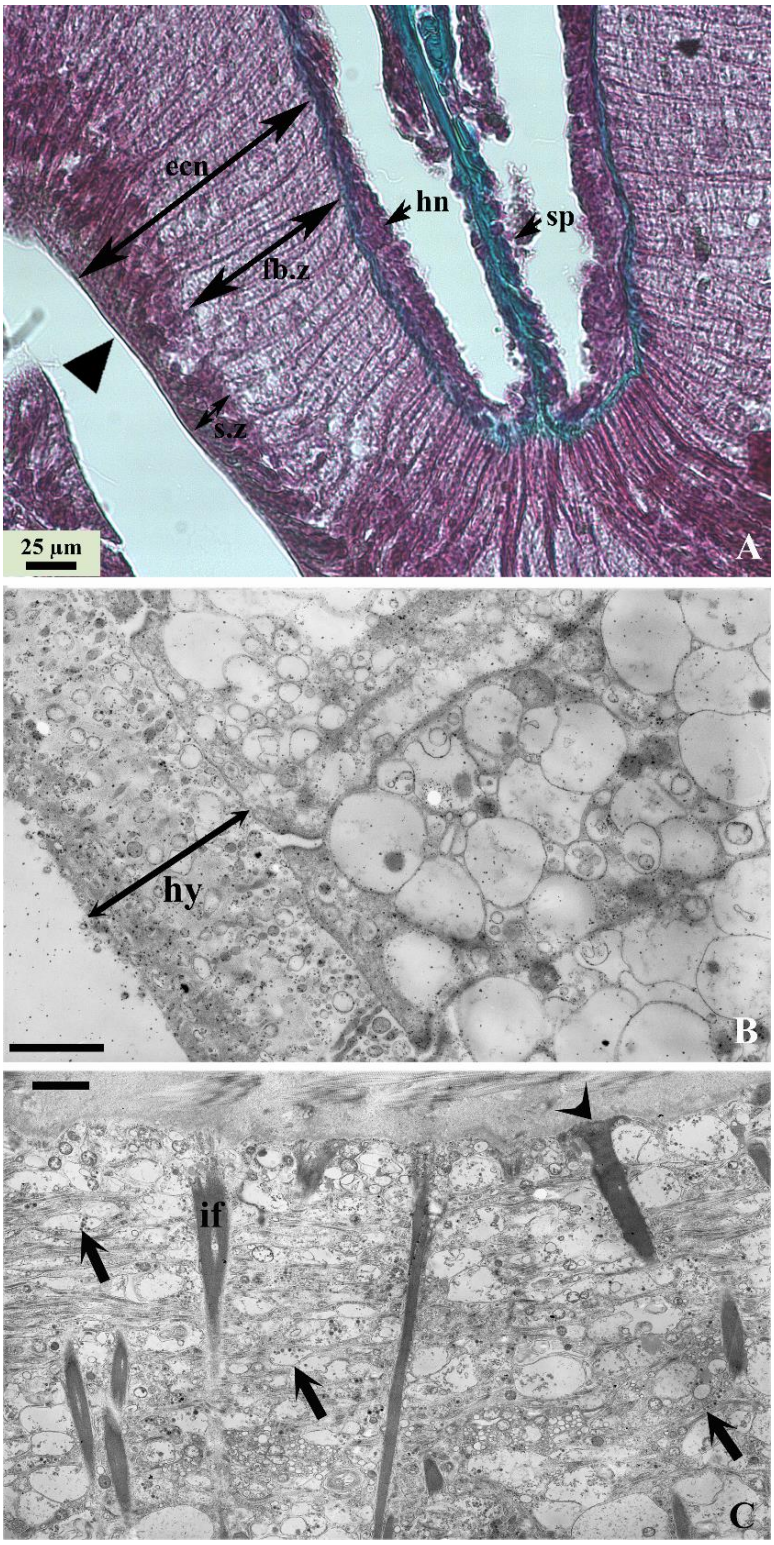


**Fig. 3.** *Main components of E. sepositus RNC*. A) Ectoneural epithelium composition: a thin hyaline layer (arrowhead) covering the surface of the cells, a somatic zone (s.z) and a fibrillar zone (fb.z). B) TEM micrograph detailing the hyaline layer (hy). C) Detail (TEM micrograph) of the basal part of the ectoneural epithelium showing the axial part of supporting cells which contain intermediate filaments bundles, their final end-feet (arrowhead) and nervous processes (arrows) with small electron-dense granules. *Abbreviations*: ecn-ectoneural epithelium, fb.z-fibrillar zone, hn-hyponeural, hy-hyaline layer, if-intermediate filaments, sp-septum, s.z-somatic zone. Scale bars: 1 µm (B), 2 µm (C).

### *3.2. Regeneration*

*3.2.1. 1 hour p.a.: wound sealing*

As shown in whole mounts and in histological sections, immediately after removal of the arm-tip, the distal portion of the stump (about 3 mm) strongly constricted (like a “haemostatic ring”) thus sealing off the open ends of the perivisceral coelom (Fig. 4A, B). Papulae present in the contracted stump body wall appeared deflated, as a consequence of the reduced coelomic hydrostatic pressure. In the contracted area the collagen fibres of the DCT apparently became more densely packed and the coelothelium showed an extensively folded profile; the rings of circular muscle fibres underlying the coelothelium appeared to be remarkably contracted, showing a more roundish and enlarged overall cross section when compared with those of more proximal area of the stump (Fig. 4C, D). This strong contraction pulled the first pair of tube feet towards the centre of the wound. The injury appeared to be sealed also by the active contribution of coelomocytes which migrated through the coelomic fluid and formed clots closing the wound (Fig. 4E). Different cytotypes could be distinguished in this area, including both apparently undifferentiated cells and differentiated coelomocytes. The presumptive undifferentiated cells were small elements, roundish or oval in shape, with a very large nucleus and a scarce granular cytoplasm not containing any specialised organelles (e.g. phagosomes). Their surface did not show filopodial processes (Fig. 4F). The differentiated coelomocytes included different populations of migratory cells, recognisable by specific morphological features (shape, size, cytoplasmic inclusions, filopodial processes, etc.). The characterisation of these cells is given in detail in stage 72 hours p.a. In any case, the microscopic analyses did not reveal any noticeable changes in the specific cellular composition of the CE either close to or far from the wound: no direct release of coelomocytes from the CE could be observed.

Even at this early stage the injured muscles showed first signs of reorganisation and dedifferentiation phenomena and evidence of release of cells towards the wound area (Fig. 4G).

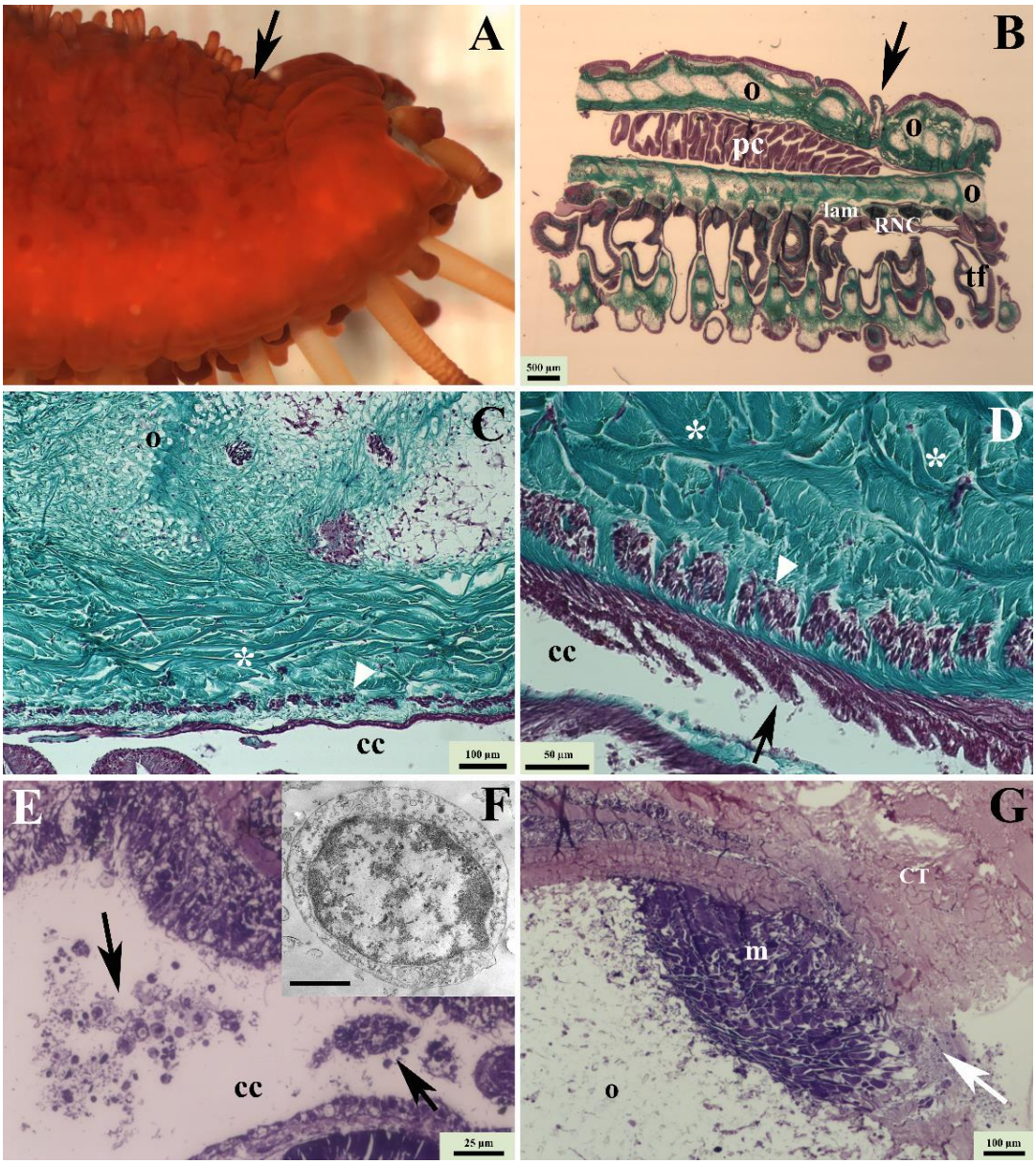


**Fig. 4.** *Wound sealing (1 hour p.a.).* A) (stereomicroscopy (SM) view) and B) (LM) haemostatic ring (arrows); the distal portion of the stump (about 3 mm) is strongly constricted. C) Normal unconstricted body wall. D) At the constriction the collagen fibres (asterisks) of the DCT become more packed, the coelothelium shows a folded profile (arrow) and the circular muscle fibres (arrowhead) appear contracted in comparison to norm (arrowhead in C). E) Coelomocytes clotting in the coelomic cavity (arrows). F) TEM micrograph of a presumptive undifferentiated cell found in the coelomic cavity. G) Injured muscle showing first signs of reorganisation and release of cells towards the wound area (arrow). *Abbreviations and symbols*: cc-coelomic cavity, CT-connective tissue, lam-lower transverse ambulacral muscle, m-muscle, n-nucleus, o-ossicle, pc-pyloric caeca, RNC-radial nerve cord, tf-tube foot, *-collagen fibres of the DCT. Scale bar (F): 1 µm.

### *3.2.2. 24 hours p.a.: wound healing*

At 24 hours p.a. the strong body wall contraction still persisted (Fig. 5A): the aboral body wall converged and folded towards the oral side (Fig. 5B). Within the end of the first day post-amputation wound healing was almost completed, including the formation of a new

thin epithelium (Fig. 5C, D). The epidermis, which seemed to converge centripetally from the edges towards the wound centre, provided cells for the formation of a new thin epithelial monolayer (Fig. 5E). At this stage, this latter was apparently composed only by partially dedifferentiated epidermal cells, derived from the stump, which were stretched in order to heal the injured area. These cells were initially flat and squamous with a prominent nucleus and cytoplasmic inclusions (granules, vacuoles, etc.) characteristic of the epidermal cells. Typical cell junction complexes, including both adherens and septate types, were detectable. Small microvilli immersed in a thin cuticle layer could be seen on the outer epithelial side, although a clearly recognisable basal lamina was still lacking (Fig. 5F). Numerous presumptive neural processes could be observed on the inner epithelial side (Fig. 5E). In some cases, beneath this wound epidermis a loose syncytial network of phagocytes was found containing several cytoplasmic inclusions and/or electron-transparent vacuoles, and creating wide and irregular lacunar areas. The syncytium appeared to form a barrier isolating extracellular matrix elements (e.g. collagen fibrils) and sparse cells that remained after ablation and/or had recently migrated to the wound area (Fig. 5G).

At this early stage the RNC was also healed: the regenerating fibrillar zone showed a rearranged pattern with a still disorganised architecture and in the most distal part only the cell body layer was visible (Fig. 5D).

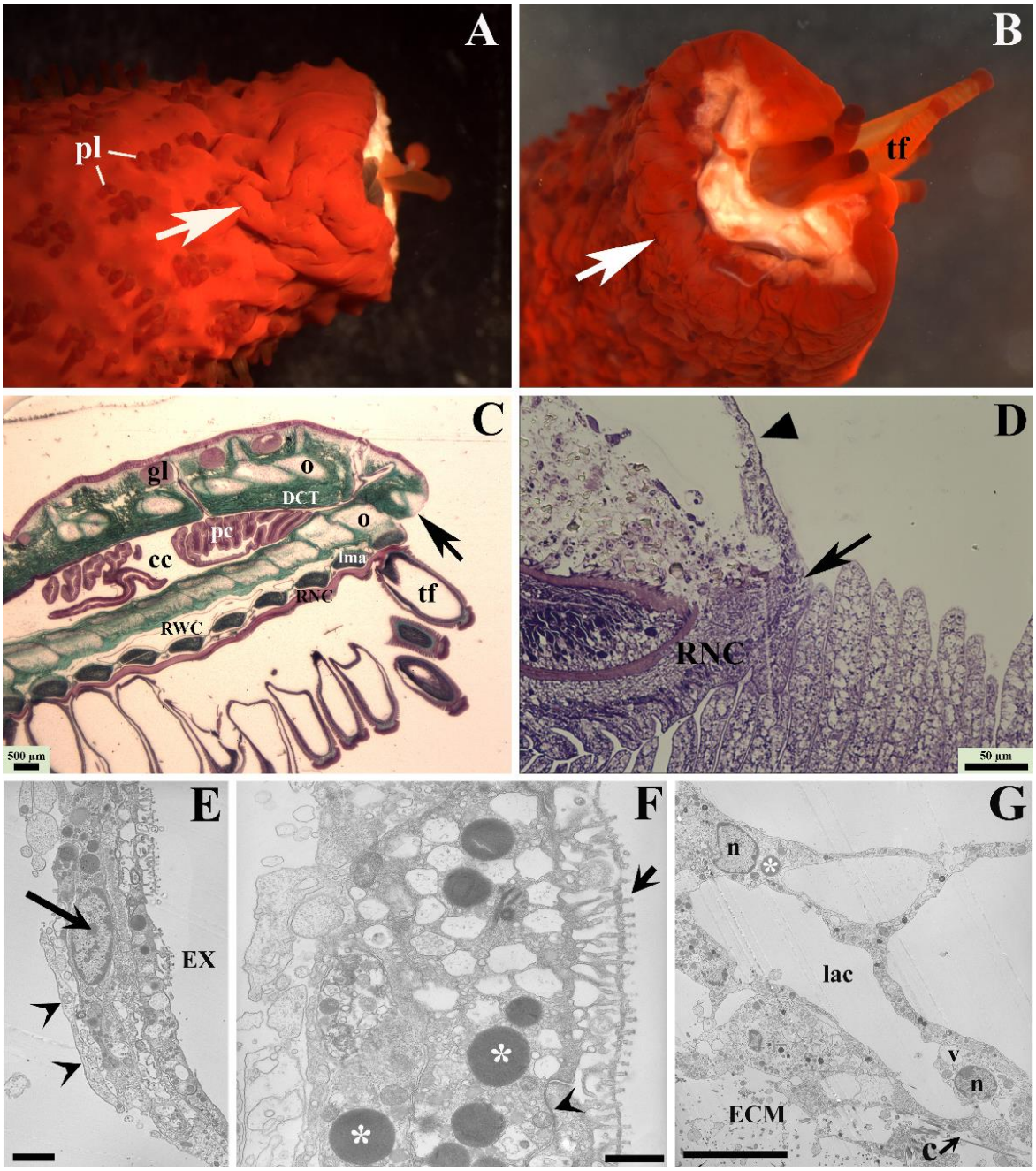


**Fig. 5.** *Wound healing (24 hours p.a.).* A) (SM view) The strong body wall contraction still persists (arrow). B) (SM view) The aboral body wall converges and folds towards the oral side (arrow). C) Complete wound healing and formation of a new thin epithelium (arrow). D) (LM) Wound epidermis (arrowhead) and neuroepithelium healing (arrow). E) TEM micrograph of the new epidermis which is composed by a monolayer of dedifferentiated epidermal cells (arrow). On its inner epithelial side numerous presumptive nervous processes are found (arrowheads). F) Detail of Fig. E on the typical cell junction complexes (arrowhead) and small microvilli (arrow) of the new epithelium together with electron-dense granules (asterisks). G) Loose syncytial network of phagocytes beneath this wound epidermis. *Abbreviations and symbols*: c-collagen fibrils, cc-coelomic cavity, DCT-dense connective tissue, oe-oedematous area, ECM-extracellular matrix, EX-external environment, gl-gland, lac-lacunar area, lam-lower transverse ambulacral muscle, LCT-loose connective tissue, n-nucleus, o-ossicle, pc-pyloric caeca, pl-papulae, RNC-radial nerve cord, RWC-radial water canal, tf-tube foot, v-vacuole, *-electron-dense granule. Scale bars: 1 µm (E-F), 10 µm (G).

*3.2.3. 72 hours p.a.: oedematous area formation*

The aboral body wall was still “moving” downward, covering the wound area (Fig. 6A). The body wall was now relaxed and the papulae protruded again, indicating that the wound was actually healed and possibly the internal hydrostatic pressure completely restored (Fig. 6A, B). The newly formed epidermis was much thicker and organised (Fig. 6C, D). The supporting cells, columnar in shape, were now more differentiated, bearing microvilli and cilia. Their roundish nucleus was basally positioned and their apical cytoplasm contained some dense or finely granular granules (Fig. 6D). Several secretory cells, filled by roughly circular electron-translucent granules (about 1.1 µm in average diameter) were present. All around the bases of these cells, well-differentiated neural processes could also be found: they were filled with a large number of small electron-dense vesicles (about 120 nm in diameter).

Just beneath the wound epidermis, clots of different cells, apparently formed by free-migrating elements, were intermixed with newly deposited collagen fibrils, leaving room for the formation of a wide empty area of oedematous area (Fig. 6E). The most numerous cell types were phagocytes, easily recognisable by their large size, irregular shape, and cytoplasmic content especially represented by large phagosomes (Fig. 6F). Furthermore, widespread presumptive fibroblasts (Fig. 6G) and some scattered morula cells or spherule cells (type III, according to the classification by Chia and Xing, 1996) were also found, these latter containing translucent granules in their cytoplasm. In addition to these cytotypes, several altered myocytes, released by the injured muscles, were found widespread in the oedematous area (Fig. 6H). These myocytes were undergoing evident dedifferentiation processes, often characterised by the presence of typical “spindle-like” structures (SLSs; Fig. 6I) in which extensive rearrangement and packaging of their contractile apparatus were occurring. Some SLSs were ingested by phagocytes. In some cases, only the contractile apparatus was ingested. Apparent flows of different cell types moved from the stump (upward from the RNC area and downward from the aboral wall) to the oedematous area. Free-circulating cells were also visible in the perivisceral coelom and the papulae.

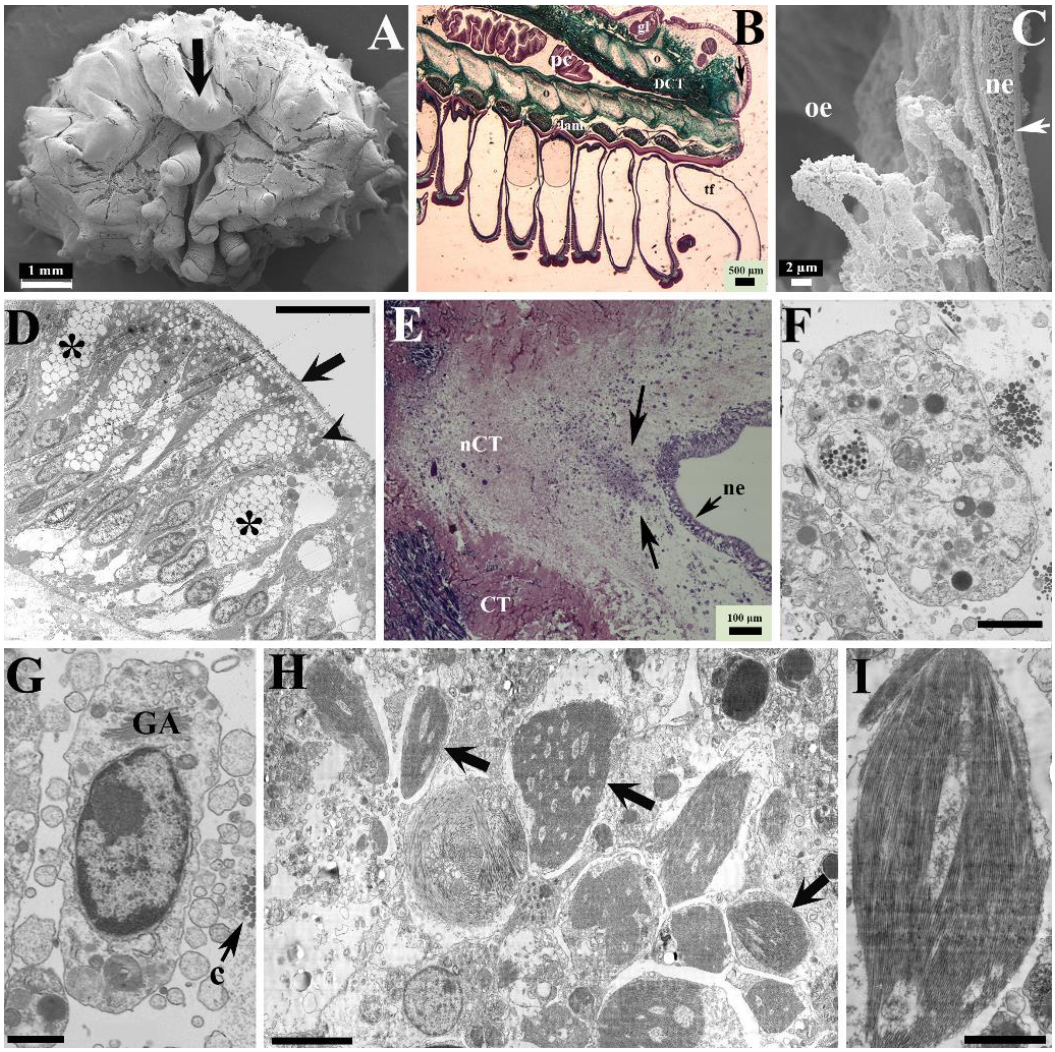


**Fig. 6.** *Oedematous area formation* (*72 hours p.a.)*. A) (SEM micrograph) The aboral body wall moves downwards (arrow). B) (LM) The body wall is relaxed and the downwards movement of the aboral body wall is visible (arrow). C) (SEM micrograph) The newly formed epidermis (arrow) is much thicker and organised. D) (TEM micrograph) The supporting cells are more differentiated (bearing microvilli and cilia (arrow)) and their apical cytoplasm contains some dense or finely granular granules (arrowhead). The secretory cells are filled by electron-translucent granules (asterisks). E) (LM) Oedematous area: intermixed cells (arrows) beneath the wound epithelium (ne). F) TEM micrograph of a phagocyte. G) TEM micrograph of a presumptive fibroblast with Golgi apparatus (GA) in full activity and an evident nucleolus. H) TEM micrograph of dedifferentiated myocytes found in the oedematous area (arrows). I) Detail of the "spindle-like" structures (SLSs) of a myocyte. *Abbreviations and symbols*: c-collagen fibrils; cc-coelomic cavity, CT-connective tissue, DCT-dense connective tissue, GA-Golgi apparatus, gl-gland, lam-lower transverse ambulacral muscle, nCT-newly deposited collagen, ne-new epidermis, o-ossicle, oe-oedematous area, pc-pyloric caeca, pl-papulae, tf-tube foot, *- electron-translucent granules. Scale bars: 10 µm (D), 2 µm (F, I), 1 µm (G), 5 µm (H).

### *4. Discussion*

In this work, we described the basic cellular mechanisms occurring during the repair phase in the Mediterranean red starfish *E. sepositus* following traumatic arm amputation.

Within one hour p.a. an immediate emergency reaction occurred. The tip of the stump was strongly constricted to seal off the perivisceral coelomic canal from the outer environment, acting like a haemostatic (coelomo-static) ring: this prevented excessive loss of coelomic fluid and, at the same time, restored and maintained the internal physiological hydrostatic pressure in the rest of the body. This was evidenced by the different conditions shown by the papulae (which are expansions of the perivisceral coelom): in fact, the papulae nearest to the coelomo-static ring looked deflated, whereas the more distant ones maintained their functional turgidity. In contrast to the papulae, those tube feet nearest to the wound surface conserved their turgor, thus indicating that the sealing of the water vascular canal was more effective and rapid than that of the perivisceral coelom.

The emergency reaction was apparently achieved by a synergic activation of different components, namely coelomocytes, muscles and scattered dermal myocytes and, possibly, also the dermal MCT. The rapid coagulation of the coelomic fluid was achieved by coelomocytes: they rapidly formed a clot of cells, facilitating the closure of the injured perivisceral coelomic canal. Only the mature coelomocytes were able to aggregate using their filopodial processes (Pinsino *et al.*, 2007). The coelomocytes coagulating in the canal were probably those already present in the coelomic liquid. However, this does not exclude the possibility that the CE produces coelomocytes immediately after wounding since the transition to the filopodial form arises within 5 to 8 minutes in fresh preparations and suspended cells (Pinsino *et al.*, 2007).

Together with coelomocytes, also myocytes were actively involved in the emergency reaction in terms of both muscular activity and cell recruitment. In terms of muscle contraction, this was in agreement with previous work carried out in *Leptasterias hexactis* where the loss of coelomic fluid is similarly stopped also by a strong contraction of the arm stump (Mladenov *et al.*, 1989). In our samples, this contraction was performed mainly by the circular muscle layer beneath the CE, which formed an internal haemostatic ring surrounding the coelomic cavity. Nevertheless, this event did not completely explain the overall constriction of the whole arm wall (*i.e.* including the aboral dermis and epidermis), its apparent reduction in thickness and the presence of a more compact dermis. This could be reasonably explained by an involvement of the myocyte network within the dermal layer: a myocyte contraction is likely to remodel the collagen bundles to which these are structurally connected. The function of the associated CE-derived granulocytes remains unknown, although their invariable co-existence with myocytes suggests a

functional relationship. Although highly speculative, the occasional presence of presumptive juxta-ligamental cells might suggest that the muscle contraction (both of the circular bundles and the dermal network) can be further supported by a stiffening of the mutable collagenous tissue (MCT) composing the dermis of the arm wall (Smith, 1990). Indeed, in many cases echinoderm MCTs can contribute or even substitute muscle functions as energy sparing mechanism during posture maintenance (e.g. in crinoids; Chia and Koss, 1994). This might be particularly important in the initial regenerative phase of *E. sepositus*, since experimental starfish do not feed during the first weeks post-amputation (personal observations).

Besides sealing off the coelom, the stump contraction reduced the injury surface, thus accelerating wound cicatrisation. This was helped also by a further downward folding of the aboral surface (which apparently slipped toward the oral side), that made the wound edges closer and increased protection of the injured site. Within 24 hours p.a. the wound healing process began: this is initially achieved recruiting and recycling the adjacent epidermal cells which were stretched and migrated over the wound, creating a thin epithelium already provided with cell junctions. It is not clear whether this epithelial covering is driven by the underlying and developing nervous plexus or by the epidermal cells themselves. The wound closure was supported by the formation of a phagocyte syncytial network separating the developing epithelium from the injured stump tissues which started to exhibit an active rearrangement process. It is well known that the fusion of phagocytic cells usually occurs after the contact between the coelomic fluid and the external environment (Isaeva and Korenbaum, 1990). In *E. sepositus*, the cell syncytia could be considered as the first barrier against loss of coelomic fluid following trauma. Also, it could represent a mechanism widely used by many organisms to eliminate foreign bodies; a syncytial-like structure has been found in the starfish *Acanthaster planci* following an injection of bile slats and other contaminants (Grand *et al.*, 2014). At the best of our knowledge, such phagocyte network formation during wound healing in invertebrates has never been documented before. However, this phenomenon is reminiscent of the formation of a network of blood vessels, which is a critical component of wound healing in mammals. The endothelial cells migrate, invade the ECM stroma, and form tube-like structures that continue to extend, branch, and create networks, which supply oxygen and nutrients to cells that are rebuilding the affected tissue (Tonnesen *et al.*, 2000). By 72 hours p.a., the wound epithelium was almost completely differentiated, thicker and permanent: epidermal cells acquired their final morphological and functional

features (prismatic shape, microvilli and cilia on the outer surface, secretory granules in the cytoplasm) and an underlying nerve plexus was well developed. The wound covering occurred in a centripetal direction, towards the RNC/water vascular canal area. This behaviour has been already observed during the ophiuroid repair phase (Biressi *et al.*, 2010) and suggests that the injured RNC or water vascular canal area released chemo-attractant molecules that direct or attract the migration of wandering cells. It is well known that echinoderm regeneration is a nerve-dependent phenomenon (Thorndyke and Candia Carnevali, 2001).

At this time an oedematous area was formed behind the newly established epidermis, composed of several cytotypes which were characterised by transmission electron microscopy (TEM). Among all intermixed cells, phagocytes represented the most abundant population, as has been described in the common sea star *A. rubens* (Pinsino *et al.*, 2007). Phagocytes are recruited at the beginning of the regeneration process and, although their number considerably varies within taxa, their involvement is usually related and restricted to the repair phase, in both arm and visceral echinoderm regeneration (Candia Carnevali *et al.*, 2009). The main characteristic of these cells is their ability to phagocytise other cells or foreign particles (Endean, 1966). The phagocytosis of foreign materials in *E. sepositus* initiated within 24 hours following amputation. Phagocytosis is an important feature of the immune response throughout the animal kingdom: in fact, it represents the first line of defence (Greenberg, 1989). It has been demonstrated that phagocytes in the sea star *Asterias vulgaris* can remove $2.6x10^7$ sea urchin coelomocytes within one hour when sea urchin cells are injected into the body cavity of the sea star (Reinisch and Bang, 1971). Moreover, phagocytes can degrade not only foreign materials but also their own particles (debris) or cells when necessary. In *E. sepositus* phagocytes began to digest SLSs/degenerated myocytes present in the oedematous area or in the area close to the wound site after 72 hours p.a.: indeed, most of these degenerating myocytes came from injured muscles at the level of the amputation plane. The first stages of dedifferentiation included the tight packaging of myofilaments in defined sarcoplasmic areas which could be eventually removed by exocytosis and subsequently ingested by phagocytes. Similar means of recycling myocytes has been described in the holothurian *Holothuria glaberrima* following evisceration of the digestive tract (García-Arrarás and Dolmatov, 2010).

In terms of cell recruitment for regeneration, several authors have shown that myocyte dedifferentiation is a common event in echinoderm regeneration processes and that the

dedifferentiated cells might play an important role in the formation of the new tissues or organs (Candia Carnevali, 2006). Indeed, in echinoderms myocytes are the most “plastic” cytotypes to be used and recycled for a potential use during the re-growth phase and this remarkable ability might be one of the key aspects of their striking regenerative capacity. It is still not clear if myocyte dedifferentiation gives rise directly to new populations of cells or if they are involved in complicated processes mediated by phagocytes in which they undergo degeneration and mainly contribute indirectly as source of important cell reserves (e.g. proteins). Tracking the fate of “myocytes” after myofilament expulsion would certainly help to clarify this issue. Regardless the implicated mechanism, direct or indirect, it is noteworthy that these processes of rearrangement/dedifferentiation at the level of the muscles were closely associated with massive cell migration.

The crucial role of phagocytes and their abundance in the oedematous area did not exclude the presence and the importance of other cell types, such as morula cells. According to Chia and Xing’s classification (Chia and Xing, 1996), we have identified a morula cell (spherule cell) type III whose granules seem to be void of content. Morula cells are reported to participate in the synthesis of a large number of humoral factors of the echinoderm immune system and inflammatory responses (Pagliara and Canicatti, 1993) as well as being associated with antibacterial activity (Haug *et al.*, 2002), extracellular matrix remodelling (García-Arrarás *et al.*, 2006) and wound healing (San Miguel-Ruiz and García-Arrarás, 2007). Other cytotypes could be present in the oedematous area, such as fibroblasts, since new extracellular matrix (ECM) including collagen was deposited progressively beneath the wound epithelium. As in mammalian wound healing processes (Diegelmann and Evans, 2004), in *E. sepositus* the ECM started to be deposited after the “immune response” phase but was delayed in comparison with them. The new collagen fibrils were widespread in the oedematous area is a still partly disorganised pattern, complete organisation being reached in the following regenerative stages. In contrast to mammalian cases (Rahban and Garner, 2003) in which fibrosis and/or over-deposition of collagen are detectable, in our samples from the wound area no signs of these phenomena were visible. As suggested for other echinoderm classes (e.g. Holothuroidea; Cabrera-Serrano and García-Arrarás, 2004), the delayed deposition of collagen and other ECM components in comparison with mammalian events might explain the effectiveness of the regenerative processes in this phylum.

The initial healing events occurred also at the level of the nerve: a thin layer of nervous tissue extending into the wound area of the regenerating arm-tip of *E. sepositus* was detectable within 24 hours p.a. The migration of cells of the radial nerve stump to cover the wound site was accompanied by disorganisation of the neurofibrillar zone of the RNC which remained over 7 days. At this stage the hyponeural system did not show any evident sign of regeneration. This delay could be related to its function, *i.e.* the innervation of the effector systems, such as tube feet, which will be regenerated later. It is well known that in many echinoderm regeneration models, the RNC starts to undergo repair first and subsequently drives the whole regenerative process (Thorndyke and Candia Carnevali, 2001).

In conclusion, in *E. sepositus* the repair phase lasted three days, during which initial wound healing occurred followed by an initial accumulation of a variety of cells, mainly phagocytes, forming an oedematous area just beneath the wound epidermis. Figure 7 summarises the most important events of these early stages. The regenerative process could be classified as morphallactic due to the absence of a true undifferentiated and localised blastema and to the remarkable rearrangement phenomena at the level of stump tissues (mainly the injured muscles). However, on the basis of what could be inferred from histological studies, the origin of most cells involved in arm regeneration was still ambiguous. It could be that cells of mixed origin might be recruited from more distant sources of stem/progenitor cells as suggested in *A. rubens* arm regeneration (Hernroth *et al.*, 2010). To help to elucidate these and other ambiguities further studies on this starfish species using markers for cell proliferation, cell ageing or cell identity (e.g. myocyte markers) are strongly recommended.

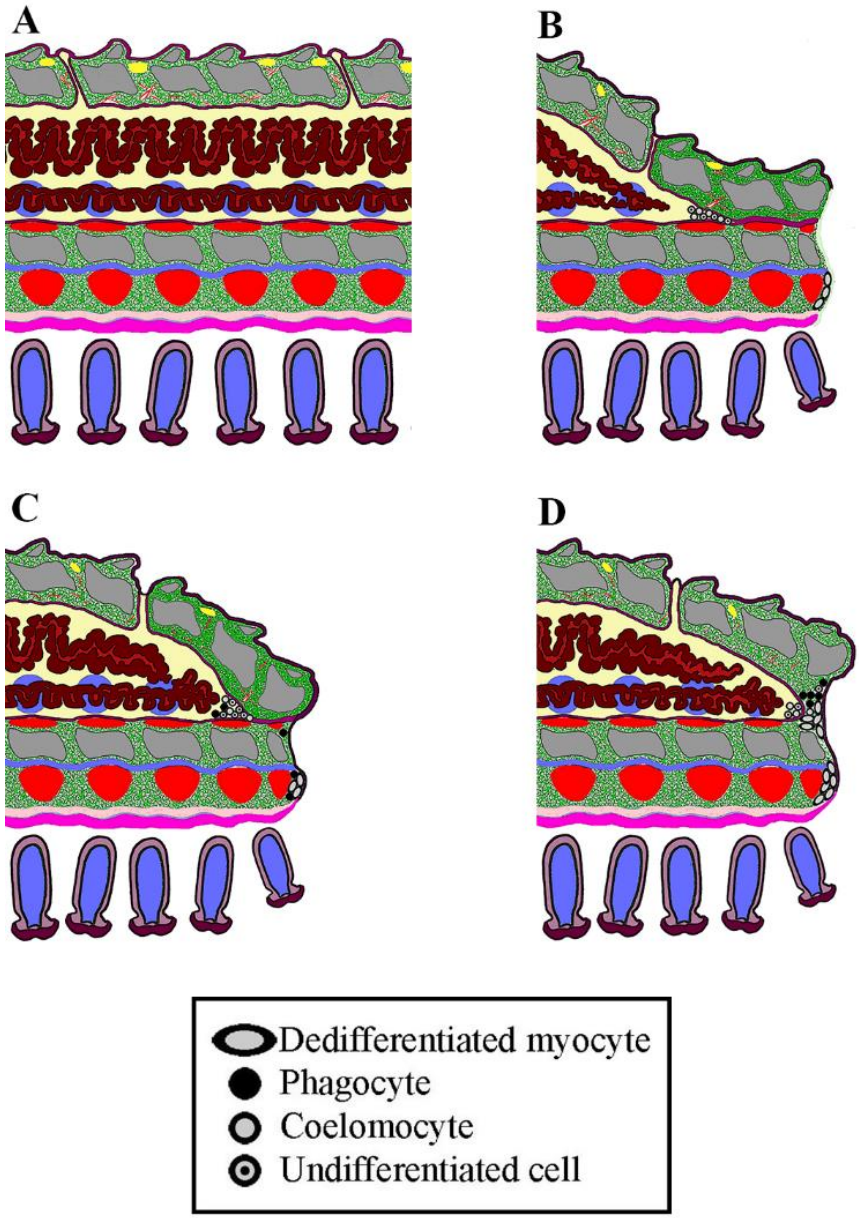


**Fig. 7.** *Diagram summarising the main events during E. sepositus repair phase*. A) Gross morphology of non-regenerating arm. B) Wound sealing (1 hour p.a.): a haemostatic ring formed by circular muscle and aboral collagen fibre contraction, and coelomocytes clotting in the coelomic cavity. C) Wound healing (24 hours p.a.): Re-epithelialisation. D) Oedematous area formation (72 hours p.a.): pool of various cells (myocytes, phagocytes, etc.) intermixed with newly deposited collagen fibrils.

## *5. Supplementary Materials*

### *5.1. Extended Materials and Methods*

*5.1.1. Microscopy analyses of regenerating samples*

*5.1.1.1. Light microscopy (LM)*

Sections were stained according to Milligan's trichrome technique (Milligan, 1946), a three-colour staining protocol that allows to distinguish the different types of tissues (for

example, green for the connective tissue and violet for the muscles). Briefly, sections were washed in clean xylene, rehydrated in a decreasing scale of ethanol and then placed into a solution of potassium dichromate and hydrochloric acid. The first staining was performed with acid fuchsin and then fixed with 1% phosphomolybdic acid; the following stainings were performed with Orange G and Fast Green. Finally, sections were dehydrated with ethanol (95% and 100%) and cleaned in xylene before mounting in Eukitt®. Stained sections were observed under a Jenaval light microscope provided with a DeltaPix Invenio 3S 3M Pixel CMOS Camera and DeltaPix ViewerLE Software.

# CHAPTER 2

## Re-growth, morphogenesis and differentiation during starfish arm regeneration

Ben Khadra Yousra, Ferrario Cinzia, Di Benedetto Cristiano, Said Khaled, Bonasoro Francesco, Candia Carnevali Maria Daniela, Sugni Michela

Wound Repair and Regeneration (2015). 23: 623-634. doi: 10.1111/wrr.12336.

***Abstract***

The red starfish *Echinaster sepositus* is an excellent model for studying arm regeneration processes following traumatic amputation. The initial repair phase was described in a previous paper in terms of the early cicatrisation phenomena, and tissue and cell involvement. In this work, we attempt to provide a further comprehensive description of the later regenerative stages in this species. Here, we present the results of a detailed microscopic and submicroscopic investigation of the long regenerative phase, which can be subdivided into two sub-phases: early and advanced regenerative phases. The early regenerative phase (1-6 weeks p.a.) is characterised by tissue rearrangement, morphogenetic processes and initial differentiation events (mainly neurogenesis and skeletogenesis). The advanced regenerative phase (after 6 weeks p.a.) is characterised by further differentiation processes (early myogenesis), and obvious morphogenesis and re-growth of the regenerate. As in other starfish, the regenerative process in *E. sepositus* is relatively slow in comparison with that of crinoids and many ophiuroids, which is usually interpreted as resulting mainly on the basis from size-related aspects and of the more conspicuous involvement of morphallactic processes. Light and electron microscopy analyses suggest that some of the amputated structures, such as muscles, are not able to replace their missing parts by directly re-growing them from the remaining tissues, whereas others tissues, such as the skeleton and radial nerve cord, appear to undergo direct re-growth. The overall process is in agreement with the distalisation-intercalation model proposed by Agata and co-workers (2007). Further experiments are needed to confirm this hypothesis.

## *1. Introduction*

Regeneration has been described at both cellular and tissue levels in adult individuals of all echinoderm classes (Moss *et al.*, 1998; Dolmatov and Ginanova, 2001; Dubois and Ameye, 2001; Candia Carnevali, 2006; Gorshkov *et al.*, 2009; Biressi *et al.*, 2010; Candia Carnevali and Burighel, 2010; García-Arrarás and Dolmatov, 2010; Hernroth *et al.*, 2010). An important point concerning all post-embryonic developmental processes, such as regeneration, is to understand the mechanisms allowing the cells of the developing structure to reform the ordered spatial pattern of differentiated tissues, at the correct place and at the right time, on the basis of positional information and morphogenetic gradients. According to Dubois and Ameye (2001), who studied starfish and sea urchin spine regeneration, during the regenerative events, the pattern of re-growth of missing parts depends on their total or partial removal: the regeneration of lost tissues is epimorphic, whereas the regenerative process of damaged tissues is morphallactic. It has been also documented that the process of regeneration changes according to the different tissue types. Dolmatov and Ginanova (2001) showed that both the intestine and aquapharyngeal complex in holothurians follow a developmental pattern similar to that of asexual reproduction, whereas regeneration of muscles and tube feet follows the same pattern observed during their embryogenic development.

Asteroids are characterised by their ability to completely regenerate arms lost after amputation: for this reason, they have been employed successfully as valuable experimental models for studies on regeneration exploring both morphological aspects (e.g. *Leptasterias hexactis* and *Asterias rubens*; Moss *et al.*, 1998; Dubois and Ameye, 2001) and molecular aspects (e.g. *Marthasterias glacialis*; Franco *et al.*, 2013). Similarly, *Echinaster sepositus* has been recently used as model species to investigate both microscopic anatomy (Ben Khadra *et al.*, 2015a) and molecular aspects (*homeobox* genes) of arm regeneration (Ben Khadra *et al.*, 2014).

As in most echinoderms, asteroid regenerative events include the following main steps: a repair phase, characterised by the first emergency reactions and the wound healing; an early regenerative phase, during which tissue reorganisation and first signs of tissue regenerative phenomena occur; an advanced regenerative phase, characterised by restoration and tissue re-growth with the formation of a new small regenerating arm consisting of the same structures of the adult arm (Candia Carnevali *et al.*, 1998; García-Arrarás and Dolmatov, 2010).

In a previous work (Ben Khadra *et al.*, 2015a) we studied the repair phase of *E. sepositus*, which lasts for one week after the traumatic amputation. This initial phase represents an important “preparation step” for the subsequent regenerative events involving the lost tissues. In the current work we go further by providing a comprehensive and detailed analysis of the following regenerative phases, focusing on the tissue and cellular aspects of growth, morphogenesis and differentiation, which will represent an indispensable morphological complement to the molecular investigations (Ben Khadra *et al.*, 2014).

## *2. Materials and Methods*

### *2.1. Ethics Statement*

All animal manipulations were performed according to the Italian law, *i.e.* no specific permits were required for the described studies since starfish are invertebrates. *Echinaster sepositus* is not an endangered or protected species. All efforts were made to minimise the animal suffering during experimental procedures. The specimens were released into their natural environment once the experimental procedures were completed.

### *2.2. Animal sampling and regeneration tests*

Adult (diameter ~ 12 cm) specimens of *Echinaster sepositus* were collected by scuba divers at depth of 5-8 m from the Marine Protected Area of Portofino (Paraggi, Ligurian Sea, Italy) between November 2012 and April 2013. They were left to acclimatise for two weeks and maintained at 18°C in aerated aquaria filled with artificial sea water (ASW; Instant Ocean, 37‰) for the whole experimental period. Chemical-physical sea water parameters were checked daily (temperature and salinity) or weekly (concentrations of nitrites, nitrates, Ca, Mg, $PO_4$ and pH) and promptly adjusted if necessary. Specimens were fed with small pieces of cuttlefish twice a week. Traumatic amputation of the distal third of one arm for each specimen was performed by scalpel. Animals were then left to regenerate in the aquaria for pre-determined periods. The regeneration pattern was monitored at 1, 3, 6, 10 and 16 week(s) post-amputation (p.a.). Four-six samples/individuals were analysed for each stage. Regenerating arm tissues were removed including about 1 cm of the stump and were subsequently processed for the different microscopic analyses.

### *2.3. Microscopic analyses*

Regenerating tissues collected at different time points were analysed by different microscopy techniques (light and electron, see below). Samples were initially observed and photographed under a LEICA MZ75 stereomicroscope provided with a Leica EC3 Camera and Leica Application Suite LAS EZ Software (Version 1.8.0).

#### *2.3.1. Light microscopy (LM)*

Both thick (paraffin) and semi-thin (resin) sections were prepared. Briefly, for thick sections three samples per stage were fixed in Bouin's fluid for about one month to allow decalcification, washed in tap water, dehydrated in an increasing ethanol series, cleared with xylene, washed in xylene:paraffin wax solution (1:1) and embedded in paraffin wax (56°-58°C). Sagittal (longitudinal-vertical) sections (5-7 µm) were cut and stained according to Milligan's trichrome technique (Milligan, 1946). For resin sections, three samples per stage were fixed in SPAFG fixative (3% glutaraldehyde, 1% para-formaldehyde, 7.5% picric acid saturated solution, 0.45 M sucrose, 70 mM cacodylate buffer) for one month to allow decalcification, washed in 0.15 M cacodylate buffer and post-fixed in 1% osmium tetroxide in the same buffer for 2 hours. Samples were rapidly washed in distilled water and then in 1% uranyl acetate in 25% ethanol (2 hours), dehydrated in an ethanol series, cleared in propylene oxide, washed in propylene oxide:Epon 812-Araldite solution (3:1 for 1 hour, 1:1 for 1 hour, 1:3 for 1 hour and 100% resin overnight) and embedded in Epon 812-Araldite. Samples were longitudinally sectioned using a Reichert Ultracut E with glass knives. The semi-thin (1 µm) sections were stained with crystal violet and basic fuchsin. Thick and semi-thin sections were observed under a Jenaval light microscope provided with a DeltaPix Invenio 3S 3M CMOS Camera and DeltaPix Viewer LE Software.

#### *2.3.2. Scanning electron microscopy (SEM)*

The regenerating samples were fixed in scanning electron microscopy (SEM) A fixative (85% ASW and 2% glutaraldehyde) for 2 hours at 4°C and left in ASW overnight at the same temperature. Samples were post-fixed in SEM C fixative (36‰ ASW with 940 mOsM glucose and 2% osmium tetroxide) for 2 hours and subsequently washed with $dH_2O$ to remove all traces of osmium. Afterwards, dehydration with an ethanol series was performed. Samples were transferred to a series of solutions of HMDS

(Hexamethyldisilazane) in absolute ethanol in different proportions (1:3, 1:1, 3:1 and 100% HMDS).

After sagittal sectioning, the remaining paraffin embedded half-samples were also used for SEM analyses. Samples were washed several times with xylene for five days in order to completely remove the paraffin wax. Then they were washed in absolute ethanol and subsequently in HMDS and ethanol (in the proportions: 1:3, 1:1, 3:1) for 15 minutes each wash, and then washed 3 times in 100% HMDS for 15 minutes. Finally, all the processed samples were mounted on stubs, covered by a thin layer of pure gold (Sputter Coater Nanotech) and observed under a scanning electron microscope (LEO-1430).

*2.3.3. Transmission electron microscopy (TEM)*

For transmission electron microscopy (TEM) analyses the same samples employed for semi-thin sections were cut sagittally with glass knives using the same Reichert Ultracut E. The thin sections (0.07-0.1 µm) were collected on copper grids, stained with uranyl acetate followed by lead citrate and finally carbon coated with an EMITECH K400X Carbon Coater. The thin sections were observed and photographed using a Jeol 100SX transmission electron microscope.

## *3. Results*

The regenerative phase was preceded by a repair phase lasting 72 hours, which was deeply described in a recent paper (Ben Khadra *et al.*, 2015a). Here, we provide a brief description of the 72 hours p.a. regenerating arm-tip morphology which represents the "background" of the subsequent regenerative events described in the present manuscript. At the end of the repair phase (72 hours p.a.), the arm-tip was completely closed over by a rather thick and differentiated epithelium, showing most the typical cell types (including epidermal cells and underlying basiepithelial nervous plexus). Beneath this latter an initial accumulation of scattered heterogeneous cytotypes occurred: these were mainly phagocytes and dedifferentiating myocytes intermixed with new fibrils of collagen, overall forming an oedematous area. The radial nerve cord (RNC) was similarly healed (Fig. 1) (see Ben Khadra *et al.*, 2015a).

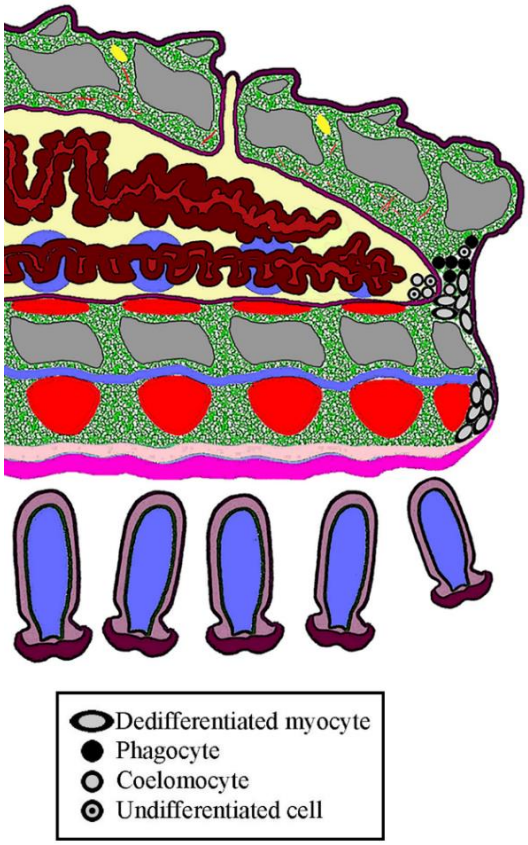


**Fig. 1.** *Diagram summarising the main morphological characteristics of E. sepositus arm-tip at the end of the repair phase (72 hours p.a.)*: Thick epithelium and oedematous area formation: pool of various cells (myocytes, phagocytes, etc.) intermixed with newly deposited collagen fibrils.

### *3.1. Early regenerative phase*

#### *3.1.1. 1 w p.a.: first sign of re-growth*

One week after traumatic amputation, the newly formed epidermis was thick and well organised (Fig. 2A, B). As already observed after 72 hours p.a. (Ben Khadra *et al.*, 2015a), the supporting cells were elongated and partly differentiated, bearing microvilli and cilia. The connective tissue underlying the wound epidermis was relatively well developed. Cellular elements, including morphologically undifferentiated cells, phagocytes and dedifferentiated myocytes, increased in number in comparison to the previous stage and were intermixed with new collagen fibrils (72 hours p.a.) (Fig. 2C; 3A, B, C, D). In some cases, a single dedifferentiating contractile apparatus (SLS: “spindle-like” structure) was observed in phagosomes (Fig. 3C, D). Large numbers of these different cell types appeared to migrate from the aboral and the oral body walls, the coelom, the nervous system and the tube feet towards the wound area (Fig. 2D, E). All these changes resulted in the oedematous area (Fig. 2) acquiring at one week both the structure and function of a fibrous cicatricial tissue (Fig. 2E).

Seven days p.a. could be considered as a separate time point in the regenerative process from which the early processes of outgrowth and differentiation started, the main changes involving the coelomic canals, the RNC and the endoskeleton. Indeed, the perivisceral coelom with its newly formed mesothelial lining (CE) started re-growing after the complete fusion of the aboral and oral body wall edges. The somatic zone of the RNC also showed first signs of regeneration. The regenerating nerve portion was composed mainly of scattered and intermixed supporting cell elements. These latter were acquiring their typical bipolar shape, producing two opposite thin cytoplasmic extensions, in which regenerating intermediate filament bundles were already visible. These cell extensions produced a series of “niches”, which started to be colonised by interspersed neurons (Fig. 3E). The apical features of the neuroepithelium were not completely differentiated: in particular cilia, microvilli and cell junctions were not visible yet and the hyaline layer consisted only of a faint fuzzy material (Fig. 3F).

At this same stage, the early signs of skeletogenesis were evident: initial mineral deposits of calcium carbonate in the form of primary plates could be detected within the new collagen network which was progressively forming in close bundles filling the former oedematous area (Fig. 2F).

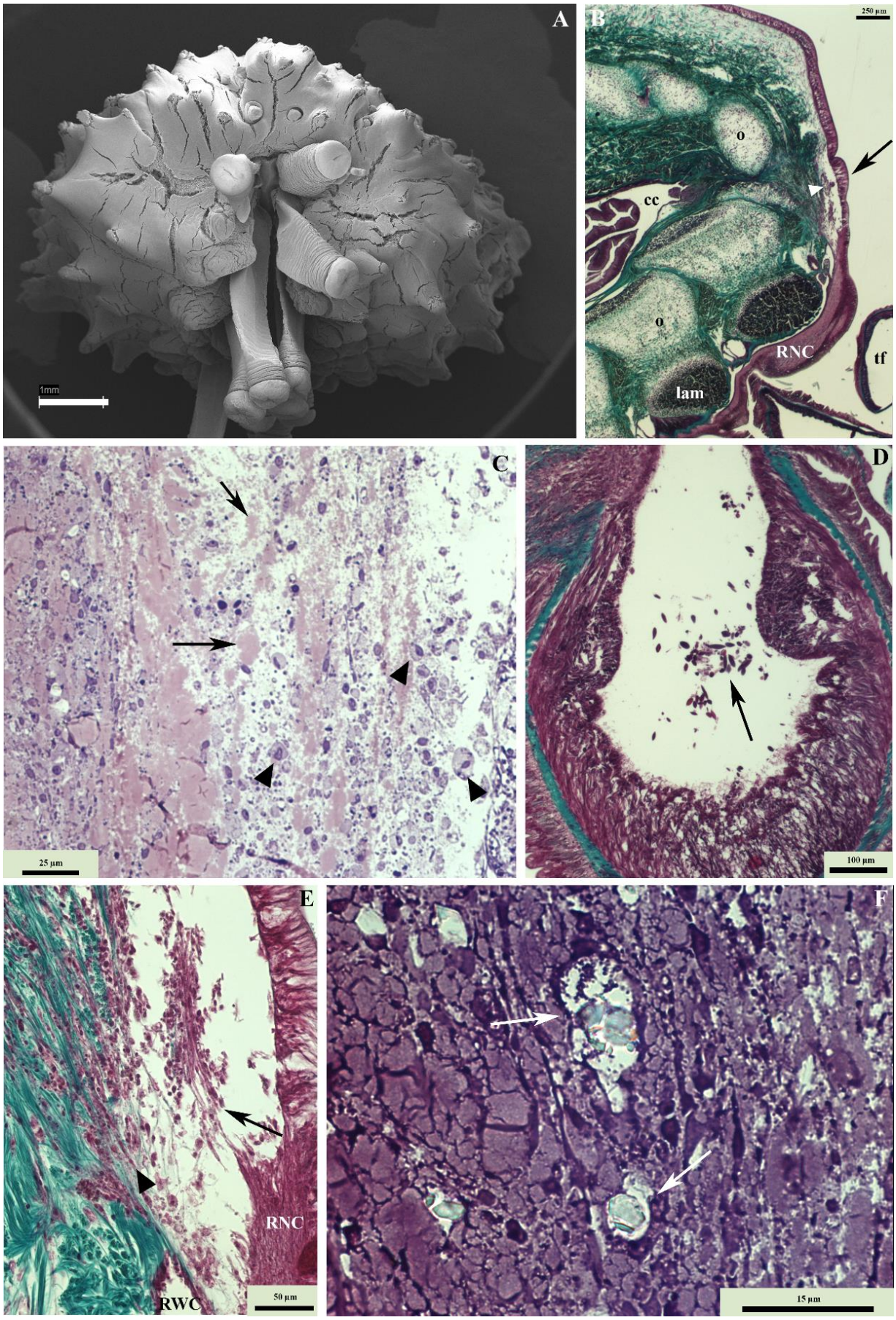


**Fig. 2.** *First sign of re-growth (1 w p.a.)*. A) (SEM photo) A front view of the regenerating sample showing the complete re-epithelialisation of the injured area. B) (Light microscopy

◀ (LM)) The newly formed epidermis is thick and well organised (arrow) and the connective tissue underlying the wound epidermis is relatively well developed (arrowhead). C) (LM) Cellular elements (arrowheads) found behind the wound epidermis intermixed with new collagen fibrils (arrows). D) (LM) Dedifferentiating myocytes migrating from the stump tube foot towards the wound area (arrow). E) (LM; a detail of B) The one week oedematous area has a fibrous cicatricial tissue structure. Large numbers of different cell types appear to migrate from the water vascular system (RWC) (arrowhead) and the nervous system (RNC; arrow). F) (LM) Early signs of skeletogenesis: first mineral deposits of calcium carbonate in form of primary plates (arrows). *Abbreviations*: cc-coelomic cavity, lam-lower transverse ambulacral muscle, o-ossicle, RNC-radial nerve cord, RWC-radial water canal, tf-tube foot.

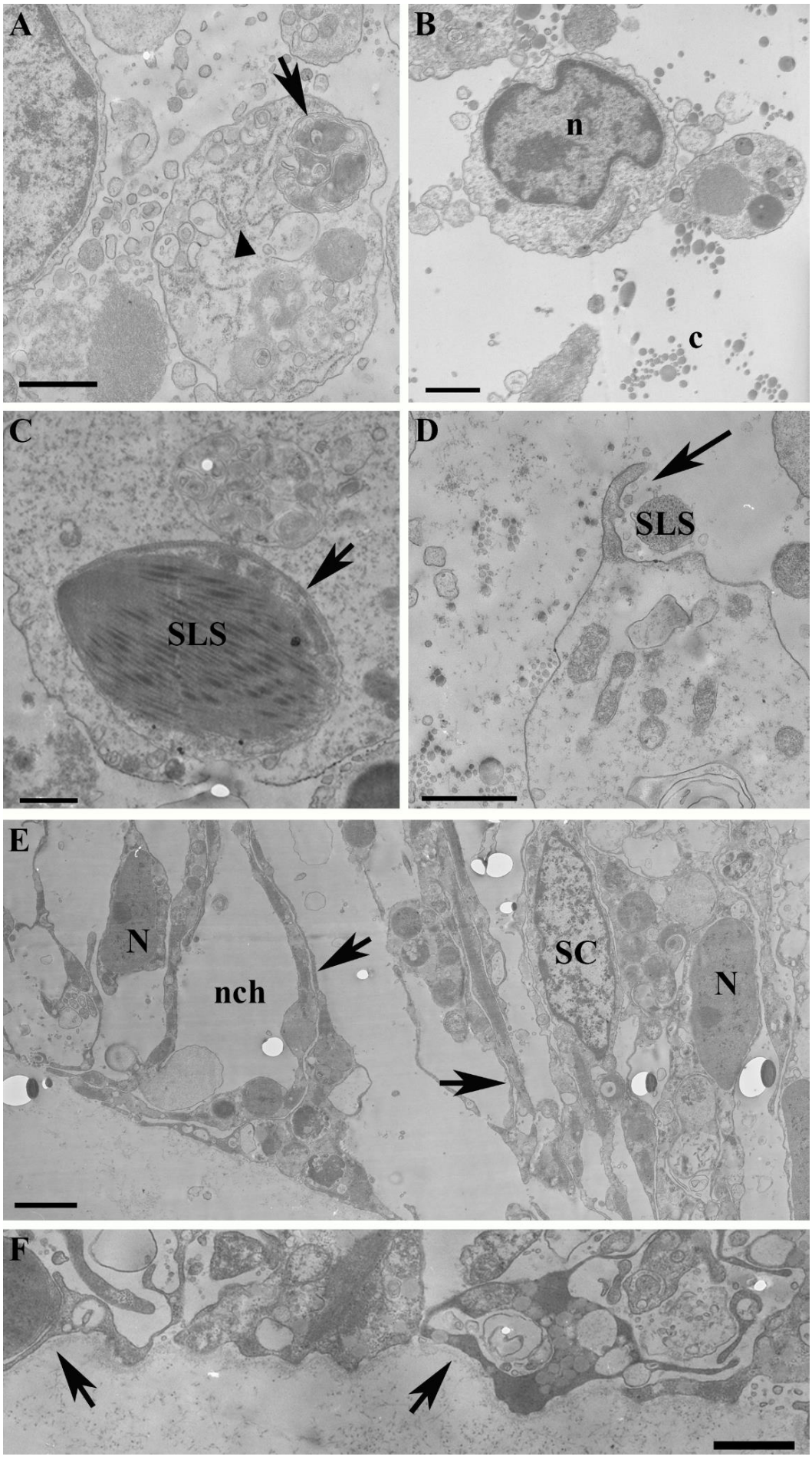
A
B
n
c
C
SLS
D
SLS
E
N
nch
SC
N
F

◀ **Fig. 3.** *TEM micrographs of migrating cells and neurogenesis (1 w p.a.).* A) A phagocyte with obvious phagosome (arrow) and RER (arrowhead). B) A presumptive undifferentiated cell with big nucleus (n). C) Single dedifferentiating contractile apparatus (SLSs) in phagosome (arrow). D) Beginning of phagocytosis of a single dedifferentiating contractile apparatus by a phagocyte (arrow). E) Regenerating nerve composed mainly of scattered supporting cell elements (SC) acquiring their typical bipolar shape in which regenerating intermediate filament bundles (arrows) are visible. “Niches” (nch) start to be colonised by interspersed neurons (N). F) A faint fuzzy material (arrows) of the apical part of the neuroepithelium. *Abbreviations*: c-collagen fibrils, n-nucleus, N-neuron, nch-niche, RER-rough endoplasmic reticulum, SC-supporting cell, SLSs-spindle-like structures. Scale bars: 1 µm (A, B, C, D, F); 2 µm (E).

*3.1.2. 3 w p.a.: the regenerate appearance*

Three weeks after amputation a small regenerate appeared (~ 1.2 mm in length; Fig. 4A, B). It was covered by an epidermis similar to that described above; although the inner stroma of connective tissue looked less compact and less organised in comparison with that of the stump, its collagen fibres appeared to be more oriented, forming a transverse meshwork. Inside the regenerate the developing ossicles were more differentiated. The mineralised part of the ossicles, the stereom, now formed a three dimensional meshwork of trabeculae. The radial water canal, which appeared to be more inflated, started regenerating the terminal tube foot (Fig. 4C, D).

During this phase, tissues demonstrated an evident overlapping of both recycling and differentiation processes. In addition to the flow of cells to the growth area, the first pair of tube feet showed a massive release of cells from their inner coelomic wall to the lumen (Fig. 4E, F). Also the most distal uninjured muscle bundles displayed evident rearrangement processes (Fig. 4G).

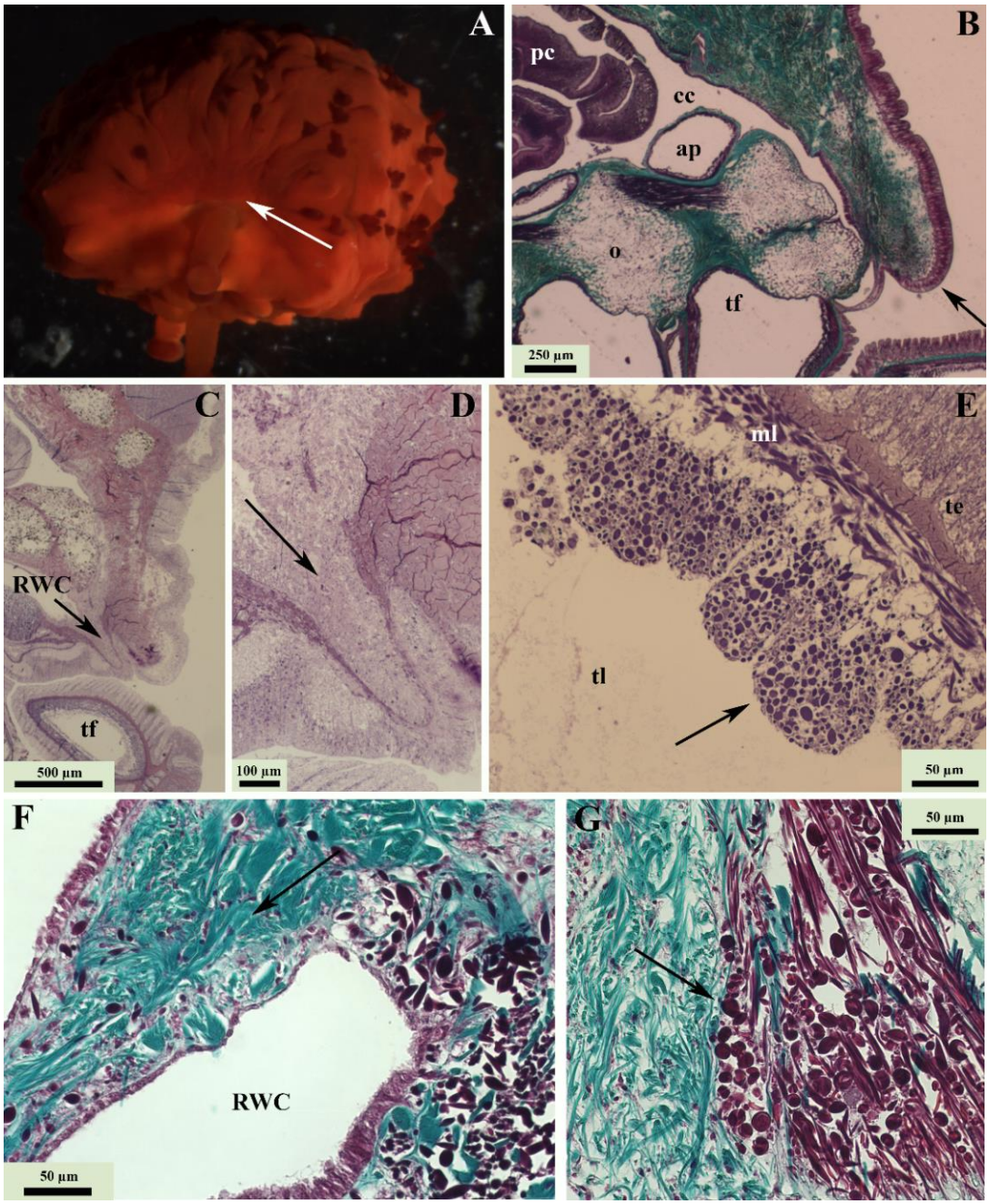


**Fig. 4.** *Appearance of the regenerate (3 w p.a.).* A) (stereomicroscopy (SM) view) and B) (LM) A regenerate measuring about 1.2 mm in length (arrows). C) and D) (a detail of C) (LM) The radial water canal (RWC) is regenerating the terminal tube foot (arrows). E) (LM) Massive release of dedifferentiating myocytes from the inner coelomic wall of the stump tube foot to its lumen (arrow). F) (LM) Flow of dedifferentiating myocytes to the growth area (arrow). G) (LM) Uninjured muscle rearrangement (arrow). *Abbreviations*: ap-ampulla, cc-coelomic cavity, ml-myoepithelial layer, o-ossicle, pc-pyloric caeca, RWC-radial water canal, te-tube foot epidermis, tf-tube foot, tl-tube foot lumen.

### *3.2. Advanced regenerative phase*

*3.2.1. 6 w p.a.: myogenesis and tube feet morphogenesis*

A new arm-tip measuring about 1.5 mm in length was clearly visible at 6 w p.a. (Fig. 5A, B). New mucous glands were present in the form of invaginations of the epidermis (Fig.

5C), under which small spines also started to develop. The stereom of the new skeletal structures (spines and ossicles) became more differentiated. The lateral processes from adjacent trabeculae tended to fuse together giving rise to the typical three-dimensional meshwork of the stereom structure. TEM analyses at this skeletogenetic stage showed a number of cells of different types in the newly formed organic stroma: putative fibroblasts *(collagen-making cells),* scleroblasts *(skeleton-making cells)* and phagocytes (Fig. 6A). The *collagen-making cells* were distinguished by the presence of “multilamellar vesicles” in their cytoplasm and of two nucleoli in their nucleus (Fig. 6A, B). Some of the presumptive phagocytes had a cilium at one pole (Fig. 6C). The *skeleton-making cells* were distinguished by their cytoplasm containing a well-developed and swollen Golgi complex, with associated vesicles, RER and other organelles. They were easily recognisable by their “calcification” vacuoles, at this stage containing only amorphous material, where calcite would be subsequently deposited (Fig. 6A, C, D). In the regenerating ossicles the new collagen exhibited transverse and longitudinal bundles and contained developing spicules enveloped by several cell processes (Fig. 6A).

First signs of myogenesis related to the lower transverse ambulacral muscles were clearly visible: they appeared as single transversal bundles of myocytes localised above the RNC (Fig. 5D). Additionally, scattered myocytes could be detected among the developing ossicles (Fig. 5E). Similarly, the longitudinal and circular muscles supporting the new CE were reorganising and regenerating, although the overall architecture of this layer (especially the circular muscles) was still incomplete and far from being definitely organised. The myocytes composing this reforming circular layer apparently derived from the CE (Fig. 5F). The regenerated epidermis and the newly formed aboral CE were furrowed.

The unpaired terminal tube foot is now well developed and protruded axially. The optic cushion started to differentiate the first pigment-cup ocelli. Six weeks p.a., new tube feet (about four pairs) were visible in the regenerate, showing proximal-distal differentiation levels (Fig. 5B). The most proximal portion included small ampullae, in which an inner and an outer coelomic lining, separated by a middle layer of connective tissue, were easily recognisable.

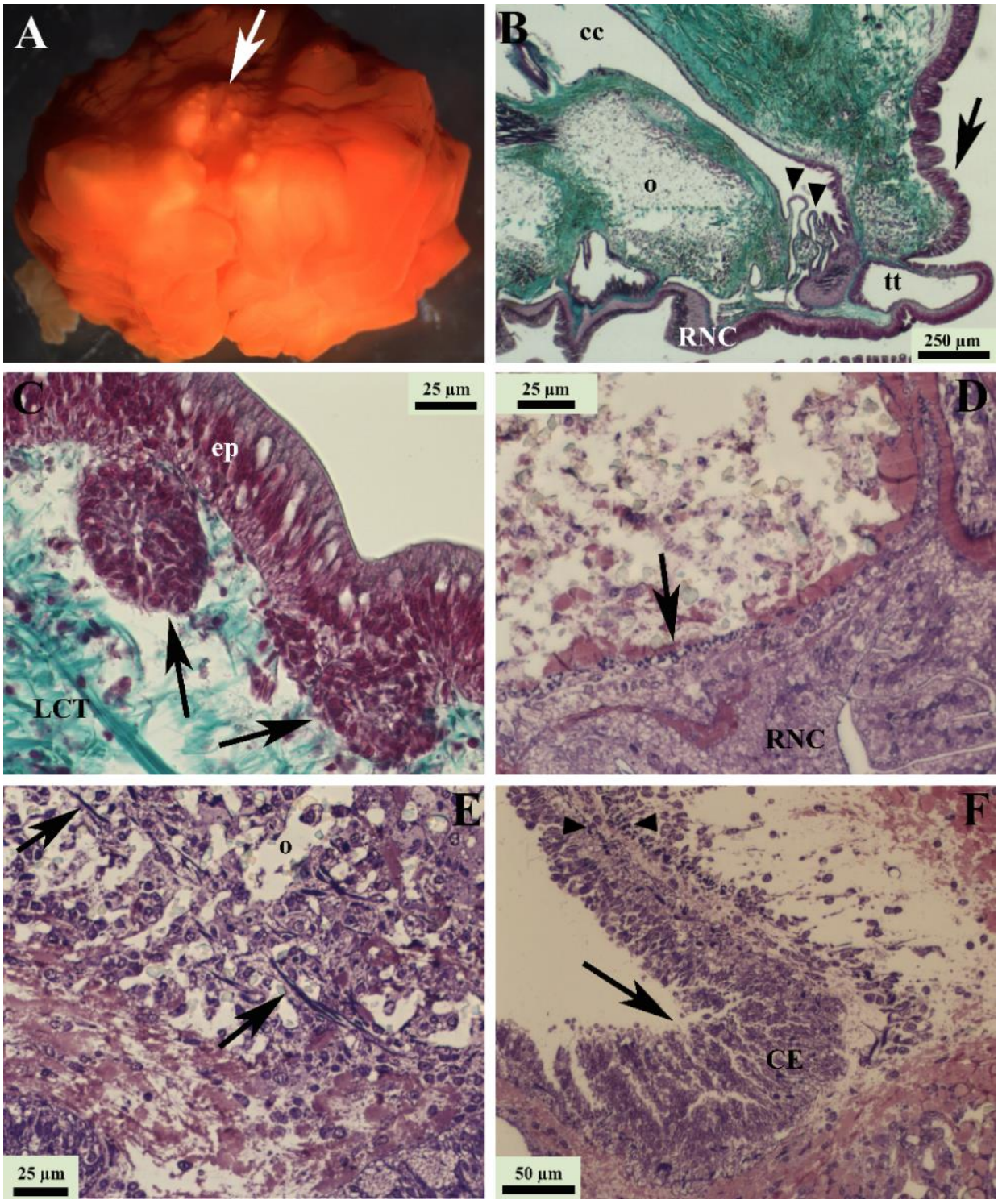


**Fig. 5.** *Myogenesis and tube foot morphogenesis (6 w p.a.).* A) (SM view) and B) (LM) A clearly visible new arm-tip (arrows). The terminal tube foot (tt) is well developed. New tube feet (about four pairs) showing proximal-distal differentiation levels are visible in the regenerate (arrowheads). C) (LM) New mucous glands forming as invaginations of the epidermis (arrows). D) (LM) First signs of myogenesis related to the lower transverse ambulacral muscle (arrow). E) (LM) Scattered myocytes detected among the developing ossicles (arrows). F) (LM) The newly formed aboral CE is furrowed (arrow) and its longitudinal and circular muscles are regenerating progressively (arrowheads). *Abbreviations*: cc-coelomic cavity, CE-coelomic epithelium, ep-epidermis, LCT-loose connective tissue, o-ossicle, RNC-radial nerve cord, tt-terminal tube foot.

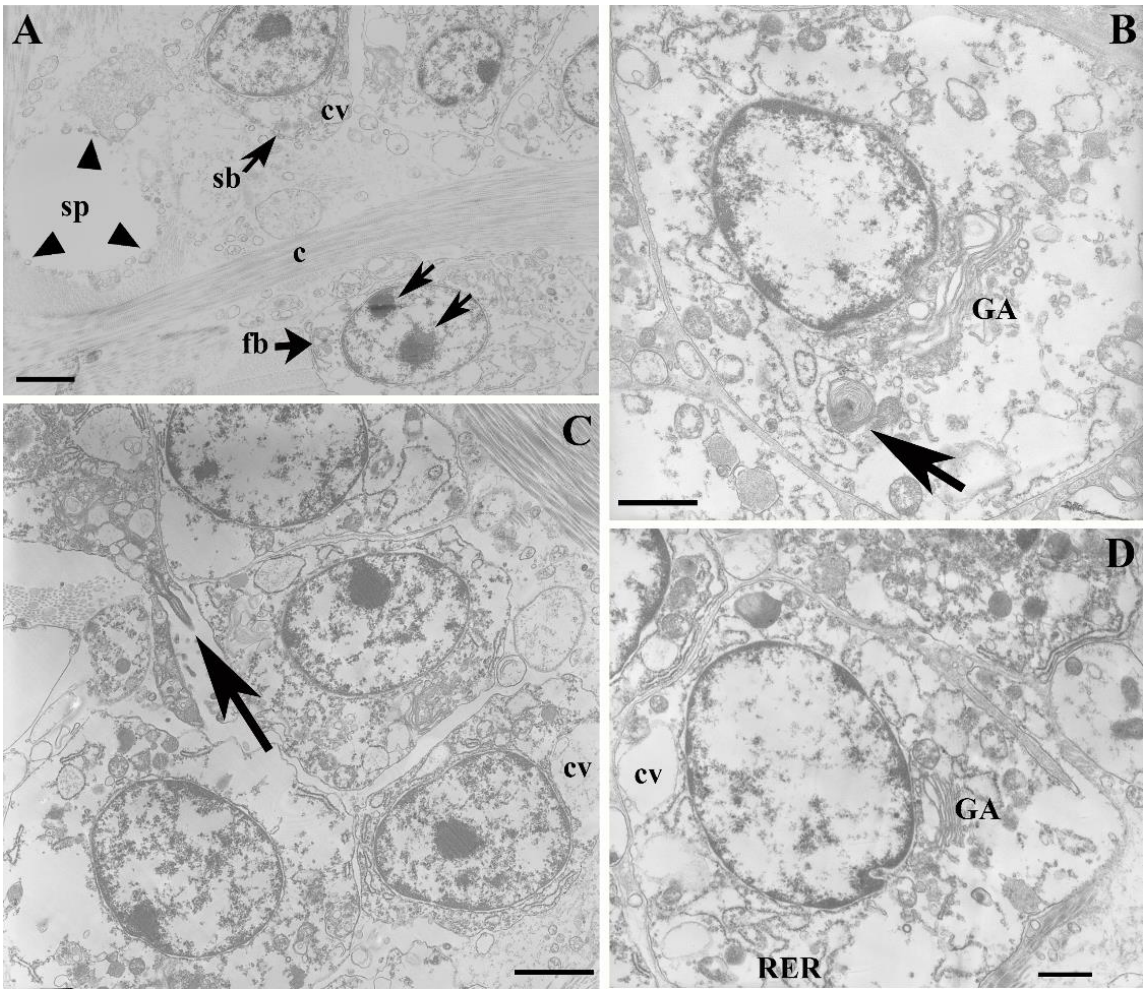


**Fig. 6.** *TEM micrographs of skeletogenesis (6 w p.a.).* A) A micrograph of the newly formed organic stroma showing putative fibroblast (fb) with two nucleoli (arrows) and scleroblast (sb) with calcification vacuole (CV), well-organised new collagen (c) and developing spicule (sp) which are enveloped by several cell processes (arrowheads). B) Detail of a collagen-making cell (fb) distinguished by the presence of "multilamellar vesicles" (arrow) and evident Golgi apparatus (GA) in its cytoplasm. C) Presumptive phagocyte with a cilium at one pole (arrow) present in the newly formed stroma. D) Detail of a skeleton-making cell (sb) which is easily recognisable by its cytoplasm containing calcification vacuoles (cv), GA and RER. *Abbreviations*: c-collagen fibrils, cv-calcification vacuole, fb-fibroblast, GA-Golgi apparatus, RER-rough endoplasmic reticulum, sb-scleroblast, sp-spicule. Scale bars: 1 μm (A, B, D); 2 μm (C).

*3.2.2. 10 w p.a.: complete restoration of the missing parts*

At this time point the regenerating tip was about 1.7 mm in length (Fig. 7A, B). The regenerative process was substantially completed: indeed, all the missing parts were restored, although still smaller in size (Fig. 7B). The new aboral and oral ossicles and spines were well developed and organised (Fig. 7B, C). The progressive development of the major muscle bundles continued, showing an increase in fibre number and size. In the TEM, each muscle bundle appeared to be composed of several tightly packed myocytes with large circular nuclei. In most cases the newly formed myofilaments were

already well arranged in ordered contractile fields distributed in the peripheral regions of the fibres (Fig. 7D). Developing muscles were not yet observed in the articulations between the new aboral ossicles. The tube feet (about six pairs), with well-differentiated ampulla and podium components, still lacked terminal suckers (Fig. 7B).

The newly regenerated segment of the radial nerve cord (RNC) gradually acquired all its components, namely a clearly recognisable optic cushion provided with several well-differentiated pigment-cup ocelli (Fig. 7E). The neural elements and the supporting cells of the regenerated part acquired their definitive shape and organisation and became indistinguishable from those of the uninjured radial nerve.

A characteristic oedematous area was visible just behind the folded distal CE (Fig. 7B). This area contained different cell types (differentiating myocytes, nervous processes, and ciliated cells) intermixed with collagen fibrils (Fig. 7F).

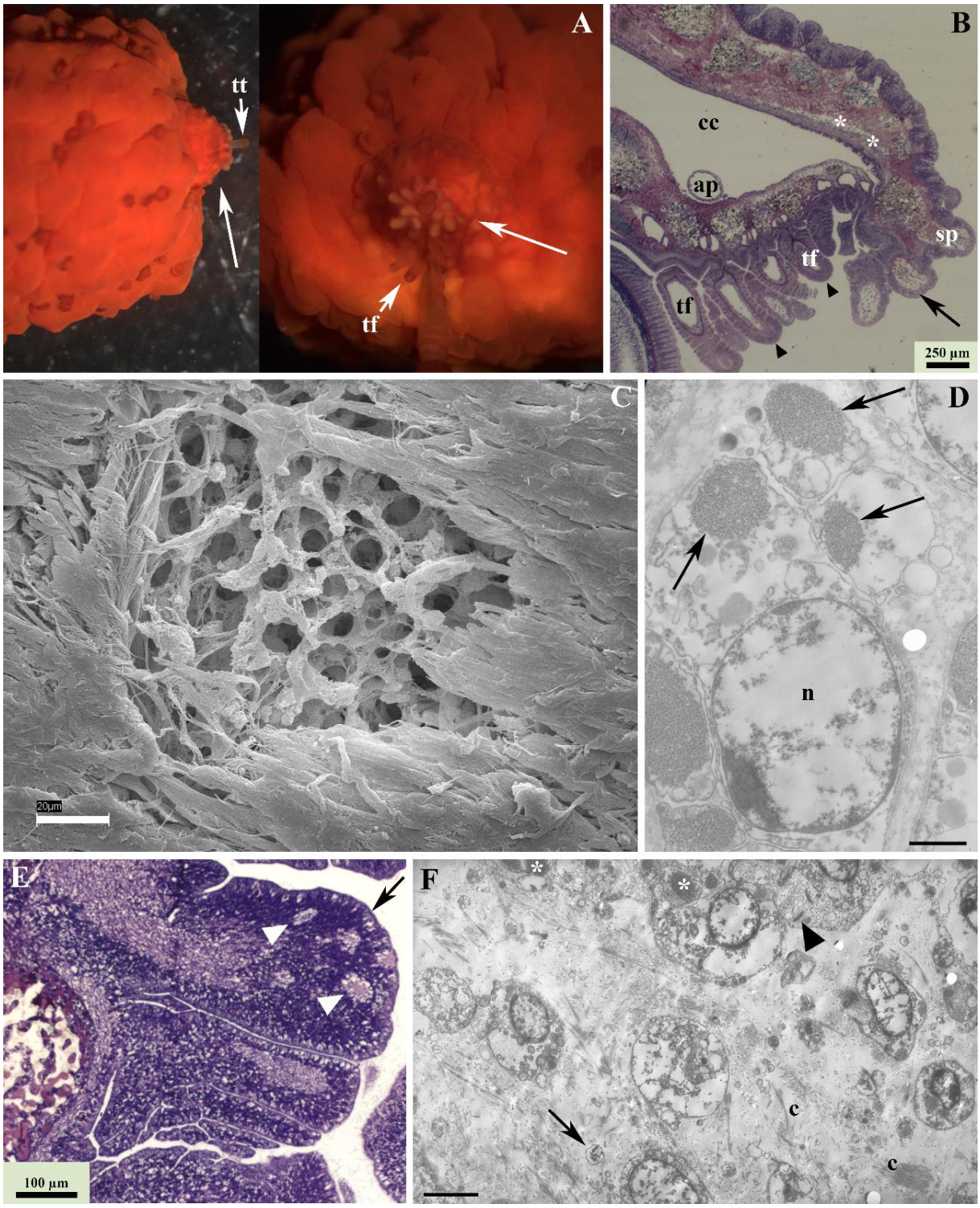


**Fig. 7.** *Complete restoration of the missing parts (10 w p.a.).* A) (SM view) A top view (left) and a front view (right) of the regenerate (arrows) showing the terminal tube foot (tt) and new tube feet (tf). B) (LM) Restoration of all the missing parts. Spines are well developed (arrow). The tube feet are well differentiated but still lack final suckers (arrowheads). An oedematous area is visible just behind the folded distal CE (asterisks). C) (SEM micrograph) A well-developed and organised new ossicle. D) (TEM micrograph) New myocytes with large circular nucleus (n) and newly formed myofilaments (arrows). E) (LM) A clearly recognisable optic cushion (arrow) provided with several well-differentiated pigment-cup ocelli (arrowheads). F) (TEM micrograph) A detail of the oedematous area just behind the folded distal CE: different cell types (differentiating

◀ myocytes (asterisks), nervous processes (arrow), and ciliated cells (arrowhead)) are intermixed with collagen fibrils (c). *Abbreviations and symbols*: ap-ampulla, c-collagen fibrils, cc-coelomic cavity, CE-coelomic epithelium, n-nucleus, sp-spine, tf-tube foot, tt-terminal tube foot, *-oedematous area (B), differentiating myocytes (F). Scale bars: 1 μm (D); 4 μm (F).

*3.2.3. 16 w p.a.: a minuscule arm*

The new arm-tip, measuring about 3 mm in length, was well differentiated and actually resembled a miniature arm, showing all the typical features of the normal arm (Fig. 8A, B). It had a terminal tube foot complete with a fully differentiated optic cushion. At least eight pairs of new tube feet were present, the most proximal pair showing developing suckers. Numerous dermal mucous glands and well-differentiated spines were present. The upper transverse ambulacral muscles and the muscle bundles joining the aboral ossicles were also developed (Fig. 8C). Although the pyloric caeca had healed, they did not extend into the coelomic cavity of the regenerate. No papulae were detectable at this stage of regeneration.


**Fig. 8.** *Regenerating arm (16 w p.a.).* A) (SM view) Front view of the regenerate measuring about 3 mm in length with complete terminal tube foot (tt) and at least six pairs of new tube feet (tf). B) (LM) Regenerate with a complete terminal tube foot (tt) and a fully differentiated optic cushion (oc). Mucous glands (arrowhead) are well differentiated. C) (LM) The lower transverse ambulacral muscles (lam) are well developed. *Abbreviations*: cc-coelomic cavity, lam-lower transverse ambulacral muscle, o-ossicle, oc-optic cushion, RNC-radial nerve cord, RWC-radial water canal, tf-tube foot, tt-terminal tube foot.

### *3.3. Rate of arm-tip regeneration*

No arm-tip was visible at 1 w p.a.; the first sign of a measurable regenerate (about 1.2 mm in length) appeared after 3 weeks p.a. Arm growth was fast during the early regenerative phase (0.32 mm/week), then it decreased regularly in the advanced regenerative phase (0.13 mm/week). The overall rate of arm-tip regeneration was about 0.2 mm/week. The lost arm could be replaced completely in about two or three years in captivity (personal observations).

To standardise for size/age effect, the measured lengths (mm) of the regenerating arm (starting from the amputation plane) were expressed as a proportion of the corresponding diameters (mm) of arm stumps measured from the top (aboral) to the base (oral), at about 1 cm far from the amputation plane of each arm, excluding the tube foot length. The normalised values are plotted against time in Fig. 9. A logarithmic curve was the best model to describe the relationship ($R^2 = 0.9796$).

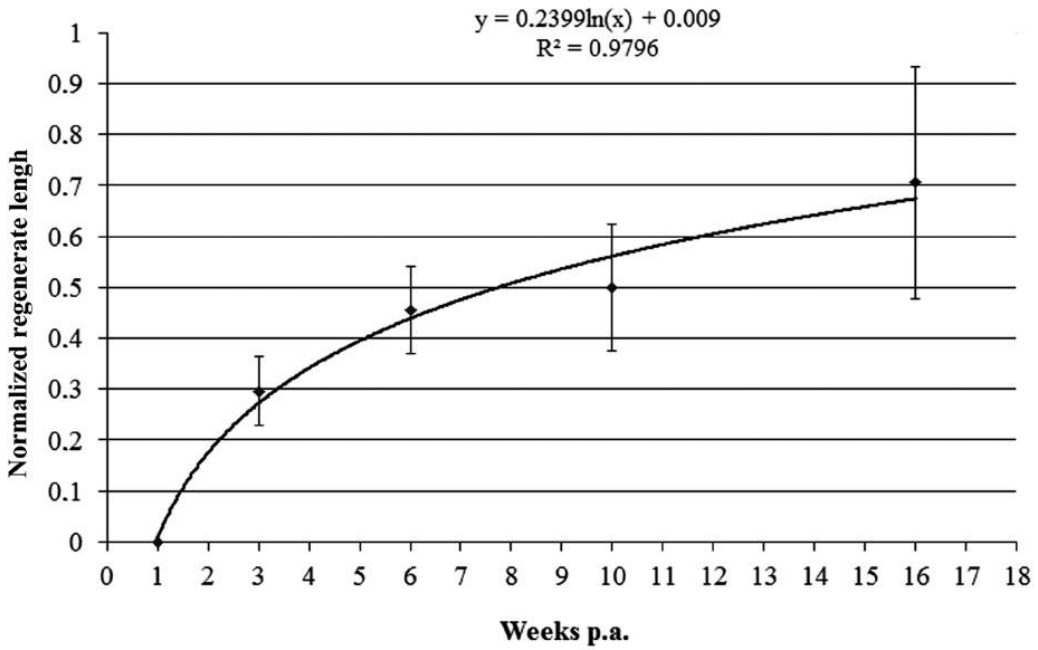


**Fig. 9.** *Time course of arm regeneration in E. sepositus.* The regenerate length is expressed as a proportion of the stump diameter. N (number of samples for each time point) = 4. Bar = mean + SD.

## *4. Discussion*

### *4.1. Regenerative phase*

The regenerative phase is the core of the regeneration process and, due to its complexity and duration, can be subdivided into early and advanced sub-phases. During the early sub-phase, the connective tissue develops at the wound site and the first calcitic skeletal

deposits are observed. The oedematous area is still evident at this stage, possibly playing a “structural” role related to the defensive function typical of the repair phase (Ben Khadra *et al.*, 2015a). Obvious cell migrations involving different cytotypes are directed to this region where the regeneration of the new tissues eventually takes place. The 1 w p.a. oedematous area is therefore an active “growth area”. This is in agreement with observations of Mladenov and co-workers (1989) who suggested that (i) the new structures are formed between the wound epidermis and the stump (in the growth area), and (ii) the radial water canal and the radial nerve cord (the only two continuous structures along the arm) are restored by outgrowth from the remains of these structures in the stump. According to Dubois and Ameye (2001) this second mechanism is similar to the developmental process during asexual reproduction which requires remaining parts of the tissues (stump); on the other hand, the *ex-novo* restoration of the lost structures, such as ossicles, muscles and tube feet, may resemble their developmental processes during embryogenesis.

*4.1.1. Skeletogenesis*

In *E. sepositus* regeneration of lost skeletal ossicles can be divided into two stages, the first (1 week p.a.) characterised by initial mineral deposits and the second characterised by stereom meshwork formation and growth. At 6 weeks p.a. TEM analyses have revealed that new ossicle formation in this starfish occurs in a manner similar to the sea urchin larval spicule (Okazaki, 1960) and primary tooth plate formation (Chen and Lawrence, 1986) and to spicule formation in holothurians (Sticker, 1985). As described in these models, skeleton formation begins with the aggregation of a population of more or less differentiated cells, including sclerocytes: these latter have one or more vacuoles where organic matrix is deposited. This initially intracellular spicule formation becomes then extracellular while the calcite crystal grows. In *A. rubens* Dubois and Jangoux (1990) reported that spicule formation might be initiated both intracellularly (lost skeleton) or extracellularly (damaged skeleton).

TEM examination at the level of the stroma in 6 weeks p.a. regenerating ossicles revealed the presence of many fibrocytes close to scleroblasts. These cells produce collagen, glycosaminoglycans and other glycoproteins usually found in the extracellular matrix. It has been demonstrated that some of these extracellular components are fundamental for normal spicule formation. Spicule development may be inhibited if the extracellular matrix lacks N-linked glycoproteins (Grant *et al.*, 1985) and inhibition of collagen formation

prevents normal spicule growth (Mintz and Lennarz, 1982; Blankenship and Benson, 1984). Hence, in addition to their role in stroma collagen formation, fibroblasts found in *E. sepositus* might also be involved in stereom construction.

The presence in the developing stereom of monociliated phagocytes is quite unusual, although previously described in *A. rubens* by Dubois and Ameye (2001). This feature further supports the hypothesis that phagocytes may derive from or share a common origin with coelomocytes.

### *4.1.2. Myogenesis*

Two different co-existing events have been observed in *E. sepositus* muscular tissues following arm amputation: dedifferentiation and differentiation. The former includes different mechanisms depending on the integrity of the muscular tissue. Standard tissue histolysis is observed at the level of injured muscles from the very first stages of the repair phase (Ben Khadra *et al.*, 2015a). A different mechanism occurs at the level of some intact muscle bundles far from the amputation site (such as the lower transverse ambulacral muscle or the myocytes composing the tube foot wall) and can be regarded as an “induced dedifferentiation”. This process becomes particularly active at 3 w p.a. in parallel with the remarkable growth of the regenerate. This observation supports the idea that these dedifferentiated myocytes, once reprogrammed, actively contribute to histogenesis and organogenesis of the regenerating structures (Candia Carnevali and Bonasoro, 2001a).

During myogenesis it is suggested that at the regeneration site some of the CE cells ingress, then they detach from the overlying epithelium and acquire the myocyte phenotype (Dolmatov and Ginanova, 2001; Franco *et al.*, 2013). This hypothesis is in agreement with what we observed in *E. sepositus* at 6 weeks p.a., where the longitudinal muscle layer of the stump CE apparently penetrates deeply into the underlying connective tissue of the regenerate giving rise to the new circular muscle layer. Similarly, during the regeneration of the somatic muscle of two holothurians (*Eupentacta fraudatrix* and *Apostichopus japonicus)* the basal regions of the coelomic epithelium detach from the surface epithelium to close up and form elongated tubular structures that eventually become new muscle bundles (Dolmatov *et al.*, 1995; Dolmatov *et al.*, 1996).

Moreover, it has been documented that myocytes do not undergo cell division once they have acquired their typical differentiated form (Dolmatov and Ginanova, 2001). According to the authors, each newly formed myocyte is derived from a new cell from the CE, which

retains the capacity to divide. This might explain the inability of *E. sepositus* to repair damaged muscles, which therefore necessitates the recycling and reformation of whole muscles.

However, there is no definitive evidence demonstrating that the origin of new myocytes is restricted only to CE elements. Dedifferentiated myocytes might also contribute directly to the development of new muscles as previously suggested for crinoids (Candia Carnevali and Bonasoro, 2001b).

### *4.1.3. Turnover zone*

After 6-10 weeks p.a. the CE at the level of the regenerating tip appears highly folded. In the underlying loose connective tissue a pool of scattered cells of various types is visible, including differentiating myocytes and phagocytes. Some of these cells might originate from the CE, as suggested for phagocytes, fibroblasts (Dubois and Ghyoot, 1995) and myocytes (Dolmatov and Ginanova, 2001). However, it cannot be excluded that this is a grouping zone of migratory cells coming from distant origins. Indeed, Hernroth and co-workers (2010) demonstrated that many cells are derived from distant tissues during arm regeneration in *A. rubens*, for example, from the pyloric caeca.

### *4.1.4. Neurogenesis*

Regeneration success in starfish depends on the presence of neurotrophic substances released by the nervous system, which acts as the primary source of regulatory factors, mitogens or morphogens (Huet, 1975; Huet and Franquinet, 1981; Dubois and Ameye, 2001; Thorndyke and Candia Carnevali, 2001; Thorndyke *et al.*, 2001). In *E. sepositus* within 72 hours p.a. the sub-epidermal nerve plexus is completely regenerated (Ben Khadra *et al.*, 2015a), whereas the RNC requires a slightly longer time: after a week p.a. the network of supporting cells with scattered neurons is visible. It has been demonstrated that neuron regeneration is guided by the radial glia cells which represent the main source of new cells in the regenerating radial nerve cord of echinoderms (Mashanov *et al.*, 2013). However, questions concerning the specific mechanisms of re-growth, such as the involvement of stem cells, dedifferentiation of local tissues or transdifferentiation in the regenerating nerve have not been fully investigated, especially in asteroids. There is some evidence suggesting that neurons in *A. rubens* are derived from locally dividing cells but it cannot be confirmed whether neurons are derived from proliferation or transdifferentiation of neuroepithelial cells, although the former mechanism is suggested

(Dubois and Ameye, 2001). In our study it was difficult to detect the origin of new neurons in the radial nerve from histological analyses alone.

### *4.2. Rate of regeneration*

As in other starfish, such as *A. rubens* and *L. hexactis* (Moss *et al.*, 1998; Dubois and Ameye, 2001), the regeneration process in *E. sepositus* is very slow in comparison with that of crinoids (Candia Carnevali and Burighel, 2010) and some ophiuroids (Biressi *et al.*, 2010): a tiny outgrowing regenerate appears only three weeks after traumatic amputation, whereas this can be seen after only 3 days in *A. mediterranea* (Candia Carnevali and Bonasoro, 2001b) or after 4 days in *A. filiformis* (Biressi *et al.*, 2010). Nevertheless, *E. sepositus* growth rate is slightly higher than that of some other larger ophiuroid species such as *Ophioderma longicaudum* (0.2 *vs* 0.17 mm/week, respectively; Biressi *et al.*, 2010). The marked differences from the crinoid *A. mediterranea* and the ophiuroid *A. filiformis* are often related to the prominent role of morphallactic processes during asteroid arm regeneration and to specimen size/age (Lawrence, 1992). Nevertheless, this is not always true as pointed out by Biressi and co-workers (2010) for ophiuroids. This concept appears valid also for asteroids in the present study: the regenerate appearance observed in *E. sepositus* (3 weeks) is comparable to that of smaller starfish like *L. hexactis* (Moss *et al.*, 1998). Overall, there is apparently an arm size threshold which affects growth rate: below this limit regeneration occurs very rapidly, whereas above it there is a high inter-specific variability. To avoid the effect of these factors, we chose *E. sepositus* adult specimens of similar size and we expressed the regenerate length as the ratio between its actual length and stump diameter. The use of this approach will certainly make easier future inter-specific comparison.

Environmental variables, such as food and physical factors *i.e.* salinity (Kaack and Pomory, 2011), temperature and pH, can affect the regeneration rate (Schram *et al.*, 2011; Clark and Souster, 2012). Nevertheless, these factors are not relevant to our experimental tests. Temperature, pH and salinity were regularly monitored and maintained constant, no hypoxia was detected and the food quality was never changed during the experimental period: all the starfish experienced the same experimental conditions.

Additionally, we noticed that specimens of *E. sepositus* apparently require little, if any, nourishment during the first two weeks of regeneration of their missing parts. The same observation has been reported for the starfish *Asterias vulgaris* (King, 1898) and *Heliaster*

*helianthus* (Barrios *et al.*, 2008): after the loss of the arm animals apparently allocate energy to the process of arm regeneration rather than to feeding activity.

### *4.3. Regenerative process in E. sepositus in relation to the old and new concepts of regeneration*

According to the classic definitions and concepts, regeneration can be classified as epimorphic or morphallactic depending on whether or not a localised blastema of proliferating progenitor cells is formed after wound healing (Agata *et al.*, 2007). A further distinctive element to be considered is the origin of cells involved in regeneration: are they undifferentiated or dedifferentiated/transdifferentiated elements? However, recent evidence indicated that these two mechanisms largely overlap and that in many cases both contribute to the overall regenerative process (Candia Carnevali and Burighel, 2010; Hernroth *et al.*, 2010).

According to classic principles the regeneration process of *E. sepositus* would be regarded as being mainly morphallactic because no distinct blastema is evident, even though a population of presumptive undifferentiated cells can be observed throughout the developing connective tissue below the wound epidermis. In agreement with our results, regeneration studies on various echinoderms report an initial accumulation, but not a proliferation, of coelomocytes beneath the wound epidermis (Moss *et al.*, 1998; Dubois and Ameye, 2001) and suggest that migrating coelomocytes are recruited for wound healing (Agata *et al.*, 2007; Hernroth *et al.*, 2010). In addition, the rearrangement of injured muscles immediately after amputation is considered a further characteristic morphallactic event. However, the old definitions of regenerative mechanisms are no longer adequate in the light of the present knowledge. Even one of the most studied models-planarian regeneration, has been described alternatively as an example of morphallaxis or epimorphosis (Agata *et al.*, 2007). According to Agata and co-workers (2003), in this model the blastema is formed as a signalling centre to reorganise body regionality rather than a place of reforming lost tissues and organs; therefore, they suggested the “distalisation-intercalation” model as a general principle for vertebrates and invertebrates’ regeneration. As the name indicates, according to this model, organisms initially form the most distal part (distalisation) of the new structure, which, by interacting with the underlying old stump tissues, induces reorganisation of positional information. The lost structures are then recovered by appropriate intercalation of newly generated tissues between the distal part and the stump.

As in all cases of asteroid arm regeneration, the terminal tube foot of *E. sepositus* (and partially the terminal ossicle) can be considered as the most distal elements (distalisation) which drive the following intercalation process: indeed, the new structures such as tube feet, muscle bundles, and so forth gradually develop between the stump and the terminal structures with a proximal-distal gradient. In those starfish species where the terminal ossicle is naturally more developed (e.g. *Marthasterias glacialis*) its contribution as a distalisation element is more clearly observable (personal observation). Other authors suggested that the concepts of distalisation and intercalation are also applicable to arm regeneration in the starfish *Linckia laevigata* and *Asterias rubens* (Hotchkiss, 2009) and in the feather star *Oxycomanthus japonicus* (Shibata *et al.*, 2010). In the crinoid *Antedon mediterranea* the most distal part of a normal arm maintains always the characteristics of an undifferentiated bud (Candia Carnevali and Bonasoro, 2001b): so, during arm regeneration, even if a clearly recognisable and differentiated distal element is apparently not present, the blastema could be regarded as the true distal element.

These concepts simplify the controversial issue regarding the presence/absence of a blastema as the distinctive character of epimorphic/morphallactic mechanism. However, this does not solve the more persistent question related to the origin of cells involved in regeneration processes. In our opinion, the regenerative event should be classified only according to the origin of the cells recruited in regenerative process, which can be stem cells, dedifferentiated cells or both. In *E. sepositus* the presence of dedifferentiated elements (myocytes) might indicate the involvement of a morphallactic mechanism but recently Hernroth and co-workers (2010) demonstrated the involvement also of progenitor undifferentiated cells in the arm regeneration of *A. rubens*.

### *5. Conclusion*

The overall process of arm regeneration in *E. sepositus* can be subdivided into three main phases: a first repair phase (0-7 days), characterised by wound healing and oedematous area formation; a second early regenerative phase (1-6 weeks p.a.), during which the first sign of neo-formation of lost parts appears; and a third advanced regenerative phase (from 6 weeks p.a.), characterised by a progressive development of the regenerating arm-tip. Figure 10 schematically summarises the main processes occurring after the repair phase. During the regenerative phase a spatial and chronological differentiation of lost and injured structures occurs, starting from neurogenesis, skeletogenesis and water vascular system (terminal tube foot) development. Later, when the regenerate is clearly

evident, myogenesis takes place between the newly formed skeletal ossicles and the tube feet start differentiating. The overall process is in agreement with the distalisation-intercalation model proposed by Agata and co-workers (2003).

Future studies should investigate the regenerative process of each new structure using immunohistochemical and molecular tools in order to clarify the origin of the cells contributing to their re-growth.

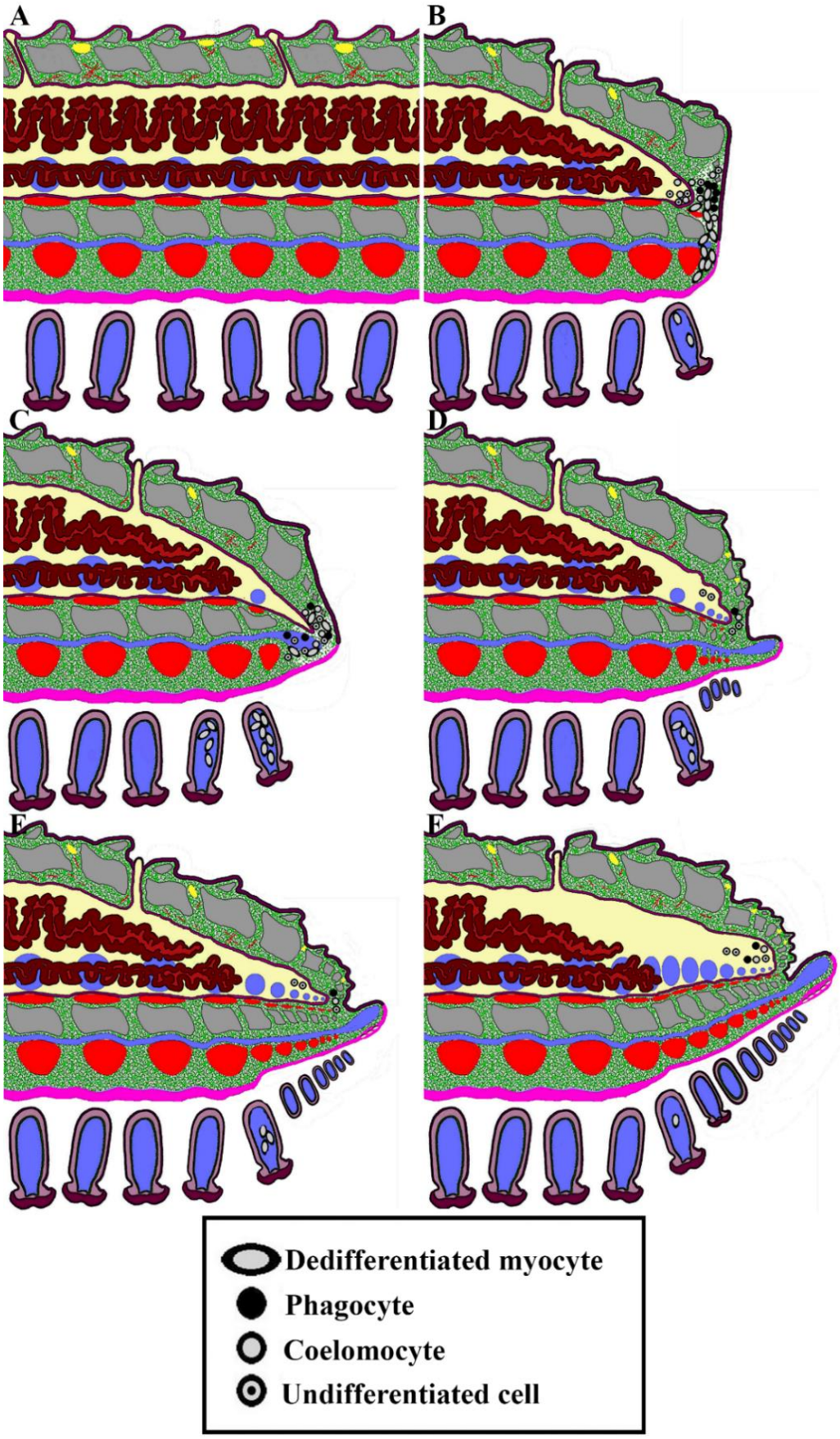


**Fig. 10.** *Diagram summarising the main events during the regenerative phase of E. sepositus.* A) Gross morphology of non-regenerating arm. B) First sign of re-growth (1 w p.a.): cellular elements are found behind the wound epidermis intermixed with new

◀ collagen fibrils and first sign of skeletogenesis. C) The regenerate appearance (3 w p.a.): massive release of dedifferentiating myocytes from their inner coelomic wall to the lumen of the tube feet. D) Myogenesis and tube feet morphogenesis (6 w p.a.): a clearly visible new arm-tip. The terminal tube foot is well developed. E) Complete restoration of the missing parts (10 w p.a.). F) A minuscule arm (16 w p.a.).

### *6. Supplementary Materials*

For Extended Materials and Methods see Chapter 1 (paragraph 5).

# CHAPTER 3

## Extracellular matrix gene expression patterns during arm regeneration in *Amphiura filiformis*

Ferrario Cinzia, Czarkwiani Anna, Piovani Laura, Candia Carnevali Maria Daniela, Sugni Michela, Oliveri Paola

*In preparation* for Cell and Tissue Research.

***Abstract***

Brittle stars are echinoderms well known for their striking regenerative abilities. They can regenerate amputated arms in only a few weeks. Among the different tissues involved in this complex process, the connective tissue plays a key role during both repair and regenerative phases.

To gather insights on the molecular role of connective tissue (mainly the extracellular matrix (ECM) component) during regeneration, the brittle star *Amphiura filiformis* was chosen as experimental model. 9 genes (5 collagen-like genes and 4 ECM-related molecule genes) were identified and cloned, and their spatial-temporal expression patterns were analysed by means of whole mount *in situ* hybridisation (WMISH) focusing on 3 regenerative stages (2, 4, and >50% DI). Wax embedding and sectioning of WMISH samples were performed to gain a better resolution of the different gene expression patterns.

Our results showed that almost all the selected collagen-like genes are not expressed at early stage of regeneration, indicating a possible delay in their activation, whereas at advanced regenerative stages they are differentially expressed mainly in coelomic epithelium, connective tissue and skeletal elements. The selected ECM-related molecule genes (e.g. laminin and tissue inhibitor of metalloproteinases) show different spatial-temporal expression patterns as well, suggesting that the gene regulation of ECM deposition/remodelling is different during the regenerative process.

Further analyses (*i.e.* quantitative RT-PCR and study of other ECM genes) will allow a better understanding of the role of the connective tissue during brittle star regeneration.

## *1. Introduction*

Regeneration, the replacement of lost body parts, is one of the most fascinating processes of animal biology. It includes many different events, such as wound healing, tissue remodelling, apoptosis, cell proliferation, dedifferentiation, trans-differentiation, and morphogenesis (King and Newmark, 2012). Both vertebrates and invertebrates are able to regenerate cells, tissues, organs or whole body parts, although the "efficiency" and extent of this ability vary according to the species (Tsonis, 2000; Brockes and Kumar, 2008; Bely and Nyberg, 2009). Among vertebrates, amphibians and zebrafish are the most extensively studied model organisms to investigate this phenomenon (Brockes and Kumar, 2002; Gemberling *et al.*, 2013), whereas *Hydra* and planarians are two of the most well-known invertebrate systems studied (Bosch, 2007; Salò *et al.*, 2009). All echinoderms possess striking regenerative abilities that caught the interest of biologists from decades ago (Hyman, 1955) till now (Candia Carnevali, 2006). Indeed, these invertebrates can regenerate internal organs, appendages or whole body parts (such as arms) after both self-induced (autotomy) or traumatic mutilations, eventually restoring completely functional structures (Thorndyke *et al.*, 1999). Moreover, they occupy a key position in the tree of life as non-chordate deuterostomes and are therefore of high interest in terms of comparative studies on regenerative potential with other deuterostomes, and humans in particular. All representatives of the five classes of the phylum present different levels of regenerative capabilities but "armed" echinoderms, *i.e.* brittle stars, starfish and crinoids, have been useful to shed light on whole complex body part (e.g. arm) regenerative process, also in view of comparative investigations with regeneration of vertebrate limbs (Nye *et al.*, 2003). So far, echinoderm regenerative mechanisms were investigated mostly through morphological and cellular investigations with few molecular studies mainly on sea cucumbers but nowadays, thanks to the increasing availability of echinoderm genome and transcriptome data (Cameron *et al.*, 2009; Janies *et al.*, 2016), molecular tools have become fundamental to understand the regenerative process itself and how genes are finely regulated to develop a new fully functional body part (Sánchez Alvarado and Tsonis, 2006).

In echinoderms, regeneration after traumatic amputation can be overall subdivided into three main phases, namely repair, early regenerative and advanced regenerative phases, each characterised by distinct events (Candia Carnevali *et al.*, 1998; Moss *et al.*, 1998; Biressi *et al.*, 2010; Ben Khadra *et al.*, 2015a, b; Czarkwiani *et al.*, 2016). Both the stump and the newly formed tissues are actively involved in this complex process. During

regeneration the connective tissue has a pivotal role ensuring structural and mechanical stability to all tissues and organs and also provides a supporting scaffold for cell migration, adhesion and proliferation (Ben Khadra *et al.*, 2015b). It is composed of different types of extracellular matrix (ECM) macromolecules, such as collagens, laminins, fibronectin, glycosaminoglycans and proteoglycans (Alberts *et al.*, 2002) and of different cytotypes, including fibroblasts. The interactions between the non-cellular and the cellular connective tissue components control both tissue development and structural integrity and ensure connective tissue maintenance and self-renewal (Gelse *et al.*, 2003). Collagen is the main ECM component of the connective tissues and is present in the metazoans from sponges to humans (Özbek *et al.*, 2010). It plays a key role throughout the whole regenerative process (Quiñones *et al.*, 2002). In echinoderms, during the repair phase, collagen and ECM-related molecules have been shown to be involved in wound closure, tissue remodelling, cell migration and proliferation (Cabrera-Serrano and García-Arrarás, 2004; Mashanov *et al.*, 2014). The delay in collagen deposition has been suggested to be strictly related to the remarkable regenerative abilities of echinoderms: indeed, in contrast with mammal, in these animals neither scar formation nor fibrosis are detectable during wound healing, thus suggesting that a proper and finely regulated ECM remodelling is crucial for the effectiveness of the subsequent regeneration (Quiñones *et al.*, 2002). Microscopic analyses on collagen deposition after arm injury in the starfish *Echinaster sepositus* have suggested that this protein plays an important role in both repair and regenerative phases creating an initial loose network of fibrils and a secondary fibre scaffold for tissue and organ reconstruction (Ben Khadra *et al.*, 2015a, b). The same observations were previously reported also for the starfish *Leptasterias hexactis* (Mladenov *et al.*, 1989) and the crinoid *Antedon mediterrenea* (Candia Carnevali and Bonasoro, 2001b).

Besides collagen, ECM remodelling is ensured also by other ECM-related molecules, such as matrix metalloproteases (MMPs) and tissue inhibitors of the MMPs (TIMPs). These enzymes regulate and modulate ECM degradation and cell behaviour in standard physiological conditions and during wound healing, tissue remodelling and regeneration. It has been shown that MMPs are involved in *Holothuria glaberrima* (Quiñones *et al.*, 2002) and *Eupentacta fraudatrix* (Lamash and Dolmatov, 2013) gut regeneration. Ortiz-Pineda and co-workers (2009) described up-regulation of three different MMPs in sea cucumber intestinal regeneration only at three and seven days post-evisceration. Recently, from transcriptome analyses, Clouse and co-workers (2015) described several

TIMPs in echinoderms but no data are available yet on their expression or specific role during regeneration.

Laminin is another important molecule of the ECM; together with collagen type IV this glycoprotein is a key component of basal laminas, which are subjected to high levels of remodelling and rearrangement during the cicatrisation phenomenon and the regeneration process itself. In the only echinoderm fully sequenced genome, the purple sea urchins *Strongylocentrotus purpuratus* (Sea Urchin Genome Sequencing Consortium, 2006), the diversity of laminin genes (4 α, 2 β and 1 γ chains; Whittaker *et al.*, 2006) is lower compared to vertebrates (e.g. in mammals at least 16 laminin complexes are described; Miner and Yurchenco, 2004). Immunohistochemical studies on *H. glaberrima* (Quiñones *et al.*, 2002) showed that laminin subunit α1 normally present in enteric and mesenteric muscle cells is no longer present in the first days of intestine regeneration, whereas it is again detectable after two weeks. On the other side, in gene expression analyses of laminin genes with two different sea cucumbers (*H. glaberrima* and *A. japonicus*) they are up-regulated during regeneration (Ortiz-Pineda *et al.*, 2009; Sun *et al.*, 2011) and the authors suggested that laminin expression could be silenced after transcription during the matrix remodelling of the early regenerative phase.

Overall, a number of morphological and molecular studies have been carried out to investigate the ECM function during single organ regeneration (e.g. intestine and radial nerve cord) in holothuroids but little is known about other echinoderms, and in case of whole body part regeneration (*i.e.* arms). Therefore, we are far from having a complete view of the ECM role during this complex process, particularly from a molecular point of view.

Among “armed” echinoderms, brittle stars (Ophiuroidea) are emerging as valid model organisms to gain a general comprehension of arm regeneration, underlining the importance of integrated cellular and molecular approaches (Dupont and Thorndyke, 2006; Biressi *et al.*, 2010; Burns *et al.*, 2012; Purushothaman *et al.*, 2015; Czarkwiani *et al.*, 2013, 2016). The burrowing brittle star *Amphiura filiformis* (O.F. Müller, 1776) is now being used for these kinds of studies mainly due to its small size, fast arm regeneration and easiness of maintenance in laboratory conditions. In this species the expression of a collagen gene (*Afi-α-coll*) was investigated by Czarkwiani and co-workers (2013). Cells expressing this gene are localised at the level of spines and lateral shields of fully regenerated arms, thus suggesting *Afi-α-coll* as a marker of skeletal differentiation. According to recent transcriptomic and proteomic data of wound healing stages (1-3 days

post-amputation, dpa) collagen IV and the ECM glycoprotein fibronectin are down-regulated (Purushothaman *et al.*, 2015), whereas collagen transcripts are present at high level during *A. filiformis* regeneration (Burns *et al.*, 2011) during early stages of regeneration (7 dpa). These data suggest the importance of the connective tissue during this species regeneration but they need to be completed with focused molecular analysis also on other ECM-related molecules, such as metalloproteases (MMPs) and their inhibitors (TIMPs), laminins, etc.

Here, we present a comprehensive study of the spatial-temporal expression of collagen and other extracellular matrix genes identified in *A. filiformis* transcriptomes (Delroisse *et al.*, 2015; Dylus *et al.*, *submitted*) involved in this brittle star arm regeneration through whole mount *in situ* hybridisation (WMISH). In order to clarify in which tissues the expression of each gene was detected, we performed classical histological analyses (paraffin wax embedding and sectioning) after WMISH. Moreover, collagen being the main protein of the extracellular matrix, the selected collagen genes of *A. filiformis* were characterised using NCBI Conserved Domain Architecture Retrieval Tool (cDART) considering as reference the collagen nomenclature described in recent literature (mainly according to Ricard-Blum, 2011). Overall, our gene expression analyses showed that in *A. filiformis* regenerating arm different collagen-like and ECM-related molecule genes are expressed at different stages and in different tissues suggesting their diverse contribution during the whole regenerative process.

## *2. Materials and Methods*

No specific permits were required since the brittle star *Amphiura filiformis* is not an endangered or protected species.

### *2.1. Animal collection and maintenance*

Adult specimens of *A. filiformis* were collected at the Sven Lovén Centre for Marine Sciences in Kristineberg (Sweden) and transported to London where they were kept in tanks with 30‰ salinity filtered artificial sea water (ASW; Instant Ocean®) at 14°C. Animals were left to acclimatise around one week before performing regeneration tests. Specimens were fed twice a week with Microvore Microdiet (Brightwell Aquatics) and ASW parameters were constantly checked and adjusted if necessary.

### *2.2. Arm regenerative samples*

Specimens were anaesthetised in 3.5% $MgCl_2(6H_2O)$ solution (pH 8.3) in a 1:1 mix of filtered ASW and milliQ water. Two arms per animal were amputated at 1 cm from the disc, performing a sharp cut with a scalpel between two subsequent arm segments under a stereomicroscope. Animals were then left to regenerate until they reached the desired stages described by Dupont and Thorndyke (2006) and Czarkwiani and co-workers (2016), namely stage 2, around 5 days post-amputation (dpa), a regenerative phase characterised by the first appearance of regenerative bud, stage 4, around 8 dpa, a regenerative phase characterised by complex structure and appearance of first metameric units, and >50% DI, after 2-3 weeks post-amputation (wpa) which corresponds to an advanced regenerative phase. Once reached the desired stages, the regenerating samples were collected together with 2-3 segments of the stump in order to easily handle them during the subsequent protocols, then processed as described below.

### *2.3. Molecular cloning and gene expression analyses*

*2.3.1. Identification of A. filiformis ECM genes*

Genes of interest were selected from:

- EchinoBase (http://www.echinobase.org/), performing a targeted gene search in *Strongylocentrotus purpuratus* and *Patiria miniata* databases with Gene ID, Gene Name or Gene Synonym;
- recent publications in other echinoderms (Ortiz-Pineda *et al.*, 2009; Sun *et al.*, 2011; Czarkwiani *et al.*, 2013; Mashanov *et al.*, 2014; Purushothaman *et al.*, 2015).

Once collected the relative sequences a search in the *A. filiformis* transcriptome (Dylus *et al.*, *submitted*) was performed using BLAST-X in order to obtain the corresponding gene sequences in *A. filiformis*. The highest score hit was then used to search back on other echinoderm database (http://www.echinobase.org/) or the non-redundant (NR) NCBI database (http://blast.ncbi.nlm.nih.gov/) to confirm they belong to general ECM genes. 38 genes were initially selected and specific cloning primers were designed using PRIMER3 Software version 4.0.0 (http://primer3.ut.ee/) with the following changes from default parameters: max Poly-X=3 and max 3' Stability=8. Supplementary Table S1 summarises the primers used for the genes further analysed in this paper.

*2.3.2. Cloning and probe synthesis*

To isolate fragments containing the desired genes, total *A. filiformis* RNA was extracted from different embryonic and adult arm regenerating stages and first strand cDNA was synthetized as described in Czarkwiani and co-workers (2013). This was used to amplify specific fragments using PCR and the PCR products for each gene of interest were subsequently ligated in pGEM®-T Easy Vector System I (Promega) and then transformed in Subcloning Efficiency Invitrogen DH5α Competent Cells (Life Technologies). Colonies containing the correct recombinant plasmid were selected by PCR and confirmed by sequencing. See Supplementary Tables S1 and S2 for the details of the cloning primers and of the clones respectively.

RNA antisense digoxigenin (DIG) probes for chromogenic enzymatic whole mount *in situ* hybridisation (WMISH) were then transcribed from specific cloned fragments and following procedures using Sp6/T7 Transcription Kit (Roche) and DIG-labelling mix (Roche) according to manufacturer's instructions.

*2.3.3. Whole mount in situ hybridisation (WMISH)*

*A. filiformis* samples of the selected regenerative stages were fixed in 4% paraformaldehyde (PFA) in 1x Phosphate Buffer saline (PBS with 0.1% Tween-20; PBT) overnight at 4°C and stored in 100% methanol at -20°C until use.

WMISH was performed with the antisense probes newly synthetized along with positive control (*Afi-c-lectin*; Czarkwiani *et al.*, 2016). For each stage at least three regenerating arms from different experimental animals were used to test each RNA antisense probe. Samples were re-hydrated in a decreasing scale of ethanol in DEPC-treated water and then washed 3 times in 1x MABT (0.1 M maleic acid pH 7.5, 0.15 M NaCl, 0.1% Tween-20). A wash with 1:1 (v/v) 1x MABT and hybridisation buffer (HB; 50% de-ionized formamide, 0.02 M Tris pH 7.5, 10% PEG, 0.6 M NaCl, 0.5 mg/ml yeast RNA, 0.1% Tween-20, 5 mM EDTA, 1X Denhardt's) was performed and then samples were incubated in HB for 1 hour at 50°-55°C. The HB was replaced with 0.02 ng/µl probes in HB and left to hybridise for 5 days at 50°C-55°C. After this period 250 µl of 1x MABT and 250 µl of HB were added and one wash with 1:1 (v/v) 1x MABT and HB was performed, followed by a wash of 10 minutes with 75% 1x MABT/25% HB. Two washes with 1x MABT were then followed by two washes with 0.1x MABT supplemented with 0.1% Tween-20. All these washes were performed at 50°C-55°C. Samples were incubated with blocking buffer (BB; 5% goat serum in 1x MABT) for 30 minutes and then for 1 hour at RT (or

overnight at 4°C) in 1:1000 alkaline phosphates conjugated antibody anti-DIG (Roche) in BB. Five washes were then performed with 1x MABT, followed by two washes with the freshly prepared alkaline phosphatase buffer (AP; 0.1 M Tris pH 9.5, 0.1 M NaCl, 0.05 M $MgCl_2$, 0.1% Tween-20, 1 mM Levamisole). Then, the staining reaction was developed using 10 µl NBT/BCIP mix (Roche) with 10% dimethylformamide in AP. The detection of the staining was monitored under the stereomicroscope. The reaction was stopped with one wash in 1x MABT with 0.5 M EDTA followed by three washes in 1x MABT (5 minutes each). Then a quick wash with 1:1 (v/v) 1x MABT and 50% glycerol was performed. Samples were then stored in 50% glycerol at 4°C and subsequently observed under a Zeiss AxioImager M1 microscope equipped with a Zeiss AxioCam HRc camera. When necessary to confirm results obtained with the previously described protocol to increase the signal, WMISH parameters were adjusted as follows on other independent samples: probe concentration 0.04 ng/µl and hybridisation time 6-7 days. If necessary, these WMISH modified parameters (from now on called second WMISH parameters) are showed in the results or in the Supplementary Materials (see figure captions for details).

*2.3.4. Post in situ sectioning*

After whole mount imaging, hybridised samples were embedded in paraffin wax and sectioned in order to gain a better resolution of the tissue-specific expression. Samples stored in 50% glycerol were washed three times in 1x PBS or 1x MABT at RT and decalcified for 1-2 days in 0.5 M EDTA in 1x PBS (pH 8) or decalcifying solution (0.3 M NaCl and 2% L-ascorbic acid in distilled water) at 4°C. They were washed twice in 1x PBS or 1x MABT, post-fixed in 4% PFA in 1x PBS or 2% glutaraldehyde in 1x MABT for 30 minutes at RT, washed twice in 1x PBS or 1x MABT, de-hydrated in an increasing scale of ethanol in distilled water (30 minutes each wash), cleared in xylene twice for 30 minutes and left overnight at RT in a 1:1 solution of paraffin wax and xylene. After three washes with new melted paraffin wax they were embedded and then sectioned with a rotary microtome (Leitz 1512). Sections (10 µm thickness) were then de-waxed in xylene, mounted with Eukitt® and observed under a Jenaval light microscope provided with a DeltaPix Invenio 3S 3M Pixel CMOS camera and DeltaPix ViewerLE Software.

### *2.4. Microscopy analyses*

Classical histological analyses (thick paraffin sections) were performed on *A. filiformis* non-regenerating arms in order to obtain a complete overview of the brittle star arm

anatomy and consequently be able to better characterise in which tissues the different gene expression patterns were detected. Sample fixation, paraffin wax embedding, sectioning and staining were performed following protocols described in Czarkwiani and co-workers (2016).

## *3. Results*

### *3.1. Collagen and other ECM genes in A. filiformis*

Supplementary Table S3 summarises the best BLAST hits of each identified *A. filiformis* transcript in EchinoBase and NCBI (see below for details).

#### *3.1.1. Collagen-like genes in A. filiformis*

One of the most abundant components of ECM is collagen in its various forms *(i.e.* fibrillar and nonfibrillar), for this reason we focused our attention on the genes highly related to collagen (see methods) present in an *A. filiformis* transcriptome (Dylus *et al.*, *submitted*). Our search identified four new genes along with the already published *Afi-αcoll* gene (Czarkwiani *et al.*, 2013).

Considering the high variety of collagen types and isoforms and the presence of repetitions of simple triplets of aminoacids (*i.e.* Gly-Pro-X) as a collagen signature, we decided to search for conserved domains in order to better characterise the identified collagen genes. The nucleotide sequences from the *A. filiformis* transcriptome were translated into the correspondent aminoacid sequences, using the tool in ExPASy (Bioinformatics Resource Portal) and then input into the NCBI Conserved Domain Architecture Retrieval Tool (cDART) on-line tool. In parallel, the best BLAST-X hits against the *Strongylocentrotus purpuratus* peptide database (http://www.echinobase.org/Echinobase/Blast/SpBlast/blast.php) and the NCBI NR database were considered. Figure 1 summarises the results of the analysis of the conserved domains and shows the different types of collagen identified.

From NCBI cDART *Afi-col-like A* (*Afi*CDS.id16823.tr6264) is a transcript that encodes for a protein that contains 20 copies of the collagen triple helix repeat (*coll*) and a *C1q* domain, a globular domain found in both collagen and complements (Fig. 1). The best BLAST hit in the sea urchin database from EchinoBase is the complement gene *Sp-C1qL* (SPU_05500), whereas from the NCBI NR database is the collagen alpha-2(VIII) chain-like [*Strongylocentrotus purpuratus*] (ref|XP_003724148.1|), which has an identical domain structure of *Afi-col-like-A*. The ascription of this transcript to a collagen type could

be controversial: indeed, considering the presence of collagen domain and *C1q* domain, it can be regarded as both a network-forming collagen or a complement C1q (the latter possessing both these domains according to Ricard-Blum, 2011). Furthermore, vertebrate protein with similar protein structure are adinopectin, TNF-α and collagen α2-typeVIII. Taking into account all the best BLAST results this transcript is considered as a nonfibrillar collagen-like protein.

From NCBI cDART *Afi-col-like B* (*Afi*CDS.id31588.tr64501) is a transcript that encodes for a protein that contains a laminin G domain (*LamG*), 20 copies of the collagen triple helix repeat (*coll*) and the fibrillar collagen C-terminal domain (*ColFI*; Fig. 1). The best BLAST hit in the sea urchin database from EchinoBase is the collagen gene *Sp-6Afcol* (SPU_009076) and from the NCBI NR database is the collagen alpha-1(V) chain isoform X2 [*Strongylocentrotus purpuratus*] (ref|XP_011679218.1|). Even if laminin G domain, also known as the LNS (Laminin-alpha, Neurexin and Sex hormone-binding globulin) domain, has not been described in Ricard-Blum (2011), it is present not only in several laminin family members but also in numerous extracellular matrix proteins among which collagen (Fallahi *et al.*, 2005). Therefore, considering the other described domains, it can be regarded as a potential fibril-forming collagen-like protein (Ricard-Blum, 2011).

From NCBI cDART *Afi-col-like C* (*Afi*CDS.id59066.tr822) is a transcript that encodes for a protein that contains a Von Willebrand factor, type C domain (*VW*; Fig. 1). The best BLAST hit in the sea urchin database from EchinoBase is the collagen *Sp-Col805b_2* (SPU_005167) and from NCBI NR database is the α-5 collagen [*Paracentrotus lividus*] (emb|CAE53096.1|). Considering that the *VW* domain can be present not only in different collagen types but also in other extracellular matrix protein and complement factors as well, a further analysis was performed in order to understand if this *A. filiformis* transcript could be considered a collagen-like protein. Hypothesising that the sequence (1360 aa) was not complete due to possible problems in the transcriptome assembly and the collagen domains could not be detected, the *Paracentrotus lividus* sequence (the best BLAST hit in NCBI; 2795 aa) was selected and a BLAST-X search in the *A. filiformis* transcriptome was performed removing the sequence corresponding to the *VW* domain. The result showed that collagen domains (triple helix repeat) are present. Considering the domains, this transcript presents a *VW* domain similar to mollusc collagens (id in UniProt database: K1QDW5) and can be compared to the mammalian fibril-associated collagens with interrupted triple helices (FACIT; Ricard-Blum, 2011) described also in

invertebrate chordate (FACIT-like protein; Exposito and Lethias, 2013). Therefore, this transcript is considered as a collagen-like protein.

From NCBI cDART *Afi-col-like D* (*Afi*CDS.id20775.tr36218) is a transcript that encodes for a protein that contains 20 copies of the collagen triple helix repeat (*coll*) and the fibrillar collagen C-terminal domain (*ColFI*; Fig. 1). The best BLAST hit in the sea urchin database from EchinoBase is the collagen *Sp-Fcolf* (SPU_013557) and from the NCBI NR database is the collagen alpha-1(XXVII) chain [*Strongylocentrotus purpuratus*] (ref|XP_011679783.1|). Taking into account the just described domains, this transcript can be regarded as a fibril-forming collagen-like protein according to Ricard-Blum (2011).

The *Afi-αcoll* sequence was obtained from NCBI (accession number: JG391435; Burns *et al.*, 2011 and Czarkwiani *et al.*, 2013) and the NCBI cDART output is a protein containing 20 copies of the collagen triple helix repeat (*coll*) and the fibrillar collagen C-terminal domain (*ColFI*; Fig. 1). The best BLAST hit in the sea urchin database from EchinoBase is the *Sp-Col805b_1* (SPU_014618) and from the NCBI NR database is the hypothetical protein BRAFLDRAFT 74778 [*Branchiostoma floridae*] (XP_002612988.1) that is a collagen. Taking into account these domains, *Afi-αcoll* can be regarded as a fibril-forming collagen (Ricard-Blum, 2011).

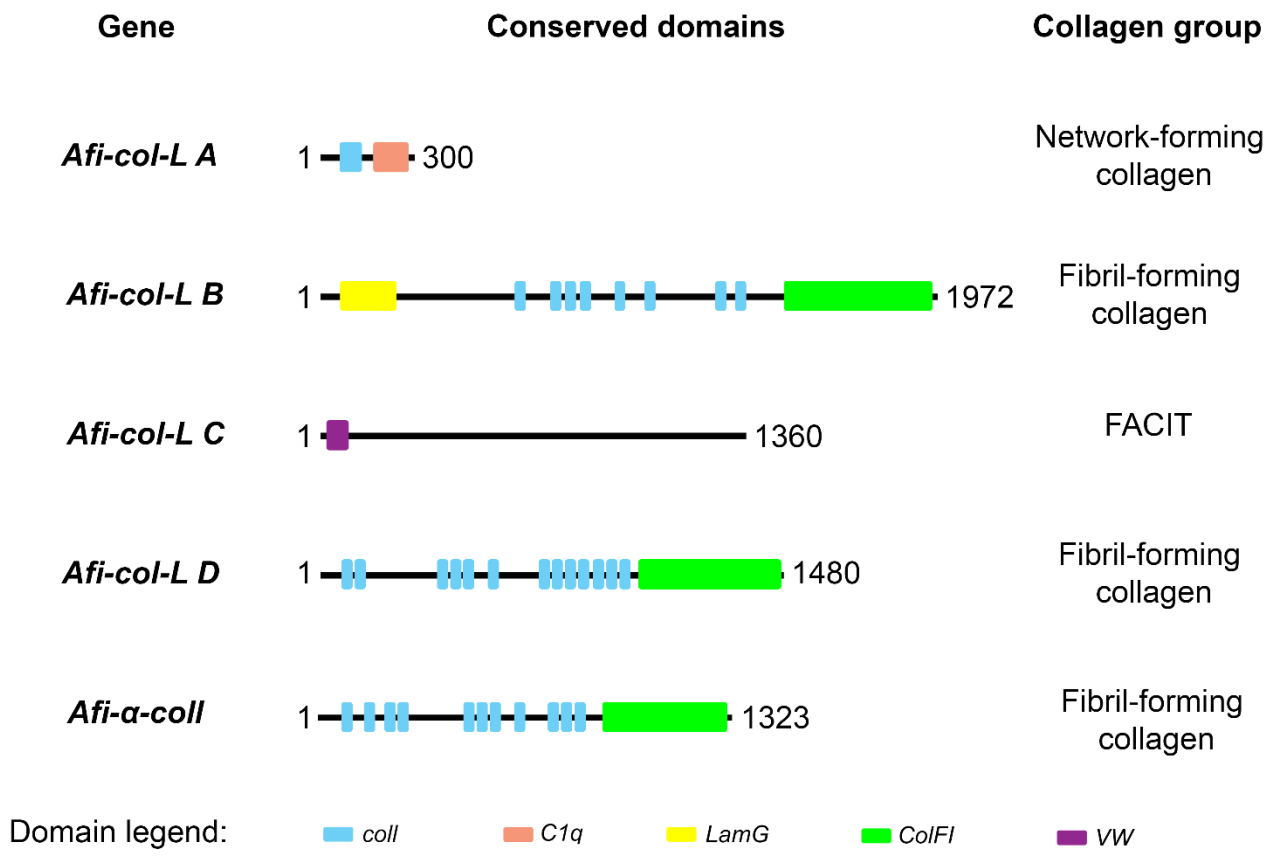

◀ **Fig. 1.** *Conserved domains of the identified collagen-like genes (transcriptome sequences) from NCBI cDART*. The transcripts were assigned to different collagen groups according to Ricard-Blum (2011). *Domain legend*: *coll* = collagen triple helix repeats; *C1q* = subunit of the C1 enzyme complex; *LamG* = laminin globular (G) domain; *ColFI* = fibrillar collagen C-terminal domain; *VW* = Von Willebrand factor, type C. Numbers: protein sequence length in aminoacids.

*3.1.2. Extracellular matrix (ECM) genes in A. filiformis*

Together with collagen, the main component of extracellular matrix, other molecules are important for its formation/structure/remodelling during regeneration, such as laminin, tissue inhibitors of metalloproteases (TIMPs) and ECM proteins. Therefore, we focused our analyses on ECM molecule-related genes present in an *A. filiformis* transcriptome (Dylus *et al.*, *submitted*). Our search identified four new genes, in particular two laminin subunits, one ECM protein and one TIMP.

For *Afi-Lamα-L* (*Afi*CDS.id50515.tr22425) the best BLAST hit in the sea urchin database from EchinoBase is *Sp-LamaLf* (SPU_020192) also called *Sp-Lama5L1_1*, whereas from the NCBI NR database is laminin subunit α-like isoform X2 [*Lingula anatina*] (ref|XP_013408769.1|). Therefore, this transcript is considered as the α subunit laminin-like.

For *Afi-Lamβ-L* (*Afi*CDS.id27309.tr36214) the best BLAST hit in the sea urchin database from EchinoBase is *Sp-LamB2Lf* (SPU_001768), whereas from the NCBI NR database is laminin subunit β-2 [*Strongylocentrotus purpuratus*] (ref|XP_793215.4|). So, this transcript is considered as the β subunit laminin-like.

For *Afi-ECM-protein* (*Afi*CDS.id38268.tr22439) the best BLAST hit in the sea urchin database from EchinoBase is *Sp-Fram1* (SPU_011688) also called FRAS1 related extracellular matrix 1, whereas from the NCBI NR database is FRAS1-related extracellular matrix protein 1 [*Strongylocentrotus purpuratus*] (ref|XP_011678210.1|). Therefore, this transcript is considered as an extracellular matrix protein.

For *Afi-TIMP3* (*Afi*CDS.id58489.tr18807) the best BLAST hit in the sea urchin database from EchinoBase is *Sp-Timp4b* (SPU_008866) or tissue inhibitor of metalloproteinase, whereas from the NCBI NR database is metalloproteinase inhibitor 3 [*Strongylocentrotus purpuratus*] (ref|XP_781027.1|). Thus, this transcript is considered as a tissue inhibitor of metalloproteinases (TIMP).

### *3.2. Spatial-temporal gene expression patterns*

In order to gather insights on the potential role of the isolated extracellular matrix genes during the process of regeneration, we studied their spatial expression in different stages of *A. filiformis* arm regeneration. Furthermore, for a better resolution of the tissue expressing the selected genes post whole mount *in situ* sample sectioning was performed. An initial histological analysis done to characterise the main tissues and structures of the brittle star arm will aid to the interpretation of the *in situ* hybridisation results. Figures 2 and 3 show the experimental model, schemes and thick paraffin sections, sagittal (longitudinal), cross (at the proximal and distal sides of the arm) and frontal, of a non-regenerating arm of *A. filiformis*. As in all ophiuroids, the arm of *A. filiformis* is subdivided in repetitive segments (Hyman, 1955) also called metameric units (Czarkwiani *et al.*, 2013, 2016). Skeletal elements (*i.e.* vertebrae, shields and spines) and muscle bundles are sequentially repeated in each segment, whereas three main structures longitudinally run along the whole arm: the aboral coelomic cavity, the radial water canal with its associated podia and accessory vesicles and the oral radial nerve cord with its associated sinuses (see Fig. 2 and 3). The distal arm-tip is characterised by the presence of a terminal cap and a terminal podium (Fig. 2e; Czarkwiani *et al.*, 2016).

In order to facilitate the understanding of the subsequent results a brief overview of the regenerative process of the arm of this species after traumatic amputation is provided below. The regenerative stages selected for this study have been detailed by Dupont and Thorndyke (2006), Biressi and co-workers (2010) and Czarkwiani and co-workers (2013; 2016). After wound healing, at ~ 5 days p.a. (stage 2) the regenerative bud appears, characterised by the first outgrowths of the three main longitudinal structures. At stage 4 (~ 8 days p.a.) the regenerate is already well differentiated and first signs of new metameric units and new podia are visible at the proximal side of the new arm-tip. After 2-3 weeks p.a. (stage >50% DI) the regenerate resembles a non-regenerating arm and it is almost completely differentiated in all its structures and tissues. New metameric units are regenerated following a proximal-distal gradient with less differentiated segments at the distal side of the regenerate: this regenerative mode of re-growth follows the distalisation-intercalation model (Czarkwiani *et al.*, 2016) and is valid for other invertebrates and echinoderms as well (Agata *et al.*, 2003; Ben Khadra *et al.*, 2015b).

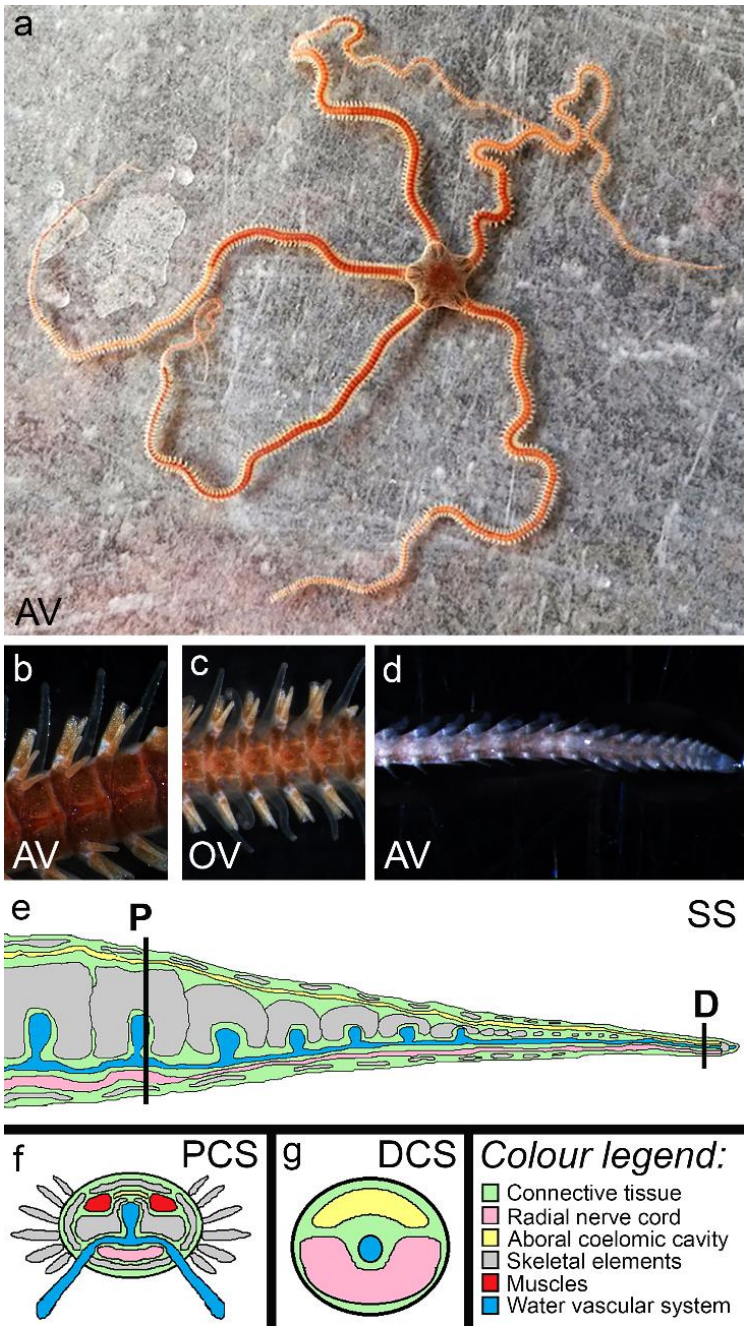


**Fig. 2.** a) Aboral view of an adult specimen of the brittle star *Amphiura filiformis*. b) Aboral view of the proximal side of a non-regenerating arm. c) Oral view of the proximal side of a non-regenerating arm. d) Aboral view of the distal tip of a non-regenerating arm. e-g) Schemes of a non-regenerating arm of *A. filiformis*. e) Sagittal (longitudinal) section scheme (SS). f) Cross section scheme at the level of the proximal side (P) of the arm. g) Cross section scheme at the level of the distal tip in the growth zone underneath the terminal ossicle (D). *Abbreviations*: AV = aboral view; D = distal; DCS = distal cross section; OV = oral view; P = proximal; PCS = proximal cross section; SS = sagittal section scheme. See colour legend embedded in the figure for the labelling of the different tissues. The epidermis is shown in black.

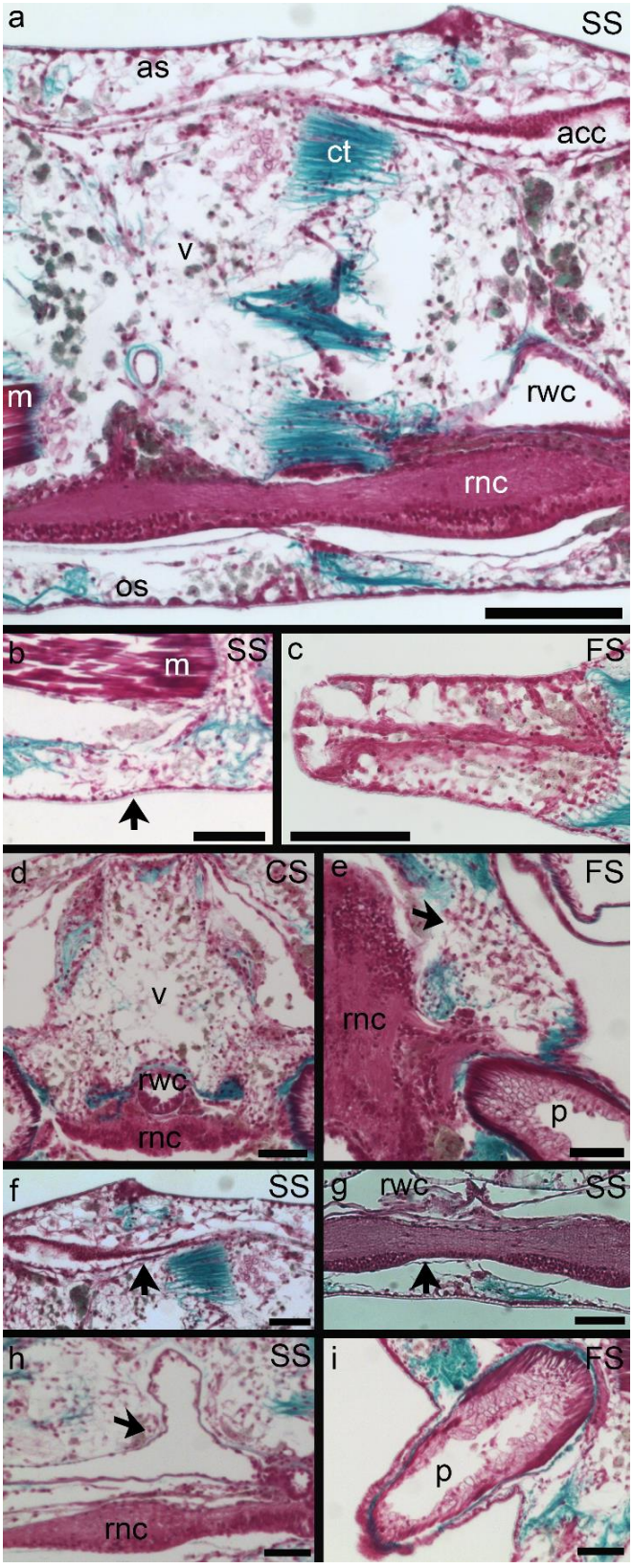


**Fig. 3.** a-i) Thick paraffin sections (Milligan trichrome staining) of non-regenerating arm of *A. filiformis*. Connective tissue (collagen) is stained in green/blue, cells are stained in pink/violet. a) Sagittal section (SS) showing the gross anatomy of an arm with its main tissues and structures. b) Sagittal section (SS) of the epidermis (arrow). c) Frontal section (FS) of the spine where the central nerve is visible. d) Cross section (CS) of the vertebra. e) Frontal section (FS) of the lateral shield (arrow). f) Sagittal section (SS) of the aboral

◀ coelomic cavity (arrow). g) Sagittal section (SS) of the radial nerve cord (arrow) with its connected sinuses. h) Sagittal section (SS) of the radial water canal (arrow) with an accessory vesicle. i) Frontal section (FS) of the podium. *Abbreviations*: acc = aboral coelomic cavity; as = aboral shield; ct = connective tissue; CS = cross section; FS = frontal section; m = muscle; os = oral shield; p = podium; rnc = radial nerve cord; rwc = radial water canal; SS = sagittal section; v = vertebra. Scale bars: a = 100 µm; b, c, d, e, f, g, h, i = 50 µm.

*3.2.1. Expression patterns of the collagen-like genes*

The expression patterns of the four newly identified collagen-like genes and of *Afi-αcoll* are analysed in three selected stages: 2 (early regenerative phase), 4 and >50% DI (advanced regenerative phases) in order to have a complete overview of their localisation during the whole regenerative process. Expression patterns in the stump tissues are investigated as well.

At stage 2 when the regenerative bud starts to appear only *Afi-col-like B* is localised in the aboral coelomic cavity epithelium (Fig. 4a, f, k), whereas all the other transcripts are not expressed (*Afi-col-like A* Fig. 5a, e, j; *Afi-col-L C* Fig. 6a, f, k; *Afi-col-L D* Fig. 7a, e, j; *Afi-αcoll* Fig. 8a, f, j).

At stage 4 when the regenerate is in an evident regenerative phase almost all the five transcripts are expressed with the exception of *Afi-col-L D* (Fig. 7b, f, k). In particular, *Afi-col-L A* is localised in the epidermis of the regenerate as visible from both whole mount samples (Fig. 5b) and post *in situ* sections (Fig. 5f, g, k), *Afi-col-like B* (Fig. 4b, g, h, l), *Afi-col-L C* (Fig. 6b, g, h, l) and *Afi-αcoll* (Fig. 8b, c, g, k) are present at the level of the aboral dermal layer of the regenerate, with the first one more localised in the aboral dermal layer of the tip of the regenerate.

In the late regenerates (>50% DI), when all the structures are differentiated, the identified collagen-like genes show different expression patterns along the proximal-distal direction. *Afi-col-L A* is confined to the aboral coelomic cavity epithelium along the whole regenerate (Fig. 5c, d, h, i, l). *Afi-col-like B* is detectable at the proximal side (Fig. 4c, d, i, m) in the inner lining of the podia, in the rim layer of the aboral intervertebral muscles, in the lateral shields, in the vertebrae and in the aboral coelomic cavity epithelium, whereas in the distal tip (Fig. 4e, j, n) it is visible only at the level of the aboral coelomic cavity epithelium. The latter and the radial water canal epithelium of the non-regenerating stump tissues show a signal as well (Fig. 4f and S1). *Afi-col-like C* shows a strong expression at the proximal side (Fig. 6c, d, i, m) in the lateral shields, the base of the spines, the aboral coelomic cavity epithelium and the rim layer of the aboral intervertebral muscles, whereas

it is confined to the lateral shields only in the distal side of the long regenerating arm (Fig. 6e, j) and no expression is detectable in the distal-most tip immediately before the terminal ossicle (Fig. 6e, n). In the non-regenerating stump tissues (Fig. S2) a signal is detectable at the level of the lateral shields and the radial water canal. Using the first WMISH conditions, *Afi-col-like D* in the long regenerate shows no signal but, in order to confirm these results, WMISH using second parameters (probe concentration 0.04 ng/µl and 5-7 days of hybridisation) was performed and a clear expression results being localised in the proximal side (Fig. 7c, h, l) of the long regenerate at the level of the aboral coelomic cavity epithelium and of the lateral shields, whereas in the distal tip (Fig. 7d, e, i, m) the signal is detectable in the aboral dermal layer and in the tip of the terminal podium. No staining is detectable at the level of the non-regenerating stump tissues (Fig. S3). *Afi-αcoll* expression pattern at stage >50% DI was described by Czarkwiani and co-workers (2013) and our results confirm a signal in the lateral shields and in the spines in the proximal side of the regenerate but reveal an expression also in the oral shield and in the aboral coelomic cavity epithelium (Fig. 8d, h, l) and in the latter also in the distal tip of the regenerate (Fig. 8e, i, m). A similar expression pattern at the level of the lateral shields, the oral shield and the spines is visible in the stump tissues as well (Fig. S4). Post *in situ* sectioning reveals that a signal is evident also at the level of the stump water vascular system and aboral coelomic cavity epithelium (Fig. S4c, d).

Overall, the expression patterns of the collagen genes we analysed showed that almost all transcripts, with the only exception of *Afi-col-L B*, are not expressed before stage 4 and that different collagen genes display different localisations suggesting that several tissues are involved in collagen production mainly from the beginning of the advanced regenerative phase. Moreover, they are all expressed in at least one regenerative stage at the level of the coelomic cavity epithelium.

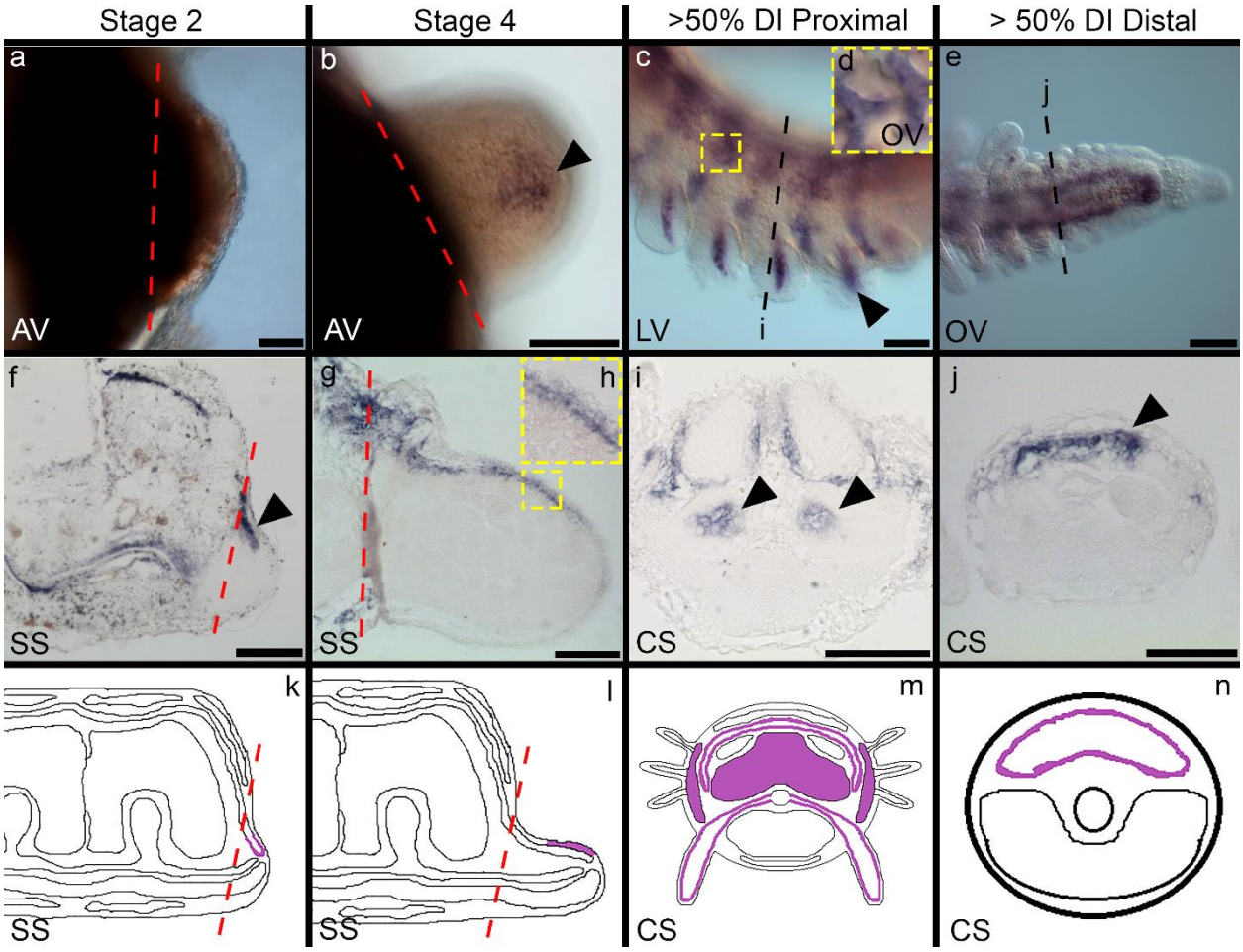


**Fig. 4.** *Afi-col-like B expression pattern at different regenerative stages*. 1st line: WMISH; 2nd line: post *in situ* sectioning; 3rd line: schemes. Stage 2 (first WMISH parameters): a, f, k. *Afi-col-like B* is expressed in the regenerative bud at the level of the aboral coelomic cavity epithelium (arrowhead). Stage 4 (first WMISH parameters): b, g, h, l. *Afi-col-like B* is expressed at the level of the aboral connective tissue of the regenerate (arrowhead). Stage >50% DI (first WMISH parameters): c, d, e, i, j, m, n. *Afi-col-like B* is expressed in the proximal side at the level of the aboral coelomic cavity epithelium, the rim layer of the aboral intervertebral muscles, the vertebrae, the lateral shields and the podia wall (arrowheads), whereas in the distal side it is detectable only at the level of the aboral coelomic cavity epithelium (arrowhead). *Abbreviations*: AV = aboral view; CS = cross section; LV = lateral view; OV = oral view; SS = sagittal section. Scale bars: a, b, e, f, g = 50 µm; c = 100 µm; i, j = 25 µm. In the schemes the gene expression pattern is shown in violet. Red dotted lines = amputation plane. Black dotted lines = levels corresponding to the cross sections shown in Fig. i and j.

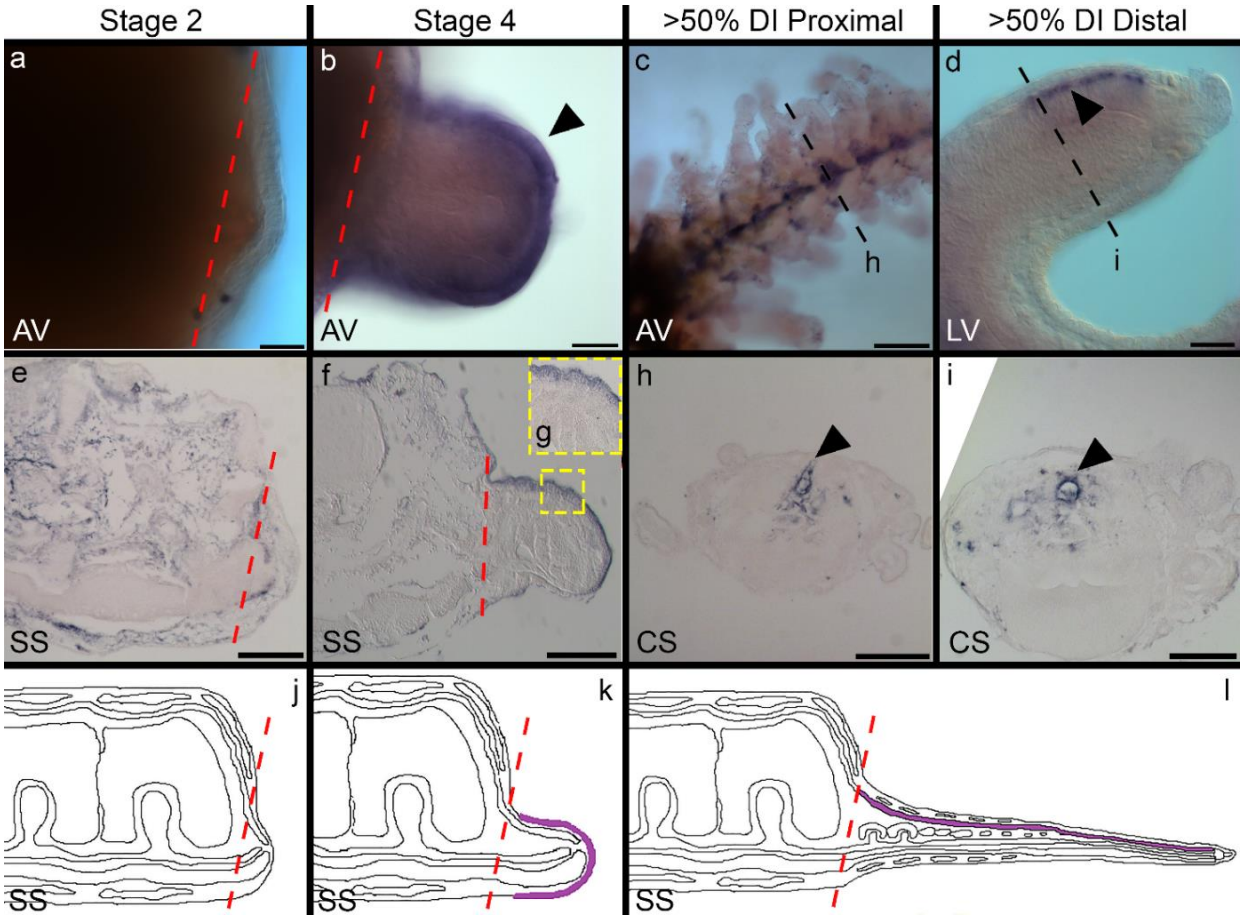


**Fig. 5.** *Afi-col-like A expression pattern at different regenerative stages*. 1st line: WMISH; 2nd line: post *in situ* sectioning; 3rd line: schemes. Stage 2 (first WMISH parameters): a, e, j. *Afi-col-like A* is not expressed in the regenerative bud. Stage 4 (first WMISH parameters): b, f, g, k. *Afi-col-like A* is expressed at the level of the epidermis (arrowhead). Stage >50% DI (first WMISH parameters): c, d, h, i, l. *Afi-col-like A* is expressed in the aboral coelomic cavity epithelium (arrowheads) along the whole regenerating arm. *Abbreviations*: AV = aboral view; CS = cross section; LV = lateral view; SS = sagittal section. Scale bars: a, b, d, e, f, h = 50 µm; c = 100 µm; i = 25 µm. In the schemes the gene expression pattern is shown in violet. Red dotted lines = amputation plane. Black dotted lines = levels corresponding to the cross sections shown in Fig. h and i.

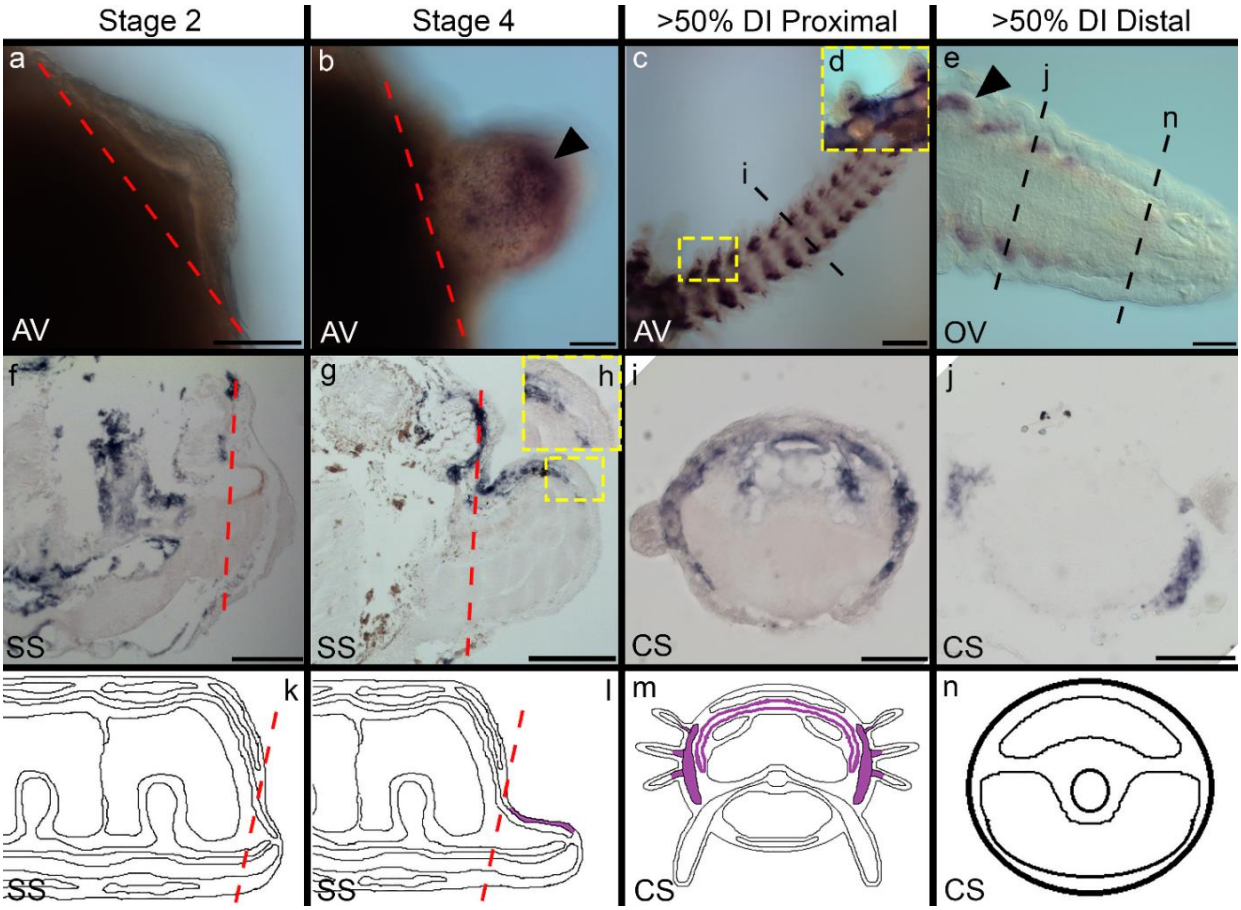


**Fig. 6.** *Afi-col-like C expression pattern at different regenerative stages*. 1st line: WMISH; 2nd line: post *in situ* sectioning; 3rd line: schemes. Stage 2 (first WMISH parameters): a, f, k. *Afi-col-like C* is not expressed in the regenerative bud. Stage 4 (first WMISH parameters): b, g, h, l. *Afi-col-like C* is expressed in the regenerate at the level of the aboral connective tissue (arrowhead). Stage >50% DI (first WMISH parameters): c, d, e, i, j, m, n. *Afi-col-like C* is expressed in the proximal side at the level of the lateral shields, at the base of the spines, in the aboral coelomic cavity epithelium and in the rim layer of the aboral intervertebral muscles, whereas in the distal side it is expressed in the developing lateral shields but not in the distal tip. *Abbreviations*: AV = aboral view; CS = cross section; OV = oral view; SS = sagittal section. Scale bars: a, b, e, f, g, j = 50 µm; h, i = 25 µm; c = 100 µm. In the schemes the gene expression pattern is shown in violet. Red dotted lines = amputation plane. Black dotted lines = levels corresponding to the cross sections shown in Fig. i, j and n.

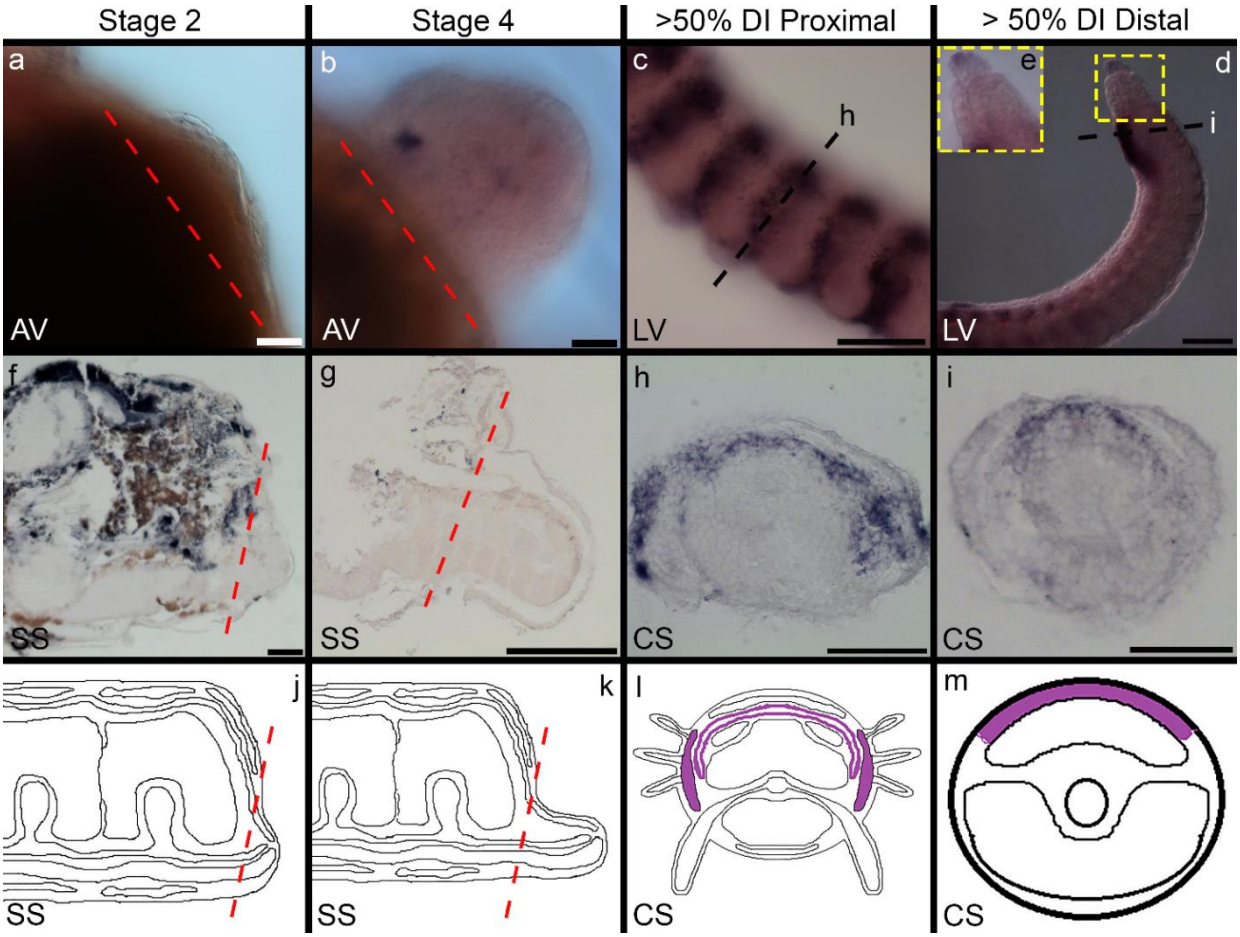


**Fig. 7.** *Afi-col-like D expression pattern at different regenerative stages*. 1st line: WMISH; 2nd line: post *in situ* sectioning; 3rd line: schemes. Stage 2 (first WMISH parameters): a, f, j. *Afi-col-like D* is not expressed in the regenerative bud. Stage 4 (first WMISH parameters): b, g, k. *Afi-col-like D* is not expressed in the regenerate. Stage >50% DI (second WMISH parameters): c, d, e, h, i, l, m. Using the first WMISH parameters no signal was detectable, whereas with higher probe concentration and increased hybridisation time, *Afi-col-like D* showed expression in the proximal side of the long regenerate at the level of the aboral coelomic cavity epithelium and of the lateral shields, whereas in the distal tip the signal is detectable in the aboral connective tissue and in the tip of the terminal podium. *Abbreviations*: AV = aboral view; LV = lateral view; CS = cross section; SS = sagittal section. Scale bars: a, b, d, f, g, h = 50 µm; c = 200 µm. In the schemes the gene expression pattern is shown in violet. Red dotted lines = amputation plane. Black dotted lines = levels corresponding to the cross sections shown in Fig. h and i.

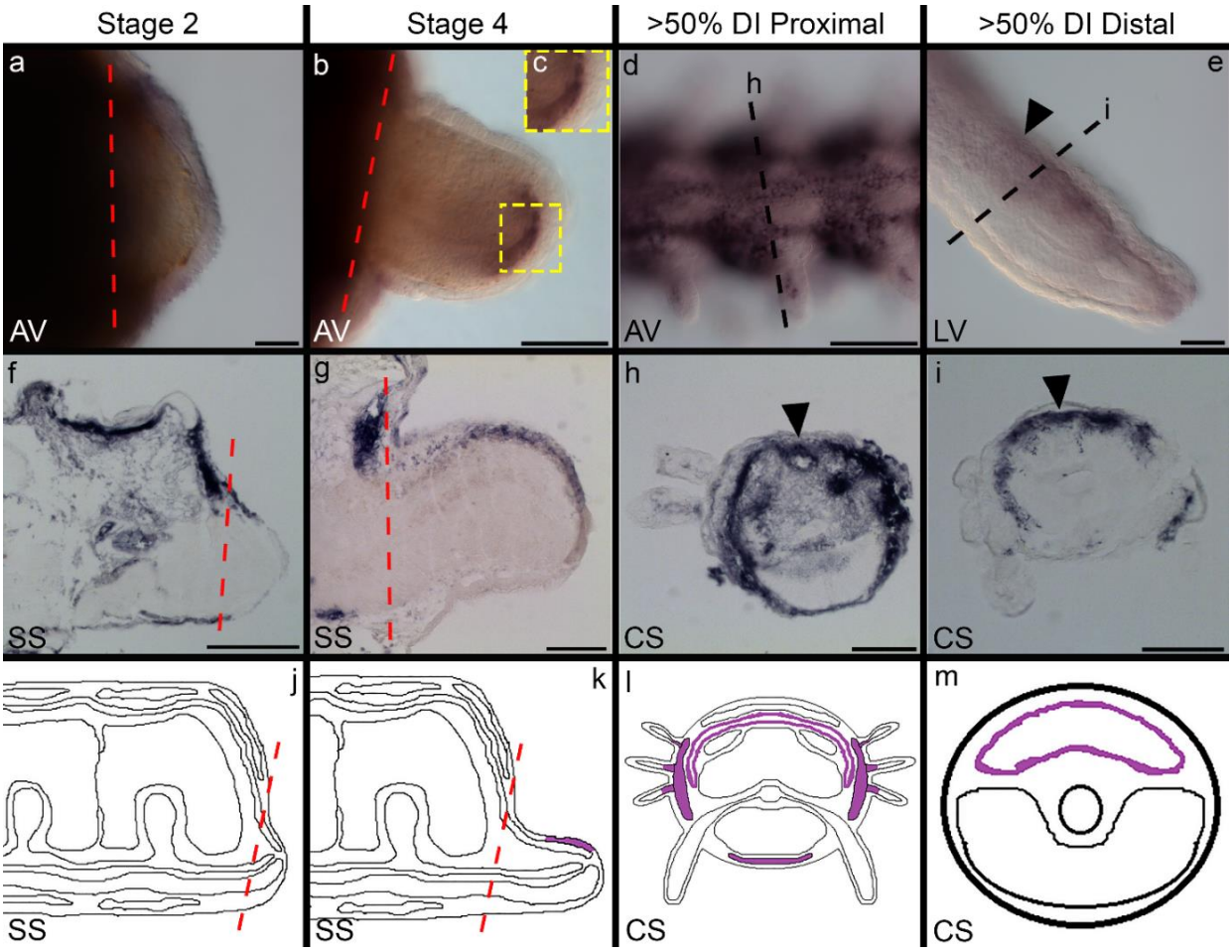


**Fig. 8.** *Afi-αcoll expression pattern at different regenerative stages*. 1st line: WMISH; 2nd line: post *in situ* sectioning; 3rd line: schemes. Stage 2 (second WMISH parameters): a, f, j. *Afi-αcoll* is not expressed in the regenerative bud. Stage 4 (first WMISH parameters): b, c, g, k. *Afi-αcoll* is expressed at the level of the aboral connective tissue of the regenerate. Stage >50% DI (second WMISH parameters): d, e, h, i, l, m. *Afi-αcoll* is detectable in the proximal side at the level of the lateral shields, the spines, the oral shield and the aboral coelomic cavity epithelium (arrowhead), whereas in the distal tip it is visible in the aboral coelomic cavity epithelium (arrowheads). *Abbreviations*: AV = aboral view; CS = cross section; LV = lateral view; SS = sagittal section. Scale bars: a, b, e, f, g, h, i = 50 µm; d = 100 µm. In the schemes the gene expression pattern is shown in violet. Red dotted lines = amputation plane. Black dotted lines = levels corresponding to the cross sections shown in Fig. h and i.

### *3.2.2. Expression patterns of the extracellular matrix (ECM) genes*

In order to better understand the role of the other ECM components during the whole regenerative process, the expression patterns of the four identified ECM molecule-related genes is analysed in the previously mentioned stages. Expression patterns in the stump tissues are investigated as well.

The two identified laminin transcripts display different expression patterns at all stages. *Afi-Lamα-L* is expressed at all stages and in different tissues. In particular, at stage 2 (Fig.

9a, g, k) and 4 (Fig. 9b, h, l) it is localised in the epidermis, whereas at stage >50% DI it is expressed in the radial water canal and in the tip of the spines in the proximal segments (Fig. 9c, d, e, i, m), and in the distal part it is visible in the epidermis but is absent in the terminal podium (Fig. 9f, j, m). On the contrary, using both first (Fig. S6) and second WMISH parameters (Fig. S8), *Afi-Lamβ-L* is not detectable neither in the regenerative tissues at all stages nor in the stump tissues.

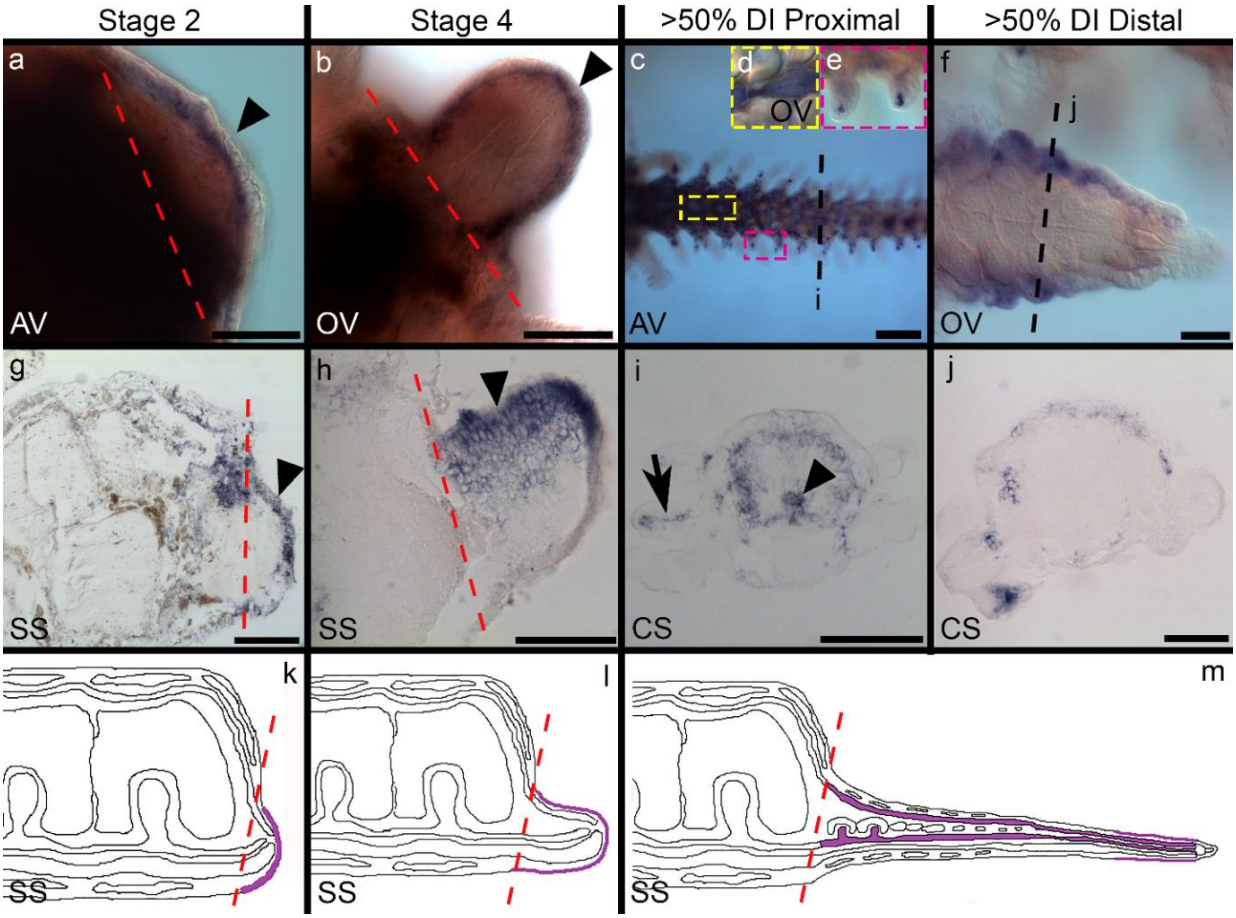


**Fig. 9.** *Afi-Lamα-L expression pattern at different regenerative stages*. 1st line: WMISH; 2nd line: post *in situ* sectioning; 3rd line: schemes. Stage 2 (first WMISH parameters): a, g, k. *Afi-Lamα-L* is expressed in the epidermis (arrowheads) of the regenerative bud. Stage 4 (first WMISH parameters): b, h, l. *Afi-Lamα-L* is expressed in the epidermis (arrowheads) of the regenerate. Stage >50% DI (first WMISH parameters): c, d, e, f, i, j, m. *Afi-Lamα-L* is expressed in the proximal side at the level of the radial water canal (arrowhead), the aboral coelomic cavity epithelium and at the tip of the spines (arrow), whereas it is expressed in the epidermis in the distal side of the long regenerate. *Abbreviations*: AV = aboral view; CS = cross section; OV = oral view; SS = sagittal section. Scale bars: a, b, f, h, j = 50 µm; c, g, I = 100 µm. In the schemes the gene expression pattern is shown in violet. Red dotted lines = amputation plane. Black dotted lines = levels corresponding to the cross sections shown in Fig. i and j.

The identified ECM protein gene, *Afi-ECM-protein*, shows no expression in the regenerative bud at stage 2 (Fig. S7a, e, i) but also in more differentiated regenerating arms at stage 4 (Fig. S7b, f, l) and >50% DI (Fig. S7c, d, g, h, m). To confirm these data, we performed WMISH using the second parameters and again no signal is visible in all stages (Fig. S8). With both WMISH parameters there is no expression at the level of the non-regenerating stump tissues as well (Fig. S7 and S8).

The newly identified TIMP gene, *Afi-TIMP3*, does not show expression neither during early regenerative phase (stage 2; Fig. 10a, e, i) nor during advanced regenerative phases, namely stage 4 (Fig. 10b, f, j) and stage >50% DI, using the first WMISH parameters. Therefore, we performed WMISH using second parameters and in this case only at stage >50% DI a faint signal at the level of the aboral coelomic cavity epithelium is detectable from both whole mount and post *in situ* sectioning at the level of the proximal side of the long regenerate (Fig. 10c, g, k) and no signal is present in the distal tip (Fig. 10d, h, k).

Overall, our results showed that different ECM molecule-related transcripts are spatially and temporally differentially expressed suggesting that ECM components are constantly remodelled during regeneration and that different tissues are involved in this process.

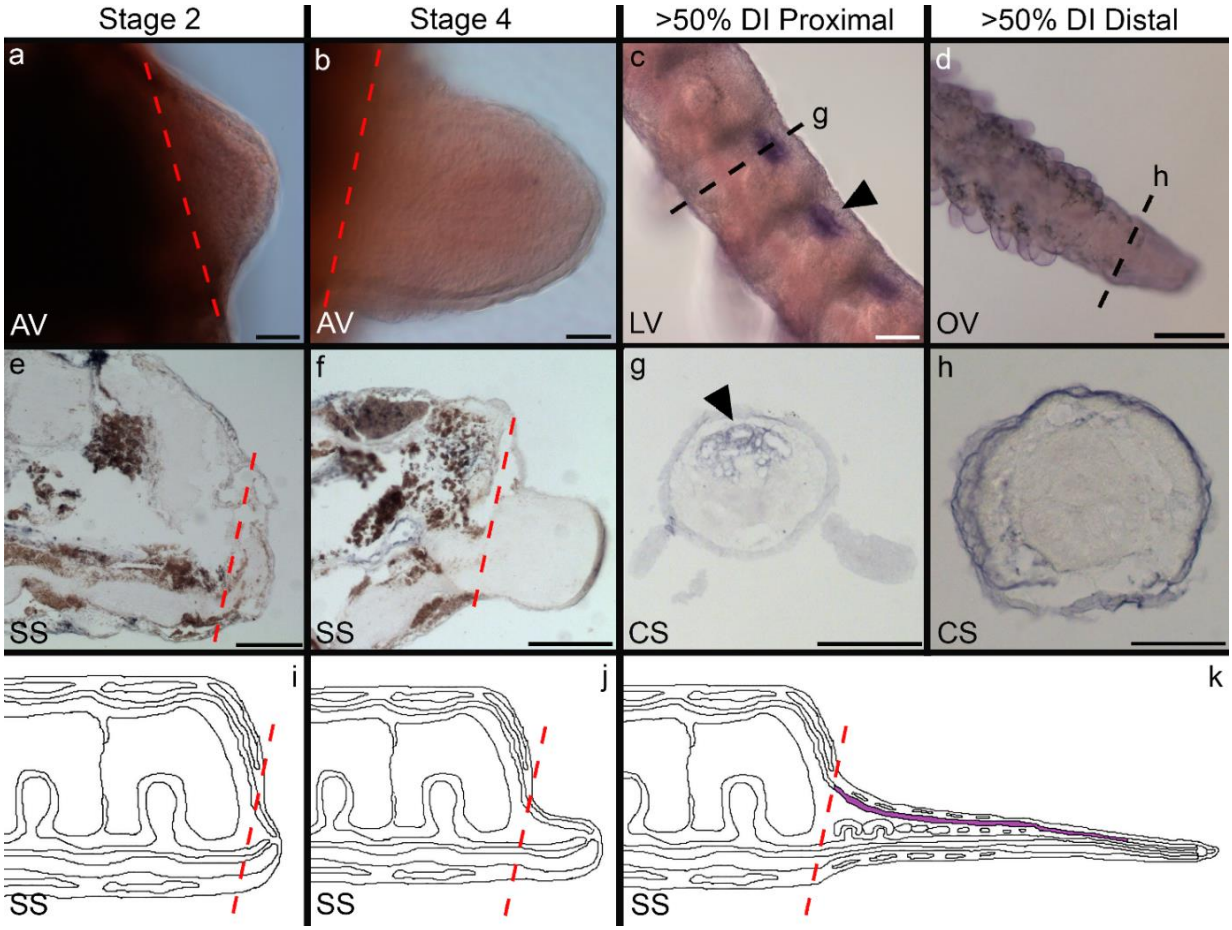


**Fig. 10.** *Afi-TIMP3 expression pattern at different regenerative stages*. 1st line: WMISH; 2nd line: post *in situ* sectioning; 3rd line: schemes. Stage 2 (first WMISH parameters): a, e, i. *Afi-TIMP3* is not expressed in the regenerative bud. Stage 4 (first WMISH parameters): b, f, j. *Afi-TIMP3* is not expressed in the regenerate. Stage >50% DI (second WMISH parameters): c, d, g, h, k. *Afi-TIMP3* is detectable at the level of the aboral coelomic cavity epithelium in the proximal side of the long regenerate, whereas no expression is visible in the distal tip. Note that the blueish staining visible in the long regenerate tip (d, h) cannot be considered a specific signal. *Abbreviations*: AV = aboral view; LV = lateral view; SS = sagittal section. Scale bars: a, b, e, f = 50 µm; c, d, g = 100 µm; h = 25 µm. In the schemes the gene expression pattern is shown in violet. Red dotted lines = amputation plane. Black dotted lines = levels corresponding to the cross sections shown in Fig. g and h.

## *4. Discussion*

### *4.1. Collagen-like genes are differentially expressed during regeneration*

Collagen, both fibrillar and nonfibrillar, is the main component of the connective tissues and basal laminas, therefore studying its gene expression is important to better understand the role of these tissues during regeneration, especially taking into account that developing structures (e.g. ossicles and muscles) normally differentiate in strict association with the dermal collagen, which actually acts as a fibrillar supporting scaffold (Okazaki and Inoué, 1976; Blankenship and Benson, 1984). We identified and studied

the gene expression patterns of five collagen-like genes and Burns and co-workers (2011) describe a high expression of collagen during *A. filiformis* regeneration at stages 4, 50% and 95% DI. Considering all the selected collagen-like genes, the overall view of their spatial-temporal expression patterns suggests a delay in their activation: indeed, most of them are not expressed at stage 2 (that can be regarded as an early regenerative phase), whereas they are differentially spatially localised at stages 4 and >50% DI, suggesting the involvement of different tissues in collagen-like molecule deposition. Collagen has been studied by immunohistochemical techniques in the sea cucumber *H. glaberrima* during intestinal regeneration (Quiñones *et al.*, 2002). The authors describe that fibrous collagen presence is reduced during the first 2 weeks after evisceration. Similarly, in the regenerating nerve cord (RNC) of the same species (Mashanov *et al.*, 2014) a reduced expression of collagen genes in comparison with normal RNC is detectable 2 days after injury followed by an up-regulation of the fibrillar collagen at the 12$^{th}$ day of regeneration. All together, these results seem partially in agreement with our findings, where a delay in collagen gene expression is observable since the selected collagen genes are mainly expressed from stage 4 onward and not during the wound healing/early regenerative events. Moreover, this delay in collagen and extracellular matrix deposition, together with collagen degradation events, has been directly connected with cell migration and proliferation during the early phases of regeneration that the authors suggest as being fundamental for the subsequent efficiency of the regenerative process (Quiñones *et al.*, 2002; Cabrera-Serrano and García-Arrarás, 2004). Our data indicate that collagen production is apparently performed by cell belonging to different tissues, such as dermal tissue, epidermis, coelomic lining and skeletal elements. Epithelia of all animals usually produce network-forming (*i.e.* nonfibrillar) collagen (e.g. type IV) for their basal laminas and skeletal elements of echinoderms present also a conspicuous collagenous component (as typical dermal skeleton; Hyman, 1955; Byrne, 1994), thus these tissues are likely to be involved in collagen production. In particular, *Afi-col-L A* expression at the level of the epidermis at stage 4 can be well explained taking into account that this transcript, according to Ricard-Blum (2011), can be regarded as a network-forming collagen. This group includes also chains forming collagen IV, typical of basal laminas, therefore, it is possible to hypothesise that the epidermis expressing this transcript is actively synthetizing/remodelling its basal lamina. Several *in vitro* and *in vivo* studies on mammal epithelial cells show that these are able to produce many components of the extracellular matrix (Green and Goldberg, 1965; Jaffe *et al.*, 1976; Alitalo *et al.*, 1980;

Campochiaro *et al.*, 1986). Czarkwiani and co-workers (2013) describe the expression of the collagen gene *Afi-αcoll* at the level of the skeletal elements (*i.e.* lateral shields and spines) in this species in long regenerating arms, thus highlighting that cells filling or associated with the trabecular stereom produce collagen during regeneration. This result is confirmed by our analyses with the same gene, which show also the expression of this transcript at the level of the oral shield and of the coelomic epithelium, suggesting a possible role of the latter tissue in collagen production as well or in the production of cells that will produce collagen. The expression at the level of the aboral dermal layer, particularly at stage 4, suggests that both the selected fibril-forming collagen genes (*Afi-col-L B* and *Afi-αcoll*) and the FACIT gene (*Afi-col-L C*) are expressed in a quite advanced regenerative phase where collagen fibrils are needed to create a well-organized scaffold for tissue re-growth. We can hypothesise that cells expressing these transcripts will be likely involved in collagen production at the level of the dermal layer of the regenerate where spicule formation is localised as well (Czarkwiani *et al.*, 2016), thus likely creating the collagen scaffold needed for skeleton regeneration. A noteworthy feature is that all selected genes are expressed at the level of the coelomic lining, even if at different regenerative stages and in different tissues of coelomic origin (*i.e.* aboral coelomic cavity epithelium or inner lining of the podia). This may indicate that the coelomic lining is actively involved in collagen production and its cells express collagen genes in both already well-differentiated tissues (e.g. proximal side of the long regenerate) and more undifferentiated tissues (e.g. re-growing area of the distal tip of the long regenerate). *Afi-col-L A* is expressed in the late stages of regeneration in this tissue, therefore, as previously suggested for the epidermis, its expression can be likely connected with basal lamina production/remodelling. *Afi-col-L B* is expressed in the tip of the aboral coelomic cavity epithelium at stage 2 and this pattern is consistent with a possible role of the "immune system activity" of the coelomic cells, circulating cells of the coelomic cavities, at this early regenerative phase. It is known that coelomocytes in echinoderms have a role in the immune response after injury and that the coelomic epithelium is one of the most likely source of these cells also during regeneration (Hernroth *et al.*, 2010). Indeed, after injury, together with phagocyte clot formation, spherule cells (one of the coelomocyte sub-population; Smith, 1981; Karp and Coffaro, 1982) produce collagen materials to help wound closure and the following regenerative process (Chia and Xing, 1996). Further analyses, e.g. cell tracking, are necessary to confirm this hypothesis.

The absence of expression of some genes in the non-regenerating stump tissues suggests that these transcripts are expressed at different stages of regeneration but are not expressed when the tissues are already well differentiated as in the stump. Another possibility could be that the genes are expressed at a so low level that are not detectable by chromogenic *in situ* technique. Quantitative analyses (e.g. RT-PCR) focused on dissected part of the regenerative arms as well as the stump tissues could help to shed light on this possibility.

In other invertebrates, e.g. planarians, collagen gene knock-down leads to faster eye regeneration (Yun, 2014), suggesting that collagen deposition can inhibit cell migration and the regenerative process in general. Studies on vertebrate regeneration, e.g. zebrafish (González-Rosa *et al.*, 2011), describe how myocardial regeneration is compatible with scar formation (*i.e.* collagen deposition) and subsequent scar regression. In amphibian limb regeneration collagen deposition is suggested being highly reduced consequently favouring the regenerative process (Satoh *et al.*, 2012). All together, these data suggest that the delay in collagen gene activation and likely protein production could avoid scar/fibrotic tissue formation, as happens for example after mammal injuries, thus likely promoting the subsequent regenerative process. Therefore, understanding the role of collagen during repair and regenerative phases in brittle star is important for comparing the striking regenerative abilities of echinoderms with those, highly reduced, of mammals.

### *4.2. ECM genes are differentially expressed during regeneration*

#### *4.2.1. Laminin*

Laminin is one of the main component of the basal laminas, thus it is involved in ECM repair and remodelling phenomena after injury where the epithelia are completely disrupted by the damage. From our analyses *Afi-Lamα-L* and *Afi-Lamβ-L* are similar to *α* and *β* laminin subunits respectively. As laminin is a heterotrimer composed of one *α*, one *β*, and one *γ* chain, it is quite surprising that expression of the *β* subunit gene is not detected at any regenerative stage. However, considering that the *A. filiformis* transcript analysed in this study is similar to subunit *β*-2 but in the sea urchin genome two different *β* subunit (1-like and 2-like) are described, it could be possible that the identified gene in *A. filiformis* is encoding for the other subunit or it is not expressed in the *A. filiformis* regenerative stages here investigated. Further studies, such as quantitative RT-PCR, are needed to clarify if its expression level could be so low that it is not detectable by chromogenic WMISH technique. On the contrary, the expression pattern of the *α* subunit

gene better fits our expectations. Indeed, laminin is synthetized by the epithelial cells and a signal in the epidermis at each regenerative stage is detected, even if its presence only in stages 2 and 4 and only in the distal tip at advanced stages could suggest that this transcript is highly involved during the first phases of repair and regeneration and at the level of the most “undifferentiated” tip at advanced stages, whereas it is not expressed or with at a highly reduced level in the epidermis when the arm is already well differentiated. The expression of this transcript at the level of the radial water canal epithelium only in the late stages of regeneration suggests that also this tissue is involved in basal lamina production and differentiation. This result is confirmed also by its expression in the same tissue at the level of the stump and in the radial nerve cord as well (Fig. S6). The signal in the tips of the spines in the long regenerate well fits with the fact that laminin is known to be involved also in nervous system development, remodelling and nervous cell migration (Barros *et al.*, 2011). Indeed, spines of brittle stars are described to possess sensory functions (Delroisse *et al.*, 2014) and we can hypothesise that the expression of this transcript in these structures is connected with these sensory functions due to nervous system presence. Its expression in the stump radial nerve cord is also consistent with the known role of laminin in nervous system development, remodelling and regeneration (Liesi *et al.*, 1984), suggesting that the differentiated radial nerve cord could be constantly involved in remodelling events. Considering other echinoderms, laminin *α* subunits have been shown to be up-regulated during *H. glaberrima* gut regeneration from 3 to 14 days post-evisceration (Ortiz-Pineda *et al.*, 2009) and *A. japonicus* gut and body wall regeneration at 4 and 7 days (Sun *et al.*, 2011), thus suggesting its involvement during both repair and regenerative phases as described for *A. filiformis*.

*4.2.2. ECM-protein*

From both EchinoBase and NCBI BLAST search, *Afi-ECM-protein* can be regarded as a FRAS1-related extracellular matrix protein 1, containing a C-type lectin-like (CTLD) domain (NCBI cDART analysis). This domain is usually present in proteins involved in extracellular matrix organisation, endocytosis, complement activation, pathogen recognition and cell-cell interactions. FRAS1-related extracellular matrix protein 1 has been shown to be fundamental for example for adhesion in mouse embryonic epidermis and epidermal structures (Short *et al.*, 2007) but, at the best of our knowledge, it has not been studied in echinoderms so far. This transcript is not expressed at all stages of regeneration here investigated and with both WMISH parameters. Nevertheless, we

cannot exclude a low expression that could be detected by quantitative RT-PCR or an expression in different regenerative stages, e.g. within few days post-amputation where transcripts encoding for proteins involved in immune response-like activities are likely to be activated. Further analyses are necessary to finally define the expression pattern of this gene at least in the three regenerative stages here considered.

*4.2.3. TIMP3*

TIMPs (*i.e.* tissue inhibitors of metalloproteinases) are important molecules for tissue remodelling and regeneration. The absence of expression of *Afi-TIMP3* during the first ~ 8 days after injury suggests that high levels of connective tissue remodelling is taking place via metalloproteinase (MMP) activity. Further molecular studies focusing on MMPs during *A. filiformis* regeneration and quantitative analyses are necessary to confirm this hypothesis. Depending on the species, between three and six tissue inhibitor of metalloproteinases (TIMPs) have recently been described in ophiuroids (Clouse *et al.*, 2015) but no molecular data have been available till now on their expression patterns during arm regeneration. From our cDART analyses, *Afi-TIMP3* contains a NTR-like domain (also called netrin module), typical of this protein class. So far, TIMP expression during regeneration has been evaluated only in another echinoderm species, the sea cucumber *H. glaberrima*. During nervous system regeneration Mashanov and co-workers (2014) discover that TIMPs are up-regulated in the radial organ complex (*i.e.* radial nerve cord, radial water canal and longitudinal muscle band) throughout the whole regenerative process. These data do not completely fit with our results where no expression is detectable before two-three weeks after arm amputation (advanced regenerative stages). In particular, *Afi-TIMP3* is homologous to the TIMP3 described as up-regulated at days two and twenty in the sea cucumber, therefore our transcript presents a diverse expression than that of the radial organ complex since, differently from sea cucumber, no expression is detectable few days post arm amputation. These differences could be explained by the great diversity in tissue complexity between the two experimental models: a more consistent tissue remodelling by MMPs could be hypothesised for brittle star arm tissues in comparison to sea cucumber radial nerve cord. However, since qualitative *in situ* hybridisation analysis on *A. filiformis* are here compared with quantitative analysis in the sea cucumber it could be as well that this latter is needed to reveal signal in the first stages of regeneration in the brittle star. Moreover, being possible that each gene encodes for more than one TIMP, a similar expression to that detected in

sea cucumber could be shown by an another *A. filiformis* TIMP here not investigated. Hence, further analyses are necessary to shed light on this issue.

### *4.3. Conclusion and perspectives*

The brittle star *Amphiura filiformis* is a good model to study the arm regenerative process after traumatic amputation from both a morphological and a molecular point of view (Biressi *et al.*, 2010; Czarkwiani *et al.*, 2016). The involvement of the connective tissue during arm regeneration has never been properly investigated in this species. Therefore, in the present work, we focused our molecular analyses on extracellular matrix (ECM) molecule-related genes, with a special attention to collagen, in order to understand their involvement during brittle star arm regeneration.

Table 1 summarises the expression patterns of the 9 identified genes considering the whole regenerative process. Our results showed that the selected collagen-like genes present different spatial-temporal expression patterns suggesting that different collagen types are involved during regeneration at different stages and in different tissues, thus differentially contributing to connective tissue remodelling and deposition. In particular, almost all collagen transcripts are not expressed in the early regenerative phase (stage 2), thus indicating that a delay in collagen gene activity and more likely of collagen protein deposition could be connected with high efficiency of regeneration, as previously suggested for other echinoderms (Quiñones *et al.*, 2002; Cabrera-Serrano and García-Arrarás, 2004). Besides collagen, other ECM-related molecule genes display dynamic spatial-temporal expression patterns, being expressed at different time points and in different tissues. Overall, our data showed that collagen and ECM-related molecule genes are differentially involved from both a spatial (tissue and structures) and temporal (regenerative stages) point of view. Other molecular analyses, *i.e.* quantitative RT-PCR, will be useful to expand and confirm *in situ* hybridisation results. Moreover, the selection of further genes (both other collagen types and ECM-molecules, such as MMPs, proteoglycans, fibronectin, integrins, etc.) will help to detail and complete the overall comprehension of the role of the connective tissue during *A. filiformis* arm regeneration in perspective of comparative studies with mammal wound closure and regenerative phenomena.

**Table 1.** *Summary of the expression patterns of the 9 identified genes during the whole regenerative process at the level of the regenerates (the expression patterns detected at the level of the stump tissues is not showed).* a) Scheme of stage 2. b) Scheme of stage

◀ 4. c) Scheme of stage >50% DI. For colour legend of the schemes see the caption of Fig. 2. Red dotted lines = amputation plane. White square = absence of expression. *Abbreviations*: ACC = aboral coelomic cavity, AS = aboral shield, CT = connective tissue, E = epidermis, LS = lateral shield, M = muscle, OS = oral shield, RNC = radial nerve cord, RWC = radial water canal, S = spine, P = podium, TO = terminal ossicle, TP = terminal podium, V = vertebra.

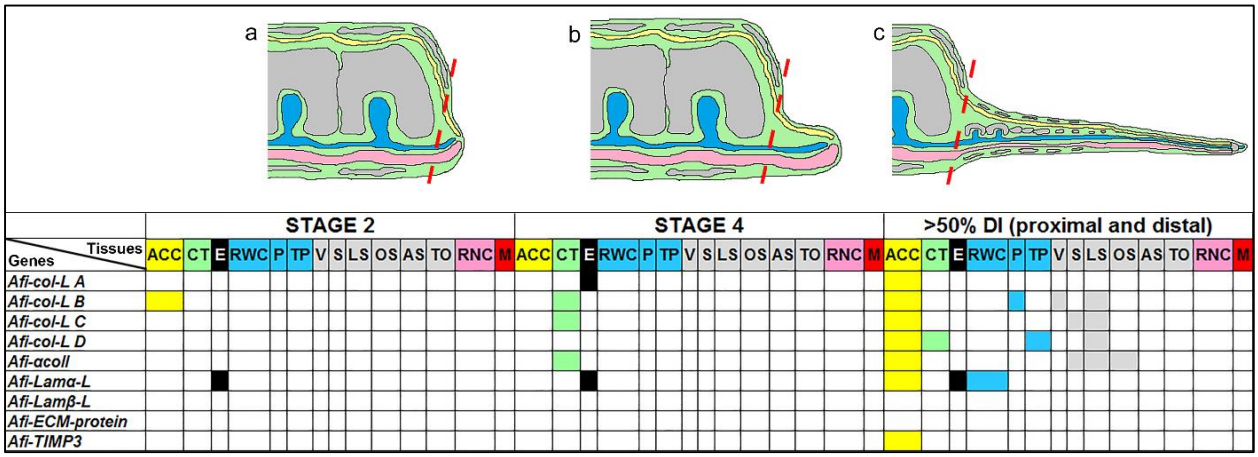


## *5. Supplementary Materials*

### *5.1. Extended Materials and Methods*

#### *5.1.1. Molecular analyses*

##### *5.1.1.1. Primer design for cloning PCR*

Primers were selected considering primer length, Tm and product length. Moreover, primer specificity was checked performing a re-BLAST to *A. filiformis* transcriptome database (Dylus *et al.*, *submitted*). Upon arrival, 100 µM stock were prepared by adding the proper volumes of NF-$H_2O$ into lyophilised products and stored at -20°C until use. Table A summarises all designed primers with their sequence, length, Tm and expected PCR product size. All primers were tested at least once using *A. filiformis* cDNA from different embryonic or regenerating (adult) stages. Only the successful ones (labelled in red in Table A) followed the subsequent steps (see below).

**Table A.** *List of the tested primers with their sequences, lengths, Tm and the expected PCR product lengths.* Only with primers in red genes were successfully cloned and the following protocols were performed. For primers of *Afi-αcoll* see Czarkwiani and co-workers (2013). *Abbreviations*: bp = base pair; Tm = primer melting temperature.

| Primer Name | Primer Sequence | Primer Length (bp) | Tm (°C) | Expected Product Length (bp) |
|---|---|---|---|---|
| ***Afi-actin F*** | ACGACGAAGTATCCGCTTTG | 20 | 60.27 | 853 |
| ***Afi-actin R*** | TCGCATTTCATGATGCTGTT | 20 | 60.23 | 853 |

| | | | | |
|---|---|---|---|---|
| ***Afi-fibr F*** | AGATGGTGGTCGCTCATTTC | 20 | 60.08 | 510 |
| ***Afi-fibr R*** | CAGATGATGCCTTTGCCATA | 20 | 59.65 | 510 |
| ***Afi-fibrillin F*** | GTTGGCTTCCAACTCAGCTC | 20 | 60 | 1605 |
| ***Afi-fibrillin R*** | ACAAGCATCGGGAAACATTC | 20 | 59.94 | 1605 |
| ***Afi-fibnec F*** | CCACCTGTGGTGGGTAAAGT | 20 | 59.74 | 941 |
| ***Afi-fibnec R*** | TCAAACGACACTGCCATCTC | 20 | 59.84 | 941 |
| ***Afi-tenascin F*** | CCAGACCCAGGTCATCCTAA | 20 | 59.92 | 312 |
| ***Afi-tenascin R*** | TGATTCAACGGCAACTTCAG | 20 | 59.84 | 312 |
| ***Afi-versican F*** | TTTGCACATTGGGTTGACAT | 20 | 59.82 | 372 |
| ***Afi-versican R*** | CAGGGTAGGCATGCTCAGTA | 20 | 58.9 | 372 |
| ***Afi-HS F*** | GCTAGCAATGAGGCTGGAAC | 20 | 59.98 | 1671 |
| ***Afi-HS R*** | GGCAGAATTGCGAGCTAAAC | 20 | 59.99 | 1671 |
| ***Afi-PG F*** | GCTAGCAATGAGGCTGGAAC | 20 | 59.98 | 1671 |
| ***Afi-PG R*** | GGCAGAATTGCGAGCTAAAC | 20 | 59.99 | 1671 |
| ***Afi-CS F*** | CAAGTTGCGGACGGTTATTT | 20 | 60 | 1325 |
| ***Afi-CS R*** | AACAGGCCGTCGTCAATATC | 20 | 59.96 | 1325 |
| ***Afi-chonss F*** | ACGGCGAGAGTTATGGAGTG | 20 | 60.28 | 2343 |
| ***Afi-chonss R*** | GCAACATCTGCCTCCTCTGT | 20 | 60.42 | 2343 |
| ***Afi-cola1 F*** | AGGAACGGTAACCGAGGTCT | 20 | 59.99 | 1914 |
| ***Afi-cola1 R*** | ATTAGGACCTGCACCACCAG | 20 | 59.99 | 1915 |
| ***Afi-col-L A F*** | CAACACCGACAGAACCAGAA | 20 | 59.72 | 778 |
| ***Afi-col-L A R*** | TGTTGTGTTGGCACCTCTTC | 20 | 59.73 | 778 |
| ***Afi-col-L B F*** | AACCGGGTATTCCTGGATTC | 20 | 60.02 | 894 |
| ***Afi-col-L B R*** | GTTCACCAACTCGTCCCACT | 20 | 60.01 | 894 |
| ***Afi-col-L C F*** | ACGTAAACGTTGGCATCTCC | 20 | 60 | 1014 |
| ***Afi-col-L C R*** | GTGATCGGCCTGATTGATCT | 20 | 60.04 | 1014 |
| ***Afi-col-L D F*** | CATAGTGCTTTCCCGGTTGT | 20 | 59.99 | 1122 |
| ***Afi-col-L D R*** | ATCACCGTCTGGTCCTATCG | 20 | 59.95 | 1122 |
| ***Afi-a2colprec F*** | CAGCTGGATTCCCAGGATTA | 20 | 60.03 | 1436 |
| ***Afi-a2colprec R*** | GAAAGGTGTTGCACGGAAAT | 20 | 59.98 | 1436 |
| ***Afi-cola1XI F*** | GATTGATGGACCACCAGGAG | 20 | 60.33 | 1652 |
| ***Afi-cola1XI R*** | ATGGCAGTTGTGCTGAAACA | 20 | 60.31 | 1652 |
| ***Afi-col4a3 F*** | TGACGACGACTTGGAAAGTG | 20 | 59.87 | 588 |
| ***Afi-col4a3 R*** | GGGTCATCTGGTGAGCTTGT | 20 | 60.12 | 588 |
| ***Afi-cola5 F*** | CGAGGGACTATGGAAGGTCA | 20 | 60.07 | 834 |
| ***Afi-cola5 R*** | TACTCGATGCCTGGAATGGT | 20 | 60.48 | 834 |
| ***Afi-a2col F*** | GGTGCCACTTGTCCTGAAAT | 20 | 59.97 | 1687 |
| ***Afi-a2col R*** | GTGATCGGCCTGATTGATCT | 20 | 60.04 | 1687 |
| ***Afi-myohc F*** | GCTTCCTAATCCGCAGACAG | 20 | 59.98 | 1994 |
| ***Afi-myohc R*** | AGGCAGACTTGGACCAGAGA | 20 | 59.99 | 1994 |
| ***Afi-myo2lc F*** | CCTTGATGCCTTCCTGTTGT | 20 | 60.11 | 404 |
| ***Afi-myo2lc R*** | TGCTCATCACCATCTTCACC | 20 | 59.64 | 404 |
| ***Afi-myoV F*** | TCAACCAAGGAAGCGATCTT | 20 | 59.81 | 1743 |
| ***Afi-myoV R*** | GGGAATACGACGGAGAAGGT | 20 | 60.33 | 1743 |
| ***Afi-MMP21 F*** | CAGGACCACCTGCTTCATCT | 20 | 60.26 | 2090 |
| ***Afi-MMP21 R*** | CCAATAATCCTCGCCTTTGA | 20 | 60.03 | 2090 |
| ***Afi-MMP16 F*** | GGGTACGCCTTACCACTTGA | 20 | 59.99 | 1559 |
| ***Afi-MMP16 R*** | CCCAGTAATGTTGGCGTTCT | 20 | 59.99 | 1559 |
| ***Afi-MMP14 F*** | CTGCTGACGGGAGAACATTT | 20 | 60,25 | 513 |
| ***Afi-MMP14 R*** | CTGTTAGTCGCGGGTAGGAC | 20 | 59,76 | 513 |
| ***Afi-TIMP1 F*** | TTTGCTGGTTCTTGGTCAAA | 20 | 59.29 | 476 |
| ***Afi-TIMP1 R*** | ATATCTGGGCGACTGGAGTG | 20 | 60.1 | 476 |
| ***Afi-TIMP3bis F*** | CTATTTGTGCAGGCCAGGAG | 20 | 60.79 | 636 |

| | | | | |
|---|---|---|---|---|
| ***Afi-TIMP3bis R*** | CATACAGTCCCGCATCTCTG | 20 | 59.27 | 636 |
| ***Afi-TIMP3 F*** | CCTTCCTAAGCACCCACAAC | 20 | 59.59 | 653 |
| ***Afi-TIMP3 R*** | AACTTGCTTGGCACAACTCA | 20 | 59.49 | 653 |
| ***Afi-ficolin F*** | CGATGGACATGATGGAAATG | 20 | 59.73 | 837 |
| ***Afi-ficolin R*** | GAGGGCCGCCAAGATATAAT | 20 | 60.27 | 837 |
| ***Afi-ECM-protein F*** | AACCCAGCAATGGTAACAGC | 20 | 60 | 1983 |
| ***Afi-ECM-protein R*** | GACACTCTGCGTTGCGATAA | 20 | 60.02 | 1983 |
| ***Afi-fibronectin F*** | ACGGTGCTCTACAGCGAGTT | 20 | 60.08 | 1027 |
| ***Afi-fibronectin R*** | CCTTTCTGTGGCCGTATTGT | 20 | 59.99 | 1027 |
| ***Afi-laminin F*** | GGGATATTTGCGTCACCAGT | 20 | 59.82 | 293 |
| ***Afi-laminin R*** | GCCTGGATCTGATTGCTCTC | 20 | 59.92 | 293 |
| ***Afi-lamα F*** | GGCACACCATCTGAAACCTT | 20 | 59.97 | 1349 |
| ***Afi-lamα R*** | TGGTCACACCTACGGTCAAA | 20 | 60 | 1349 |
| ***Afi-lama2 F*** | GTGTGTGTCGGGAAGATGTG | 20 | 60 | 1170 |
| ***Afi-lama2 R*** | ACCTATCACATGTGCGTCCA | 20 | 59.99 | 1170 |
| ***Afi-Lamα-L F*** | GTGCTACCGGACCTCAATGT | 20 | 60 | 1017 |
| ***Afi-Lamα-L R*** | CTTCAGCTTGGCCTTGTAGG | 20 | 60.01 | 1017 |
| ***Afi-Lamβ-L F*** | CACATTAGGCACGGTGAATG | 20 | 59.99 | 1494 |
| ***Afi-Lamβ-L R*** | AACCCATCTTTGCACTGGTC | 20 | 59.97 | 1494 |
| ***Afi-P4H F*** | TCTCCAATCATGGGCCTACT | 20 | 59.51 | 1513 |
| ***Afi-P4H R*** | ACAGGTTTGCAGCCCATTT | 19 | 60.51 | 1513 |

*5.1.1.2. Amplification of specific cDNA fragments*

cDNA of *A. filiformis* at different embryonic and regenerative stages were already available in the laboratory and was used as template to perform gradient PCRs (see below for details). Amplified fragments of the correct molecular weight were then purified using the NucleoSpin® gel and PCR clean-up kit (Macherey-Nagel) according to manufacturer's instructions and eluted in a final volume of 18-19 µl of NE buffer; nucleic acid concentration was checked using a NanoDrop Spectrophotometer.

The gradient PCRs with *A. filiformis* cDNA were performed using Invitrogen reagents as follows:

| | |
|---|---|
| 10X buffer-$MgCl_2$ | 2.5 µl |
| 50 mM $MgCl_2$ | 0.75 µl |
| 10 mM dNTPs | 0.5 µl |
| 10 µM forward primer | 1.25 µl |
| 10 µM reverse primer | 1.25 µl |
| 10 ng cDNA of interest | 5 µl |
| 5 U/µl DNA *Taq* polymerase | 0.1 µl |
| NF-$H_2O$ | up to 25 µl |

Reactions were amplified as follows (ROCHEPR2 program):

| | | |
|---|---|---|
| 94°C | 3’ | 1 cycle |
| 94°C | 30’’ | 10 cycles |
| T gradient* | 30’’ | |
| 72°C | 1’30’’ | |
| 94°C | 30’’ | 25 cycles |
| T gradient* | 30’’ | |
| 72°C | Variable** | |
| 72°C | 7’ | 1 cycle |

*The temperatures of the gradient from the highest to the lowest were: 65°C, 62.5°C, 59.5°C and 55.9°C. In some cases, only two temperatures were used with a reaction volume of 50 µl. **The extension times were optimised according to the predicted product length (about 1 minute per 1000 bp).

1 or 2 µl of the PCR products were checked at NanoDrop Spectrophotometer to know the DNA concentration and 2 µl were loaded on a 1% TBE agarose gel to check the validity of the purification step. The remaining 15 µl were stored at -20°C for the following steps.

*5.1.1.3. Cloning of PCR fragments*

*5.1.1.3.1. Ligation*

In order to clone the genes of interest the amplified fragments were ligated into pGEM®-T Easy Vector System I (Promega; Fig. A) using the following ligation protocol:

| | |
|---|---|
| 2X or 10X ligation buffer | 5 or 1 µl |
| pGEM®-T Easy Vector (50 ng/µl) | 0.5 µl |
| Fragment of interest | x* |
| 3 Weiss units/µl T4 DNA Ligase | 1 µl |
| NF-$H_2O$ | Up to 10 µl |

*The fragment of interest was added in the reaction using an insert:vector molar ratio either 6:1 or 3:1 employing the following formulas:

- [25 ng vector x sample size (kb)/vector size (~ 3 kb)] x 6/1 or 3/1 = fragment in ng;
- fragment in ng/fragment concentration = volume of fragment in µl.

If the sample concentration was low the maximum possible volume (3.5 µl or 7.5 µl depending on the used ligation buffer) was added. The ligation reactions were then incubated overnight at 14°C.

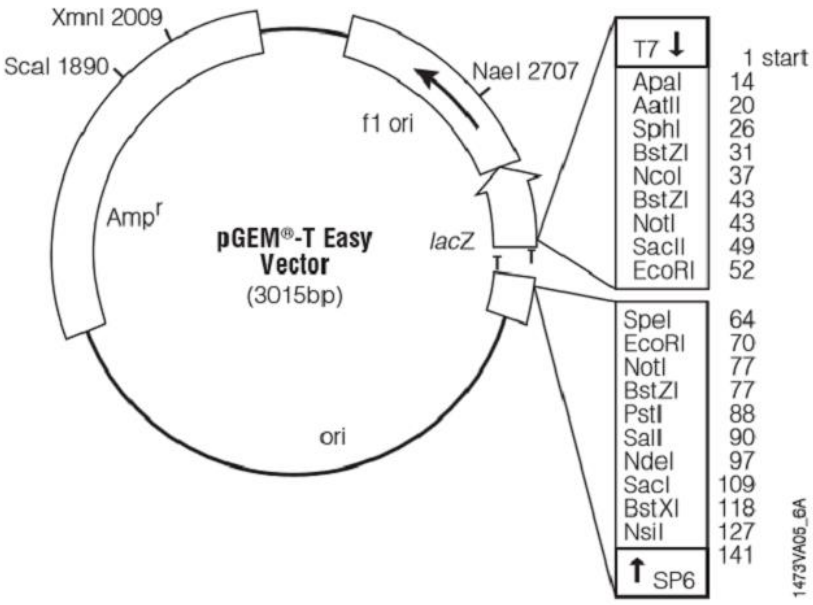


**Fig. A.** *Vector map of pGEM®-T Easy Vector System I (Promega).* Note the presence of Sp6, T7 and EcoRI restriction enzyme.

*5.1.1.3.2. Transformation*

Plasmid with the inserted fragment of interest were then transformed in Subcloning Efficiency™DH5α™ Competent cells (Invitrogen). 5 µl of the ligation were added to 50 µl of bacterial aliquots and incubated 30 minutes on ice. Heat shock was then performed in a water bath at 42°C for 20 seconds followed by a cooling step on ice for 2 minutes. 950 µl of S.O.C. medium (Life Technology) were added and the samples were incubated at 37°C for 1 hour at 225 rpm. Samples were centrifuged at 11000 g for 30 seconds to concentrate them and reduce the volume. The remaining 100 µl, after re-suspension, were plated onto agarose plate with 100 µg/ml ampicillin and 20 µg/ml X-gal for the subsequent colony selection (see below). In some cases, the bacteria suspension was directly supplemented with further 100 µg/ml ampicillin (5 µl) to avoid satellite colonies. Plates were then incubated overnight at 37°C. The day after colonies in each plate were counted to check the transformation efficiency and the colony PCR was performed only on the successful plates (see below). Plates were stored at 4°C till the results of the colony PCR (see below).

*5.1.1.3.3. Colony selection through colony PCR*

The pGEM®-T Easy Vector System I (Promega; Fig. A) contains ampicillin resistance gene and *lacZ* gene used to select the successfully transformed colonies, with the insertion of a fragment (white). At least 6 white single colonies and 1 negative control

(blue), possibly without insertion of the fragment of interest, were picked from the plates, added to 20 µl of LB Broth with 100 µg/ml ampicillin and incubated at 37°C for 1 hour. Colony PCR was performed to assess the size of the cloned fragment using Invitrogen reagents as follows:

| | |
|---|---|
| 10X buffer-$MgCl_2$ | 2 µl |
| 50 mM $MgCl_2$ | 0.6 µl |
| 10 mM dNTPs | 0.4 µl |
| 10 µM Sp6 primer | 0.8 µl |
| 10 µM T7 primer | 0.8 µl |
| Colony | 2 µl |
| 5 U/µl DNA *Taq* polymerase | 0.2 µl |
| NF-$H_2O$ | up to 20 µl |

Reactions were amplified as follows (AGACOLON program):

| | | |
|---|---|---|
| 95°C | 1’ | 1 cycle |
| 94°C | 30’’ | 30 cycles |
| 55°C | 30’’ | |
| 72°C | 1’30’’ | |
| 72°C | 10’ | 1 cycle |

PCR products were loaded on a 1% TBE agarose gel using 10 µl of PCR product and 2.5 µl of 6x Loading Buffer and run for 25 minutes at 100 V. Only colonies showing the right bands were selected and 5 µl of the bacteria suspension were added to 4 ml of LB with 100 µg/ml ampicillin and incubated overnight at 37°C at 225 rpm in order to grow the corresponding bacteria and subsequently prepare the glycerol stocks (see below).

*5.1.1.3.4. Plasmid purification*

To prepare the glycerol stocks 750 µl of bacteria suspension were added at 750 µl of 50% glycerol, well mixed and immediately stored at -80°C.

The remaining 3.25 ml of bacteria (from the starting 4 ml) were used to purify plasmids with the NucleoSpin® Plasmid Mini-Prep kit (Macherey-Nagel) following manufacture’s protocol. Plasmids were eluted from the column in 50 µl of AE buffer or 10 mM Tris. The DNA concentration was checked with a NanoDrop Spectrophotometer using 2 µl of purified plasmids. The remaining 48 µl were stored at -20°C for the following steps.

*5.1.1.3.5. Diagnostic digestion*

When colony PCR results were not clear plasmids were digested with EcoRI restriction enzyme (Promega) with the following protocol:

| | |
|---|---|
| 10X Restriction buffer H (Promega) | 2 µl |
| NF-$H_2O$ | 15.8 µl |
| Plasmid sample | 2 µl |
| 12 U/µl EcoRI restriction enzyme | 0.2 µl |

The reaction mixes were incubated at 37°C for 1-2 hours and subsequently checked on an agarose gel using 10 µl of digestion product and 2.5 µl of 6x Loading Buffer and run for 25 minutes at 100 V.

*5.1.1.3.6. Orientation PCR*

Given the fact that the ligation of the fragment in pGEM-T vectors is not directional, the orientation of the cloned fragment needs to be assessed to then transcribe an antisense probe. To check the orientation of the fragment we used PCR with an internal (fragment specific) and an external (vector specific) primer and the purified plasmid as template (see Fig. B). Two different equivalent strategies were followed using the purified plasmid as template. The first one using Invitrogen reagents as follows:

| | |
|---|---|
| 10X buffer-$MgCl_2$ | 2 µl |
| 50 mM $MgCl_2$ | 0.6 µl |
| 10 mM dNTPs | 0.4 µl |
| 10 µM specific F/R primer* | 0.8 µl |
| 10 µM Sp6/T7 primer* | 0.8 µl |
| 1 ng/µl purified plasmid | 1 µl |
| 5 U/µl DNA *Taq* polymerase | 0.2 µl |
| NF-$H_2O$ | up to 20 µl |

*For each fragment of interest four tubes were prepared using the following primer combinations:

1) Sp6 and specific reverse;
2) Sp6 and specific forward;
3) T7 and specific forward;
4) T7 and specific reverse.

Reactions were amplified as follows (AGACOLON program):

| | | |
|---|---|---|
| 95°C | 1’ | 1 cycle |
| 94°C | 30’’ | 30 cycles |
| 55°C | 30’’ | |
| 72°C | 1’30’’ | |
| 72°C | 10’ | 1 cycle |

The second one was performed using Invitrogen reagents as follows:

| | |
|---|---|
| 10X buffer-$MgCl_2$ | 5 µl |
| 50 mM $MgCl_2$ | 3 µl |
| 10 mM dNTPs | 1 µl |
| 10 µM primer* | 1.5 µl |
| 10 µM primer* | 1.5 µl |
| 1 ng/µl purified plasmid | x µl |
| 5 U/µl DNA *Taq* polymerase | 0.5 µl |
| DEPC-treated $H_2O$ | up to 50 µl |

*For each fragment of interest four tubes were prepared using the following primer combinations:

1) M13F and specific reverse;
2) M13F and specific forward;
3) M13R and specific forward;
4) M13R and specific reverse.

Reactions were amplified as follows (WMISH1 program):

| | | |
|---|---|---|
| 95°C | 5’ | 1 cycle |
| 95°C | 30’’ | 10 cycles |
| 50°C | 30’’ | |
| 72°C | * | |
| 95°C | 30’’ | 20 cycles |
| 50°C | 30’’ | |
| 72°C | ** | |
| 72°C | 8’ | 1 cycle |

*variable extension time depending on the fragment length (1min/kb), **1 minute and 30 seconds + 5 s/each cycle.

In both cases only two of the four reactions gave a band at the right molecular weight, thus it was possible to understand the orientation (sense or antisense) of the fragment of interest relative to T7 and Sp6 promoters in the plasmid (see Fig. B).

After both strategies PCR products were checked on an agarose gel using 10 µl of PCR product and 2.5 µl of 6x Loading Buffer and run for 25 minutes at 100 V.

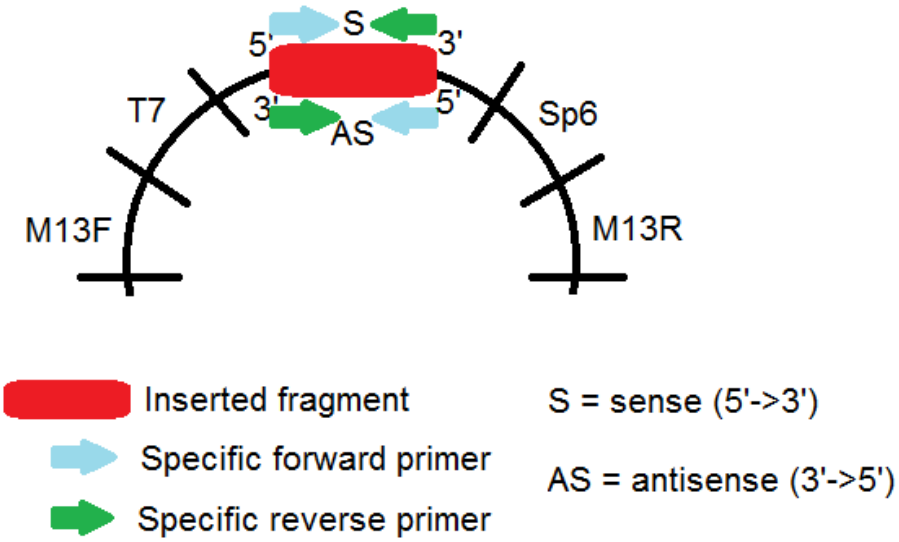


**Fig. B.** *Scheme illustrating the position of M13F, M13R, T7, Sp6 and target gene (inserted fragment) in the plasmid.*

*5.1.1.4. Template PCR*

After orientation PCR, a template PCR was performed using Invitrogen reagents as follows:

| | |
|---|---|
| 10X buffer-$MgCl_2$ | 5 µl |
| 50 mM $MgCl_2$ | 3 µl |
| 10 mM dNTPs | 1 µl |
| 10 µM M13F primer | 1.5 µl |
| 10 µM M13R primer | 1.5 µl |
| 1 ng/µl purified plasmid* | 1 µl |
| 5 U/µl DNA *Taq* polymerase | 0.5 µl |
| DEPC-treated $H_2O$ | 36.5 µl |

Reactions were amplified using the above described WMISH1 program.

The DNA templates were then purified using the NucleoSpin® gel and PCR clean-up kit (Macherey-Nagel) and eluted in a final volume of 18-19 µl of NE buffer; concentration was checked at NanoDrop Spectrophotometer and purity of the fragment (absence of

primer dimers or non-specific bands) was checked on a 1% TBE agarose gel. The remaining 15 µl were stored at -20°C. As above mentioned, since not for all the purified plasmids the subsequent orientation PCR was successful (e.g. due to conflicting results or technical problems) and considering that all the fragments need to be checked in order to be sure that the starting fragment of interest have been cloned, all the purified plasmids were prepared for sequencing and 10 µl of samples at 100 ng/µl (note that the concentration was lower in case the samples did not have a concentration higher than 100 ng/µl) were sent to the company (Source Bioscience Sequencing).

*5.1.1.5. Transcription of the RNA antisense probes*

To produce antisense RNA probe labelled with DIG to detect the expression of mRNA *in situ*, transcription was performed as follows using Sp6/T7 Transcription Kit (Roche), the use of Sp6 and T7 depending on the fragment orientation:

| | |
|---|---|
| 10X Transcription buffer | 2 µl |
| 10X DIG RNA Labelling Mix (Roche) | 2 µl |
| DNA template (100-500 ng) | x µl |
| 20 U/µl RNA polymerase (Sp6 or T7) | 1.6 µl |
| 10 U/µl RNAse inhibitor | 0.4 µl |
| DEPC-treated $H_2O$ | Up to 20 µl |

The mix was incubated for 5 hours at 37°C and then 1 µl of DNAse/RNAse free mix and 2 µl DNAse/RNAse free 10X buffer (Roche) were added and incubated for 15 minutes at 37°C. 30 µl of DEPC-treated $H_2O$ and 25 µl of 7.5 M LiCl were added and precipitated overnight at -20°C. 200 µl of 80% EtOH were added, then thoroughly mixed and centrifuged for 10 minutes at maximum rpm and the supernatant was completely removed without touching the pellet. This latter was then air-dried for 5-15 minutes (no more than 15 minutes in order to not have re-suspension problems), re-suspended in 50 µl of DEPC-treated $H_2O$ and well mixed.

The concentration of the antisense RNA probe was then measured with a NanoDrop Spectrophotometer and then diluted (if possible depending on the resulting concentration) at the working concentration of 50 ng/µl, aliquoted, 10 µl/Eppendorf tube, and stored at -80°C until use. 100 ng of the probe was checked on an 1% TBE agarose gel for purity and absence of degradation.

### *5.2. Microscopy analyses*

*5.2.1. Paraffin embedding and sectioning*

Samples were embedded as follows: after fixation in Bouin fixative for about one month to allow decalcification, they were washed in tap water, dehydrated in an increasing ethanol series, cleared with xylene, washed in xylene:paraffin wax solution (1:1) and embedded in paraffin wax (56°-58°C). Sagittal, cross and frontal sections (5-7 µm in thickness) were sectioned with Leica RM2155 or Leitz 1512 microtomes and stained according to Milligan's trichrome technique (Milligan, 1946). Slides were then mounted with Eukitt® and subsequently observed under a Jenaval light microscope as previously described or a Zeiss AxioImager M1 microscope equipped with a Zeiss AxioCamHRc camera.

**Table S1.** *Primers of the cloned genes with their sequences, lengths, Tm and expected PCR product lengths from PRIMER3 Software.* For *Afi-αcoll* primers see Czarkwiani and co-workers (2013). *Abbreviations*: bp = base pair; F = forward primer; R = reverse primer; Tm = primer melting temperature.

| Primer Name | Primer Sequence | Primer Length (bp) | Tm (°C) | Expected Product Length (bp) |
|---|---|---|---|---|
| ***Afi-col-L A F*** | CAACACCGACAGAACCAGAA | 20 | 59.72 | 778 |
| ***Afi-col-L A R*** | TGTTGTGTTGGCACCTCTTC | 20 | 59.73 | 778 |
| ***Afi-col-L B F*** | AACCGGGTATTCCTGGATTC | 20 | 60.02 | 894 |
| ***Afi-col-L B R*** | GTTCACCAACTCGTCCCACT | 20 | 60.01 | 894 |
| ***Afi-col-L C F*** | ACGTAAACGTTGGCATCTCC | 20 | 60 | 1014 |
| ***Afi-col-L C R*** | GTGATCGGCCTGATTGATCT | 20 | 60.04 | 1014 |
| ***Afi-col-L D F*** | CATAGTGCTTTCCCGGTTGT | 20 | 59.99 | 1122 |
| ***Afi-col-L D R*** | ATCACCGTCTGGTCCTATCG | 20 | 59.95 | 1122 |
| ***Afi-TIMP3 F*** | CCTTCCTAAGCACCCACAAC | 20 | 59.59 | 653 |
| ***Afi-TIMP3 R*** | AACTTGCTTGGCACAACTCA | 20 | 59.49 | 653 |
| ***Afi-Lamα-L F*** | GTGCTACCGGACCTCAATGT | 20 | 60 | 1017 |
| ***Afi-Lamα-L R*** | CTTCAGCTTGGCCTTGTAGG | 20 | 60.01 | 1017 |
| ***Afi-Lamβ-L F*** | CACATTAGGCACGGTGAATG | 20 | 59.99 | 1494 |
| ***Afi-Lamβ-L R*** | AACCCATCTTTGCACTGGTC | 20 | 59.97 | 1494 |
| ***Afi-ECM-protein F*** | AACCCAGCAATGGTAACAGC | 20 | 60 | 1983 |
| ***Afi-ECM-protein R*** | GACACTCTGCGTTGCGATAA | 20 | 60.02 | 1983 |

**Table S2.** *Details of the clones of the identified genes.* For *Afi-αcoll* see Czarkwiani and co-workers (2013). The vector is pGEM®-T Easy Vector System I (Promega) with ampicillin resistance. *Abbreviations*: bp = base pair.

| Clone name | Fragment size (bp) | Orientation | Vector |
|---|---|---|---|
| ***Afi-col-L A*** | 778 | Sense, transcribed with Sp6 | pGEM-T Easy |
| ***Afi-col-L B*** | 894 | Sense, transcribed with Sp6 | pGEM-T Easy |
| ***Afi-col-L C*** | 1014 | Sense, transcribed with Sp6 | pGEM-T Easy |
| ***Afi-col-L D*** | 1122 | Sense, transcribed with Sp6 | pGEM-T Easy |
| ***Afi-TIMP3*** | 653 | Antisense, transcribed with T7 | pGEM-T Easy |
| ***Afi-Lamα-L*** | 1017 | Sense, transcribed with Sp6 | pGEM-T Easy |
| ***Afi-Lamβ-L*** | 1494 | Sense, transcribed with Sp6 | pGEM-T Easy |
| ***Afi-ECM-protein*** | 1983 | Sense, transcribed with Sp6 | pGEM-T Easy |

**Table S3.** *Best BLAST hits of the identified genes in EchinoBase (SPU Best BLAST) and in NCBI (NCBI Best BLAST).*

| Gene | Afi Transcriptome id (Afi-CDSnt_v2) | CDS size (nt) | Spu Best Blast (SPU) | Score | E-value |
|---|---|---|---|---|---|
| ***Afi-col-L A*** | AfiCDS.id16823.tr6264 | 903 | Sp-C1qL (SPU_05500) | 207 | 8,00E-54 |
| ***Afi-col-L B*** | AfiCDS.id31588.tr64501 | 507 | Sp-6Afcol (SPU_009076) | 353 | 1,00E-96 |
| ***Afi-col-L C*** | AfiCDS.id59066.tr822 | 4080 | Sp-Col805b_2 (SPU_005167) | 895 | 0 |
| ***Afi-col-L D*** | AfiCDS.id20775.tr36218 | 4443 | Sp-Fcolf (SPU_013557) | 447 | E-125 |
| ***Afi-αcol*** | AfiCDS.id59033.tr18060 | 3972 | Sp-Col805b_1 (SPU_014618) | 228 | 3,00E-59 |
| ***Afi-Lamα-L*** | AfiCDS.id50515.tr22425 | 11016 | Sp-LamaLf (SPU_020192) | 2160 | 0 |
| ***Afi-Lamβ-L*** | AfiCDS.id27309.tr36214 | 5982 | Sp-LamB2Lf (SPU_001768) | 1570 | 0 |
| ***Afi-ECM-protein*** | AfiCDS.id38268.tr22439 | 6807 | Sp-Fram1 (SPU_011688) | 2023 | 0 |
| ***Afi-TIMP3*** | AfiCDS.id58489.tr18807 | 771 | Sp-Timp4b (SPU_008866) | 150 | 1,00E-36 |

| Gene | Afi Transcriptome id (Afi-CDSnt_v2) | CDS size (nt) | NCBI Best Blast (ID) | Score | E-value |
|---|---|---|---|---|---|
| ***Afi-col-L A*** | AfiCDS.id16823.tr6264 | 903 | alpha-2(VIII) chain-like [*S. purpuratus*] (gi\|390335431\|ref\|XP_003724148.1) | 203 | 1,00E-60 |
| ***Afi-col-L B*** | AfiCDS.id31588.tr64501 | 507 | collagen alpha-1(V) chain isoform X2 [*S. purpuratus*] ref\|XP_011679218.1\| | 350 | 2,00E-94 |
| ***Afi-col-L C*** | AfiCDS.id59066.tr822 | 4080 | alpha-5 collagen [*P. lividus*] emb\|CAE53096.1\| | 865 | 0 |
| ***Afi-col-L D*** | AfiCDS.id20775.tr36218 | 4443 | PREDICTED: collagen alpha-1(XXVII) chain [*S. purpuratus*] ref\|XP_011679783.1\| | 350 | 4,00E-101 |
| ***Afi-αcol*** | AfiCDS.id59033.tr18060 | 3972 | hypothetical protein BRAFLDRAFT 74778 [*B. floridae*] | 274 | 5,00E-80 |
| ***Afi-Lamα-L*** | AfiCDS.id50515.tr22425 | 11016 | laminin subunit alpha-like isoform X2 [*Lingula anatina*] ref\|XP_013408769.1\| | 2615 | 0 |
| ***Afi-Lamβ-L*** | AfiCDS.id27309.tr36214 | 5982 | PREDICTED: laminin subunit beta-2 [*S. purpuratus*] ref\|XP_793215.4\| | 1436 | 0 |
| ***Afi-ECM-protein*** | AfiCDS.id38268.tr22439 | 6807 | PREDICTED: FRAS1-related extracellular matrix protein 1 [Spu] ref\|XP_011678210.1\| | 2018 | 0 |
| ***Afi-TIMP3*** | AfiCDS.id58489.tr18807 | 771 | PREDICTED: metalloproteinase inhibitor 3 [*S. purpuratus*] ref\|XP_781027.1\| | 138 | 1,00E-136 |

### *5.3. Extended results*

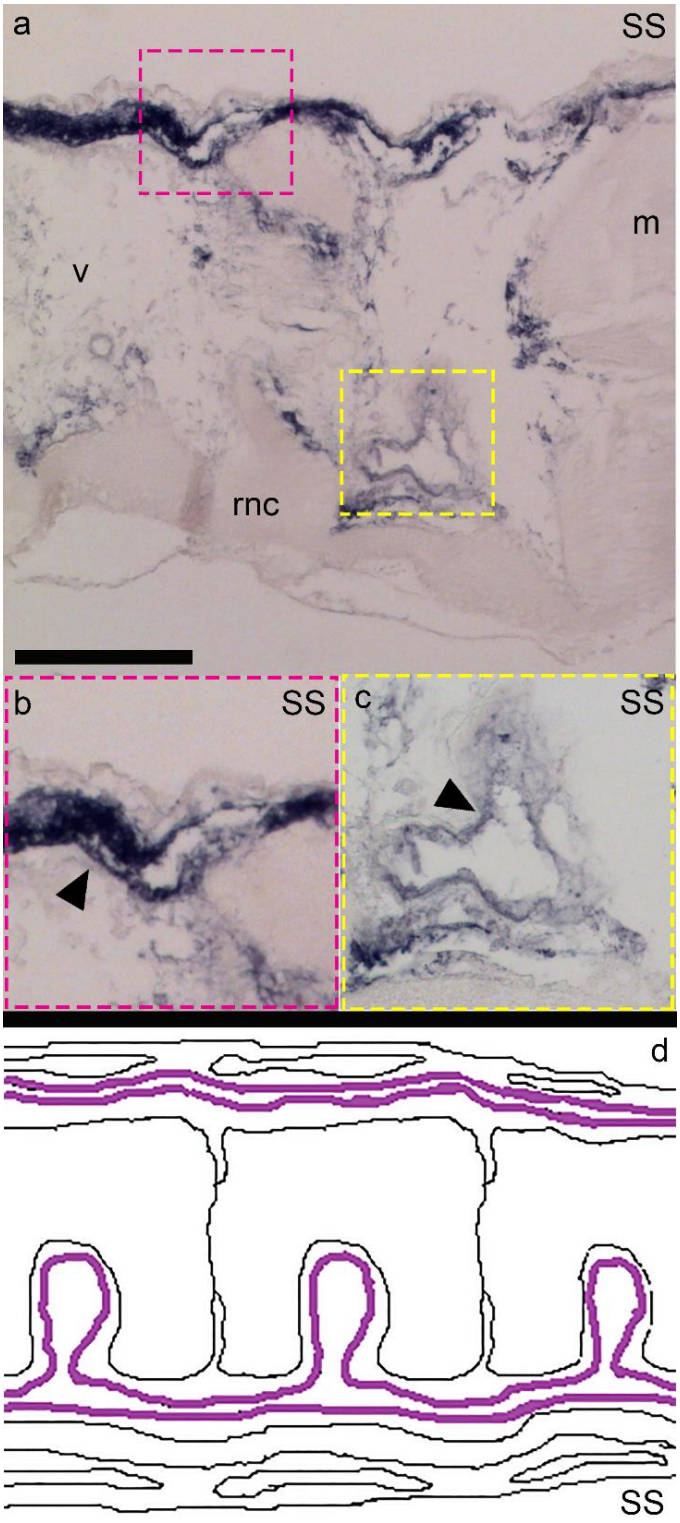


**Fig. S1.** a) Post *in situ* sagittal section showing that in the stump *Afi-col-L B* is expressed in the aboral coelomic cavity epithelium and in the radial water canal epithelium. Scale bar = 100 µm. b) Detail of Fig. a on the signal at the level of the aboral coelomic cavity epithelium (arrowhead). c) Detail of Fig. a on the signal at the level of the radial water canal epithelium. d) Sagittal section scheme showing the *Afi-col-L B* expression pattern at the level of the stump. Violet = presence of signal. *Abbreviations*: m = muscle; rnc = radial nerve cord; SS = sagittal section; v = vertebra.

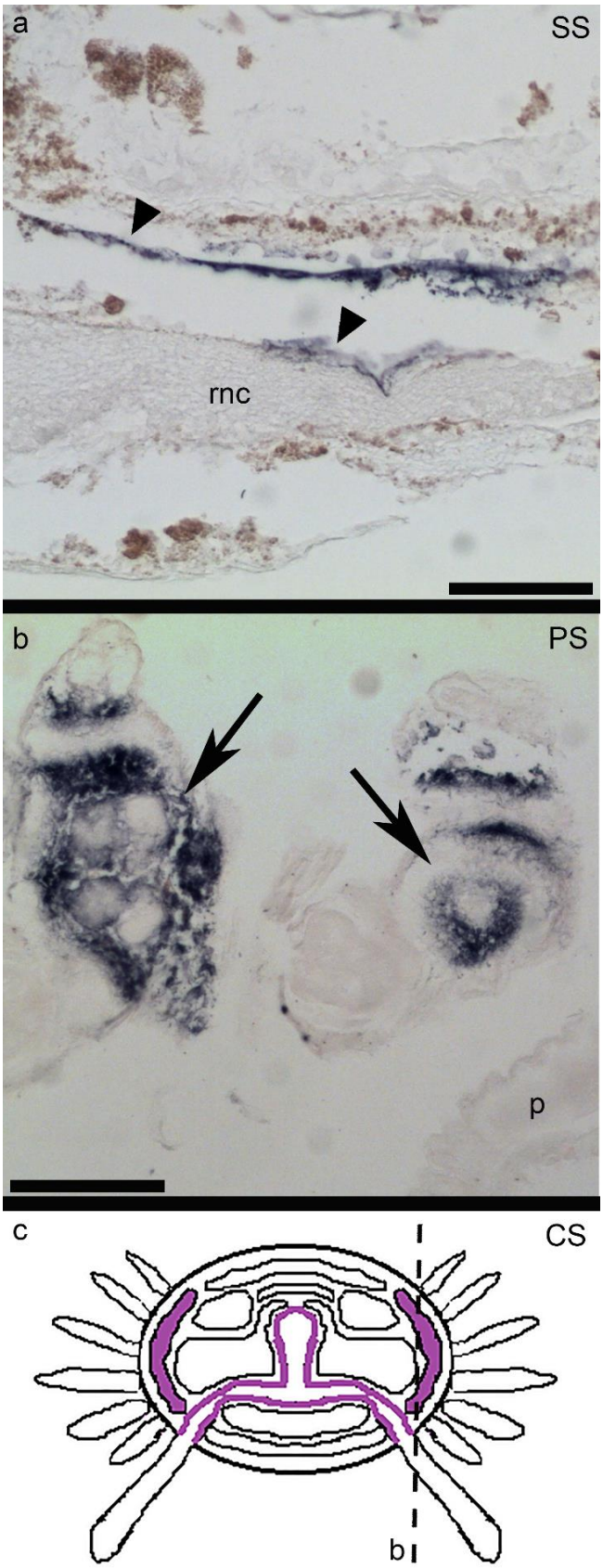


**Fig. S2.** a) Post *in situ* sagittal section showing that *Afi-col-L C* is expressed in the stump at the level of the radial water canal epithelium (arrowheads). Scale bar = 50 µm. b) Post *in situ* parasagittal section showing that *Afi-col-L C* is expressed in the stump at the level of the lateral shields (two adjacent shields are visible, arrows). Scale bar = 100 µm. c)

◀ Cross section scheme showing expression at the level of the stump in the lateral shields and in the radial water canal epithelium. Violet = presence of signal. Black dotted line = level at which the section in Fig. b has been performed. *Abbreviations*: CS = cross section; p = podium; PS = parasagittal section; rnc = radial nerve cord; SS = sagittal section.

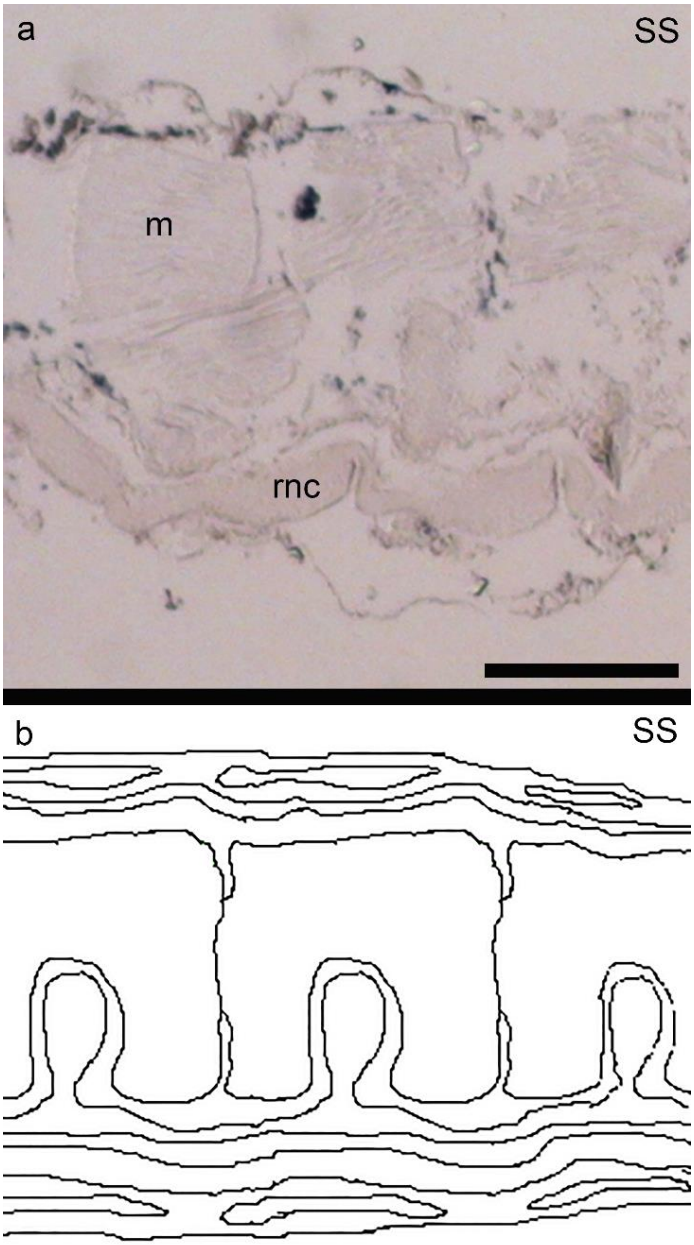


**Fig. S3.** a) Post *in situ* sagittal section showing that *Afi-col-L D* is not detectable at the level of the non-regenerating stump tissues. Blue dots visible in the section are residues of calcium carbonate crystals, thus is not a specific signal. Scale bar = 200 µm. b) Sagittal section scheme showing the absence of *Afi-col-L D* expression pattern at the level of the stump. *Abbreviations*: m = muscle; rnc = radial nerve cord; SS = sagittal section.

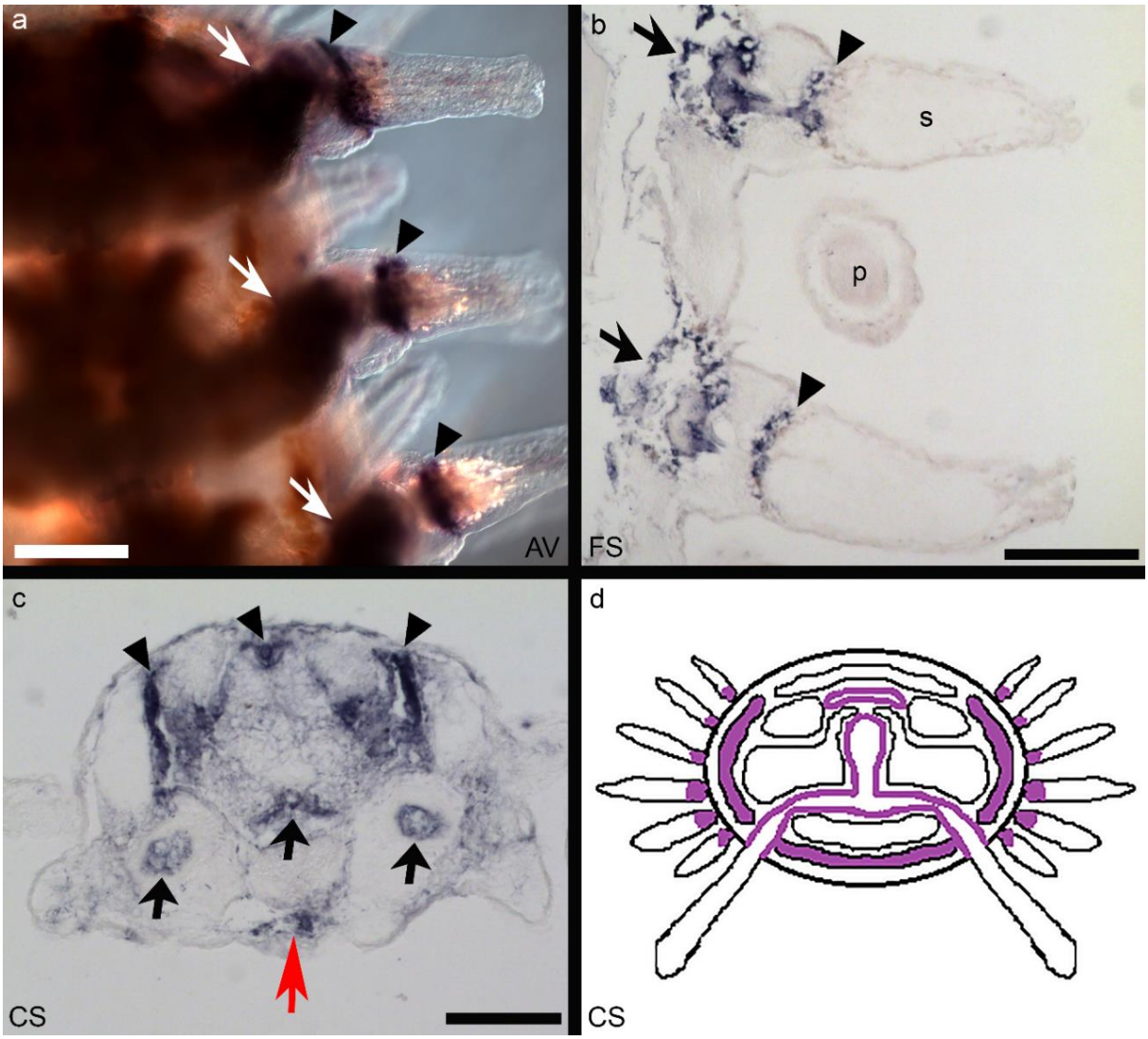


**Fig. S4.** a) Aboral view (AV) of a WMISH sample at the level of the stump. It is visible that *Afi-αcoll* is expressed at the level of the lateral shields (arrows) and at the base of the spines (arrowheads). Scale bar = 100 µm. b) Post *in situ* frontal section (FS) of the stump showing that *Afi-αcoll* is expressed in the lateral shields (arrows) and at the base of the spines (arrowheads). Scale bar = 100 µm. c) Post *in situ* cross section (CS) of the stump showing that *Afi-αcoll* is expressed also in the aboral coelomic cavity epithelium (arrowheads), in the oral shield (red arrow) and in the water vascular system (black arrows). Scale bar = 50 µm. d) Cross section scheme (CS) summarising the expression pattern of this gene in the stump tissues. Violet = presence of signal. *Abbreviations*: AV = aboral view; CS = cross section; FS = frontal section; p = podium; s = spine.

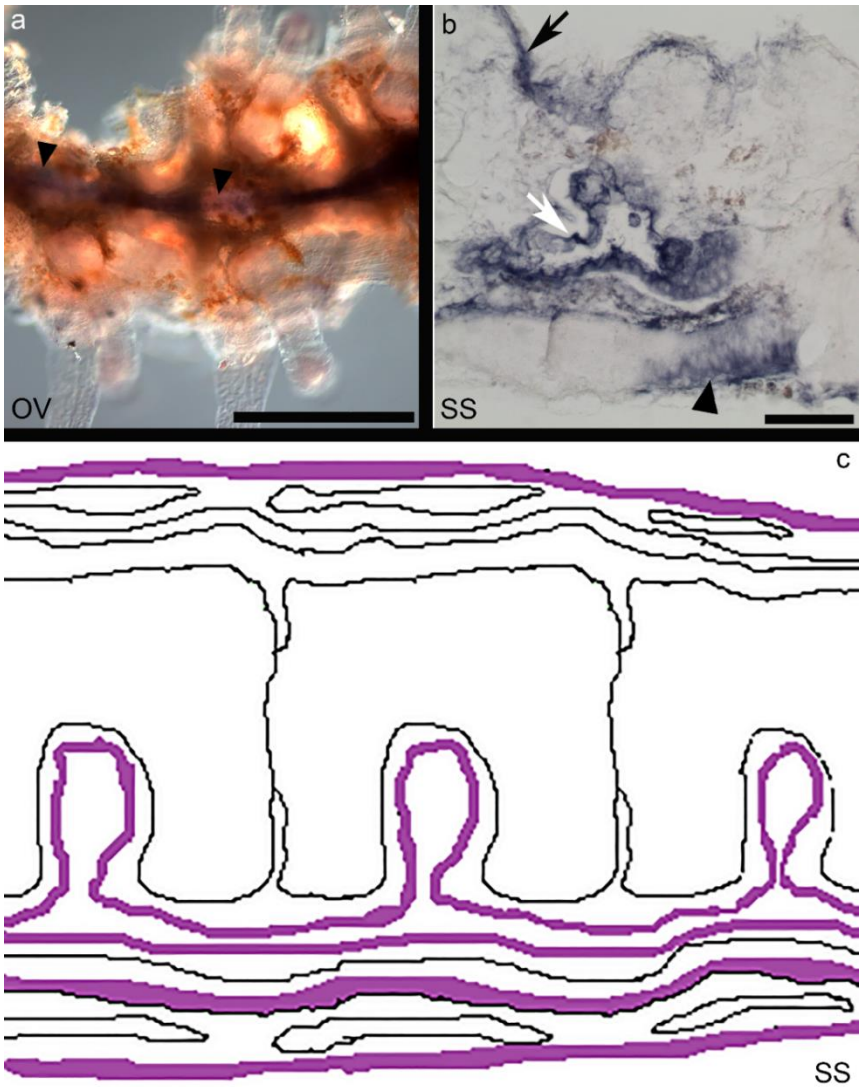


**Fig. S5.** a) Oral view of *Afi-lamα-L* WMISH sample at the level of the stump. *Afi-lamα-L* is expressed at the level of the radial water canal (arrowheads). Scale bar = 200 µm. b) Post *in situ* sagittal section of the stump showing that *Afi-lamα-L* is expressed not only at the level of the radial water canal epithelium (white arrow) as visible from whole mount samples but also at the level of the epidermis (black arrow) and of the ectoneural system of the radial nerve cord (arrowhead). Scale bar = 50 µm. c) Sagittal section scheme showing the expression pattern of *Afi-lamα-L* in the stump tissues. Violet = presence of signal. *Abbreviations*: OV = oral view; SS = sagittal section.

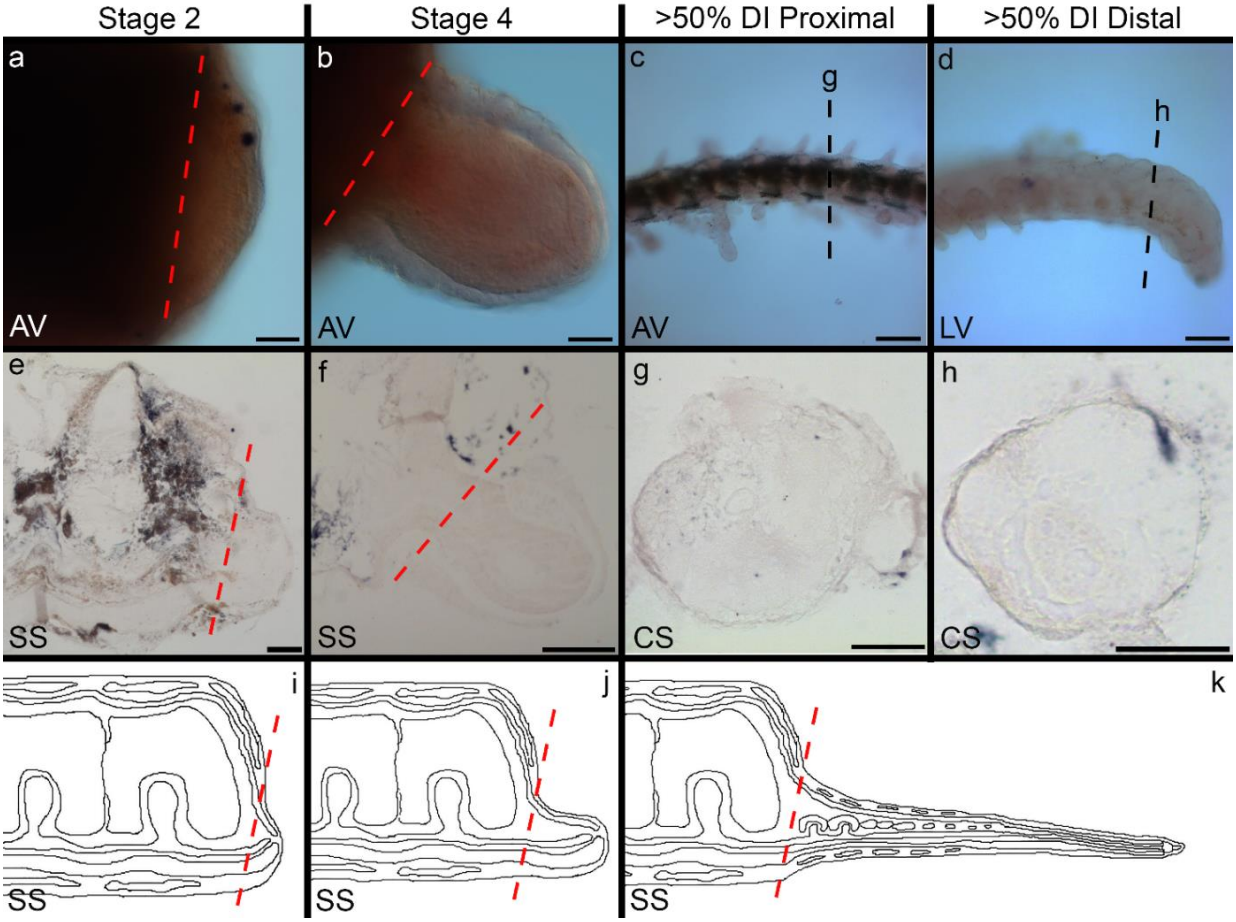


**Fig. S6.** *Afi-Lamβ-L expression pattern at different regenerative stages*. 1st line: WMISH; 2nd line: post *in situ* sectioning; 3rd line: schemes. Stage 2 (first WMISH parameters): a, e, i. *Afi-Lamβ-L* is not expressed in the regenerative bud. Stage 4 (first WMISH parameters): b, f, j. *Afi-Lamβ-L* is not expressed in the regenerate. Stage >50% DI (first WMISH parameters): c, d, g, h, k. *Afi-Lamβ-L* is not expressed along the whole regenerate length. Note that the dark pigmentation visible in the long regenerate is due to light reflection of the skeletal elements and it is not an actual WMISH staining, as clarified by post *in situ* sections. *Abbreviations*: AV = aboral view; CS = cross section; LV = lateral view; SS = sagittal section. Scale bars: a, b, d, e, f, g = 50 µm; c = 100 µm; h = 25 µm. Red dotted lines = amputation plane. Black dotted lines = levels corresponding to the cross sections shown in Fig. g and h.

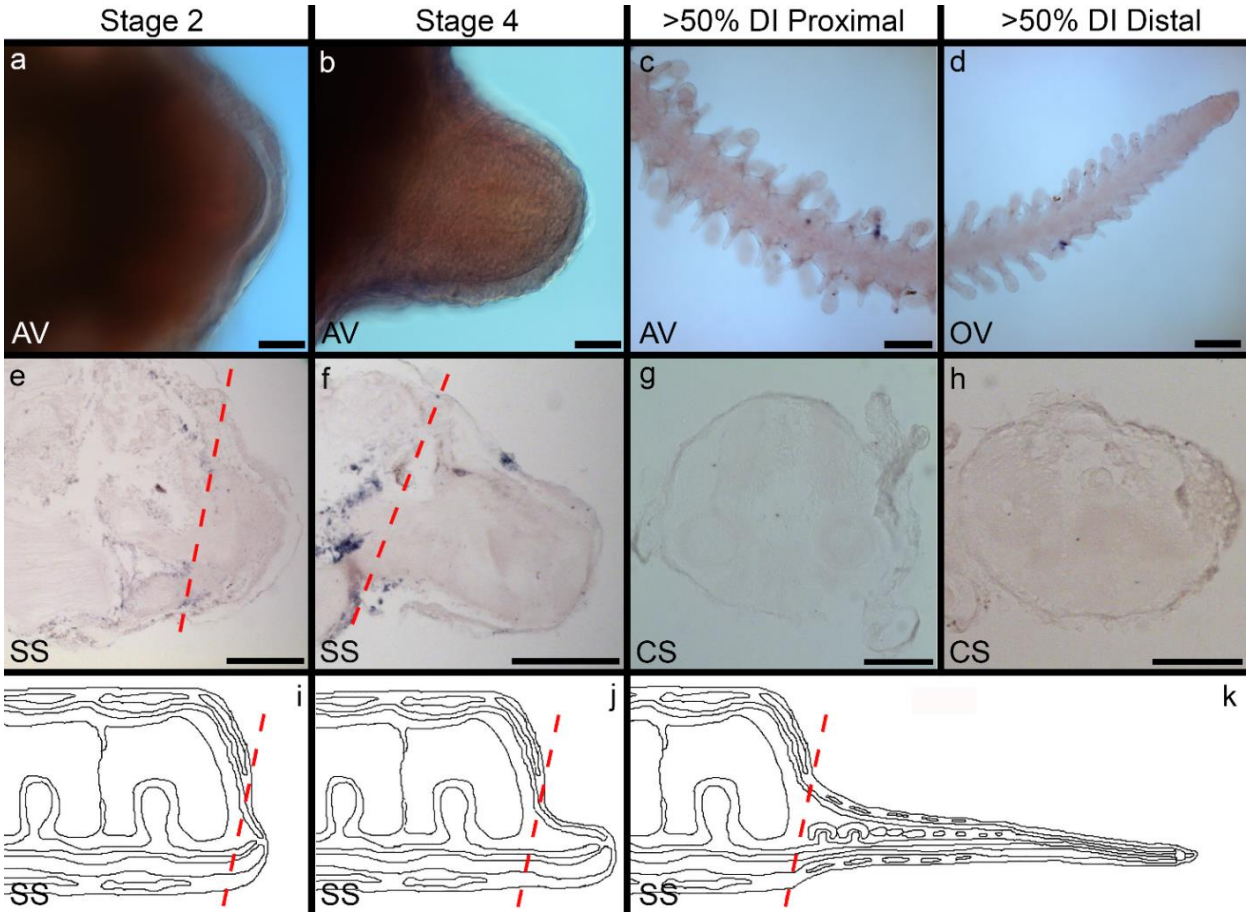


**Fig. S7.** *Afi-ECM-protein expression pattern at different regenerative stages*. 1st line: WMISH; 2nd line: post *in situ* sectioning; 3rd line: schemes. Stage 2 (first WMISH parameters): a, e, i. *Afi-ECM-protein* is not expressed in the regenerative bud. Stage 4 (first WMISH parameters): b, f, k. *Afi-ECM-protein* is not expressed in the regenerate. Stage >50% DI (first WMISH parameters): c, d, g, h, k. *Afi-ECM-protein* is not expressed along the whole regenerate length. *Abbreviations*: AV = aboral view; CS = cross section; OV = oral view; SS = sagittal section. Scale bars: a, b, d, f, g, h = 50 µm; c, e = 100 µm. Red dotted lines = amputation plane.

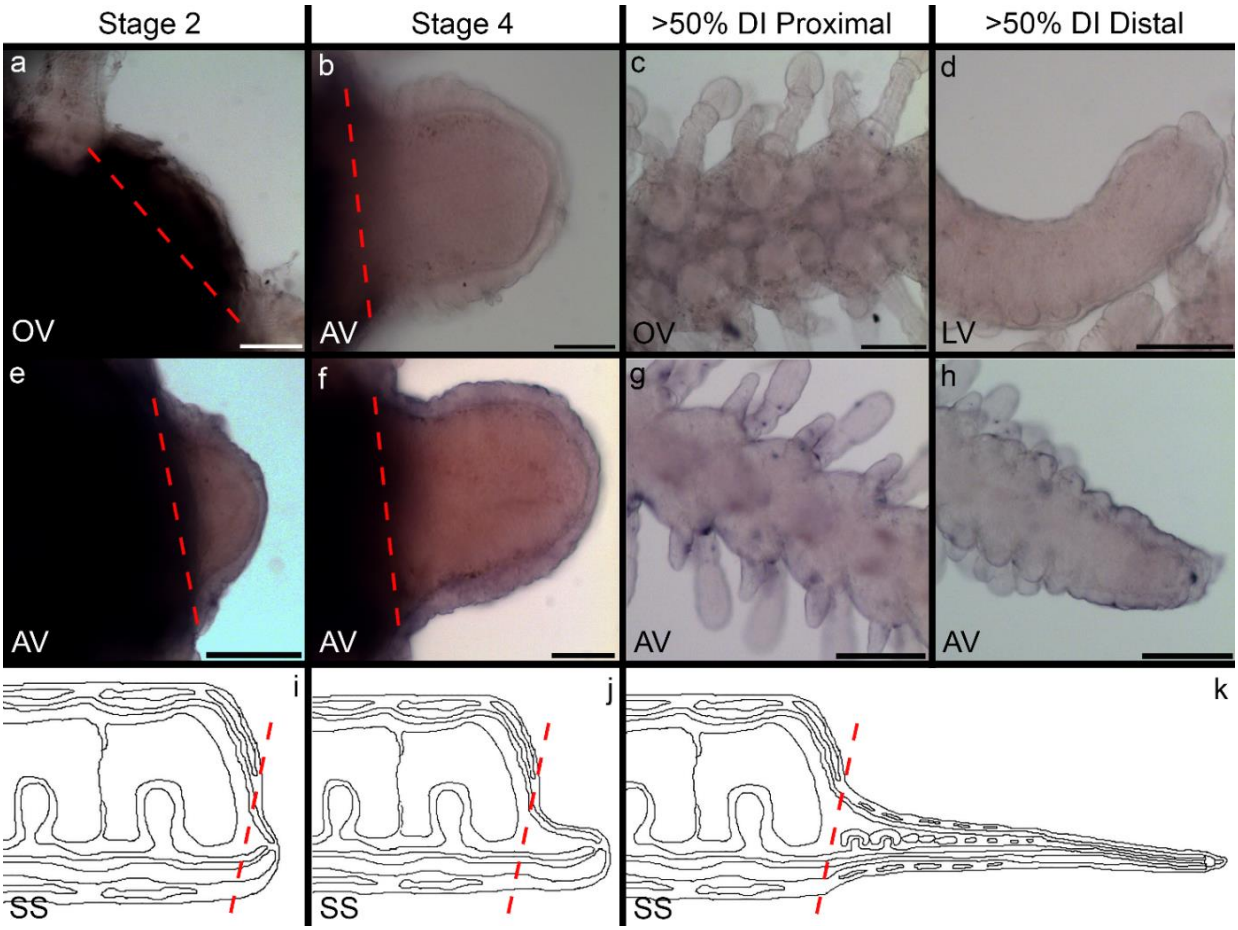


**Fig. S8.** *Afi-lamβ-L* and *Afi-ECM-protein expression patterns at the selected regenerative stages using the second WMISH parameters*. 1st line: *Afi-lamβ-L* WMISH; 2nd line: *Afi-ECM-protein* WMISH; 3rd line: sagittal section schemes valid for both genes. As visible from all images no expression is detectable in all stages for both genes. AV = aboral view; LV = lateral view; OV = oral view; SS = sagittal section. Scale bars: a, b, f = 50 µm; c, d, e, g, h = 100 µm. Red dotted lines = amputation plane.

# CHAPTER 4

## Comparative aspects of the repair phase in echinoderm arm regeneration

Ferrario Cinzia, Ben Khadra Yousra, Czarkwiani Anna, Zakrzewski Anne, Martinez Pedro, Ascagni Miriam, Bonasoro Francesco, Candia Carnevali Maria Daniela, Oliveri Paola, Sugni Michela

*In preparation* for Developmental Biology.

***Abstract***

Regeneration is a post-embryonic developmental process that ensures complete morphological and functional restoration of lost body parts. The repair phase is a key step for the effectiveness of the subsequent regenerative process: in vertebrates, post-injury connective tissue remodelling and rapid immune response are fundamental aspects for the success of this phase, their impairment leading to an inhibition or total prevention of regeneration.

Among deuterostomes, echinoderms display a unique combination of striking regenerative abilities and diversity of useful experimental models, although still largely unexplored. The starfish *Echinaster sepositus* and the brittle star *Amphiura filiformis* were here used to investigate the presence and expression of extracellular matrix (*i.e.* collagen) and immune system molecules during the repair phase using both microscopy and molecular tools.

Our results showed that emergency reaction and wound healing are faster and more effective in echinoderms than in mammals and delayed and less abundant collagen deposition at the wound site (absence of fibrosis) can be important features ensuring their subsequent efficient regeneration. Immunodetection of TNF-α-like in brittle star showed a comparable signal to that of mammals. The gene expression patterns of starfish *fibrinogen-like* and brittle star *ficolin* were described for the first time during echinoderm regeneration providing promising starting points to investigate the immune system's role in these regeneration models.

Overall, these data suggest that the repair processes in echinoderms are key events of the regenerative phenomenon which distinguish them from scarcely regenerating animals, such as mammals. Deeper analyses will shed light on the evolution (loss/potentiation) of these abilities along the deuterostomian lineage.

### *1. Introduction*

Along with metamorphosis, regeneration is one of the most fascinating post-embryonic developmental processes in the animal kingdom, both at larval and adult stages (Candia Carnevali, 2006). However, contrary to embryogenesis and metamorphosis, regeneration occurs after lesions, damage and loss of whole body parts due to predation, diseases or autotomy, thus following both unpredictable and predictable events. Moreover, the cellular and tissue context in which it takes place is largely different from those other developmental processes. Indeed, during regeneration new cells arise in the context of differentiated tissues of adults or larvae that are morphologically and functionally characterised, whereas in a developing embryo the new dividing cells constitute the new structures (Candia Carnevali, 2006) and in metamorphosis larval tissues are completely reorganised to build up the adult morphology (Tata, 1993).

Regardless the life stage or age of the individual, all animals face and heal minor wounds, though the final result of the restoration process can be remarkably different. Vertebrates, humans included, are able to heal minor injuries but most of them possess a limited capacity of regeneration in case of loss of complete body parts (Sánchez Alvarado, 2000). One of the causes of this limited regenerative ability is the occurrence of fibrosis, *i.e.* the deposition of excess fibrous connective tissue during the first phases of repair. Indeed, in mammals the cicatrisation phenomenon frequently leads to an “exaggerated” inflammatory response that leads to fibrosis or to more severe problems e.g. keloid formation (Bock and Mrowietz, 2002; Rahban and Garner, 2003). These latter are conditions provoked by over-deposition of scarcely remodelling collagen (Diegelmann and Evans, 2004) that are directly connected with fibro-proliferative disorders (Tredget *et al.*, 1997; Singer and Clark, 1999) and with impossibility to regenerate damaged tissues. Among vertebrates, notable exceptions to fibrotic wound healing and, therefore, limited regeneration are exemplified by some fishes, amphibians and reptiles, which fully regenerate body appendages such as fins, limbs and tails (Akimenko *et al.*, 2003; Brockes and Kumar, 2002; Bateman and Fleming, 2009). However, regenerative capabilities are even more remarkable in some invertebrate clades: cnidarians (Bosch,

2007), planarians and annelids (Saló and Baguñá, 2002; Saló *et al.*, 2009) and echinoderms (Candia Carnevali, 2006) are the most representative examples.

In particular, echinoderms show the maximum extent of regenerative potential among deuterostomes: indeed, this physiological phenomenon is displayed by representatives of all the five extant classes (Hyman, 1955) and is described in fossils as well (Oji, 2001), suggesting that regeneration is an ancient feature of the phylum, virtually present in all its members. Moreover, echinoderms regenerate not only body appendages (e.g. spines, pedicellariae, whole arms; Mladenov *et al.*, 1989; Dubois and Ameye, 2001; Candia Carnevali and Bonasoro, 2001b; Candia Carnevali, 2006; Biressi *et al.*, 2010) but also internal organs, such as the visceral mass (Mozzi *et al.*, 2006; Mashanov and García-Arrarás, 2011), and even whole animals from an isolated body fragment (Ducati *et al.*, 2004). Therefore, they are promising models to study this phenomenon allowing us to compare their efficiency in regenerating whole body parts with the scarce regenerative abilities displayed by humans and mammals overall.

Among the numerous echinoderm models, nowadays starfish and brittle stars (belonging to the classes Asteroidea and Ophiuroidea respectively) are becoming valid experimental models to study the regenerative process of whole arms after traumatic amputation (Mladenov *et al.*, 1989; Biressi *et al.*, 2010; Czarkwiani *et al.*, 2013; Ben Khadra *et al.*, 2015a, b). However, till now only a few of these studies focused on describing arm regeneration using an integrated perspective, including both morphological and molecular aspects (Czarkwiani *et al.*, 2016).

The regenerative phenomenon in echinoderms is usually subdivided into three main phases: the repair phase, characterised by wound closure events, the early regenerative and the advanced regenerative phases, during which morphogenesis and differentiation occur.

As in all animals, in echinoderms during the first hours/days immediately after arm injury different events take place at the level of the wound site and several tissues/cell types are involved. Wound closure is the first reaction after damage, which is important to avoid loss of fluid from the body cavities (that could be more or less conspicuous). This is quickly achieved mainly by wound edge approach and clotting phenomena of the circulating coelomocytes (Gross *et al.*, 1999; Pinsino *et al.*, 2007; Ben Khadra *et al.*, 2015a).

A quick inflammation response is activated as well. As described for the mammal immune response to injury (Martin, 1997; Wilgus, 2008), in echinoderms many molecules, humoral factors, complement and immune system components have been described

mainly in sea urchins and sea cucumbers and are thought to be involved in the emergency reaction after damage (Pancer *et al.*, 1999; Rast *et al.*, 2006; Ramírez-Gómez *et al.*, 2008, 2009, 2010; Ramírez-Gómez and García-Arrarás, 2010; Smith *et al.*, 2010). In mammals, fibrinogen, cytokines e.g. TNF-α and TGF-β, interleukins *i.e.* IL-1 and IL-6, lectins and ficolins are just some of the key players during the inflammation process and their presence/role should be comparatively investigated in echinoderm healing phenomena to better characterise these important events and shed light on possible evolutionary differences.

The inflammatory response is followed by quick re-epithelialisation (Biressi *et al.*, 2010; Ben Khadra *et al.*, 2015a) and in some species by oedema appearance (Ben Khadra *et al.*, 2015a, b). At this stage in echinoderms the first observed changes occur in the connective tissue, with both its extracellular matrix (ECM) and cellular components, therefore suggesting its importance during regeneration. In particular, both fibrillar and nonfibrillar collagens, the main ECM components, are important during the whole repair phase and later on during the regenerative phases since the fibrillar collagen network likely provides the scaffold for subsequent tissue reconstruction (Ben Khadra *et al.*, 2015b). The importance of collagen as scaffold for tissue development has been described also in the context of sea urchin larval spicule formation (Okazaki and Inoué, 1976; Blankenship and Benson, 1984). As previously underlined, during wound closure and cicatrisation both collagen and ECM are remodelled and re-deposited. A few studies focused on sea cucumbers suggested that these events may be directly related to their high ability and efficiency of regeneration: a delayed collagen production was suggested as important for the subsequent regenerative process (Quiñones *et al.*, 2002; Cabrera-Serrano and García-Arrarás, 2004).

Considering both starfish and brittle stars, the cellular/tissue and molecular aspects of the initial repair phase have never been comparatively and extensively studied. Therefore, investigating cell/molecule/enzyme/gene involvement during wound repair will help understanding if the absence of fibrosis during the healing process in these two classes is key for effective echinoderm regeneration, as suggested for sea cucumbers (Quiñones *et al.*, 2002; Cabrera-Serrano and García-Arrarás, 2004).

Hence, the aims of this research are to characterise and compare the phenomena occurring during the repair phase after traumatic arm amputation in the starfish *Echinaster sepositus* (Asteroidea) and the brittle star *Amphiura filiformis* (Ophiuroidea), using an integrated approach including histological, ultrastructural, immunohistochemical and

molecular techniques. The focus will be on ECM (and collagen) and on immune system involvement during the repair phase in order to understand if the “secrets” of the high efficient regeneration in echinoderms are linked to their highly effective initial response to damages without the fibrosis event. A deeper knowledge on how echinoderms heal severe wounds and start and complete the regenerative process will shed light on similarities and/or differences with animals less or not capable of regenerating whole body parts, humans included. In the future, this could serve the regenerative medicine field in finding actual clinical solutions to severe injuries or amputations.

## *2. Materials and Methods*

### *2.1. Animal collection, maintenance and regeneration tests*

#### *2.1.1. Starfish*

Adult (diameter ~ 12 cm) specimens of *Echinaster sepositus* were collected by scuba divers at depth of 5-8 m in the Marine Protected Areas of Portofino (Ligurian Sea, Italy) and of Bergeggi Island (Ligurian Sea, Italy). They were left to acclimatise for about two weeks and maintained at 18°C in aerated aquaria of artificial sea water (ASW; 37‰ salinity, Instant Ocean®). Chemical-physical ASW parameters were constantly checked and adjusted if necessary. Specimens were fed twice a week with small pieces of cuttlefish. Traumatic amputation of the distal third of one arm for each specimen was performed using a scalpel. Animals were then left to regenerate in the aquaria for pre-determined periods, namely 24 and 72 hours (h) and 1 week (w) post-amputation (p.a.). Regenerating arm tissues were collected including about 1 cm of the stump and differently processed depending on the subsequent analyses.

#### *2.1.2. Brittle stars*

Adult (central disc diameter ~ 0.5 cm) specimens of *Amphiura filiformis* were collected at the Sven Lovén Centre for Marine Sciences in Kristineberg (Sweden) and kept in tanks with filtered ASW (30‰ salinity; Instant Ocean®) at 14°C. Animals were left to acclimatise for about one week before performing regeneration tests. Specimens were fed twice a week with Microvore Microdiet (Brightwell Aquatics) and ASW parameters were constantly checked and adjusted when necessary. Animals were anaesthetised in 3.5% $MgCl_2$ ($6H_2O$) solution (pH 8.3) in a 1:1 mix of filtered ASW and milliQ water and maximum of two arms per animal were amputated under a stereomicroscope at 1 cm from the disc and using a scalpel. They were then left to regenerate until they reached the desired

stages, namely 8, 16, 24, 48, 72 hours (h) and 5 days (d; stage 2) post-amputation (p.a.). Samples at 8d (stage 4) and 2-3 weeks (w) p.a. (>50% DI) were collected and processed as well but they will not be further discussed. All the regenerates were collected together with 2-3 segments of the stump in order to easily handle them.

### *2.2. Microscopy analyses*

*2.2.1. Light (LM) and transmission electron microscopy (TEM)*

For paraffin wax embedding starfish and brittle star regenerating samples were fixed in Bouin fixative that was left for one month at 4°C to allow decalcification. Then, they were washed in tap water, dehydrated in an increasing ethanol series, cleared with xylene or Histoclear, washed in xylene (or Histoclear):paraffin wax solution (1:1) and embedded in paraffin wax (56-58°C). After sectioning, sagittal, frontal and cross thick sections (5-7 µm) were stained according to Milligan's trichrome technique (Milligan, 1946).

For Epon resin embedding starfish and brittle star regenerating samples were fixed in 2% glutaraldehyde in 0.1 M sodium cacodylate (pH between 7.2-7.4) with 1.4% (starfish) or 1.2% (brittle star) NaCl and washed overnight at 4°C in 0.1 M cacodylate buffer. They were post-fixed in 1% osmium tetroxide in the same buffer for 2 hours, rapidly washed in distilled water, decalcified at 4°C for at least 2-3 days using a 1:1 solution (v/v) of 2% L-ascorbic acid and 0.3 M NaCl in distilled water, washed with distilled water and then in 1% uranyl acetate in 25% ethanol (2 hours). Dehydration was performed in an increasing scale of ethanol and samples were then cleared in propylene oxide, washed in propylene oxide:Epon 812-Araldite solution (3:1 for 1 hour, 1:1 for 1 hour, 1:3 for 1 hour and 100% resin overnight) and embedded in pure resin. Semi-thin sections (1 µm) were obtained using a Reichert-Jung Ultracut E with glass knives and stained with crystal violet and basic fuchsin.

Both thick and semi-thin sections were then observed under a Jenaval light microscope provided with a DeltaPix Invenio 3S 3M CMOS camera and DeltaPix Viewer LE Software or a Zeiss AxioImager M1 microscope equipped with a Zeiss AxioCamHRc camera.

For transmission electron microscopy (TEM) the same samples used for semi-thin sections were used to obtain thin sections (0.07-0.1 µm) which were collected on copper grids, stained with 1% uranyl acetate and lead citrate and finally carbon coated with an EMITECH K400X Carbon Coater. Grids were observed and photographed using a Jeol 100SX or a Zeiss EFTEM Leo912ab transmission electron microscope.

*2.2.2. Scanning electron microscopy (SEM) of starfish samples*

After sagittal sectioning, the remaining paraffin embedded half-samples of regenerating starfish were used for scanning electron microscopy. Briefly, they were washed several times with xylene for at least 5 days, then in absolute ethanol and were later transferred to a series of solutions of HMDS (Hexamethyldisilazane) in absolute ethanol in different proportions (1:3, 1:1, 3:1, and 100% HMDS). Finally, they were mounted on stubs, covered by a thin layer of pure gold (Sputter Coater Nanotech) and observed under a scanning electron microscope (LEO-1430).

*2.2.3. Immunofluorescence microscopy (IF)*

For immunohistochemical analysis starfish regenerating samples underwent different fixation and embedding protocols depending on the antibody employed: no fixation and cryo-embedding in OCT or 4% paraformaldehyde (PFA) in 1x Phosphate Buffer Saline (PBS) and paraffin embedding. All samples were decalcified using 6% trichloroacetic acid (TCA) in distilled water for at least 2 days at 4°C. Brittle star regenerating samples were fixed in 4% PFA in 1x PBS, decalcified in 6% TCA for at least two days and embedded in paraffin wax. Starfish regenerating samples were embedded in paraffin wax following the protocol described in paragraph 2.2.1 or directly in OCT medium following standard procedures. Briefly, samples were rapidly passed in liquid nitrogen-cooled isopentane (VWR) for 1 minute, then in liquid nitrogen for few minutes, and left at -80°C until processed. Paraffin-embedded samples of both species were sectioned at 10 µm in thickness with a microtome, whereas starfish OCT-embedded samples were sectioned at 10 µm of thickness using a cryostat (Leica) on positively charged slides (Superfrost Plus, Thermo Scientific).

Table 1 summarises tested antibodies with concentration and exposure time and temperature. Primary antibodies were used as follows: anti-HgfCOL monoclonal antibody raised in mouse (from Quiñones *et al.*, 2002; Hg=*Holothuria glaberrima*) was tested to detect fibrous collagen and anti-TNF-α monoclonal antibody raised in mouse (ab1793; Abcam) was used to detect the presence of this cytokine. Paraffin-embedded slices were de-waxed in toluene with two washes at room temperature (RT) and then washed three times in 1x PBS. OCT-embedded slices were washed once in 1x PBS and then both types of slides underwent the same protocol. Briefly, slices were permeabilised in 0.1% PBSTT (1x PBS with 0.1% Tween-20 and 0.1% Triton X-100) for 20 minutes at RT and washed three times in 1x PBS. Then, they were blocked with 10% goat serum (Sigma-

Aldrich) in 0.05% PBSTT (1x PBS with 0.05% Tween-20 and 0.05% Triton X-100) for 90 minutes at RT. Several washes in 1x PBS were performed and slides were incubated with primary antibodies (for details see Table 1) in 5% goat serum in 0.05% PBSTT. After six washes in 1x PBS slides were washed in 0.05% PBSTT with 1% Bovine Serum Albumin (Sigma-Aldrich) for one hour at RT and then washed several times in 1x PBS. Samples were later incubated with secondary antibodies (for details see Table 1) in 5% goat serum in 0.05% PBSTT. After six washes in 1x PBS, slides were counterstained with 1:1000 4',6-diamidino-2-phenylindole (DAPI) for 30 minutes at RT, washed three times in 1x PBS and mounted with Fluoroshield (Sigma-Aldrich). Finally, slides were examined under a Leica TCS SP2 Laser Scanning Confocal microscope (Leica Microsystems).

**Table 1.** *Summary of primary and secondary antibodies (Life Technologies-Molecular Probes) used for starfish and brittle star slides with concentration, exposure time and temperature. Abbreviations*: HgfCOL=anti-fibrous collagen from *H. glaberrima* (Quiñones *et al.*, 2002); O/N=overnight; TNF-α=anti-tumour necrosis factor-α. Note that antibody concentrations were optimised with several trials and the table shows only the best tested conditions.

| Primary antibody | Secondary antibody |
|---|---|
| **Anti-HgfCOL** 1:2 O/N 4°C | Alexa Fluor ® 488 goat anti-mouse IgG (H+L) 1:200 O/N 4°C or TRITC goat anti-mouse 1:200 O/N 4°C |
| **Anti-TNF-α** 1:50 O/N 4°C | |

### *2.3. Molecular analyses*

#### *2.3.1. Candidate gene identification in starfish*

The identified gene of interest in starfish was the collagen biosynthesis enzyme *prolyl-4-hydroxylase* (*p4h*). Due to the absence of any transcriptome for this species, degenerate primers were designed to clone it using PCR. Degenerate primers from Zhang and Cohn (2006) for collagen genes were tested as well (see Table 2). As positive controls, *actin 1* and *ets1/2* were selected: the nucleotide sequence of *actin 1* (NCBI accession number: KC858258.1, GI: 525327359) was used to design specific primers and clone this gene, whereas to clone *ets1/2* degenerate primers already available in the laboratory were used (see Table 2). For the positive control genes, since the expected product length was lower than 300 bp to obtain longer RNA antisense probes for *in situ* hybridisation, 3'RACE was performed using a mixed cDNA samples from regenerate stages and the FirstChoice® RLM-RACE Kit (Ambion) according to manufacturer's instructions. For actin the protocol was successful and both PCR products were used to transcribe RNA antisense probes.

For *ets1/2* the 3'RACE was not successful and the degenerate PCR product was used to transcribe the probe.

*2.3.2. Candidate gene identification in brittle star*

Genes of interest were identified from EchinoBase (http://www.echinobase.org), starting with a targeted gene search in *Strongylocentrotus purpuratus* Gene bank with Gene ID, using Gene Name or Gene Synonym. BLAST-X analyses were performed over the *Afi* transcriptome (Dylus *et al.*, *submitted*) in order to obtain the corresponding gene sequences in *Amphiura filiformis*. The genes of interest were the collagen biosynthesis enzyme *prolyl-4-hydroxylase* (*p4h*) and *ficolin*. *Actin* (*Afi-actin*) was used as positive control.

*2.3.3. Primer design*

To identify the genes of interest in *E. sepositus* and *A. filiformis* different design strategies were followed depending on the gene selected. For the specific primers in both species PRIMER3 Software version 0.4.0 (http://primer3.ut.ee/) was used optimising the following parameters: max 3' stability was set at 8.0 and max polyX at 3. Primers were selected considering primer length and product length and for brittle star their specificity was checked performing a re-BLAST to the *A. filiformis* transcriptome (Dylus *et al.*, *submitted*). For degenerate primers, after a search by name in EchinoBase (including both *Strongylocentrotus purpuratus* and *Patiria miniata* genomes), EchinoDB (http://echinodb.uncc.edu/) and NCBI databases, a multialignment was performed in order to manually design them. Vertebrate collagen-specific degenerate primers designed by Zhang and Cohn (2006) were tested on *E. sepositus* cDNA. For both species degenerate primers were used to clone the second positive control, *ets1/2*. Table 2 summarises *E. sepositus* and *A. filiformis* primers used in this project.

**Table 2.** *List of E. sepositus (Ese) and A. filiformis (Afi) primers with corresponding primer length. Abbreviations and symbols:* bp=base pair; F=forward primer; R=reverse primer; *=degenerate primers; **=collagen-specific degenerate primers from Zhang and Cohn (2006).

| Primer Name | Primer Sequence (5'-3') | Primer Length (bp) |
|---|---|---|
| ***Ese-actin F*** | GTGCCCAGAAGCCTTGTTC | 19 |
| ***Ese-actin R*** | AGGATAGAGCCACCGATCC | 19 |
| ***ets1/2 deg F**** | CA(A/G)GA(A/G)CGNCUNGGNAU(A/C/U)CCNAA(A/G) | 24 |
| ***ets1/2 deg R**** | (A/G)TC(A/G)CANAC(A/G)AANCG(A/G)TANAC(A/G)TA | 24 |
| ***col deg F*** ** | GGCCCTCCCGGCCTGCARGGNATGCC | 26 |
| ***col deg R*** ** | GGGGCCGATGTCCACGCCRAAYTCYTG | 27 |
| ***p4h deg F**** | GGNCAYTAYGARCCNCAYTTYGAY | 24 |
| ***p4h deg R**** | DATCCADATRTTNGCNACCCAYTT | 24 |
| ***Afi-actin F*** | ACGACGAAGTATCCGCTTTG | 20 |
| ***Afi-actin R*** | TCGCATTTCATGATGCTGTT | 20 |
| ***Afi-ficolin F*** | CGATGGACATGATGGAAATG | 20 |
| ***Afi-ficolin R*** | GAGGGCCGCCAAGATATAAT | 20 |
| ***Afi-p4h F*** | TCTCCAATCATGGGCCTACT | 20 |
| ***Afi-p4h R*** | ACAGGTTTGCAGCCCATTT | 19 |

*2.3.4. RNA extraction, cDNA synthesis, gene cloning and antisense probe transcription*

For *A. filiformis* RNA was extracted and antisense probes were prepared as described by Ferrario and co-workers (*in preparation*). RNA of *E. sepositus* at different regenerating stages of interest (24 h, 72 h and 1 w p.a.) was extracted from 5 specimens per stage with the RiboPure Kit (Ambion) following manufacturer's instructions. cDNA synthesis was performed using the RETROscript kit (Ambion) following manufacturer's instructions and using 1 µg of RNA. Reactions were conducted as follows: 25°C for 5', 42°C for 30', 85°C for 5'. A pool of cDNA was prepared and used to perform different PCRs. The amplification protocol using Invitrogen reagents (*Taq* DNA Polymerase (Invitrogen) or Q5 High-Fidelity DNA Polymerase (New England BioLabs)) was optimised for each gene of interest (for details see Supplementary Materials). Moreover, when necessary 3'RACE was performed to obtain longer PCR products (for details see Supplementary Materials). All PCR products were subsequently ligated into pGEM®-T Easy Vector System I (Promega) and transformed in Subcloning Efficiency Invitrogen DH5α (Life Technologies) or Top 10 Competent Cells *E. coli* (Fisher Scientific) according to manufacturer's instructions. RNA antisense digoxigenin (DIG) labelled probes were then transcribed following classic procedures and using the Sp6/T7 Transcription Kit (Roche) plus a DIG-labelling mix (Roche), always following the manufacturer's guidelines.

*2.3.5. In situ hybridisation (ISH) on starfish sections*

For *in situ* hybridisation analysis starfish regenerating samples were fixed in 4% PFA in 0.1 M MOPS (pH 7) and 0.5 M NaCl or in 4% PFA in 1x PBS with 0.1% Tween-20 (PBST),

decalcified in Morse's solution (10% sodium citrate and 20% formic acid in DEPC-treated water) overnight at 4°C and embedded in paraffin wax as previously described (see paragraph 2.2.1). Samples were sectioned at 10 µm thickness with a Leica RM2155 microtome and, after optimisation steps, two different protocols were performed. The first protocol was modified from the whole mount protocol performed for *A. filiformis* samples. Briefly, sections were warmed up 30 minutes at 55°C and cooled down at RT for 15 minutes. Slides were de-waxed with Histoclear and rehydrated in a decreasing scale of ethanol in DEPC-treated water, washed twice in 1x MABT (0.1 M maleic acid pH 7.5, 0.15 M NaCl, 0.1% Tween-20 in DEPC-treated water) and post-fixed in 4% PFA in 1x MABT for 20 minutes at RT. After one wash in 1x MABT supplemented with 0.1% Tween-20, slides were washed in 1:1 solution of 1x MABT and hybridisation buffer (HB; 50% de-ionized formamide, 0.02 M Tris pH 7.5, 10% PEG, 0.6 M NaCl, 0.5 mg/ml yeast RNA, 0.1% Tween-20, 5 mM EDTA, 1X Denhardt's) for 5 minutes at RT. Then, slides were pre-hybridised in HB for 1 hour at 45°-55°C. Probes in HB were subsequently added at a final concentration ranging from 0.02 to 1 ng/µl and left for 1 or for 5 days at 45°-55°C in humid chamber. After several washes with 1:1 solution of 1x MABT and HB at 45°-55°C and in 1x MABT only at 45°-55°C, 2 washes in 0.1x MABT supplemented with 0.1% Tween at 45°-55°C were performed and then slides were blocked in 5% sheep serum in 1x MABT (blocking buffer, BB) for 30 minutes at RT and incubated in 1:1000 alkaline phosphates (AP) conjugated antibody anti-DIG (Roche) in BB for 1 hour at RT. After at least 5 washes in 1x MABT slides were washed twice in AP buffer (0.1 M Tris pH 9.5, 0.1 M NaCl, 0.05 M $MgCl_2$, 0.1% Tween-20, 1 mM Levamisole) and stained with NBT/BCIP mix (Roche) with 10% dimethylformamide in AP buffer. When staining was complete the reaction was stopped with one wash in 1x MABT with 0.5 M EDTA followed by three washes in 1x MABT. Finally, slides were mounted with 50% glycerol and stored at RT till observation.

The second protocol performed was described by Etchevers and co-workers (2001) and modified by Gillis and co-workers (2012). Briefly, slides were de-waxed with Histoclear (2x 5 minutes) and rehydrated in a decreasing series of ethanol in DEPC-treated 1x PBS. Slides were then subsequently rinsed in DEPC-treated water, DEPC-treated 1x PBS with 0.1% Tween-20 and 2x SSC solution. After preparing the hybridisation mix (1x salt solution, 50% formamide, 10% dextran sulfate, 1 mg/ml yeast tRNA, 1x Denhardt's solution in DEPC-treated water; salt solution: 0.2 M NaCl, 0.89 mM Tris HCl, 0.11 mM Tris base, 5 mM $NaH_2PO_4xH_2O$, 5 mM $Na_2HPO_4$, 5 mM EDTA), probes at 1 ng/µl were added and slides were incubated under glass coverslip at 65°-70°C overnight in humid

chamber. Two washes of 30 minutes each in pre-warmed 50% formamide, 1x SSC and 0.1% Tween-20 were performed at 65°-70°C in order to remove the coverslips and slides were washed 3x 10 minutes in 1x MABT at RT. Slides were then blocked for 2 hours at RT in 1% Roche blocking reagent in 1x MABT with 20% sheep serum (Sigma-Aldrich). Later on, 1:1000 anti-DIG-AP in the same solution was added and left overnight at RT in humid chamber. Slides were washed 4-5 times in 1x MABT and then equilibrated in NTMT (0.1 M NaCl, 0.1 M Tris pH 9.5, 5 mM $MgCl_2$ and 0.1% Tween-20 in milliQ water). Staining was performed by adding BM Purple AP substrate (Roche) at RT in the dark and stopped with 1x PBS. Slides were post-fixed for 5 minutes in 4% PFA in 1x PBS, washed with 1x PBS and mounted with DAPI Fluoromount-G® (SouthernBiotech).
After both protocols, the slides were imaged under a Zeiss AxioImager M1 microscope equipped with a Zeiss AxioCamHRc camera.

*2.3.6. Whole mount in situ hybridisation (WMISH) on brittle star samples and post in situ sectioning*

Brittle star regenerating samples were fixed in 4% PFA in 1x PBST and stored in 100% methanol at -20°C till performing whole mount *in situ* hybridisation (WMISH). WMISH was performed together with positive controls as previously described (Ferrario *et al.*, *in preparation*). After imaging, WMISH samples were embedded in paraffin wax and sectioned according to Ferrario and co-workers (*in preparation*) in order to better define the tissue-specific expression pattern of the RNA antisense probes. Slides were observed under a Jenaval light microscope provided with a DeltaPix Invenio 3S 3M Pixel CMOS camera and DeltaPix ViewerLE Software.

## *3. Results*

Before describing the events occurring during the regenerative process, a brief summary of the gross morphology of starfish and brittle star arms is here provided in order to facilitate the understanding of the subsequent results. Further details are provided in Ben Khadra and co-workers (2015a) for *E. sepositus* and Czarkwiani and co-workers (2016) for *A. filiformis*. Figure 1 shows schemes of cross sections of both experimental animal arms.

The starfish arm is mainly occupied by a spacious perivisceral coelom containing the pyloric caeca (part of the digestive tract), and the ampullae, the inner outgrowths of the tube feet or podia. Two rows of podia orally run along the whole arm together with the

externally exposed radial nerve cord and the radial water canal. The body wall is mainly occupied by calcitic ossicles and spines embedded in an abundant dermal layer and joined by muscle bundles.

The brittle star arm is subdivided in repetitive segments each one mainly occupied by a set of skeletal elements, namely the central vertebra, the inner aboral, oral and lateral shields and the external spines, embedded in a thin dermal layer. Muscle bundles and ligaments link the adjacent segments and allow the typical snake-like movements of the arms. Only three main structures uninterruptedly run along the whole arm: the aboral coelomic cavity (that is much reduced if compared to the starfish one), the radial water canal, and the radial nerve cord, the latter, differently from starfish, is located inside the arm. Differently from starfish, the digestive tract is not hosted in the arm.

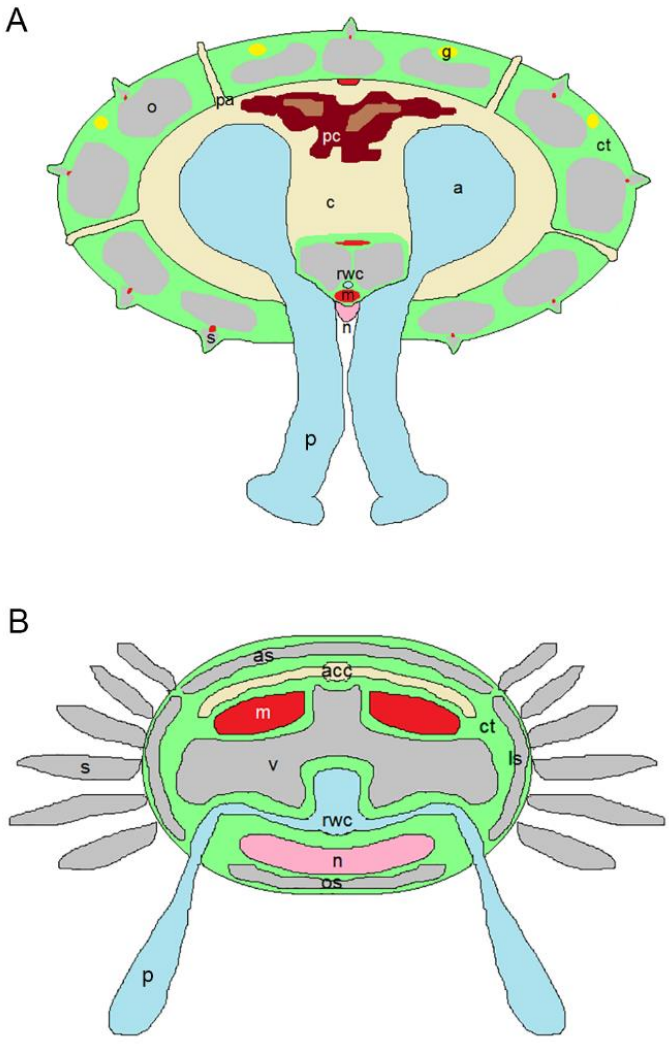


**Fig. 1.** *Gross morphology of starfish and brittle star arms.* A) Schematic cross section of an arm of *Echinaster sepositus* showing its main features. B) Schematic cross section of an arm of *Amphiura filiformis* showing its main structures. *Abbreviations*: a=ampulla;

◀ acc=aboral coelomic cavity; as=aboral shield; c=coelom; ct=connective tissue; g=mucous gland; ls=lateral shield; m=muscle; n=radial nerve cord; o=ossicle; os=oral shield; p=podium; pa=papula; pc=pyloric caeca; rwc=radial water canal; s=spine; v=vertebra.

### *3.1. Microscopic anatomy of the repair phase*

#### *3.1.1. Emergency reaction and re-epithelialisation*

Immediately after traumatic amputation both starfish and brittle star respond to the injury with actions aimed to avoid coelomic fluid loss and the entrance of debris, pathogens and microorganisms.

In less than one hour p.a. in starfish a circular contraction of the body wall close to the amputation plane forms, providing a first sealing of the wide perivisceral coelomic cavity (Fig. 2A). Sealing of the perivisceral canal is further achieved in the following 24-48 hours by a downward folding of the aboral wall and apical shrinkage of the wound edges. In brittle star no evident haemostatic ring is visible. The coelomic cavities and vessels (the aboral coelomic cavity and the radial water canal) are simply sealed by a downward and upward bending respectively of the first aboral and oral shields proximal to the amputation plane (Fig 2C). The muscular valves along the radial water canal proximal to the injury apparently remain opened until stage 2 (3-5d p.a.; Fig. 2B) when they get closed possibly to allow an increase of hydrostatic pressure within the radial water canal (Fig. 2D). In both animal models the narrowing of the wound edges allows a reduction of the wound surface and protect it from external insults; additionally, clotting phenomena of circulating cells are visible at the level of the coelomic cavity, close to the amputation plane (Fig. 2F): coelomocytes and other cytotypes are actively recruited also from tissues around or even far from the amputation plane throughout the whole repair phase e.g. papulae in starfish (Fig. 2E). In both starfish and brittle star signs of histolysis and remodelling of injured tissues (mainly muscles) are soon detectable (Fig. 2C, 5F, 5G).

Almost simultaneously to the first emergency reaction, the actual healing of the injury begins. In both models this is initially achieved by stump epidermal cells.

In starfish the first wound epithelium (Fig. 3A, B), already presenting microvilli projecting through the cuticle that covers it (Fig. 4A), is visible within 24-48h p.a. and is mainly composed of stretched epithelial cells of the wound edges which dramatically change from a columnar to a squamous morphology and centripetally migrate over a network-shaped syncytium of phagocytes and other cytotypes e.g. dedifferentiating myocytes (Fig. 3C, D, 4B; Ben Khadra *et al.*, 2015a), without losing their junctional connections. The

basement membrane is not visible till around 72 hours p.a. though several nervous processes of the sub-epithelial nervous plexus are already detectable (Fig. 4A).

In brittle star, an almost complete wound epidermis is present already within 8 hours p.a. (Fig. 3E). This already possesses a well-defined cuticle presenting microvilli in the subcuticular space and microvillar tips on top of the homogeneous layer (Fig. 4C). Epidermal cells do not remarkably stretch, apparently maintaining the flat-cubic morphology of non-regenerating conditions: they have big roundish patchy nucleus and in the apical portion are jointed together by junctional complexes (Fig. 4D). The analysis of serial sections of samples at different regenerative stages shows that, similarly to starfish, the epidermal sheet centripetally migrates over the wound. No basal membrane is visible underneath the new epithelium. In both the subcuticular space and the wound area underlying the wound epithelium numerous bacteria are present (Fig. 4C, E). At 16 hours p.a. (Fig. 3F) several phagosomes are visible in this tissue (Fig. 4F) suggesting a high phagocytic activity, likely on bacteria and debris still present in the wound area (Fig. 4F, G). No phagocyte syncytium is detectable underlying the wound epidermis.

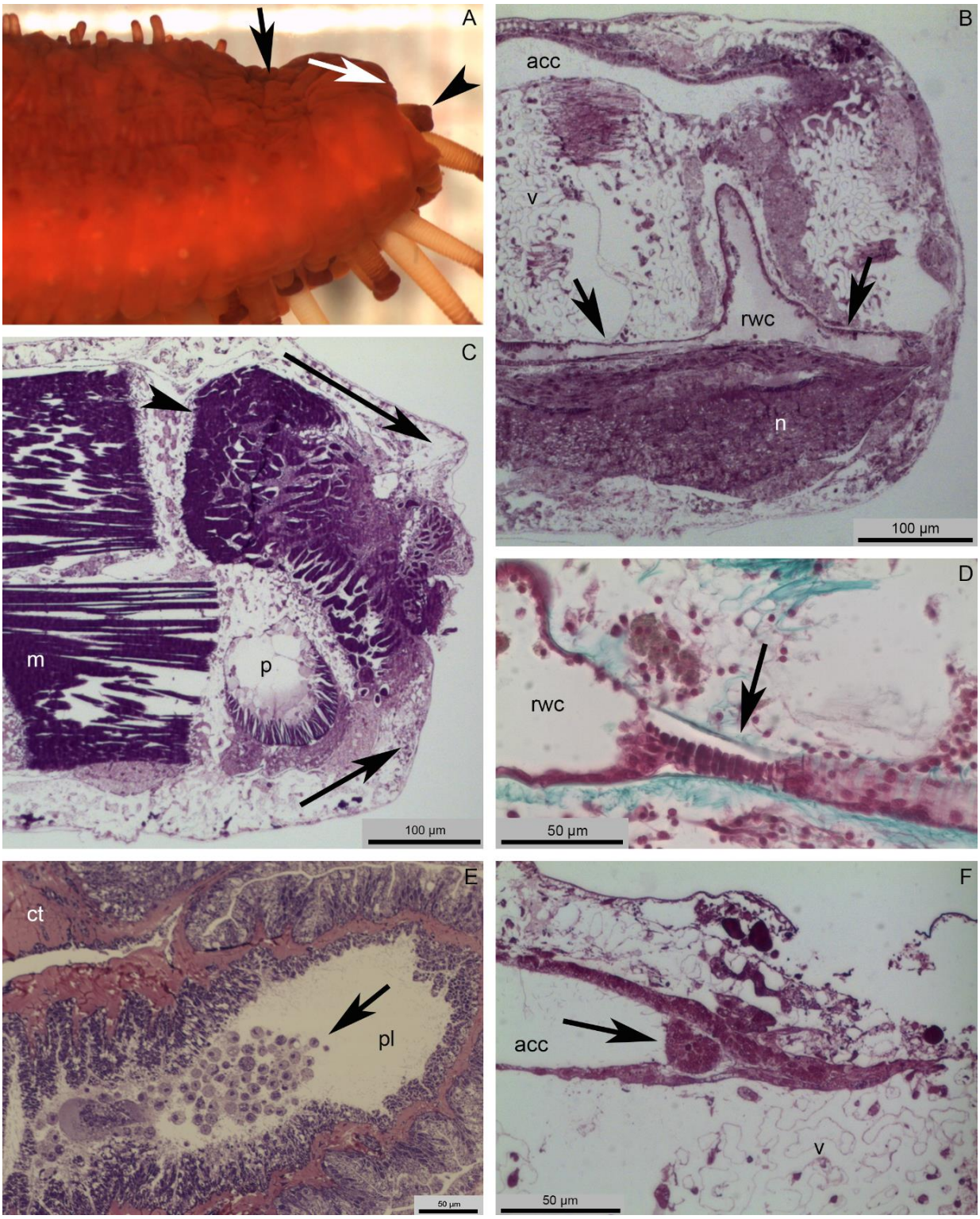


**Fig. 2.** *Emergency reaction*. A) Stereomicroscope lateral view of the starfish arm stump one hour p.a. The haemostatic ring is visible (black arrow) immediately behind the amputation plane. The first pair of podia (arrowhead) is contracted at the level of the injury in order to help wound closure by reducing its surface. The aboral body wall moves toward the oral side (white arrow). B) Semi-thin sagittal section of the brittle star arm stump 16 hours p.a. showing that the radial water canal is completely pervious (arrows). C) Semi-thin sagittal section of the brittle star arm stump 16 hours p.a. showing the downward and upward movements of the aboral shield and of the oral shield respectively (arrows) to help wound closure. The intervertebral muscles involved in the amputation already show

◀ rearrangement phenomena (arrowhead). D) Thick sagittal section of the brittle star arm stump 5 days p.a. showing a valve of the radial water canal (arrow) that is closed to increase inner hydrostatic pressure. E) Semi-thin sagittal section of a starfish papula far from the amputation plane showing circulating cells (presumptive coelomocytes) that are recruited for regeneration at 72 hours p.a. F) Semi-thin sagittal section of a brittle star arm 8 hours p.a. showing that at the level of the aboral coelomic cavity lumen cells are clotting (arrow) in order to seal the cavity and avoid loss of fluid. *Abbreviations*: acc=aboral coelomic cavity; ct=connective tissue; m=muscle; p=podium; pl=papula lumen; n=radial nerve cord; rwc=radial water canal; v=vertebra.

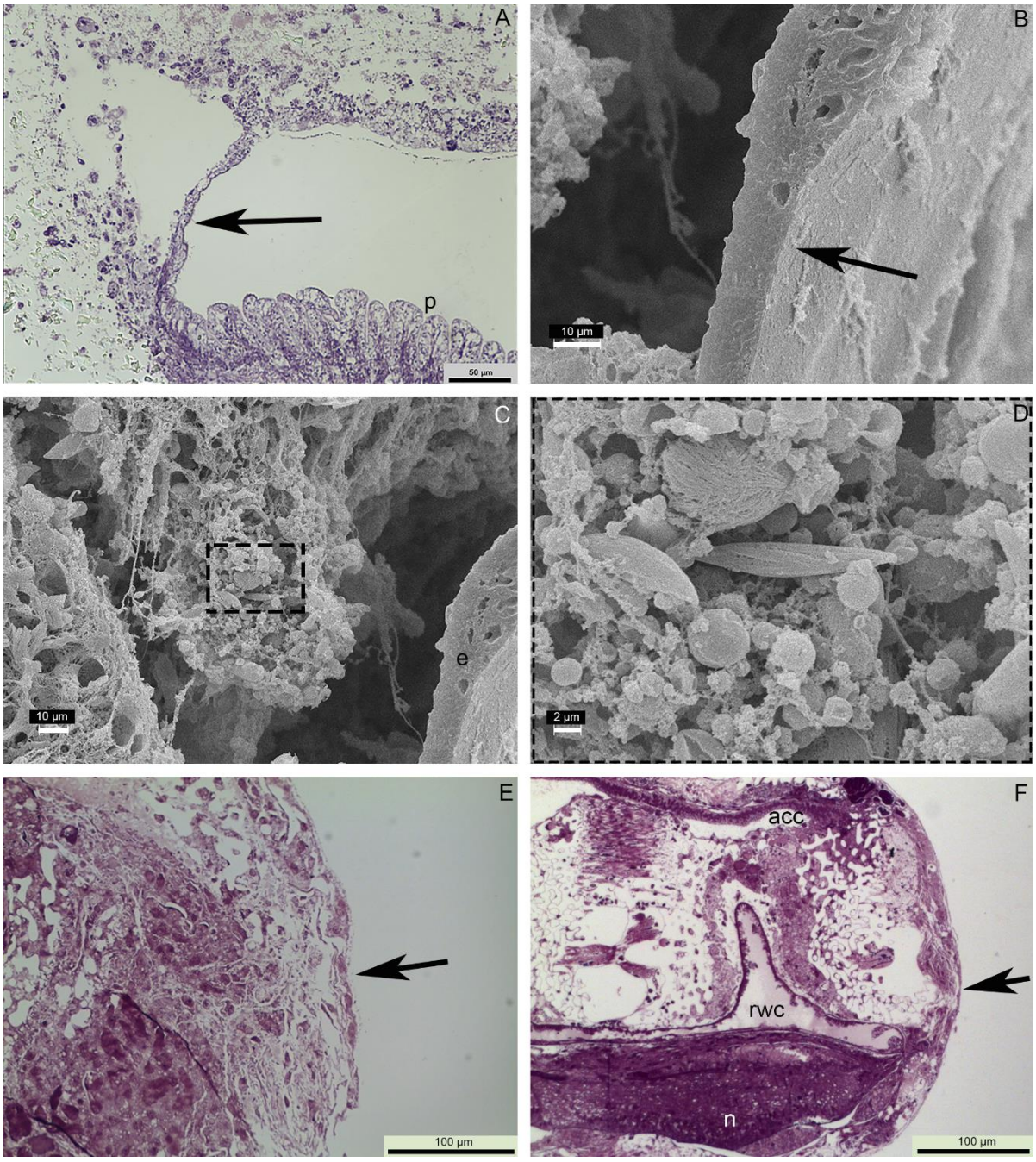


**Fig. 3.** *Wound closure*. A) Semi-thin parasagittal section of the starfish regenerating arm 24 hours p.a. where the new thin epithelium covering the wound is visible (arrow). B) SEM sagittal view of the starfish new epithelium (arrow) 24 hours p.a. C) SEM sagittal view of the starfish wound area 24 hours p.a. showing that immediately behind the new

epithelium a clot of cells is visible. D) Detail of C showing cells of the clot with different shapes. Roundish cells (possibly phagocytes) and spindle-like cells (dedifferentiating myocytes) are visible. E) Semi-thin parasagittal section of the brittle star regenerating arm 8 hours p.a. showing that the wound is already healed by a thin new epithelium (arrow). F) Semi-thin sagittal section of the brittle star regenerating arm 16 hours p.a. where the new epithelium covers the whole wound surface (arrow). *Abbreviations*: acc=aboral coelomic cavity; e=epithelium; n=radial nerve cord; p=podium; rwc=radial water canal.

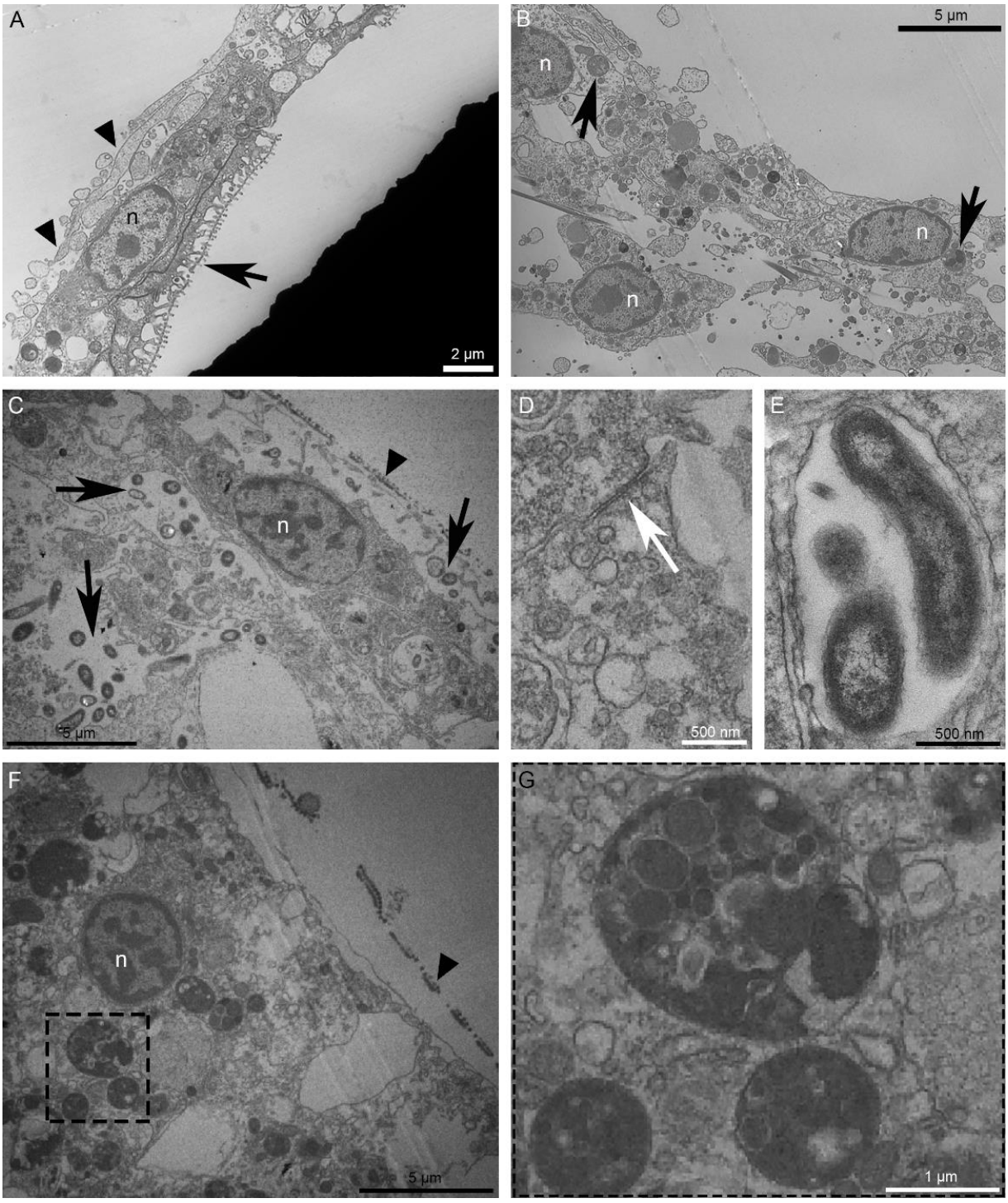


**Fig. 4.** *Re-epithelialisation phenomenon*. A) TEM micrograph of the starfish new epithelium 24 hours p.a. The epithelial cells present nucleus (n) with a well-defined nucleolus and bearing microvilli (arrow). The basement membrane is not visible but

◀ numerous processes of the sub-epithelial nervous plexus (arrowheads) are detectable. B) TEM micrograph of the starfish clot of cells immediately behind the new epithelium 24 hours p.a. This clot is mainly composed of phagocytes displaying almost roundish nuclei (n) and several phagosomes (arrows). C) TEM micrograph of the brittle star new epithelium 8 hours p.a. Epithelial cells present a nucleus (n) with well-defined nucleolus and cuticle. Numerous bacteria (arrows) are present both underneath the epithelium and in the subcuticular space. D) TEM micrograph detail on a junction complex (arrow) between epithelial cells of the new brittle star epithelium 8 hours p.a. E) TEM micrograph detail of bacteria present during brittle star re-epithelialisation 8 hours p.a. They are enveloped by a thin membrane. F) TEM micrograph of the brittle star new epithelium 16 hours p.a. Epithelial cells show a well-defined cuticle (arrowhead) and spread within them phagocytes are detectable with patchy nucleus (n) and several phagosomes. G) Detail of F on phagosomes. *Abbreviation*: n=nucleus.

*3.1.2. Collagen appearance and immunolocalisation*

In starfish at one week p.a. the damaged area is completely healed (Fig. 5A, B) with podia protecting the delicate regenerating area from external insults (Fig. 5C). At the level of the regenerating zone the new epidermis is well differentiated already at 72 hours p.a. (Fig. 6A, B) and an oedematous area is detectable behind it (Fig. 5C, D, E, 6C) composed of different cytotypes (Fig. 6; Ben Khadra *et al.*, 2015a) interspersed in an initially nonfibrillar collagenous material and wide empty lacunar spaces (Fig. 5D, E, 6D, E). Collagen fibrils organised in small bundles are detectable in the oedematous area starting from one week p.a. (Fig. 6F, G, H) providing the first meshwork scaffold for cell migration and tissue regeneration.

In brittle star, an oedematous area comparable to that described in starfish is never detectable (Fig. 5F). Muscles damaged by the amputation event are actively remodelled with myocytes showing spindle-like structures composed of their packed contractile apparatus (Fig. 5F, G). Behind the new epidermis extracellular matrix deposition starts around 3 days p.a. and collagen is detectable in a thin dermal layer (Fig. 5G). The outgrowths of the regenerating radial nerve cord, radial water canal and aboral coelomic canal (the main structures composing the axial core) (Fig. 5F) are then surrounded and supported by an already well-organised thin dermal layer which becomes slightly more evident from around 8 days p.a. onwards (Fig. 5H, I, J).

As previously mentioned, collagen deposition occurs differently in the two experimental models. In the starfish collagen fibrils are detectable only from around 7 days p.a. onwards. Instead, in brittle star collagen deposition is detectable earlier, a thin layer of well-organised connective tissue being already visible 3 days p.a. In parallel to histological and ultrastructural analyses and to better define the timing of collagen

deposition onset, we evaluated the presence of fibrous collagen at the level of the wound area by using an antibody raised against the fibrous collagen of the sea cucumber *H. glaberrima* (Quiñones *et al.*, 2002, HgfCOL).

In starfish sections a faint immunolabelling is visible at the level of the epidermis in one week p.a. regenerating samples, in both the apical (cuticle) and basal portions of the epidermis (Fig. 7). In the latter the specific intra- or extra-cellular localisation could not be determined.

Similarly, in brittle star the anti-HgfCOL labels the regenerating epidermis at both 24 and 48 hours p.a. (Fig. 8); however, in the latter the signal is increased and more widespread, being detectable also deeper in the underlying connective tissue layer (new dermal layer). The same staining is not visible in the connective tissue of the stump.

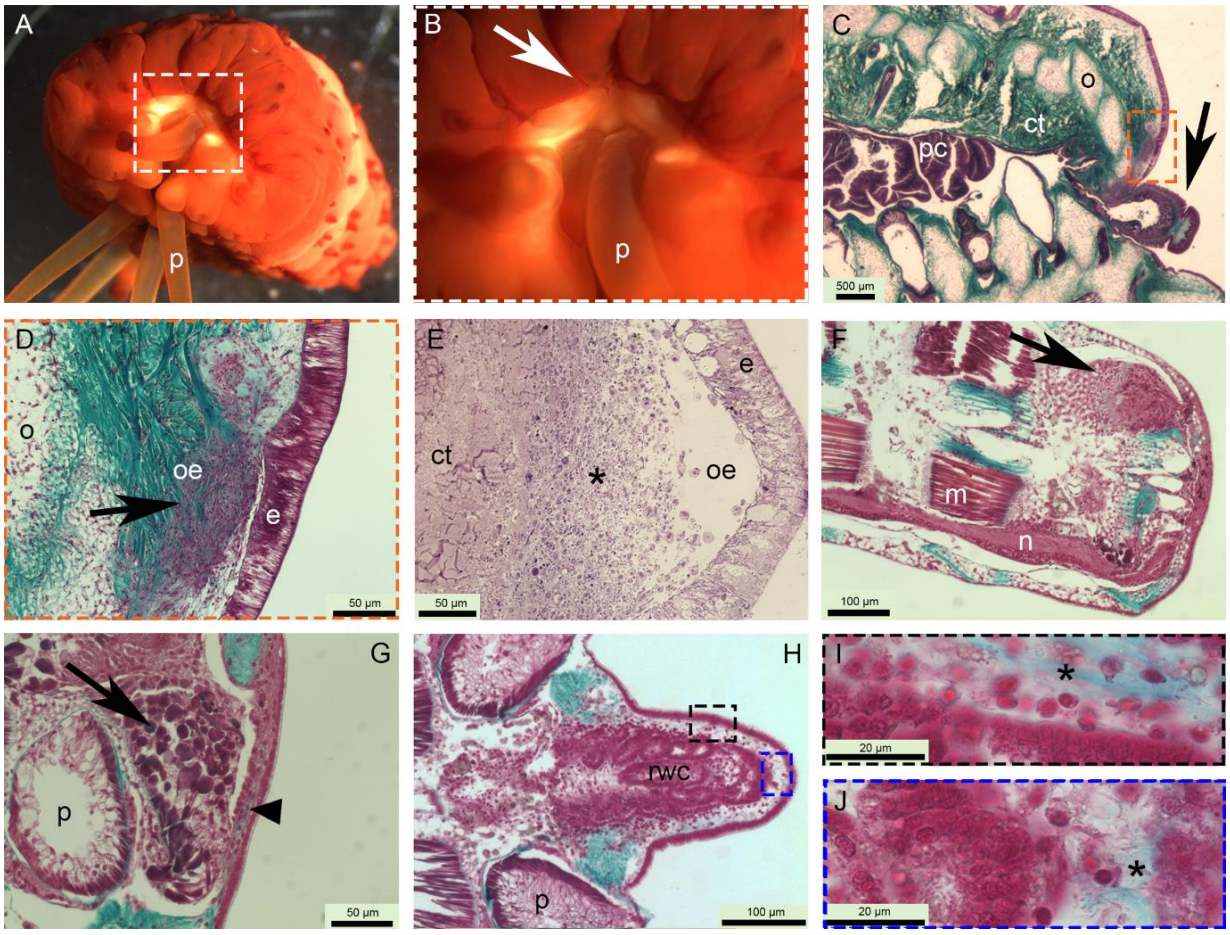


**Fig. 5.** *Oedematous area formation and collagen deposition in starfish and brittle star regenerating arms.* A-E starfish regenerating arms; F-J brittle star regenerating arms. A) Stereomicroscope frontal view of the regenerating arm one week p.a. showing the complete healing of the damaged area. B) Detail of A on the cicatrisation area (arrow). C) Thick parasagittal section of the regenerating arm one week p.a. showing the oedematous area forming at the level of the cicatrisation area and the persistent upward position of the first pair of podia (arrow) possibly to protect the delicate regenerating area.

◀ D) Detail of C on the oedematous area. One week p.a. the new epidermis resembles the stump epidermis and immediately behind it an oedematous area (arrow) of cells and extracellular matrix (ECM) is present. E) Semi-thin parasagittal section of the regenerating arm one week p.a. where the oedematous area is visible underneath the new epidermis. Cell and newly-deposited ECM are detectable (*). F) Thick sagittal section of the regenerating arm 72 hours p.a. showing massive rearrangement of the muscles directly involved in the injury (arrow). At the level of the regenerating area both the radial nerve cord and the aboral coelomic cavity show signs of re-growth. G) Thick parasagittal section of the regenerating arm 72 hours p.a. where behind the new epidermis an injured muscle (arrow) is rearranging and myocytes present the typical spindle-like shape. New collagen is already visible underneath the new epidermis (arrowhead). H) Thick frontal section of the regenerating arm around 8 days p.a. (stage 4) where together with the main longitudinal structures the podia are regenerating immersed in a thicker and more organised dermis. I) Detail of K on the lateral oral dermis. New collagen is labelled in green/cyan (*). J) Detail of K in the distal-most dermis of the tip. New collagen is labelled in green/cyan (*) and the dermis appears slightly less organised than that in the proximal side of the regenerate. *Abbreviations and symbols*: ct=connective tissue; m=muscle; n=radial nerve cord; o=ossicle; oe=oedematous area; p=podium; pc=pyloric caeca; rwc=radial water canal; * in E=oedematous area; * in I and J=newly deposited collagen.

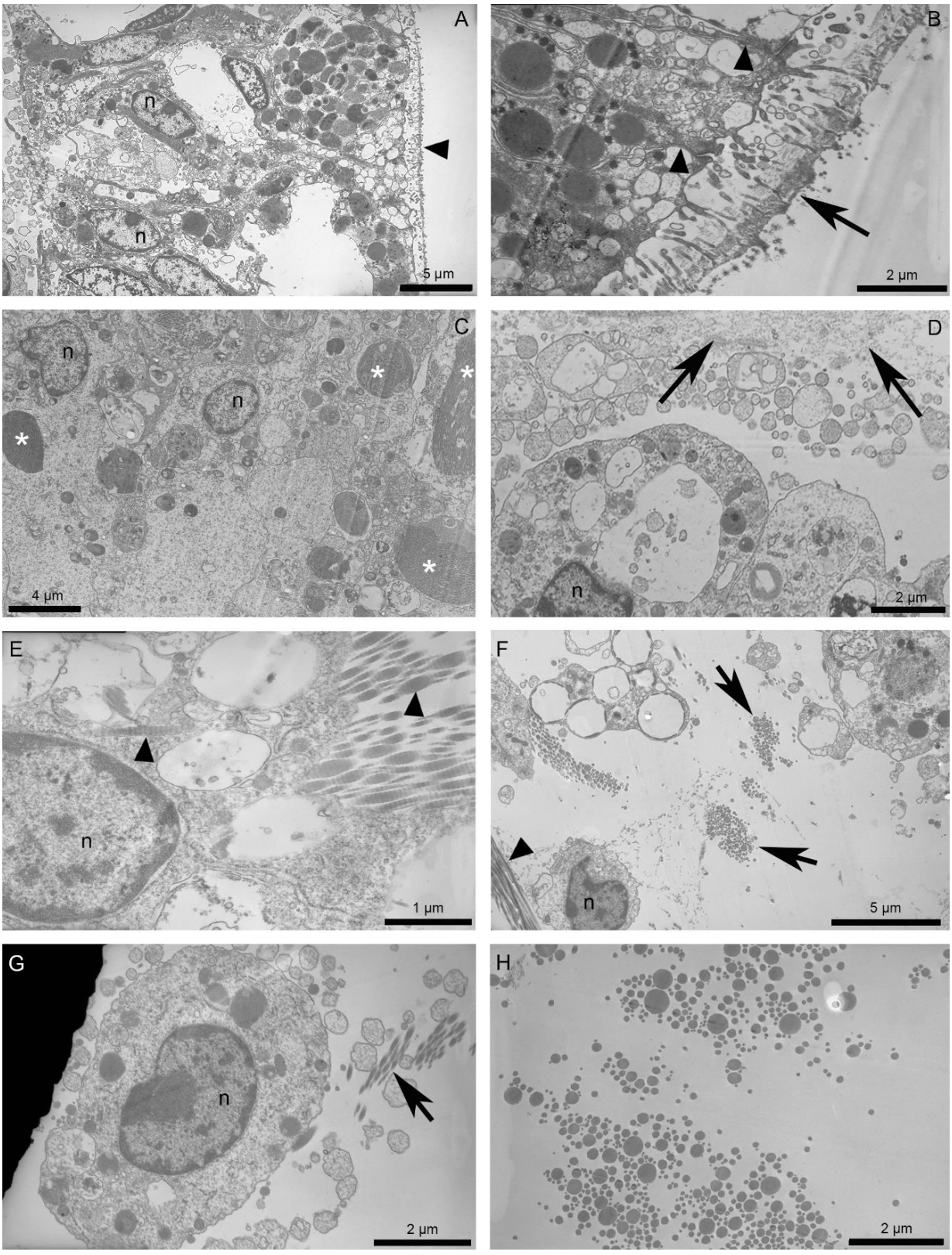


**Fig. 6.** *Starfish oedematous area 72 hours and one week p.a.* A) TEM micrograph of the new epidermis 72 hours p.a. It is thicker and more differentiated than that at 24 hours p.a. with a well-defined cuticle (arrowhead). B) TEM micrograph detail of the apical part of the new epidermis 72 hours p.a. showing cell junctions between adjacent epithelial cells (arrowheads) and microvilli projecting through the fuzzy coat and the double-layered cuticle that covers it (arrow). C) TEM micrograph at the level of the oedematous area 72 hours p.a. Where cells are crowded together new collagen fibrils are not detectable. The

predominant cytotype is the dedifferentiating myocyte recognisable by the spindle-like structure (*) indicating the rearrangement and loss of their contractile apparatus. D) TEM micrograph at the level of the oedematous area 72 hours p.a. where cells are immersed in a nonfibrillar collagenous material (arrows). E) TEM micrograph of a presumptive fibroblast in the oedematous area 72 hours p.a. Collagen fibrils in longitudinal section (arrowheads) are visible. F) TEM micrograph of the oedematous area one week p.a. where more numerous new collagen fibrils in cross section (arrows) and longitudinal section (arrowhead) are visible spread among oedematous cells. G) TEM micrograph of a presumptive undifferentiated cell in the oedematous area one week p.a. This cell presents a big roundish nucleus with a well-defined nucleolus and new collagen fibrils (arrow) are spread around it. H) TEM micrograph detail on new collagen fibrils present in the oedematous area one week p.a. The fibrils in cross section show highly different diameters. *Abbreviation and symbols*: n=nucleus; *=spindle-like structure.

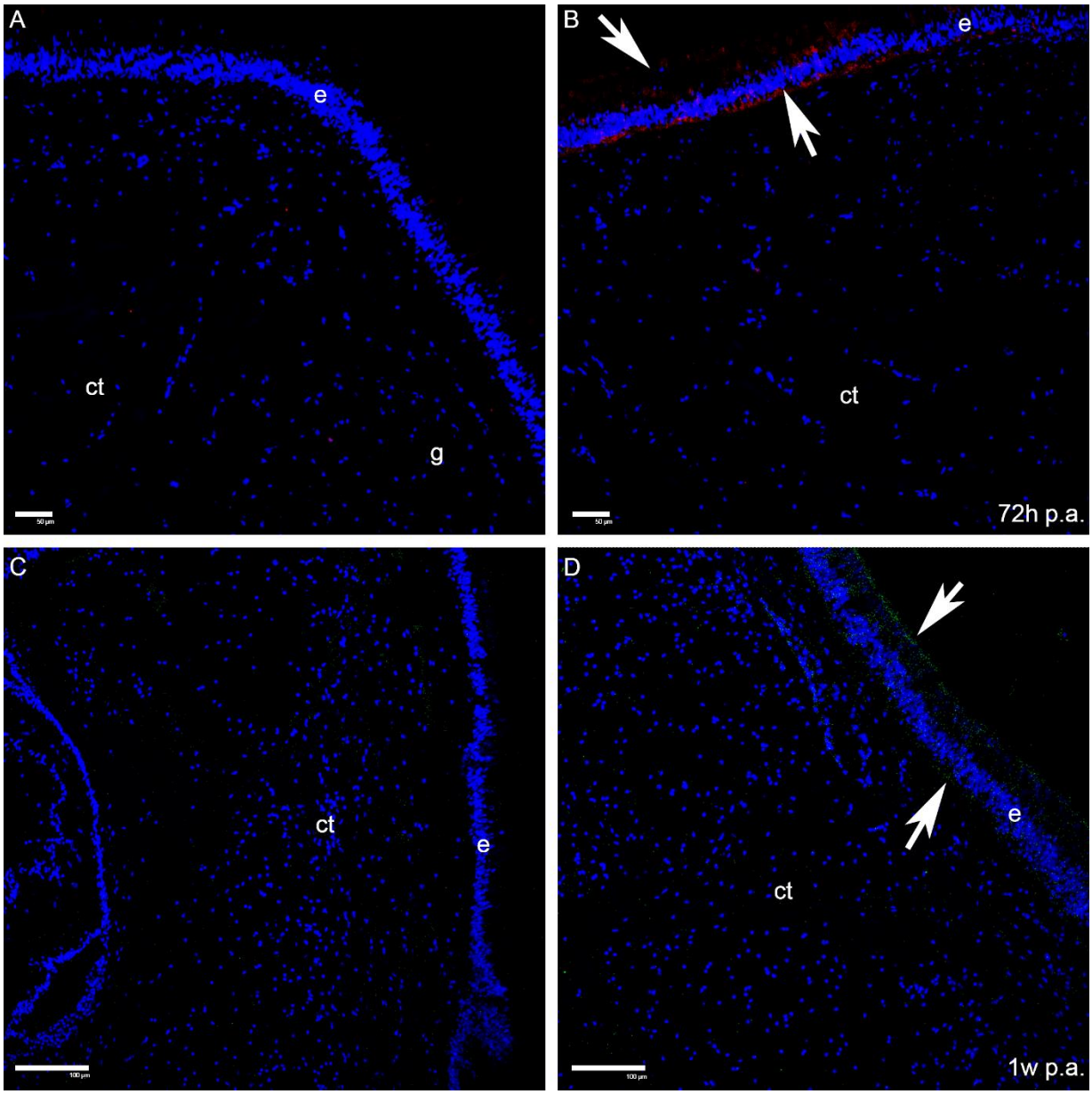


**Fig. 7.** *Immunohistochemistry on starfish sections using anti-HgfCOL.* Nuclei are labelled in blue (DAPI). In all images brightness and contrast values were increased to 90 and 23 respectively using Photoshop CC (2014) in order to better visualise the immunostaining.

◀ A) Negative control (no primary Ab) on the stump aboral body wall. B) On the stump aboral body wall of a 72 hours p.a. sample anti-HgfCOL is present at the level of the apical (cuticle) and basal layers of the epidermis (arrows). C) Negative control (no primary Ab) on the regenerating area. D) On the regenerating area one week p.a. anti-HgfCOL is faintly present at the level of the apical (cuticle) and basal layers of the new epidermis (arrows). *Abbreviations*: ct=connective tissue; e=epidermis; g=mucous gland.

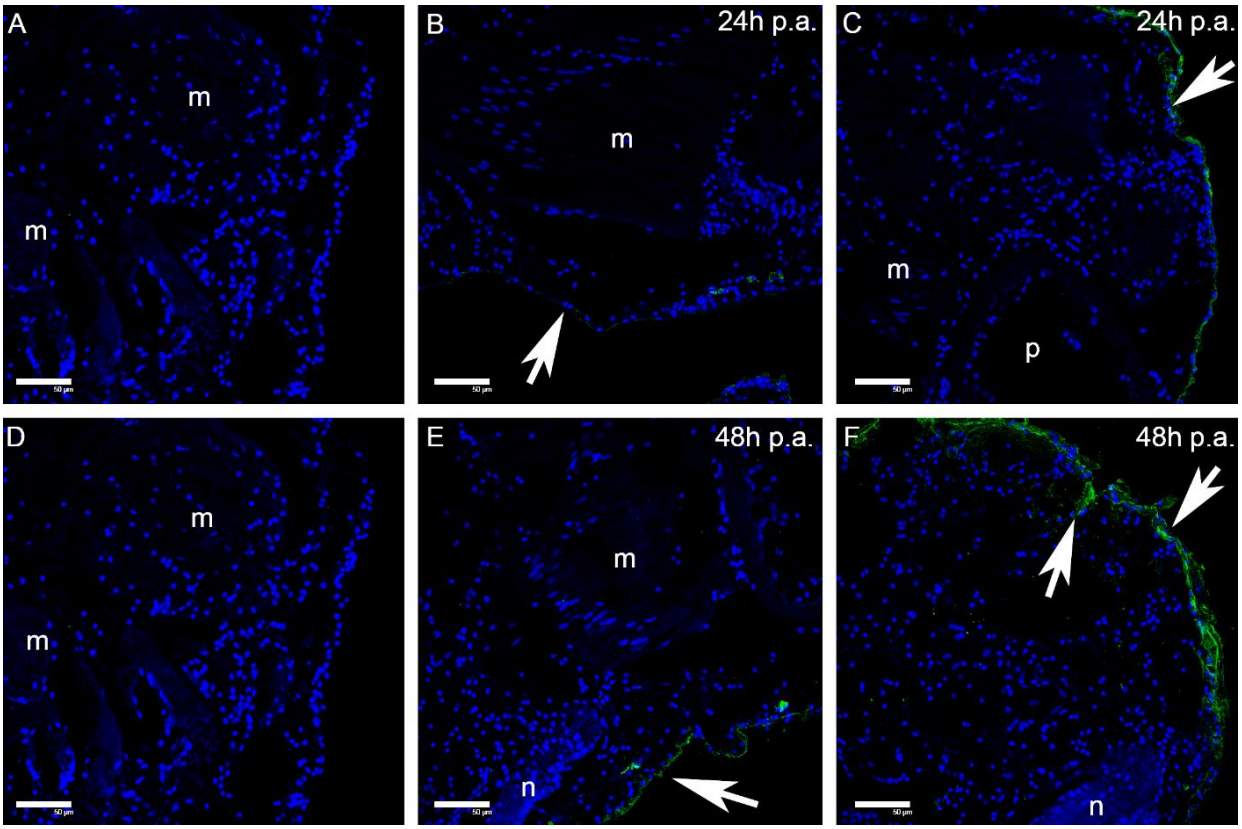


**Fig. 8.** *Immunohistochemistry on brittle star sections using anti-HgfCOL.* Nuclei are labelled in blue (DAPI). In all images brightness and contrast values were increased to 90 and 23 respectively using Photoshop CC (2014) in order to better visualise the immunostaining. A) Negative control (no primary Ab) on the regenerating area 48 hours p.a. B) On the stump oral area of a 24 hours p.a. sample anti-HgfCOL is present at the level of the epidermis (arrow). C) On the regenerating area of a 24 hours p.a. sample anti-HgfCOL is present at the level of the epidermis (arrow). D) Negative control (no primary Ab) on the regenerating area 48 hours p.a. E) On the stump oral area of a 48 hours p.a. sample anti-HgfCOL is present at the level of the epidermis (arrow). F) On the regenerating area of a 48 hours p.a. sample anti-HgfCOL is present at the level of the epidermis and in the connective tissue immediately underneath (arrows). *Abbreviations*: m=muscle; n=radial nerve cord; p=podium.

### *3.1.3. TNF-α-like immunolabelling*

TNF-α (cytokine) is a marker of wound healing response usually expressed in mammals mainly in macrophages and epidermal cells (Pastar *et al.*, 2014). In order to investigate the immune response after traumatic amputation in echinoderms a commercial mouse anti-TNF-α was used.

As it is shown in Fig. 9, in starfish the antibody faintly labels the new epidermis at both 72 hours and one week p.a. A weak signal is detectable also in the stump epidermis. In brittle star a much stronger TNF-α-like immunolabelling is detected in the wound epidermis as well at both 24 and 48 hours p.a., showing a time-dependent decrease (Fig. 10). At 24 hours p.a. the signal is localised also deeper in the tissues below the new epidermis. A faint labelling is also detected in the stump epidermis although to a much less extent.

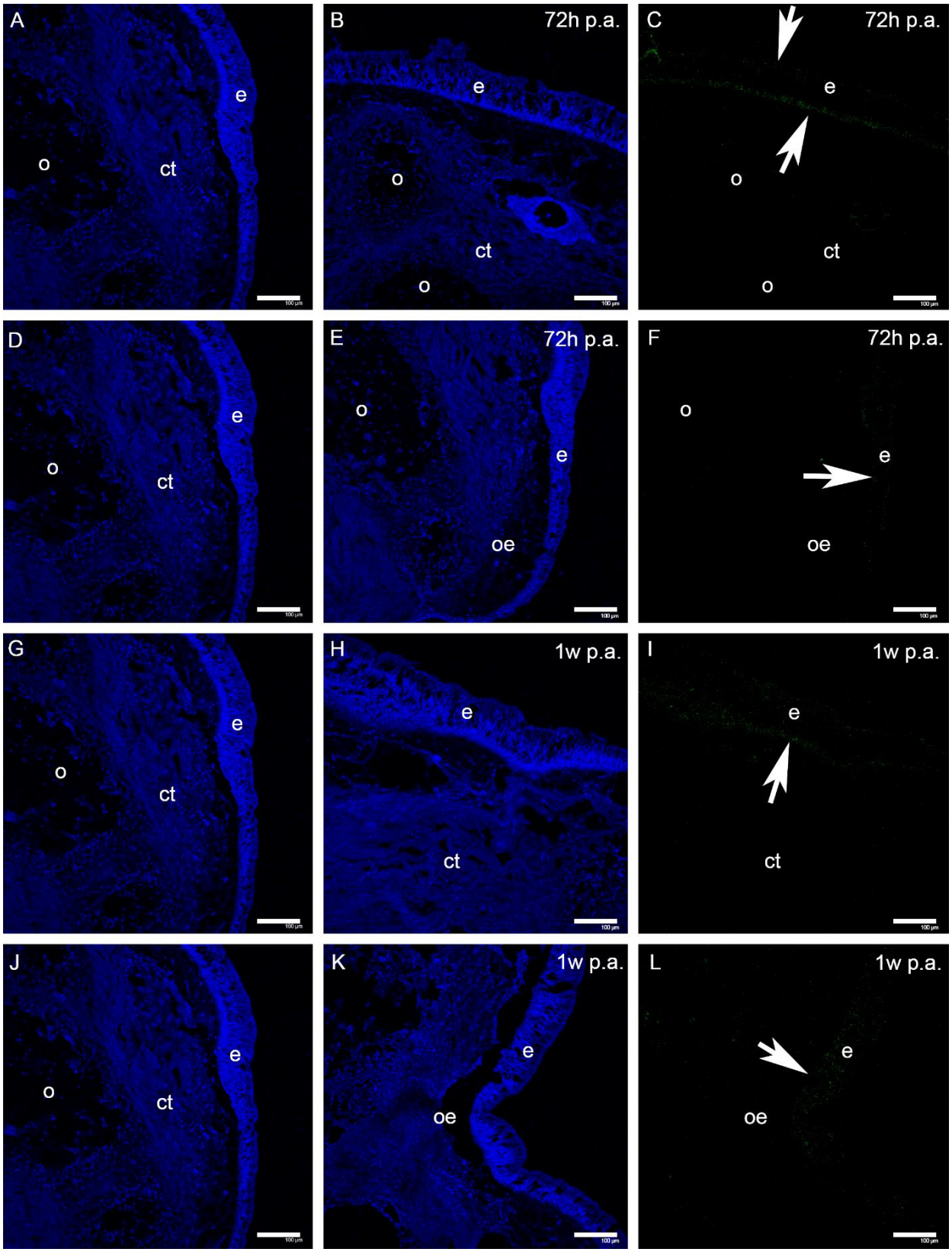


**Fig. 9.** *Immunohistochemistry on starfish sections using anti-TNF-α-like antibody.* Nuclei are labelled in blue (DAPI). In all images brightness and contrast values were increased to 90 and 23 respectively using Photoshop CC (2014) in order to better visualise the immunostaining. A) Negative control (no primary Ab) on the regenerating area 72 hours p.a. B) Stump aboral area of a 72 hours p.a. sample labelled with DAPI. C) Corresponding green channel of B showing that anti-TNF-α-like presents a faint signal in the apical and

basal parts of the stump epidermis (arrows). D) Negative control (no primary Ab) on the regenerating area 72 hours p.a. E) Regenerating oedematous area of a 72 hours p.a. sample labelled with DAPI. F) Corresponding green channel of E showing that anti-TNF-α-like presents a faint signal in the apical and basal parts of the new epidermis (arrow). G) Negative control (no primary Ab) on the regenerating area 72 hours p.a. H) Stump aboral area of a one week p.a. sample labelled with DAPI. I) Corresponding green channel of H showing that anti-TNF-α-like presents a faint signal in the stump epidermis (arrow). J) Negative control (no primary Ab) on the regenerating area 72 hours p.a. K) Regenerating oedematous area of a one week p.a. sample labelled with DAPI. L) Corresponding green channel of K showing that anti-TNF-α-like presents a faint signal in the new epidermis (arrow). *Abbreviations*: ct=connective tissue; e=epidermis; o=ossicle; oe=oedematous area.

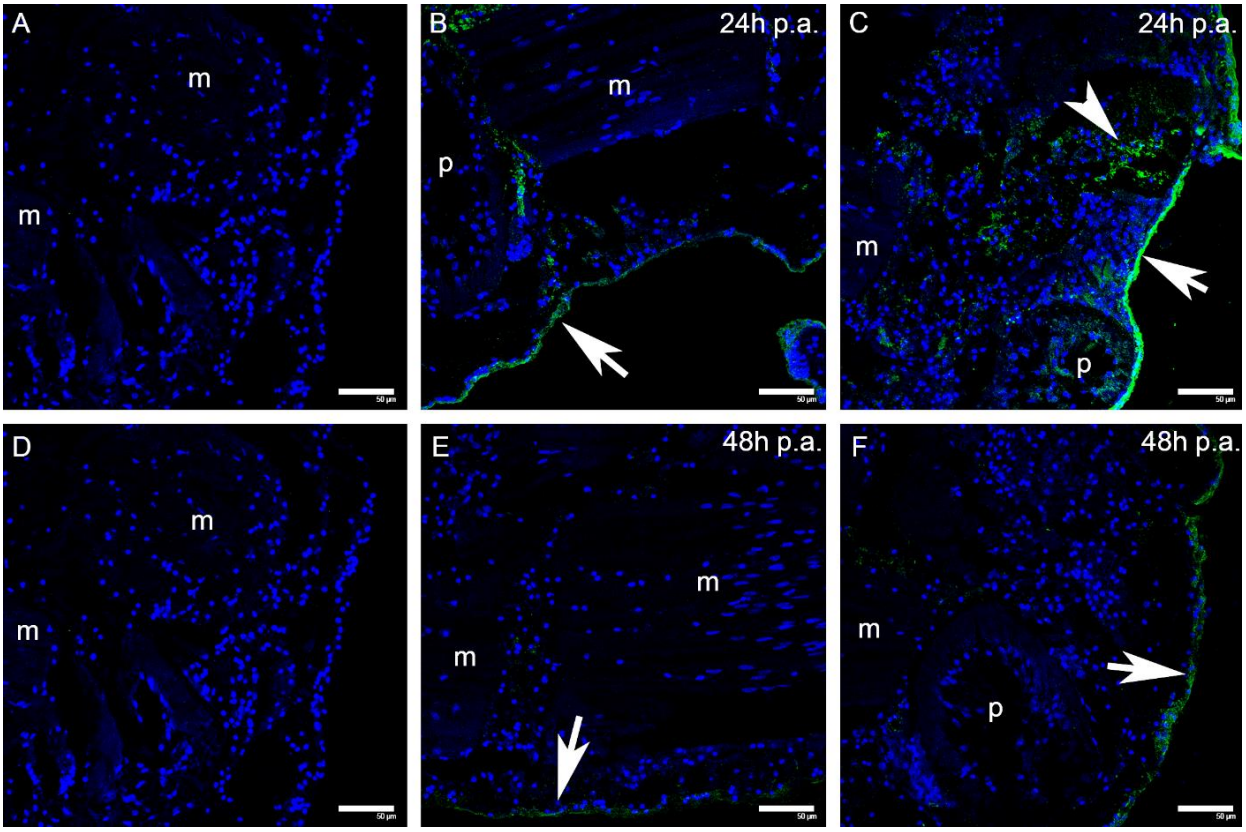


**Fig. 10.** *Immunohistochemistry on brittle star sections using anti-TNF-α-like antibody.* Nuclei are labelled in blue (DAPI). In all images brightness and contrast values were increased to 90 and 23 respectively using Photoshop CC (2014) in order to better visualise the immunostaining. A) Negative control (no primary Ab) on the regenerating area 48 hours p.a. B) Stump oral area of a 24 hours p.a. sample showing that anti-TNF-α-like is present in the epidermis (arrow) and in the dermis. C) Regenerating area of a 24 hours p.a. sample where anti-TNF-α-like is mainly present in the new epithelium covering the injury (arrow) and in the rearranging area immediately behind it (arrowhead). D) Negative control (no primary Ab) on the regenerating area 48 hours p.a. E) Stump oral area of a 48 hours p.a. sample showing that anti-TNF-α-like is faintly expressed in the epidermis (arrow). F) Regenerating area of a 48 hours p.a. sample where anti-TNF-α-like is detectable at the level of the new epithelium (arrow). *Abbreviations*: m=muscle; p=podium.

### *3.2. Molecular results*

*3.2.1. Positive controls: actin and ets1/2*

To optimise and validate the protocols of whole mount *in situ* hybridisation for brittle star and *in situ* hybridisation on paraffin sections for starfish three transcripts were identified and used as controls, *Afi-actin* (brittle star) and *Ese-actin* and *ets1/2 deg* (starfish).

The description of the transcripts and their expression patterns are detailed and shown in the Supplementary Materials (see Fig. S1, S2, S3, S4) but the results will not be discussed in the following paragraphs. However, the localised expression patterns of all these positive controls gave us confidence on the effectiveness of the techniques used in both experimental models.

*3.2.2. Collagen biosynthesis enzyme gene: p4h*

Collagen is one of the key component of the extracellular matrix and plays an important role during the repair phase. Its biosynthesis needs to be finely regulated, therefore, we focused our attention on one gene encoding for an enzyme important in this process, prolyl-4-hydroxylase. We identified the alpha-subunit genes in both experimental models and analysed their expression patterns during the repair phase.

After cloning with degenerate PCR, *p4h deg* sequence was checked performing a BLAST-X (*vs* non-redundant sequence database) and the best BLAST hit is the prolyl-4-hydroxylase alpha-1 subunit (XP_018564257.1). Using cDART tool (NCBI) the 2OG-Fe(II) oxygenase superfamily domain is detected. This domain is characteristic of prolyl-4-hydroxylase (P4H), therefore confirming it is the desired collagen biosynthesis enzyme.

For *Afi-p4h* (AfiCDS.id43946.tr460) the best BLAST hit in the sea urchin genome from EchinoBase is prolyl-4-hydroxylase alpha-1 subunit precursor (SPU_027669), whereas from the NCBI non-redundant sequence database the best BLAST hit is prolyl-4-hydroxylase subunit alpha-1 (XP_012689665.1). The cDART tool (NCBI) confirms the presence of a prolyl-4-hydroxylase alpha subunit domain. Therefore, this transcript is considered as prolyl-4-hydroxylase (*p4h*).

In starfish *p4h deg* expression pattern is summarised in Fig. 11G. Specifically, in the stump it is localised at the level of the epidermis (Fig. 11A, B, C), the pyloric caeca (Fig. 11E) and in almost all coelom-derived epithelia: the perivisceral coelom (Fig. 11E) and associated papulae (Fig. 11D), the radial water canal (Fig. 11F) and the podia (Fig. 11A, C). Both the ectoneural and the hyponeural components of the stump's radial nerve cord

show an expression of this transcript as well (Fig. 11F). The new epithelium covering the wound also expresses this transcript (Fig. 11C).

In brittle star *Afi-p4h* is expressed in the new epidermis in the regenerative bud at stage 2 (Fig. 12). This transcript is expressed also at the level of the inner lining of the podia in the stump (Fig. S7). Its localisation in the advanced regenerative stages is described in the Supplementary Materials and shown in Fig. S8 but it will not be discussed.

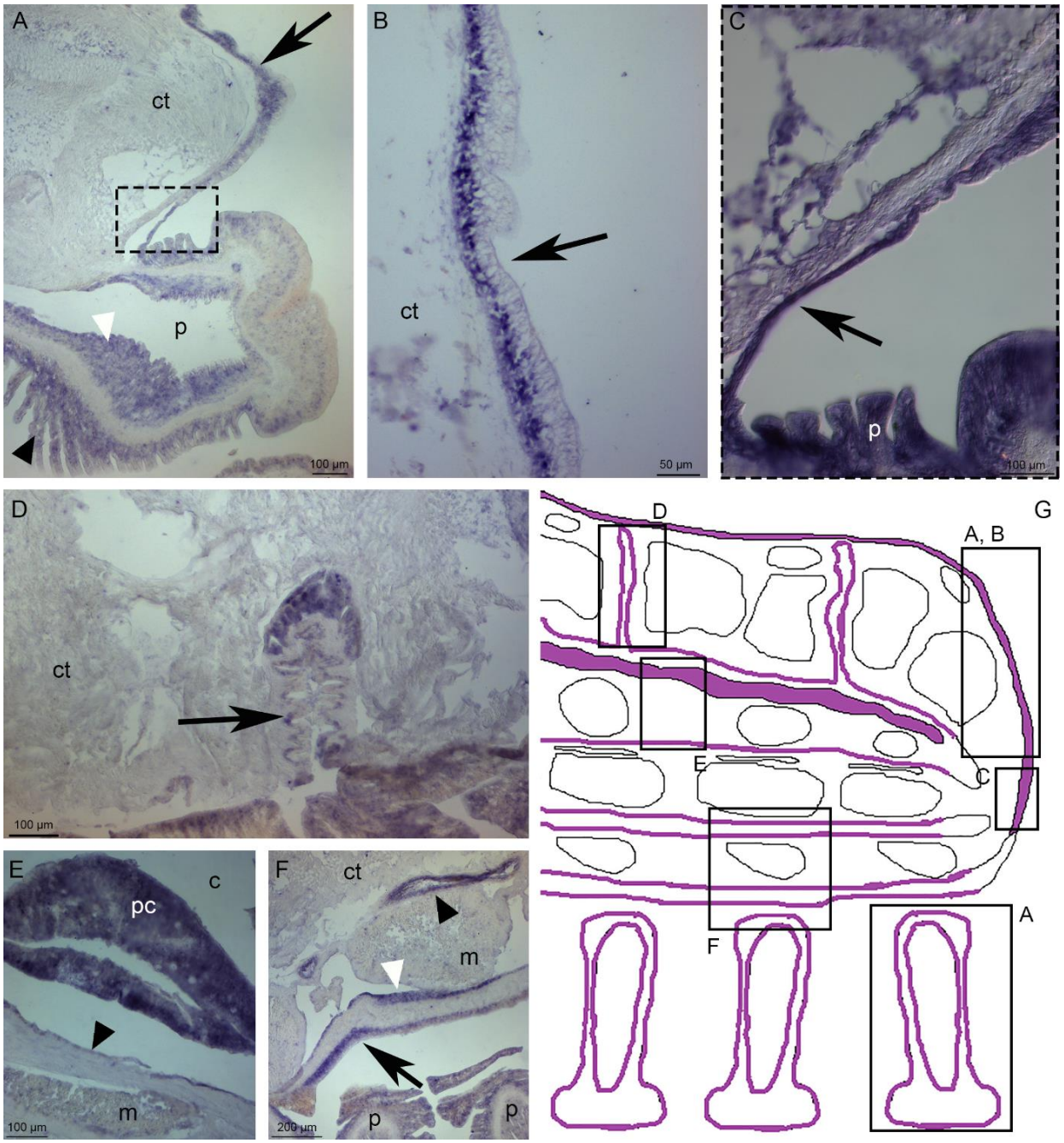


**Fig. 11.** *Expression pattern of p4h deg on regenerating arm 72 hours and one week p.a. using ISH on paraffin sections.* A) *p4h deg* is expressed in the epidermis of the stump (arrow) and in the epidermis of the podium (black arrowhead), as well as in the inner lining

◀ of the podium (white arrowhead). B) This transcript is expressed in the stump epidermis (arrow). C) The new epithelium shows a signal (arrow). D) *p4h deg* is expressed at the level of the coelomic lining of the papulae (arrow). E) The transcript is expressed in the pyloric caeca (pc) and in the perivisceral coelom (arrowhead). F) The signal is localised in the radial water canal epithelium (black arrowhead) and in the ectoneural (arrow) and hyponeural (white arrowhead) systems of the radial nerve cord of the stump. G) Sagittal section scheme summarising *p4h deg* expression pattern. Signal is highlighted in violet and black boxes indicate corresponding images of this figure to facilitate expression pattern understanding. *Abbreviations*: c=coelom; ct=connective tissue; m=muscle; p=podium; pc=pyloric caeca.

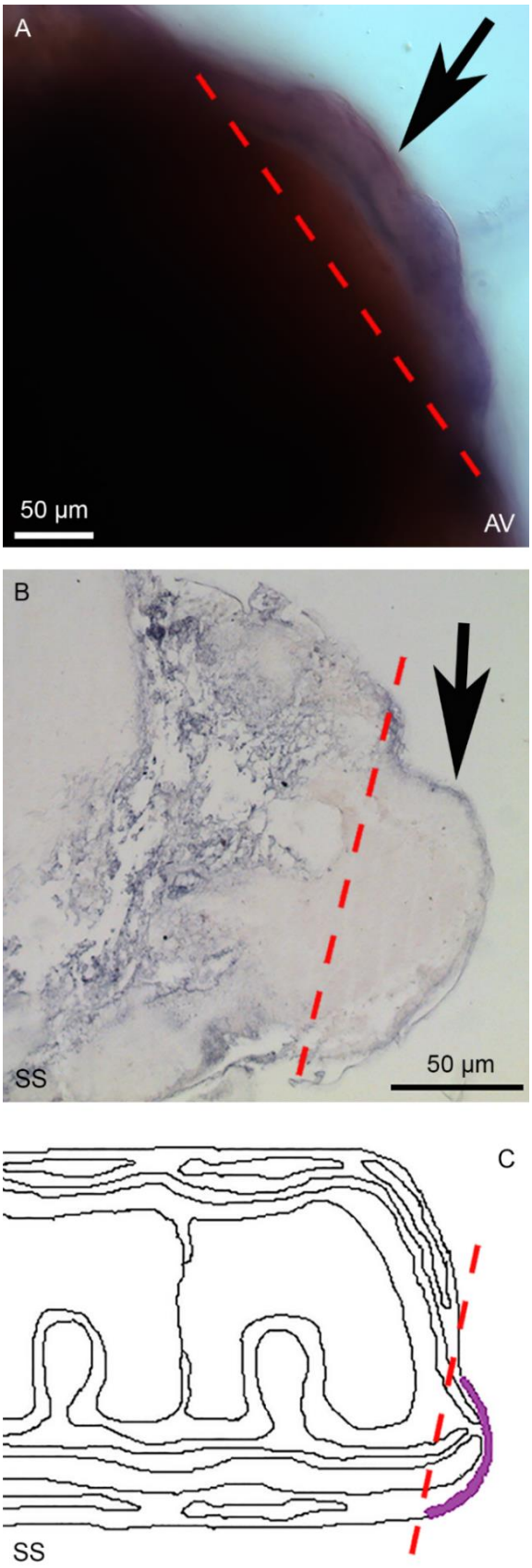


**Fig. 12.** *Afi-p4h expression pattern at stage 2.* A) WMISH. B) Post *in situ* sectioning. C) Scheme. *Afi-p4h* is expressed in the regenerative bud at the level of the epidermis (arrows). *Abbreviations*: AV=aboral view; SS=sagittal section. Red dotted lines=amputation plane.

*3.2.3. Immune response-related genes: col deg and ficolin*

Immune response after injury is one of the key events happening in order to heal the wound and start the subsequent regenerative process. The precise regulation of these mechanisms are strongly necessary. Therefore, we focused our attention on two genes we identified in the two experimental models: *col deg* (starfish) and *Afi-ficolin* (brittle star). *col deg* is a transcript belonging to the FReD superfamily. Using the cDART tool (NCBI) the FReD domain is confirmed. It is usually present in fibrinogen, a glycoprotein that helps in the formation of blood clotting in vertebrates forming bridges between platelets and being the precursor of fibrin. Therefore, *col deg* is here considered as fibrinogen-like.

The *col deg* transcript is expressed in the stump at the level of the epidermis (Fig. 13A, B) and in the coelomic epithelium lining the papulae (Fig. 13B, C). Free-circulating coelomocytes present a signal as well (Fig. 13C). Moreover, the perivisceral coelom epithelium and the circular coelomic muscles express also this transcript (Fig. 13D). Both non-regenerating and regenerating radial nerve cords show expression of *col deg* (Fig. 13E, F), in particular at the level of the ectoneural and hyponeural systems. At the level of the stump water vascular system, the radial water canal epithelium (Fig. 13H) and the lining of podia (Fig. 13I) and ampullae (Fig. 13J) show a clear signal. *col deg* expression is localised also in the new epithelium covering the wound (Fig. 13K). No expression is detected in the mucous glands of the stump (Fig. 13B) and in the injured muscles in the process of active rearrangement (Fig. 13G). The scheme in Fig. 13L summarises the expression pattern of this transcript in both stump and regenerating tissues.

For *Afi-ficolin* (*Afi*CDS.id39565.tr647) the best BLAST hit in the sea urchin genome from EchinoBase is *Sp-Fic1* (SPU_000045), whereas from the NCBI non-redundant sequence database the best BLAST hit is hypothetical protein BRAFLDRAFT_88602 [*Branchiostoma floridae*] (XP_002604312.1). This transcript is considered as ficolin.

*Afi-ficolin* is not expressed in the regenerative bud at stage 2 (Fig. 14), whereas at the level of the stump it is localised in the radial water canal epithelium (Fig. S6). The expression pattern in the advanced regenerative phases is described in the Supplementary Materials and shown in Fig. S5 but it will not be further discussed.

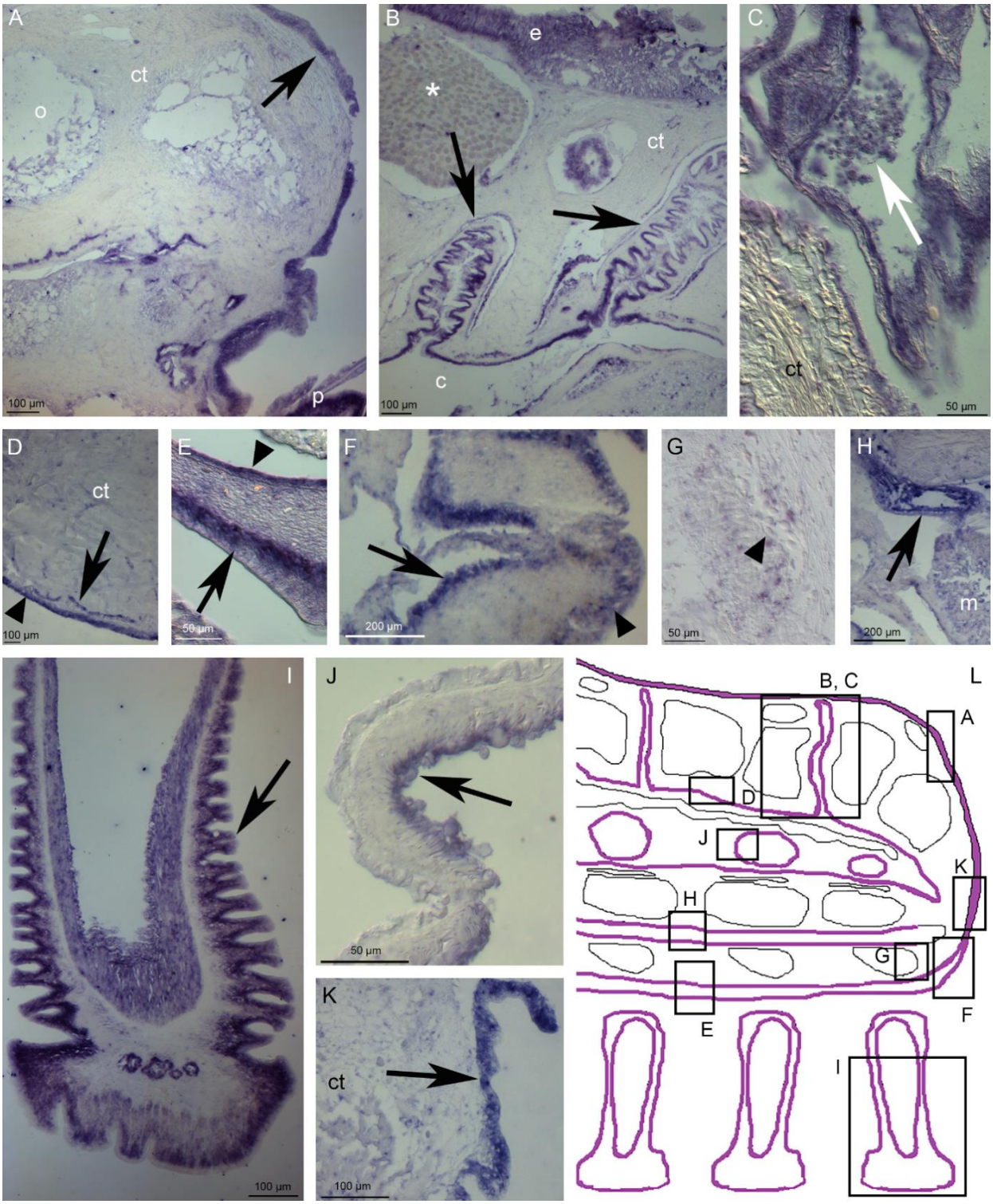


**Fig. 13.** *Expression pattern of col deg on regenerating arm 24 hours, 72 hours and one week p.a. using ISH on paraffin sections.* A) This transcript is expressed in the epidermis of the stump (arrow). B) Expression is detectable in the coelomic lining of the papulae (arrows) and in the epidermis of the stump but no signal is present in the mucous gland (*). C) Cells in the papulae (possibly coelomocytes) are stained (arrow). D) The coelomic epithelium (arrowhead) and the circular coelomic muscles (arrow) show expression of this transcript. E) The ectoneural (arrow) and the hyponeural (arrowhead) systems of the stump radial nerve cord show a signal. F) The new regenerating radial nerve cord is stained in both ectoneural (arrowhead) and hyponeural (arrow) systems. G)

◀ Dedifferentiating myocytes at the level of an injured oral muscle do not express this transcript. H) *col deg* is expressed at the level of the radial water canal epithelium (arrow) of the stump. I) The epidermis of the podia is stained (arrow). J) The inner lining of the ampullae (arrow) expresses this transcript. K) *col deg* is detectable in the new epithelium (arrow). L) Sagittal section scheme summarising *col deg* expression pattern. Signal is highlighted in violet and black boxes indicate corresponding images of this figure to facilitate expression pattern understanding. *Abbreviations and symbols*: c=coelom; ct=connective tissue; e=epidermis; m=muscle; o=ossicle; p=podium; *=mucous gland.

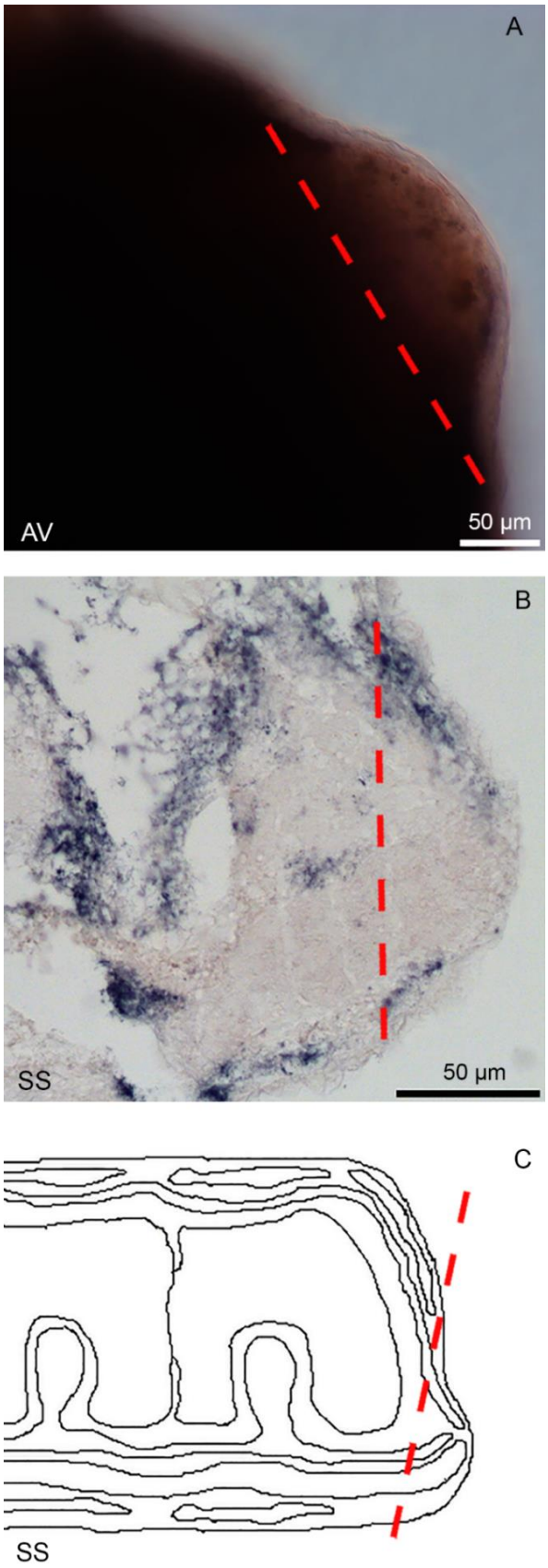


**Fig. 14.** *Afi-ficolin expression pattern at stage 2.* A) WMISH. B) Post *in situ* sectioning. C) Scheme. *Afi-ficolin* is not expressed in the regenerative bud. *Abbreviations*: AV=aboral view; SS=sagittal section. Red dotted lines=amputation plane.

## *4. Discussion*

### *4.1. Emergency reaction and re-epithelialisation are fast in both experimental models*

Both echinoderm models show a quick response to traumatic injury. The aims of the emergency reaction are to seal the coelomic cavities through constriction and clotting and decrease the exposed wound surface through shrinkage. The circular constriction visible in starfish, due to contraction of coelomic muscle layer and possibly connective tissue stiffening (Ben Khadra *et al.*, 2015a), is not detectable in brittle star. This is consistent with the different anatomy of the animals: in starfish the presence of a spacious coelomic cavity has necessarily led to the evolution of a more “efficient” constriction/sealing system, which, on the contrary, is not necessary and even hardly feasible in brittle star due to the conspicuous skeletal element development and the absence of circular muscle bundles. The sealing of the coelomic cavities is ensured also by the apical contraction of the body walls. This event is likely to be sufficient to seal the aboral coelomic cavity and the radial water canal in brittle star. Similar events have been described also in other echinoderms (Mladenov *et al.*, 1989; Candia Carnevali *et al.*, 1993; Moss *et al.*, 1998) and they are of primary importance for both wound closure and reduction of the surface to be healed. Wound contraction and blood vessel constriction have been well studied in mammal wound healing (Pastar *et al.*, 2014; Ibrahim *et al.*, 2015) and, although the involved structures (e.g. blood vessel and coelomic cavity) can be markedly different in anatomy and embryological origin (Hyman, 1955; Gilbert, 2000), comparative aspects with echinoderms can be profitably derived. In mammals while vasoconstriction is an almost immediate reaction, wound contraction is delayed in comparison to echinoderms: in human skin wound shrinkage weakly starts almost immediately after injury but its main peak is 10-15 days after the damage (Shultz *et al.*, 2005), whereas in echinoderms it is perfectly visible and functional within 1-2 days p.a., and involves the whole body walls (Fig. 2A, C). This delay in humans is due to fibroblasts in the injury neighbourhood that have to emerge from quiescence, migrate and then transform into myofibroblasts (Martin, 1997). Evolutionary constrains leading to the more efficient sealing of the body cavities/vessels and wound contraction in echinoderms are unknown but might be one of the features promoting their effective regeneration. Haemostasis in echinoderms is also mediated by cell clotting at the level of the coelomic cavities. The cells involved are mainly coelomocytes that contribute to both avoiding fluid loss and eliminating cell debris or microorganisms thanks to their phagocytic function (Pinsino *et al.*, 2007, Gorshkov *et al.*,

2009; Ben Khadra *et al.*, *in press*). This clotting and the presence of phagocytes behind the new epidermis (in starfish) are comparable to the presence of platelets and thrombocytes described in mammalian injury (Peacock, 1984; Clark, 1988; Ibrahim *et al.*, 2015).

Re-epithelialisation starts almost simultaneously with the emergency reaction and it is very rapid in both starfish and brittle star, although in the latter it is accomplished earlier (8-16 hours p.a. *versus* 24-48 hours p.a.), most likely due to its smaller arm size, whereas in mammals it takes longer than in both echinoderm models (Pastar *et al.*, 2014). Delayed re-epithelialisation or defects in this process could lead to inhibition of functional wound healing and regeneration (Sivamani *et al.*, 2007), therefore the quick re-epithelialisation displayed in echinoderms can be regarded as an important feature contributing to their subsequent effective wound healing. Moreover, in both experimental models the new epithelium is composed by epithelial cells deriving from the adjacent wound edges. These cells retain the junction complexes (Fig. 4D; Ben Khadra *et al.*, 2015a), thus ensuring a continuous covering layer that is immediately functional as barrier against pathogens and further fluid loss. This is markedly different from what happens in mammals where at the level of the wound edges cell-cell junctions are disrupted to allow migration of single keratinocytes over the wound area (Pastar *et al.*, 2014). Briefly considering *A. filiformis*, the presence of bacteria in the epidermis has been suggested having a symbiotic non pathological role (Burnett and McKenzie, 1997; Byrne, 1994) and the intriguing hypothesis that bacteria help/quicken the healing process in brittle star in comparison to starfish (without bacteria), disregarding different wound size, deserves to be investigated.

### *4.2. Oedematous area present in starfish does not characterise brittle star repair phase*

The repair phase events occurring after re-epithelialisation differ between the two experimental models. Indeed, the regenerating area of starfish arm is characterised by a temporary (3-7 days p.a.) oedematous area that is not detectable in brittle star.

The oedematous area of starfish is actually a “filling tissue” developing at the level of the wound and characterised by the presence of different cytotypes intermixed by a sparse nonfibrillar extracellular matrix. Cells at this stage are mainly phagocytes, coelomocytes, undifferentiated cells, fibroblasts and dedifferentiating myocytes (Ben Khadra *et al.*, 2015a, b). Phagocytes and coelomocytes can be regarded as cells involved in the immune response (Glínski and Jarosz, 2000; Pinsino *et al.*, 2007; Smith *et al.*, 2010) and

can be functionally compared to monocytes and macrophages of mammals (Martin, 1997; Pastar *et al.*, 2014) whose presence is fundamental for effective wound debridement and healing (Koh and DiPietro, 2011). The oedematous area progressively matures (see below) and this “filling tissue” is functionally (and partially histologically) comparable to the granulation tissue of mammals, although in this latter the matrix deposition is much more conspicuous than in echinoderms (Martin, 1997; Pastar *et al.*, 2014).

In brittle star immediately after re-epithelialisation the tissues damaged during the injury, e.g. muscle bundles, are actively remodelled but no sign of granulation tissue-like structures are visible as already described by Biressi and co-workers (2010) and Czarkwiani and co-workers (2016). After only 2-3 days p.a. regeneration of the main longitudinal structures (*i.e.* radial nerve cord, aboral coelomic cavity and radial water canal) occurs. Therefore, brittle star repair phase is accomplished much earlier than that of starfish and of mammals as well. Size-related aspects likely play a significant role in this better efficiency; however, the existence of specific cellular or molecular mechanisms cannot be excluded and would be “justified” by an evolutionary selective pressure playing on the very fragile arms of *A. filiformis* and their frequent loss. Regardless, both echinoderm models, although presenting some differences in repair phase events and timing, are clearly more efficient and rapid than mammals in healing an injury that, moreover, is much more complex than a mammal skin wound. This underlines that the different regenerative abilities of echinoderm and mammals diverge since the very first reparative events and do not only depend on differences in re-growth capacity.

### *4.3. Extracellular matrix during regeneration: a focus on collagen*

As previously mentioned, the fibrillar reorganisation of the extracellular matrix (ECM) occurs earlier in brittle star than in starfish. In particular, in brittle star regenerating arm collagen is already present in the thin dermal layer underneath the new epidermis at the middle/end of the repair phase, whereas in starfish collagen fibrils and small fibril bundles start being visible at the level of the oedematous area only at the end of the repair phase. After the repair phase the ECM continuously matures creating a more organised collagen network for cell migration and tissue regeneration, ensuring both physical scaffold and first mechanical resistance. Few studies have focused on ECM deposition during echinoderm regeneration processes. By using an anti-fibrous collagen antibody (HgfCOL*)* specifically raised in an echinoderm species (the sea cucumber *Holothuria glaberrima*), Quiñones and co-workers (2002) have observed a decrease in the protein content during

the first 2 weeks of visceral regeneration of this species, suggesting extensive collagen remodelling. This time period corresponds to the repair and first regenerative phases. Therefore, we decided to use the same antibody (HgfCOL*)* to detect collagen presence during the repair phase of both *E. sepositus* and *A. filiformis*. The antibody consistently labels the basal portion (probably the basement membrane) of both the stump and the regenerating epidermis and, in brittle star, also the connective tissue underling the wound epithelium. Noteworthy is the fact that this latter signal is absent in the stump, suggesting that this fibrous collagen could be a characteristic of the new connective tissue.

In order to better characterise collagen involvement during the repair phase, the gene encoding for a key collagen biosynthesis enzyme (prolyl-4-hydroxylase; *p4h*) has been preliminarily studied in terms of its expression pattern during regeneration. In both experimental models a signal is localised at the level of the regenerating epidermis, further supporting a role of this tissue in collagen biosynthesis. In starfish this transcript is present also in the coelomic epithelium of different structures of the stump, in the pyloric caeca and in the radial nerve cord suggesting that different tissues are involved in collagen production. At the best of our knowledge, this enzyme has been previously investigated in echinoderms only by Sugni and co-workers (2014) who have described collagen synthetic activity in presumptive fibroblast-like cells of the sea urchin compass depressor ligaments using immunodetection. Few studies have been focused on *p4h* of invertebrates in general (Veijola *et al.*, 1994; Abrams and Andrew, 2002) and of marine invertebrates in particular (Pozzolini *et al.*, 2015). In humans P4H is detected in several different tissues e.g. capillary endothelial cells, liver, kidney, skeletal myocytes, and developing bones, therefore, confirming that collagen synthesis is performed in tissues of highly different origin and function (Nissi *et al.*, 2001). Moreover, in a rabbit model Kim and co-workers (2003) have described that inhibition of P4H leads to reduced collagen deposition and improvement in hypertrophic scars (*i.e.* keloids), thus indicating a possible clinical way to reduce fibrotic scar formation and subsequently improve tissue regeneration. These findings suggest that diverse tissues are involved in collagen synthesis and this aspect needs to be further investigated in order to confirm the hypothesis that delayed fibrous collagen deposition in echinoderms could be an advantage in terms of regenerative capacity. Furthermore, these kinds of studies could hold great biomedical potential that could hopefully lead to possible solutions to problematic clinical complications e.g. keloids or severe amputations in humans.

Overall, differences occur between echinoderm and mammal collagen deposition during wound healing. Indeed, in mammals, collagen starts to be deposited almost immediately after injury (around 10 hours) at the beginning of the repair phase and it is later constantly remodelled (Prockop and Kivirikko, 1995). The deposition of collagen in echinoderms starts only at the middle/end of the repair phase and the delay in fibrillar extracellular matrix organisation and the presence of a “loose” connective tissue at the level of the regenerating area provide a more “dynamic and plastic” environment for tissue regeneration. Moreover, contrary to mammals (Bock and Mrowietz, 2002; Rahban and Garner, 2003), in echinoderms no fibrotic scar or keloid formation are normally detected (Quiñones *et al.*, 2002).

### *4.4. Immune system contribution during regeneration*

It is well known that the immune system plays a key role during the initial haemostasis and throughout the whole inflammation phase after injury. In both starfish and brittle star, we have evaluated the presence of a pro-inflammatory cytokine, the tumour necrosis factor-α-like (TNF-α-like), during the first days after amputation. TNF-α is one of the main players in vertebrate wound repair and it is up-regulated during this process (Grellner *et al.*, 2000); it is involved in inflammatory response (Bradley, 2008) as well as keratinocyte activation, migration and differentiation and fibroblast activation (Pastar *et al.*, 2014). Gene homologous to the mammalian TNF-α has been described in echinoderms (Matranga *et al.*, 2005) and it is found in both the sea urchin *Strongylocentrotus purpuratus* and the starfish *Patiria miniata* genomes (Cameron *et al.*, 2009) as well as in the *Amphiura filiformis* transcriptome (Dylus *et al.*, *submitted*). Due to the absence of genome or transcriptome of *Echinaster sepositus* it has not been possible to definitively confirm its presence at a genomic/transcriptomic level in this species. Our results showed that, at least in the brittle star, a TNF-α-like signal is detectable in the regenerating epidermis and the underlying tissues during the first 24 hours p.a. Later (48 hours p.a.) it apparently decreases in intensity and it is localised only in the regenerating epidermis. This is consistent with what reported for mammals, where epithelial cells and macrophages infiltrating the wound express this fundamental regulative factor (Pastar *et al.*, 2014). Apparently, in the brittle star a “basal” level of TNF-α-like is constitutively expressed also in the stump epidermis. Whether this is related to the subcuticular presence of bacteria and, therefore, to a constantly activated “basal” inflammatory response is a fascinating hypothesis to test.

Together with immunolocalisation, molecular analyses on two genes important during the repair phase after injury have been performed. For starfish the gene encoding for a protein containing a FReD (fibrinogen-related) domain has been identified. This domain is typical of fibrinogen, a glycoprotein that in vertebrates is fundamental for blood clotting, being the precursor of fibrin. Fibrinogen-like presence in echinoderms has been described only by Xu and Doolittle (1990) in the sea cucumber *Parastichopus parvimensis* but no expression data are available in these marine organisms. To the best of our knowledge, these are the first results on *fibrinogen-like* gene expression pattern in echinoderms. *col deg* is mainly expressed in coelomic structures and cells suggesting that both the stump and the regenerating coelomic epithelium could be involved in direct production or release of cells that express this gene. The signal at the level of the new epidermis suggests that also this tissue could be involved in production of fibrinogen-like during the repair phase. In mammals, fibrinogen is fundamental for granulation tissue formation and cell migration (Drew *et al.*, 2001) and in humans in particular, it is mainly produced by hepatocytes and lung epithelium and is the major coagulation protein having a central role in platelet aggregation during wound healing (Guadiz *et al.*, 1997; Laurens *et al.*, 2006). Therefore, further analyses are necessary to understand if *fibrinogen-like* gene expression leads to subsequent fibrin-like formation and if something similar to mammal fibrin clot (Clark, 2001) could be transiently present in echinoderms as well.

For brittle star the gene encoding for a ficolin has been identified. *Afi-ficolin* is also a transcript containing a fibrinogen-related domain (FReD) and it is involved in immune response after injury. In both vertebrates and invertebrates ficolin is a lectin important in the innate immune response (Fujita, 2002; Iwanaga and Lee, 2005; Matsushita, 2009). The absence of its expression in the regenerative bud of *A. filiformis* is quite surprising. However, in the absence of its genome and considering that in the sea urchin genome four potential *ficolin* genes are present (http://www.echinobase.org/), we cannot exclude the presence of other *ficolin* genes and, therefore, their expression during regeneration. Moreover, a localised expression in the stump at the level of the radial water canal epithelium suggests that it is actively produced in this tissue. Hence, it is possible to hypothesise that proteins are synthetized in the stump tissue and subsequently released at the level of the coelomic fluid of the water vascular system (comparable to vertebrate circulatory system in terms of function) to reach the regenerating area. At the best of our knowledge, this is the first results on this transcript expression during arm regeneration in this species and more detailed analyses are necessary to confirm this hypothesis.

### *4.5. Conclusion*

In this study the starfish *E. sepositus* and the brittle star *A. filiformis* have been used as models to compare the repair phase after arm amputation between these two echinoderm species as well as with mammals. The main similarities/differences between them are summarised in Table 3 and Fig. 15.

Our results showed that both starfish and brittle star are more efficient in haemostasis, wound contraction and re-epithelialisation of the injury in comparison to mammals in terms of both rate and efficiency. The extracellular matrix (ECM) fibrillar organisation in echinoderms is delayed and less conspicuous in comparison to mammals and, together with the absence of over-deposition of collagen (fibrosis), suggests a possible advantage for echinoderms because their temporary loose ECM is likely more “plastic” than the collagen/fibrin clot of mammals. As suggested for other echinoderms (Quiñones *et al.*, 2002) this “plasticity” could be directly connected to the subsequent efficiency of regeneration.

The involvement of the immune system during the repair phase has been investigated through immunodetection of TNF-α-like and expression patterns of *fibrinogen-like* and *ficolin* genes for starfish and brittle star respectively. Overall, our data showed that TNF-α-like presence in brittle star is preliminary comparable to that of mammals. *Fibrinogen-like* and *ficolin* transcripts are both involved in echinoderm immunity but further analyses are necessary to understand if they could have a similar role to that of mammals during wound healing.

In general, we provided the first evidences of the importance of ECM fibrillar organisation and immune system molecules during starfish and brittle star regeneration and highlighted interesting differences (mainly in wound healing and ECM organisation) among echinoderm and mammal responses to injury that suggest that their different regenerative abilities diverge since the very first repair events and do not only depend on differences in re-growth capacity. Moreover, our findings showed that echinoderms are valid alternative models to study biological processes (e.g. wound healing and regeneration) can also be important to hopefully help solving human health problems (Gurtner *et al.*, 2008).

**Table 3.** *Summary of the main differences between the events occurring during the repair phase of echinoderms and mammals.* *=data from Martin, 1997, Werner and Grose, 2003, Pastar *et al.*, 2014.

| EVENT | STARFISH | BRITTLE STAR | MAMMALS* |
|---|---|---|---|
| **Constriction of the cavities/canals** | Sealing of the coelomic cavities (haemostatic ring) | Sealing of the coelomic cavities (no haemostatic ring) | Vasoconstriction of the blood vessels |
| **Wound contraction** | Aboral body wall moves toward the oral side (within 24 hours p.a.) | Aboral and oral body walls move toward the wound (within 24 hours p.a.) | Contraction of the wound edges (after 3-4 days post injury) |
| **Clotting in the cavities/canals** | Coelomocytes | Coelomocytes | Platelets and thrombocytes |
| **Phagocytosis** | Coelomocytes | Coelomocytes | Macrophages |
| **Re-epithelialisation direction** | Centripetal | Centripetal | Centripetal |
| **Epidermal cell junction disruption** | No | No | Yes |
| **Oedematous area formation** | Yes | No | Granulation tissue (only partially similar to starfish oedematous area) |
| **Canal/vasa infiltration** | No | No | Yes (angiogenesis) |
| **ECM deposition at the wound site** | Not conspicuous | Not conspicuous | Conspicuous |
| **Fibrosis** | No | No | Yes |
| **Scar formation** | No | No | Yes |
| **TNF-α-like detection during the repair phase** | Faint | Yes | Yes |

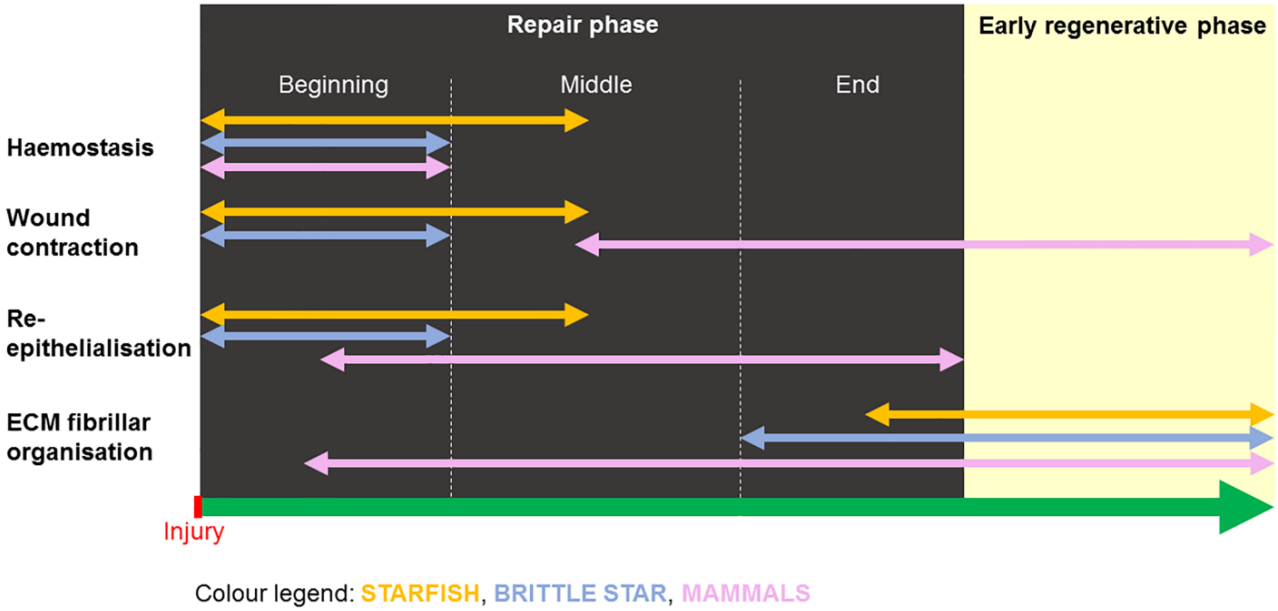


**Fig. 15.** *Main similarities/differences in the repair phase events among starfish, brittle star and mammals*. See colour legend embedded in the figure.

## *5. Supplementary Materials*

### *5.1. Extended Materials and Methods*

#### *5.1.1. 3'RACE and degenerate PCR protocols for starfish cDNA amplification*

For *actin* standard gradient PCR was performed and the transcript was successfully cloned. However, since the PCR product was short (less than 300 bp), 3'RACE was performed using a mixed cDNA samples from regenerate stages and the FirstChoice® RLM-RACE Kit (Ambion) according to manufacturer's instructions optimising annealing temperature (55°C) and cycles (40) in order to obtain a longer product (predicted length ~ 1 kb) and, thus, a longer RNA antisense probe. Primers used for 3'RACE are listed in Table S1. Also these PCRs were successful, therefore both PCR products were cloned and used to transcribe RNA antisense probes as previously described.

For *ets1/2* degenerate primers (100 µM) were used on a mixed cDNA samples from regenerate stages as follows: 95°C for 5' followed by 35 cycles of 95°C for 30'', temperature gradient for 30'' and 72°C for 30'' and a final 7' elongation at 72°C. The temperatures of the gradient from the highest to the lowest were: 60°C, 54.5°C, 48°C and 45°C. The amplification was successful for all of them but the PCR product was short (around 300 bp). Therefore, specific primers were designed to perform 3'RACE using a mixed cDNA samples from regenerate stages and the FirstChoice® RLM-RACE Kit (Ambion) according to manufacturer's instructions in order to obtain a longer PCR product (predicted length ~ 3.5 kb) and, thus, a longer RNA antisense probe. Primers are listed in Table S1. The annealing temperature (55°C) and cycles (40) were optimised. Since this PCR was not successful, the short PCR product was cloned and used to obtain the RNA antisense probe.

Collagen-specific degenerate primers (20 µM) from Zhang and Cohn (2006) were used on a mixed cDNA samples from regenerate stages. To optimise the amplification, the following protocol was tested and subsequently modified: 94°C for 1' followed by 35 cycles of 94°C for 45'', temperature gradient for 45'' and 68°C for 2' and a final 10' elongation at 68°C. The temperatures of the gradient from the highest to the lowest were: 60°C, 54.5°C, 50.8°C and 45°C. 50.8°C was selected as best amplification temperature and cycles were increased to 40. The PCR product was then purified with NucleoSpin® gel and PCR clean-up kit (Macherey-Nagel) and cloned as described before.

For *p4h*, degenerate primers (Table 2; 100 µM) were used with Q5 High-Fidelity DNA Polymerase (New England BioLabs) and Invitrogen reagents and the following protocol was performed: 98°C for 30'', 35 cycles of 98°C for 10'', temperature gradient for 30'' and

72°C for 30'' and a final 2' elongation at 72°C. After purification with NucleoSpin® gel and PCR clean-up kit (Macherey-Nagel), cloning and RNA antisense probe transcription were performed as described before.

**Table S1.** *List of 3' outer and inner primers used for E. sepositus 3'RACE PRCs (FirstChoice® RLM-RACE Kit; Ambion) for Ese-actin and ets1/2 deg.* All primers were used at a concentration of 10 µM. *Abbreviations and symbols*: bp, base pair; F, forward primer; R, reverse primer; *=specific primer already present in Table 2.

| Primer Name | Primer Sequence (5'-3') | 3' RLM-RACE PCR | Primer Length (bp) |
|---|---|---|---|
| ***Ese-actin SO**** | GTGCCCAGAAGCCTTGTTC | Specific outer | 19 |
| ***Ese-actin SI*** | CATCATGAAGTGTGACGTGGA | Specific inner | 21 |
| ***ets1/2 deg SO*** | CCATTCAGCTGTGGCAGTT | Specific outer | 19 |
| ***ets1/2 deg SI*** | ACCGAACCTGCCAACATATC | Specific inner | 20 |
| ***3' RACE inner*** | CGCGGATCCGAATTAATACGACTCACTATAGG | Kit inner primer | 32 |
| ***3' RACE outer*** | GCGAGCACAGAATTAATACGACT | Kit outer primer | 22 |

### *5.2. Extended results*

*5.2.1. Description of the positive control transcripts and of their expression patterns*

*Ese-actin* is a transcript whose sequence is available in NCBI (GenBank: KC858258.1, around 300 bp long). This is *actin 1* and a BLAST-X (*vs* non-redundant sequence database) in NCBI shows that it is a *β-actin*. Using cDART tool (NCBI) the actin domain is confirmed. The sequence of the longer actin has been checked as well, confirming the previous result.

After cloning through degenerate PCR, *ets1/2 deg* sequence is checked with NCBI BLAST-X (*vs* non-redundant sequence database) and it shows 100% identity with *ets1/2* transcription factor of the starfish *Patiria pectinifera*. Moreover, using cDART tool (NCBI) the *ets* domain is detected. Therefore, this transcript is confirmed being the transcription factor *ets1/2*.

For *Afi-actin* (*Afi*CDS.id2787.tr9243) the best BLAST hit in the sea urchin database from EchinoBase is *Sp-CskaI* (SPU_009481) also called *CyI*, whereas from the NCBI non-redundant (NR) database is an *actin related protein 1* [*Strongylocentrotus purpuratus*] (NP_999634.1 GI:47550921). Here this transcript is considered as *actin*.

The expression patterns of *Ese-actin*, *ets1/2 deg* and *Afi-actin* are described below. Schemes are provided in order to facilitate expression pattern understanding (Fig. S1I for *Ese-actin*, Fig. S3 for *ets1/2 deg* and Fig. S4 for *Afi-actin*). For *A. filiformis*, stages of the advanced regenerative phase are described as well.

*Ese-actin* is expressed in the stump at the level of the coelomic lining of the perivisceral cavity (Fig. S1A), of the papulae (Fig. S1B), of the ampullae (Fig. S1C) and of the podia (Fig. S1D) and in the pyloric caeca (Fig. S1A). Moreover, it is present also in the epidermis of the podia (Fig. S1D) and of the body wall (Fig. S1E). The expression is detectable also in the non-regenerating radial nerve cord, in particular in the ectoneural and hyponeural systems (Fig. S1F). In the regenerating area the signal is present at the level of the new epidermis (Fig. S1G), the regenerating radial nerve cord and radial water canal (Fig. S1H).

*ets1/2 deg* is expressed in the stump at the level of the epidermis of body wall and podia (Fig. S2A). The coelomic epithelium presents a signal at the level of the inner lining of the podia (Fig. S2A), the radial water canal (Fig. S2F), the papulae (Fig. S2B), the ampullae (Fig. S2G) and the perivisceral coelom in both the stump area (Fig. S2D) and the regenerating area (Fig. S2E). This transcript is localised also in the pyloric caeca (Fig. S2D) and in the stump radial nerve cord at the level of the ectoneural and hyponeural systems (Fig. S2F). The new epidermis shows a signal as well (Fig. S2C). No expression is detectable at the level of the main muscle bundles (Fig. S2F) and of the ossicles (Fig. S2A, C).

Both WMISH and post *in situ* sections show that *Afi-actin* is expressed in the regenerative bud epidermis at stage 2 (Fig. S4A, F, I) and the same expression pattern is detectable at stage 4 (Fig. S4B, G, J). At the late stage, >50% DI, *Afi-actin* is expressed in the proximal side of the long regenerate at the level of the epidermis covering spines and podia (Fig. S4C, D, H, K) and not at the level of other structures (e.g. oral, aboral and lateral sides). In the distal tip this gene is expressed in the epidermis as well (Fig. S4E, I, L).

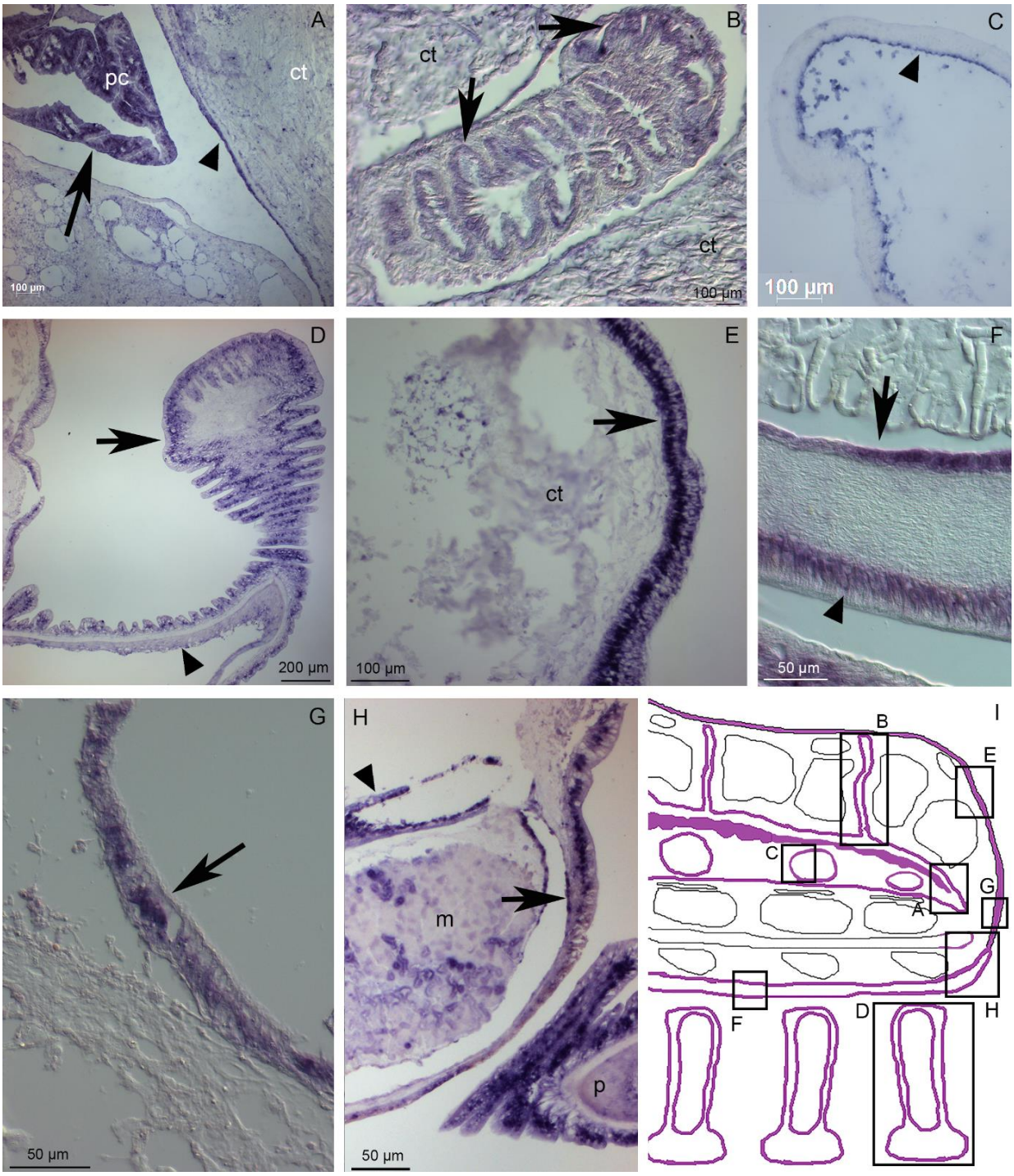


**Fig. S1.** *Expression pattern of Ese-actin on starfish regenerating arm 24 hours p.a. using ISH on paraffin sections.* A) *Ese-actin* is expressed in the coelomic cavity epithelium (arrowhead) and in the pyloric caeca (pc; arrow) of the stump. B) The inner lining of the stump papulae (*i.e.* coelomic epithelium) shows expression of this transcript. C) *Ese-actin* is expressed at the level of the inner lining of the stump ampulla (*i.e.* coelomic epithelium). D) *Ese-actin* is expressed in the epidermis of the stump podia (arrow) and in the inner coelomic lining (arrowhead). E) This transcript is expressed in the stump epidermis (arrow). F) *Ese-actin* shows an expression in the stump radial nerve cord, in particular at the level of the ectoneural (arrowhead) and of the hyponeural systems (arrow). G) *Ese-actin* is expressed in the new epithelium (arrow). H) The regenerating radial nerve cord (arrow) and radial water canal (arrowhead) show expression of this transcript. I) Sagittal section scheme summarising *Ese-actin* expression pattern. Signal is highlighted in violet

◀ and black boxes indicate corresponding images of this figure to facilitate expression pattern understanding. *Abbreviations*: ct=connective tissue; m=lower transverse ambulacral muscle; p=podium; pc=pyloric caeca.

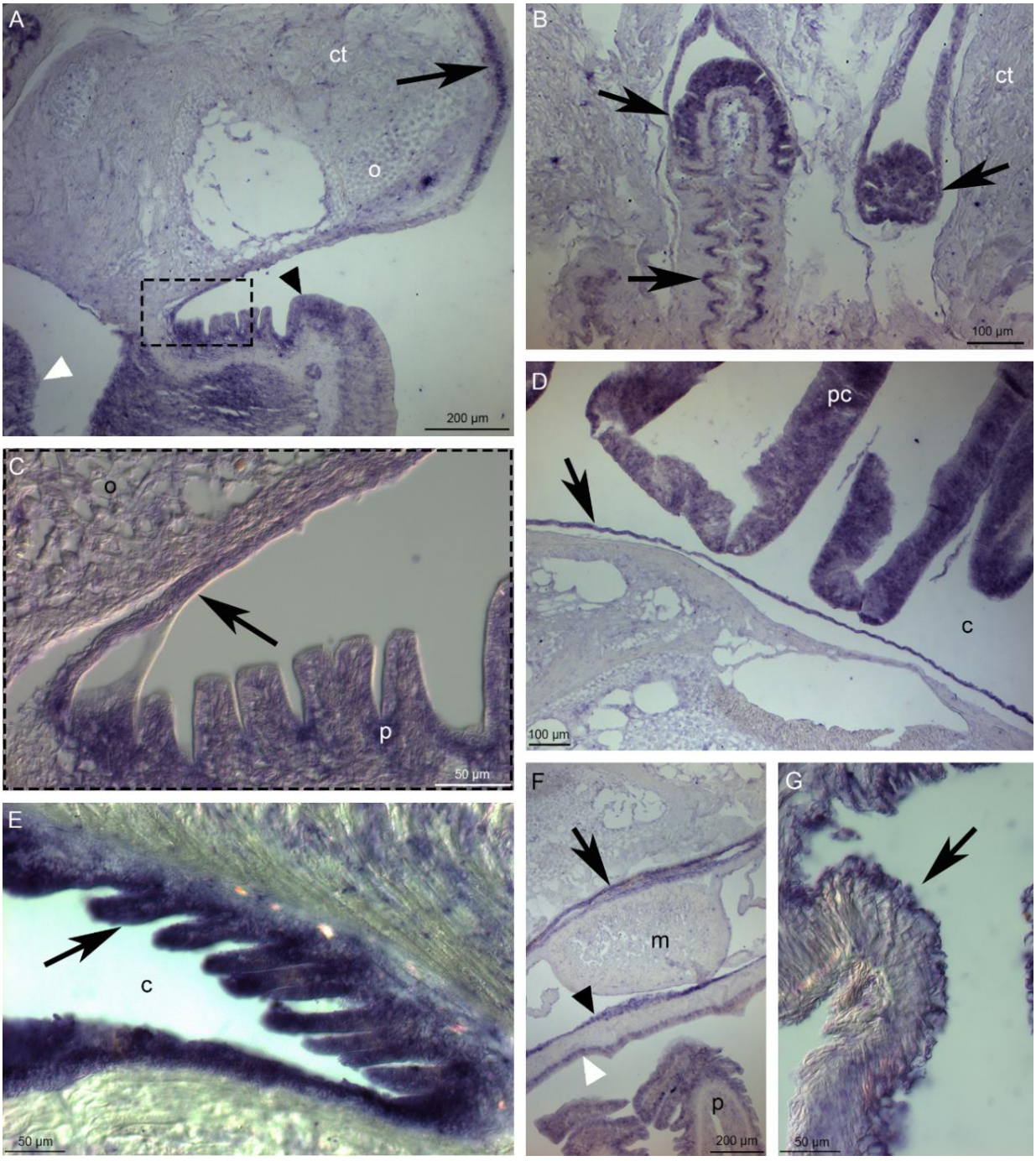


**Fig. S2.** *Expression pattern of ets1/2 deg on starfish regenerating arm 24 hours and 72 hours p.a. using ISH on paraffin sections.* A) *ets1/2 deg* is expressed in the stump at the level of the epidermis (arrow) and of the podium, in particular in the epidermis (black arrowhead) and in the inner coelomic lining (white arrowhead). B) The papulae (arrows) present a signal. C) The new epidermis (arrow) shows expression of this transcript. D) *ets1/2 deg* is expressed in the pyloric caeca (pc) and at the level of the coelomic epithelium (arrow). E) This transcript is expressed in the new coelomic epithelium (arrow). F) In the stump the radial water canal (arrow) and the radial nerve cord show a clear expression pattern. In particular, in the radial nerve cord both the ectoneural (white

◀arrowhead) and the hyponeural (black arrowhead) systems show a signal. G) The inner lining of the ampullae (arrow) shows expression of this transcript. *Abbreviations*: c=coelom; ct=connective tissue; m=muscle; o=ossicle; p=podium; pc=pyloric caeca.

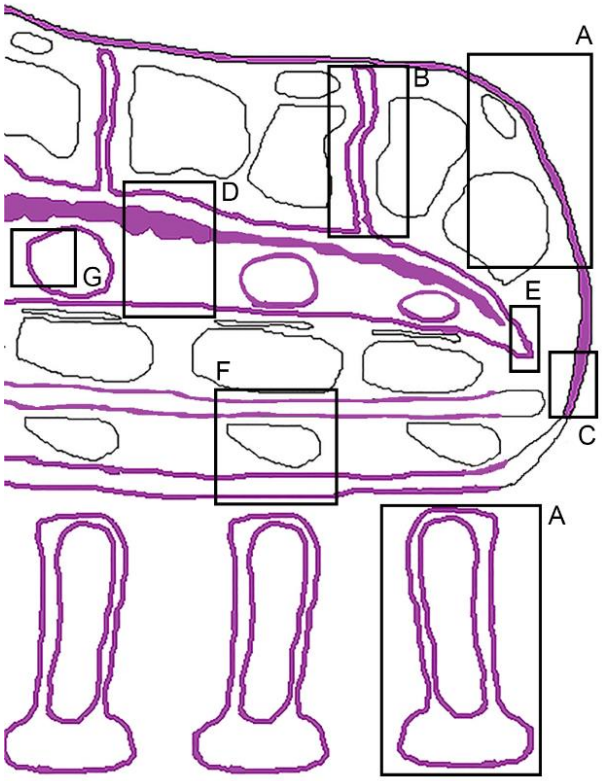


**Fig. S3.** *Sagittal section scheme of the starfish regenerating arm summarising ets1/2 deg expression pattern.* Signal is highlighted in violet and black boxes indicate corresponding images of figure S2 to facilitate expression pattern understanding.

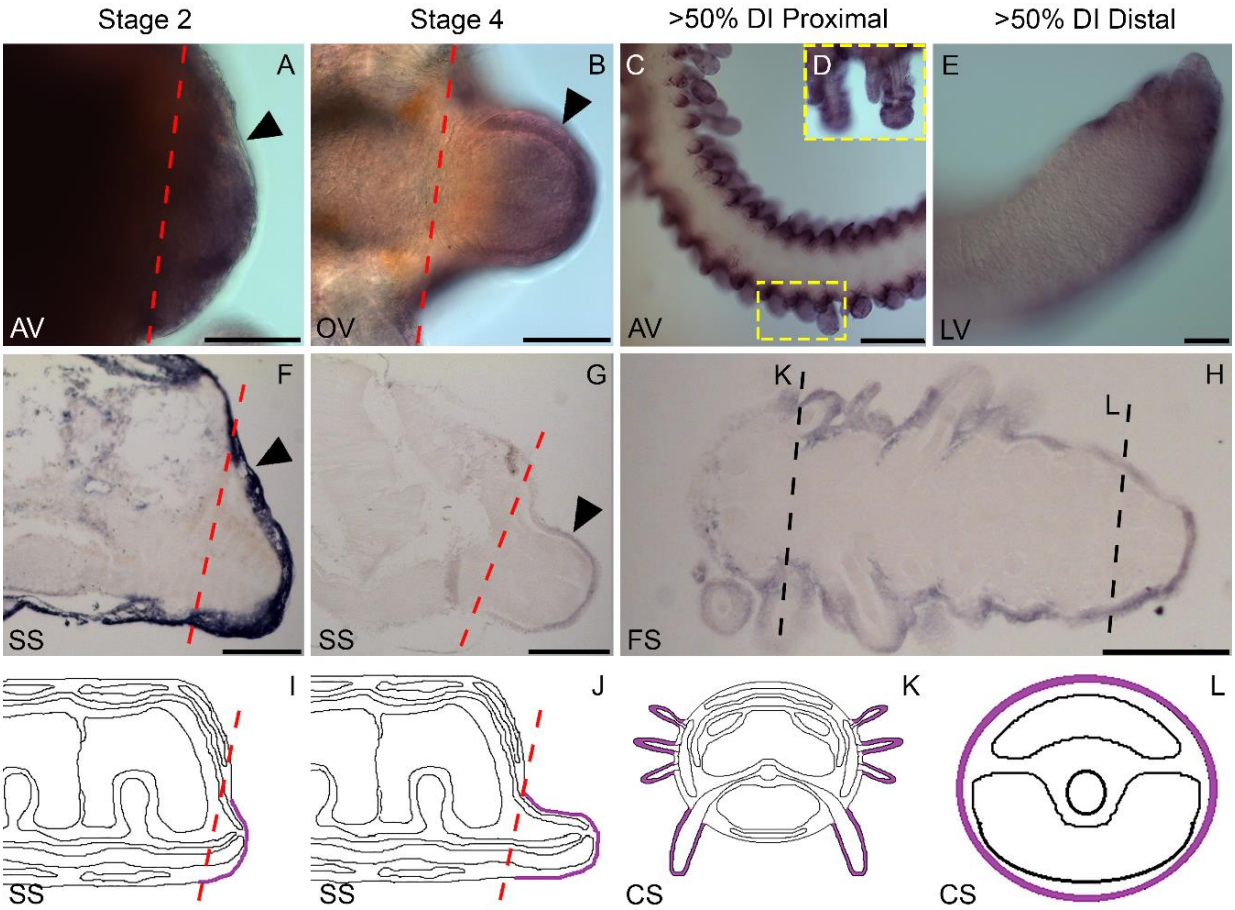


**Fig. S4.** *Afi-actin expression pattern at different regenerative stages*. 1st line: WMISH; 2nd line: post *in situ* sectioning; 3rd line: schemes. Stage 2: A, F, I. *Afi-actin* is expressed in the epidermis (arrowheads) of the regenerative bud. Stage 4: B, G, J. *Afi-actin* is expressed in the epidermis (arrowheads) of the regenerate. Stage >50% DI: C, D, E, H, K, L. *Afi-actin* is expressed in the proximal side at the level of the spine and podia epidermis, whereas in the distal side is expressed in the whole epidermal layer. *Abbreviations*: AV=aboral view; CS=cross section; FS=frontal section; LV=lateral view; OV=oral view; SS=sagittal section. Scale bars: A, B, E, F, G = 50 µm; C, H = 100 µm. In the schemes the gene expression pattern is shown in violet. Red dotted lines=amputation plane. Black dotted lines=levels corresponding to the cross section schemes of Fig. K and L.

*5.2.2. Expression patterns of the A. filiformis genes in the advanced regenerative stages*

*Afi-ficolin* and *Afi-p4h* expression patterns in the advanced regenerative stages (stage 4 and >50%DI) are here described but not further discussed.

*Afi-ficolin* (Fig. S5) is not expressed neither in the regenerate at stage 4 nor at stages >50% DI in both proximal and distal sides.

*Afi-p4h* (Fig. S8) is expressed at the level of the epidermis in the regenerate at stage 4. In the >50% DI stage at the proximal side the expression is localised in the epidermis of podia and spines and in the aboral coelomic cavity epithelium, whereas at the distal side expression is detectable only at the level of the epidermis.

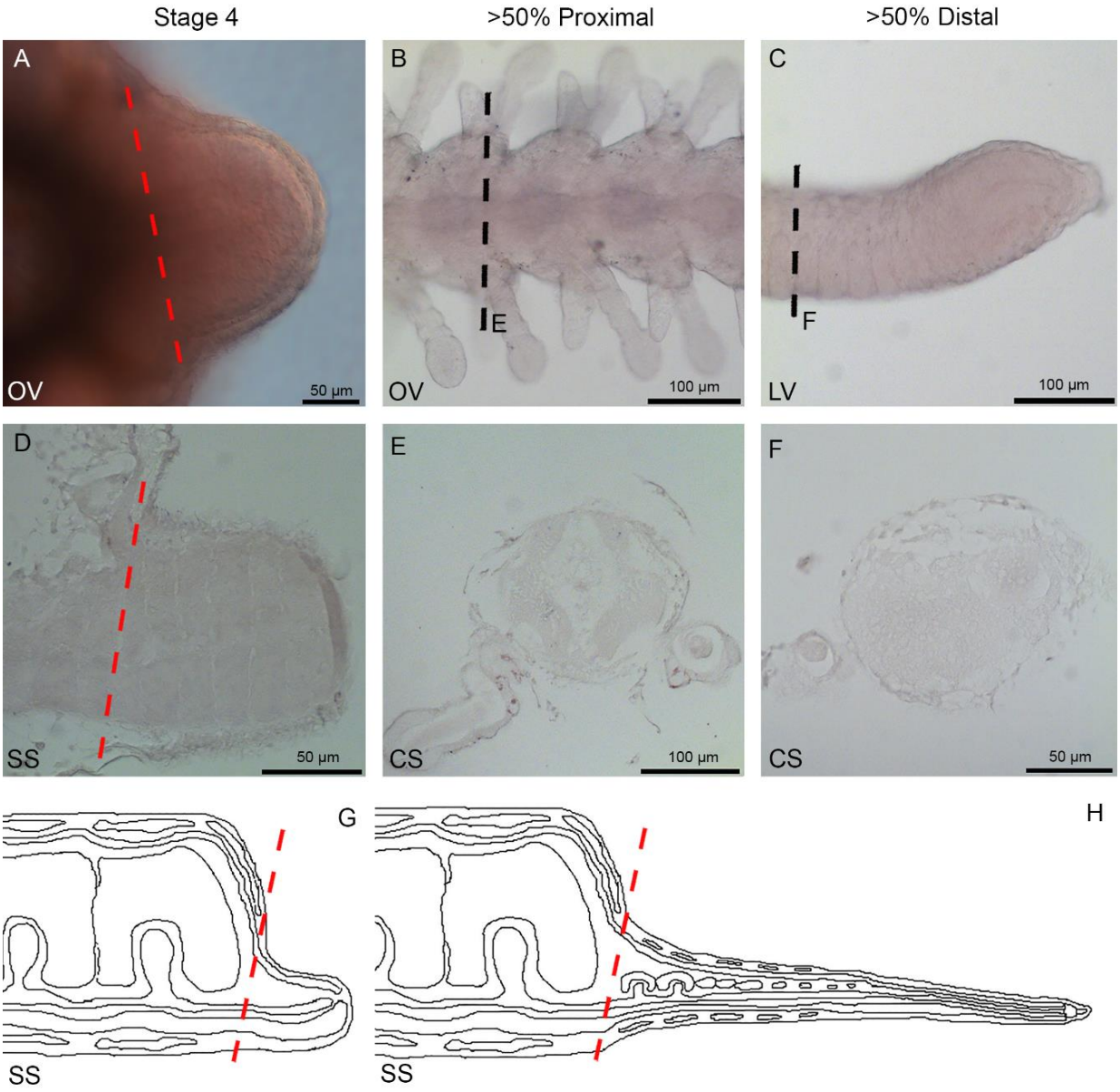


**Fig. S5.** *Afi-ficolin expression pattern in the advanced regenerative stages.* 1st line: WMISH; 2nd line: post *in situ* sectioning; 3rd line: scheme. Stage 4: A, D, G. *Afi-ficolin* is not expressed in the regenerate. Stages >50% DI: B, C, E, F, H. *Afi-ficolin* is not expressed in both proximal and distal side of the late regenerate. *Abbreviations*: CS=cross section; LV=lateral view; OV=oral view; SS=sagittal section. Red dotted lines=amputation plane. Black dotted lines=levels corresponding to the cross sections shown in Fig. E and F.

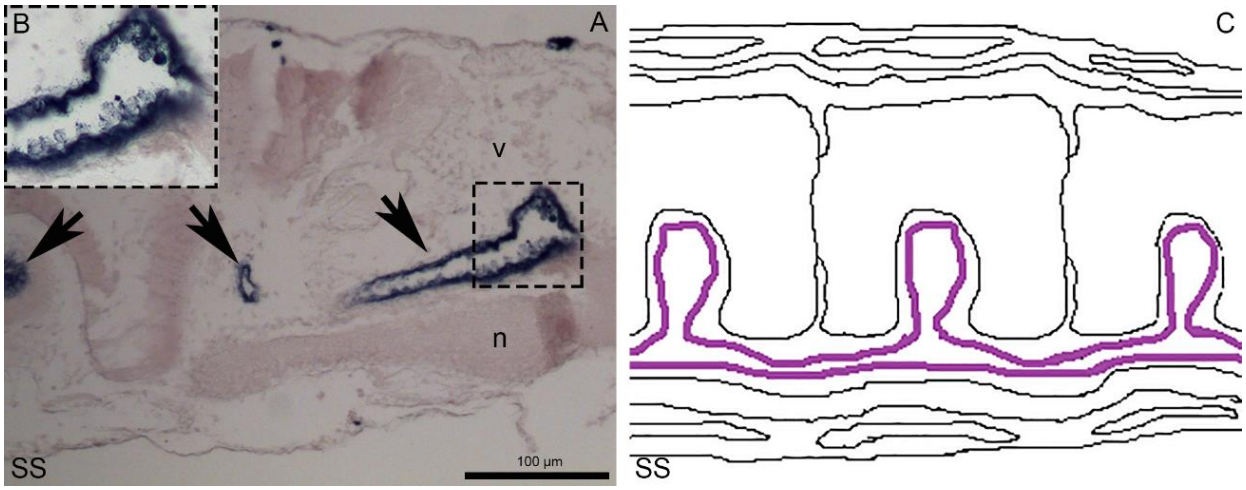


**Fig. S6.** *Afi-ficolin expression pattern in the brittle star stump tissues.* A) This transcript is expressed in the radial water canal epithelium (arrows). B) Detail of A on the staining at the level of the radial water canal epithelium. C) Sagittal section scheme showing the localisation of the signal (violet). *Abbreviations*: n=radial nerve cord; SS=sagittal section; v=vertebra.

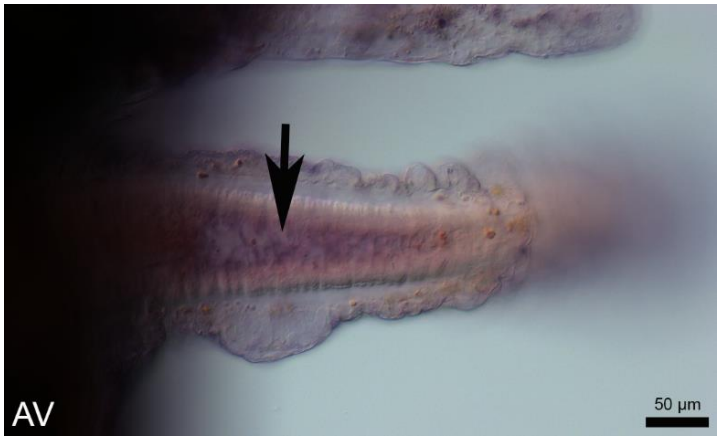


**Fig. S7.** *Afi-p4h expression pattern in the brittle star stump.* This transcript is expressed in the inner lining of the podia (arrow) of the stump. *Abbreviation*: AV=aboral view.

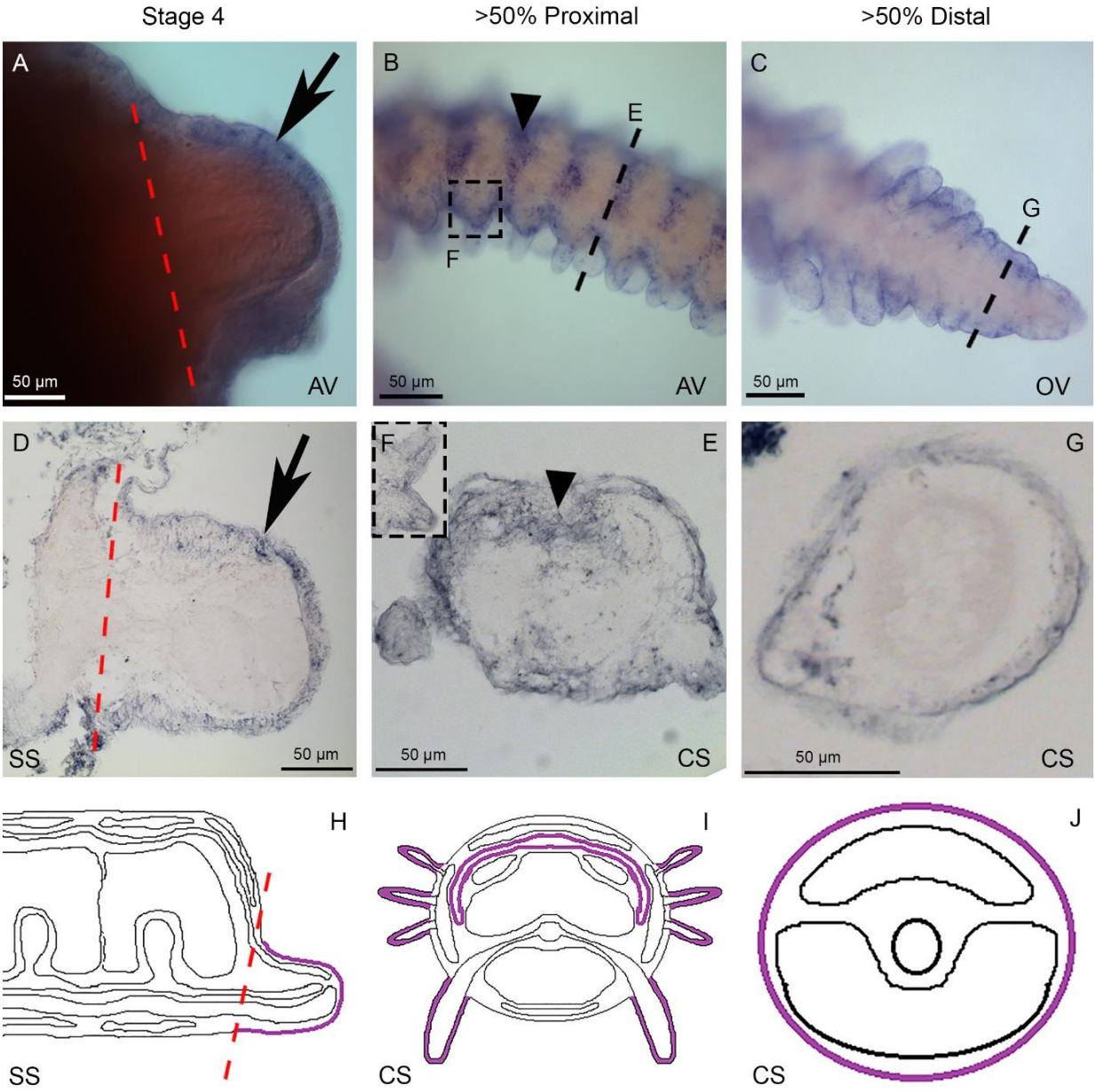


**Fig. S8.** *Afi-p4h expression pattern in the advanced regenerative stages.* Stage 4: A, D, H. This transcript is expressed in the epidermis of the regenerate (arrows). Stages >50% DI: B, C, E, F, G, I, J. *Afi-p4h* is expressed in the proximal side at the level of the aboral coelomic cavity epithelium (arrowheads) and of the epidermis of podia and spines, whereas in the distal side its expression is localised in the epidermis only. *Abbreviations*: AV=aboral view; CS= cross section; OV=oral view; SS=sagittal section. In the scheme the signal is shown in violet. Red dotted lines=amputation plane. Black dotted lines=level corresponding to the cross sections shown in Fig. E and G.

# 3) INTRODUCTION TO CHAPTER 5

As previously underlined, echinoderm regenerative abilities have been suggested being connected with “dynamic” connective tissue (MCTs) presence (Wilkie, 2001). The possibility of increasing human regenerative abilities exploiting knowledge from other animal peculiar features/adaptations has always fascinated scientists. The marine ecosystem has been a valid and continuous source of inspiration and of experimental models to study regeneration from both “basic research” and application perspective. In particular, echinoderm MCTs can be considered not only a source of inspiration but also of biomaterials for future biotechnological application (e.g. regenerative medicine). The exploration of the potential of collagen, their main component, is one of the most appealing in biotechnological viewpoint.

### *3.1. Collagen*

Collagen is the most abundant protein in the animal body and constitutes the main component of the extracellular matrix (ECM) and therefore of connective tissue. It ensures structural integrity, mechanical resistance and elasticity depending on connective tissue function (Wilkie, 2005). Together with other molecules strictly associated (e.g. glycosaminoglycans and proteoglycans), collagen possesses also a physiological function, being responsible for cell response and behaviour, such as migration, proliferation and differentiation (Shuppan *et al.*, 1998; Di Lullo *et al.*, 2001; Gelse, 2003; Czirok *et al.*, 2004; Pawelec *et al.*, 2016). Therefore, it is important in several processes and in tissue and organ repair and regeneration as well. Till now almost 30 types of collagen have been described (Exposito *et al.*, 2010). This protein is characterised by the repetition of Gly-Xaa (usually proline)-Yaa (usually hydroxyproline) tripeptide sequences which permits the formation of alpha helix domains. Single triple helices constitute the tropocollagen which is then subjected to several post-translational modifications that lead to the great variety of collagen types and forms present in animals. Indeed, collagen is usually classified according to the different supramolecular aggregations in fibrillar and nonfibrillar forms, these latter comprehending e.g. collagen type IV, typical of basement membranes. The most common fibrous types are: type I, present in skin, tendons and bones, type II, typical of cartilages, and type III, usually forming reticular fibres. Type I collagen is one of the better characterised fibrillar collagen from both ultrastructural and mechanical point of view (Kuhn, 1987; Shoulders and Raines, 2009). It is composed of

three alpha chains which fold creating the characteristic banding pattern with a periodicity (D-period) of generally around 67 nm (Fig. 12). This fibrillar collagen is typical of vertebrate tissues but numerous invertebrates, both terrestrial and marine, present collagen type I-like collagens, e.g. sponges (Heinemann *et al.*, 2007), cnidarians (Addad *et al.*, 2011), molluscs (Nagai *et al.*, 2001, 2002) and echinoderms (Nagai and Suzuki, 2000; Di Benedetto *et al.*, 2014).

Due to its peculiar features and its involvement in several biological processes, both vertebrate-derived and invertebrate-derived collagens are nowadays intensively investigated as potential biomaterials for human biotechnological applications since collagen can be exploited e.g. to create tools for clinical/biomedical purposes (Lee *et al.*, 2001).

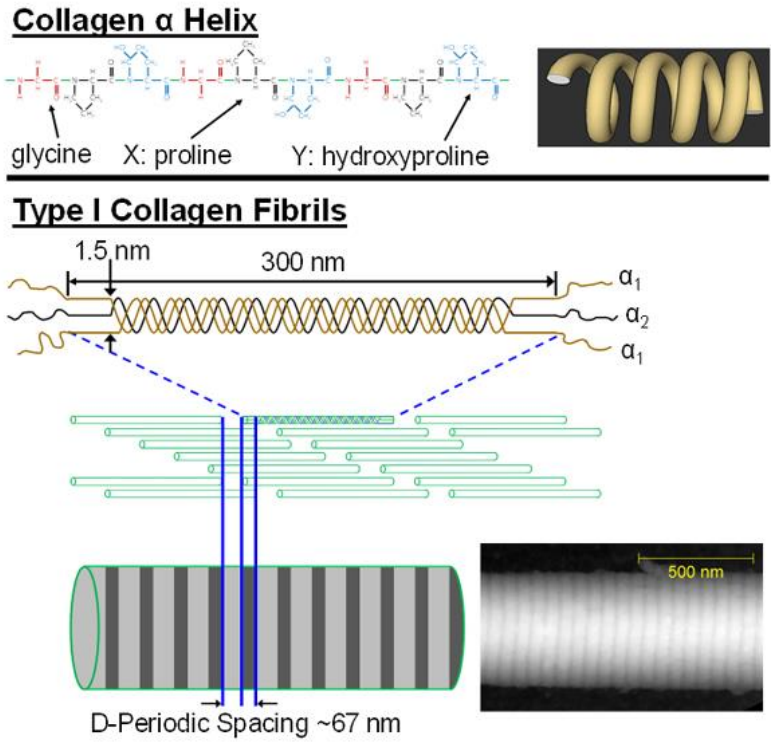


**Fig. 12.** *Collagen type I structure from aminoacid sequence to fibril organisation (from iupui.edu).*

### *3.2. Marine-derived collagen and its potential*

Marine animals are nowadays intensively studied, among the other reasons, as source of biomolecules and biomaterials for human health applications (Jha and Zi-rong, 2004; Silva *et al.*, 2014). Within marine animals, invertebrates are becoming the most interesting sources of bioactive compounds: sponges, corals, nudibranchs, bryozoans and sea slugs are just few of these examples (Donia and Hamann, 2003; Haefner, 2003). Among the

different molecules obtained from these animals, collagens have attracted the interest of researchers because they present several interesting features in comparison to those of mammal origin which are nowadays the most commonly used in biotechnological/biomedical applications (Parenteau-Bareil *et al.*, 2010; Silva *et al.*, 2014). Industrially available collagen is mainly of bovine and porcine origin which carries a risk of transmission of serious diseases (e.g. Bovine Spongiform Encephalopathy or BSE), whereas marine-derived collagen usually presents low antigenicity (Yamamoto *et al.*, 2014). Moreover, it is preferred to mammal collagen also due to allergy problems (Silvipriya *et al.*, 2015), religious and social/life style constraints (Jenkins *et al.*, 2010) and high costs of recombinant technologies (Silva *et al.*, 2014), all problems that have to be faced when using mammal-derived collagen. This latter is usually employed in its hydrolysed form but for many applications collagen in its native fibrillar conformation could better mimic the *in situ* connective tissue environment, *i.e.* the extracellular matrix and its complex scaffold/network structure. Collagen has a wide range of possible biotechnological applications, such as biomaterials for regenerative medicine (Pawelec *et al.*, 2016), cell culture, tissue engineering (TE), guided tissue regeneration (GTR; Ferreira *et al.*, 2012; Tal *et al.*, 2012), pharmaceutical, ophthalmological, biomedical, cosmetic and food industries (Lee *et al.*, 2001). The wide application potential of this protein makes its study fundamental for human health purposes.

### *3.3. Echinoderm-derived collagen and its potential*

As previously described, echinoderms possess peculiar connective tissues (MCTs) whose main component is collagen. Echinoderm collagen has been characterised from both ultrastructural and biochemical point of view. Fibril D-period, diameter, length and chain composition are some of the features investigated in different echinoderm classes. For starfish species (Matsumura, 1973; Kimura *et al.*, 1993; Ferrario, 2013) collagen fibrils have a mean D-period between 50 and 60 nm and a fibril diameter between 20 and 600 nm. These values are comparable with those of other echinoderms, whose D-period ranges from 44 nm (sea urchin) to 67 nm (sea cucumber; Sugni *et al.*, 2013) and fibril diameter between 11 nm and 184 nm (sea urchin) and between 20 and 410 nm (sea urchin; Ribeiro *et al.*, 2011). Overall, according to biochemical analyses, echinoderm collagen is comparable to invertebrate type I-like and vertebrate type I collagens (Di Benedetto *et al.*, 2014; Barbaglio *et al.*, 2015), thus suggesting that it might replace mammal-derived collagen in biotechnological/biomedical applications.

In this perspective, our laboratory recently started exploiting echinoderm connective tissues as valid alternative source of fibrillar collagen (Di Benedetto *et al.*, 2014). Besides being potentially safer in comparison to mammal-derived collagen, echinoderm-derived collagen may be even more appealing for material design addressed to regenerative medicine and tissue engineering. Indeed, considering echinoderm regenerative process the developing structures (especially ossicles and muscles) normally differentiate in strict association with the dermal collagen, which actually acts as a fibrillar scaffold. Thus, considering this intrinsic properties/functions, echinoderm collagen fibrils maybe an optimal material to develop biomimetic, mechanically resistant and growth-promoting scaffold for cell culture studies and regenerative medicine. Other main advantages of echinoderm-derived collagens are: the possibility of easily and efficiently extracting fibrillar collagen in its native conformation (*i.e.* maintaining its ultrastructural integrity; Matsumura, 1974; Trotter *et al.*, 1994; Barbaglio *et al.*, 2012, 2013; Di Benedetto *et al.*, 2014) and the opportunity of exploiting eco-friendly sources e.g. food industry wastes as suggested by Di Benedetto and co-workers (2014). With fibrillar collagen it will be possible to produce both two- and three-dimensional membranes and scaffolds that can be used in the previously suggested medical fields. To assess the suitability of these innovative biomaterials both *in vitro* and *in vivo* tests need to be performed in order to evaluate their biocompatibility and effectiveness for human applications.

# CHAPTER 5

## Marine-derived collagen biomaterials from echinoderm connective tissues

Ferrario Cinzia, Leggio Livio, Leone Roberta, Di Benedetto Cristiano, Guidetti Luca, Coccè Valentina, Ascagni Miriam, Bonasoro Francesco, La Porta Caterina A.M., Candia Carnevali Maria Daniela, Sugni Michela

Marine Environmental Research, Special Issue “Blue Growth” (2016). S0141-1136(16)30032-0. doi: 10.1016/j.marenvres.2016.03.007.

***Abstract***

The use of marine collagens is a hot topic in the field of tissue engineering. Echinoderms possess unique connective tissues (Mutable Collagenous Tissues, MCTs) which can represent an innovative source of collagen to develop collagen barrier-membranes for Guided Tissue Regeneration (GTR). In the present work we used MCTs from different echinoderm models (sea urchin, starfish and sea cucumber) to produce echinoderm-derived collagen membranes (EDCMs). Commercial membranes for GTR or soluble/reassembled (fibrillar) bovine collagen substrates were used as controls. The three EDCMs were similar among each other in terms of structure and mechanical performances and were much thinner and mechanically more resistant than the commercial membranes. Number of fibroblasts seeded on sea urchin membranes were comparable to the bovine collagen substrates. Cell morphology on all EDCMs was similar to that of structurally comparable (reassembled) bovine collagen substrates. Overall, echinoderms, and sea urchins particularly, are alternative collagen sources to produce efficient GTR membranes. Sea urchins display a further advantage in terms of eco-sustainability by recycling tissues from food wastes.

### *1. Introduction*

The marine ecosystem and its inhabitants have always been sources of food, biomaterials, active compounds or simply ideas for human applications (e.g. medicine, cosmetics, biotechnology, biofuels, etc.). Many examples of sustainable exploitation of

“blue resources” have been reported so far including: 1) professional swimsuits inspired by shark skin, 2) algae and marine sponge bioactive substances (Gupta and Abu-Ghannam, 2011; Dembitsky *et al.*, 2005; Rao *et al.*, 2006; Guzmàn *et al.*, 2011) for pharmacological use (anti-cancer or anti-neurodegeneration drugs), 3) structural molecules (*i.e*. chitin and collagen) from different marine animals as alternative biomaterials for biomedical applications (Gomez d’Ayala *et al.*, 2008; Gomez-Guillen *et al.*, 2011). Basic research on ocean life and applied research on possible industrial applications are the key activities in terms of “blue growth” in biotechnology and bioeconomy (European Commission, 2012): the sustainable exploitation of “blue resources” and the eco-friendly management of industrial wastes are nowadays two of the most challenging aspects in this field.

To date, marine invertebrates (e.g. sponges, jellyfish and molluscs), are among the most promising groups of animals for this kind of studies because of their variety and abundance in all seas. However, a wide range of marine biodiversity is still unexplored from this point of view. Echinoderms are marine invertebrates widespread in all the oceans and employed as source of food for decades (e.g. sea cucumbers and sea urchins; Conand, 2004; Barrington *et al.*, 2009). They are well known also for their peculiar connective tissues, called Mutable Collagenous Tissues or MCTs, which are able to rapidly change their passive mechanical properties (stiffness and viscosity), under the nervous system control (Wilkie, 2005). MCTs are a unique feature of echinoderms and, although their presence was not described in all known species, their ubiquity throughout the phylum is highly probable: indeed, MCTs have been described in all the five extant classes (Wilkie, 2005) and in fossil specimens as well (Baumiller and Ausich, 1996), thus indicating they are probably an ancestral character. This type of tissue has been recently proposed as possible source of inspiration for “smart dynamic biomaterials” for tissue engineering and regenerative medicine applications (Barbaglio *et al.*, 2012, 2013). Particularly, the sea urchin peristomial membrane (a well-known MCT) has been proposed as a sustainable and eco-friendly source of native fibrillar collagen to produce thin membranes for regenerative medicine applications (Di Benedetto *et al.*, 2014). Indeed, the peristomial membrane is a sea urchin food industry waste that can be transformed in a highly valuable by-product.

Among the “blue biomaterials” marine collagen has the most promising perspectives as valid candidate for replacing the most commonly used mammal-derived collagen. This latter is routinely employed in a wide range of human applications (Karim and Bath, 2008;

Silva *et al.*, 2014; Silvipriya *et al.*, 2015), from large-scale uses, such as food (Djagny *et al.*, 2010), pharmaceutical/nutraceutical industry (Sahithi *et al.*, 2013) and cosmetics (Buck II *et al.*, 2009), to more targeted fields, such as cell cultures (Lee *et al.*, 2008) and biomedical/clinical applications (Tsai *et al.*, 2005; Glowacki and Mizuno, 2008). However, due to allergy problems (Silvipriya *et al.*, 2015), religious and social/life style constraints (Jenkins *et al.*, 2010), disease transmission-connected reasons (e.g. bovine spongiform encephalopathy or BSE) and high costs of recombinant technologies, collagen sources alternative to mammals are constantly investigated (Silva *et al.*, 2014). In this sense marine animals, and echinoderms in particular, are surely appealing (Shimomura *et al.*, 1962; Nagai and Suzuki, 2000; Nagai *et al.*, 2000; Swatschek *et al.*, 2002; Song *et al.*, 2006; Uriarte-Montoya *et al.*, 2010; Barros *et al.*, 2014; Di Benedetto *et al.*, 2014). A further advantage of echinoderm MCTs is the relative easiness to obtain high amount of native collagen fibrils, which maintain their original structure (Matsumura, 1974; Trotter *et al.*, 1994; Di Benedetto *et al.*, 2014). Indeed, most mammalian collagen is usually employed in its hydrolysed (acid-solubilised) form, a characteristic that strongly reduces the mechanical performances of the produced membrane/scaffold and that can be a limit in those biomedical applications where highly resistant materials, with fibril three-dimensional organisation, are required e.g. tendon/ligament regeneration (Kew *et al.*, 2011) or dermis reconstruction (Ruszczak, 2003). Echinoderm MCTs can be useful to easily and rapidly produce fibrillar collagen membranes with a high similarity in terms of both ultrastructural and mechanical characteristics to the physiological situation of connective tissue. A specific regenerative medicine field where fibrillar collagen membranes are commercially used is Guided Tissue Regeneration (GTR; Ferreira *et al.*, 2012; Tal *et al.*, 2012). One of the aims of GTR is to reduce post-surgical tissue adhesions, a common and only partially solved complication (Parker *et al.*, 2001), which prevents proper tissue regeneration. These latter are abnormal attachments or mixture of cells forming between tissues or organs after surgery or due to local inflammation. Only recently researchers have tried to produce effective and satisfactory tools to overcome them. Indeed, barrier/membranes composed by several different biomaterials (e.g. chitosan and hyaluronic acid) have been tested for GTR but none of them displayed all the necessary functional properties, the most important of which is avoiding cell penetration into the underlying anatomical compartment (Tang *et al.*, 2007). Collagen-based membranes seem promising from this point of view because their porosity/three-dimensional structure can be modified as desired. However, their use is still limited by the

weak mechanical resistance. This, for example, reduces their efficacy in prevention of wound dehiscence or in tendon repair.

The present work was addressed to evaluate if echinoderm-derived collagen membranes could represent a valuable “blue alternative” to the commercially available (mammal-derived) membranes employed for GTR. This was done by considering different aspects, including ultrastructural properties, mechanical performances as well as the behaviour of human skin-derived fibroblasts (hSDFs) when seeded on these substrate types. Considering the high biodiversity of echinoderms, we also evaluated which animal/MCT source might be more suitable for this biotechnological application. To accomplish this, representatives of different echinoderm classes were used: the sea urchin *Paracentrotus lividus*, the starfish *Echinaster sepositus* and the sea cucumber *Holothuria tubulosa*.

## *2. Materials and methods*

### *2.1. Experimental animals*

Adult specimens of the sea urchin *P. lividus*, the starfish *E. sepositus* and the sea cucumber *H. tubulosa* were collected by scuba divers in Paraggi (Marine Protected Area of Portofino, Ligurian Sea, Italy), transferred to the Department of Biosciences (University of Milan) and immediately dissected. Samples of sea urchin peristomial membranes (PM; Fig. 1A and B), starfish aboral arm walls (AW; Fig. 1C and D) and sea cucumber whole body walls (BW; Fig. 1E-G) were collected and stored at -20°C for the subsequent collagen extraction protocol (see paragraph 2.2). Animal collection and experimental manipulation were performed according to the Italian law.

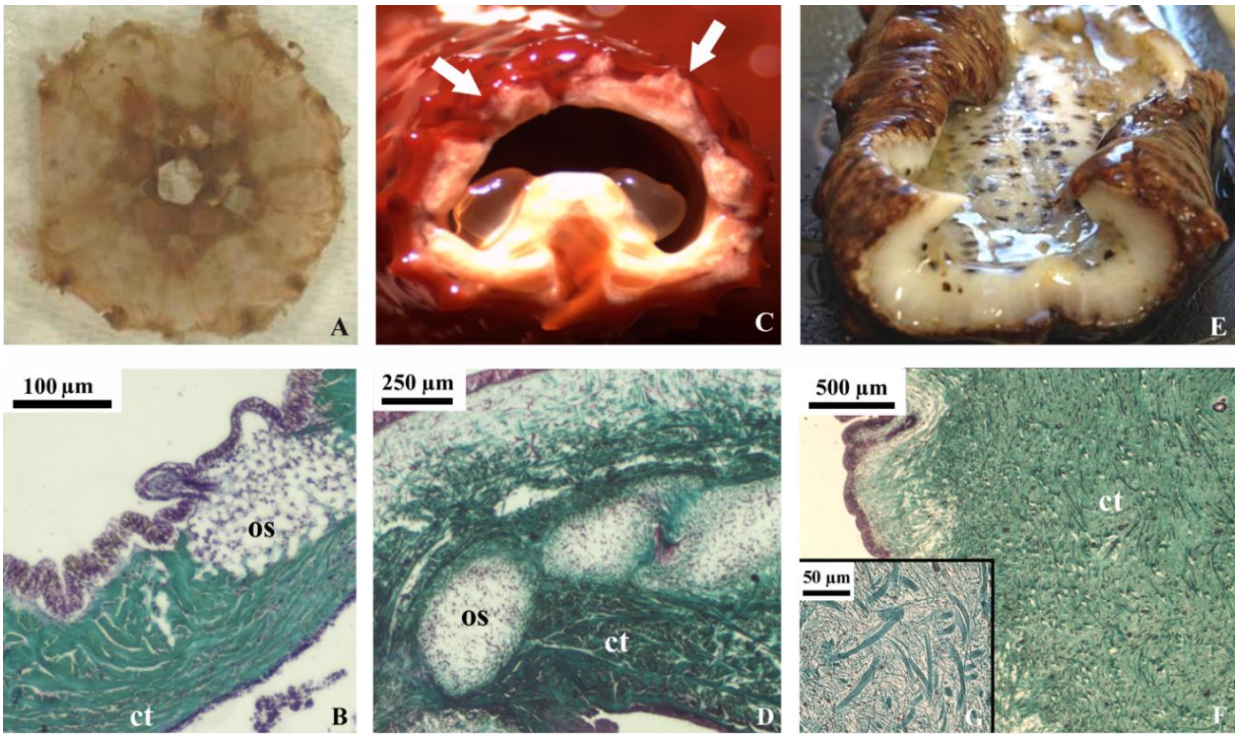


**Fig. 1.** *Echinoderm tissues for the collagen extraction protocol in vivo (stereomicroscopy) and in histological sections (light microscopy, Trichrome Milligan staining; collagen is stained in green)*. A) Sea urchin peristomial membrane (PM). B) PM connective tissue characterised by highly packed collagen fibrils and fibres (ct) with quite large ossicles (os). C) Starfish aboral arm wall (AW; arrows). D) AW connective tissue characterised by dense collagen fibre bundles (ct) in which large ossicles (os) are widespread. E) Sea cucumber body wall (BW). F) BW connective tissue with small spicules and absence of highly packed collagen fibres (ct). G) Detail of figure F on the loosely packed collagen fibrils.

### *2.2. Echinoderm collagen extraction*

Sea urchin collagen was extracted from the peristomial membranes as previously described by Di Benedetto and co-workers (2014). Starfish aboral arm walls followed the same protocol with only slight modifications. Briefly, the frozen tissues of both animals were dissected in small pieces, rinsed in artificial sea water and left in a hypotonic buffer (10 mM Tris, 0.1% EDTA) for 12 hours at room temperature (RT) and then in a decellularising solution (10 mM Tris, 0.1% Sodium Dodecyl Sulphate) for 12 hours at RT. After several washings in phosphate-buffered saline (PBS), samples were placed in disaggregating solution (0.5 M NaCl, 0.1 M Tris-HCl pH 8.0, 0.1 M β-mercaptoethanol, 0.05 M EDTA-Na). The obtained collagen suspension was filtered and dialysed against 0.5 M EDTA-Na solution (pH 8.0) for 3 hours at RT and against $dH_2O$ overnight at RT. Starfish samples underwent an additional step in 1 mM citric acid (pH 3-4) between decellularising and disaggregating solutions in order to remove as much as possible the calcium carbonate ossicles present in the fresh tissue. All the steps were carried out

under stirring conditions. Sea cucumber collagen was extracted from the whole body wall following a different protocol. Briefly, the starting tissue was cut into small pieces, placed in PBS and gentamicin (40 µg/ml) and left in stirring conditions at RT for at least 5 days in order to obtain a collagen suspension that was subsequently filtered. Suspensions obtained from the three experimental models were then stored at -80°C until use.

### *2.3. Ultrastructural characterisation of isolated echinoderm collagen fibrils*

#### *2.3.1. D-period measurements*

A drop of fibril suspension was placed on a 300 mesh copper grid with FORMVAR membrane. The excess was removed after 5 min and the grid was stained with potassium phosphotungstate (pH 7.3) for 1 min. All the grids were then observed and photographed under a transmission electron microscope (TEM JEOL SX100, Tokyo, Japan) and the D-period was measured from digital images by Adobe Photoshop CS3 Extended Software (Version 10.0.1).

#### *2.3.2. Glycosaminoglycan (GAG) visualisation*

A 10 µl drop of suspension of each type of collagen was added to FORMVAR-coated grids which, after excess removal, were processed according to the following steps: filtered $dH_2O$ (30 s x3), 500 mM NaCl (1 min), fixative solution (2.5% glutaraldehyde, 300 mM $MgCl_2$, 25 mM sodium acetate, pH 5.6; 1 min), 0.2% Cuprolinic Blue (1 min), fixative solution (30 s x2), 1% sodium tungstate (1 min) and filtered $dH_2O$ (30 s x3). The grids were then observed and photographed under a transmission electron microscope (TEM JEOL SX 100, Tokyo, Japan).

### *2.4. Production of echinoderm-derived collagen membrane (EDCM)*

Membranes of the three echinoderm collagen types were prepared as previously described for sea urchin membrane by Di Benedetto and co-workers (2014) to produce substrates for both mechanical and *in vitro* tests (see paragraphs 2.5.2 and 2.6 respectively). Briefly, 500 µl of the collagen suspensions were dried overnight in a silicon mould at 37°C. The resulting collagen sheets were weighted in order to calculate the original collagen concentrations. The remaining suspensions were centrifuged for 10 min at 50xg to remove eventual precipitated debris and then for 20 min at 2000xg (sea urchin), 1500xg (starfish) or 4000xg (sea cucumber). The pellet was re-suspended in 0.01% Triton X-100 for cell culture substrates or in autoclaved filtered $dH_2O$ for membranes for

mechanical tests to reach a 2 mg/ml final collagen concentration. 300 µl of the former suspensions were placed in 24x multiwells dishes and 800 µl of the latter in rubber silicone moulds (10 mm-16 mm) and left dry overnight at 37°C. The obtained collagen membranes were then immersed in EDC/NHS (1-ethyl-3-(3-dimethylaminopropyl)carbodiimide/N-hydroxysuccinimide) cross-linker solution (30 mM EDC/15 mM NHS in 100 mM MES (2-(N-morpholino)ethanesulfonic acid) buffer, pH 5.5; Song *et al.*, 2006; Yang, 2012) for 4 hours at RT and then washed with PBS, $dH_2O$ and 70% EtOH.

### *2.5. Collagen membrane characterisation*

#### *2.5.1. Ultrastructural analysis: scanning electron microscopy (SEM)*

Collagen membranes for both cell cultures and mechanical tests were fixed with 2% glutaraldehyde in 0.1 M cacodylate buffer (2 hours, 4°C) and post-fixed with 1% osmium tetroxide in 0.1 M sodium cacodylate buffer (2 hours, RT). After careful washings with $dH_2O$, samples were dehydrated with an increasing concentration ethanol and then transferred to a series of solutions of Hexamethyldisilazane (HMDS)/absolute ethanol in different proportions (1:3, 1:1, 3:1 and 100% HMDS). Membranes were then mounted on stubs, covered with pure gold (Agar SEM Auto Sputter, Stansted, UK) and observed under a scanning electron microscope (LEO-1430, Zeiss, Oberkochen, Germany). Measurements of collagen membrane thickness, mesh size (superficial porosity), fibril diameter and length were performed with Adobe Photoshop CS3 Extended Software. SEM analyses were carried out also on both reassembled (fibrillar) bovine collagen (BCMs; see paragraph 2.6) and commercial membranes (CMs; bovine collagen) in order to compare their ultrastructural characteristics with the EDCM ones.

#### *2.5.2. Mechanical analysis: force-extension tests*

Echinoderm and commercial collagen membranes were cut into small strips (2 mm-10 mm) whose ends were fixed to rigid plastic supports with cyanoacrylate cement (Superattak®, Heckel, Düsseldorf, Germany). Each strip was photographed under a LEICA MZ75 stereomicroscope provided with a Leica EC3 Camera and Leica Application Suite LAS EZ Software (Version 1.8.0) to allow digital width measurements. For details on the experimental apparatus and conditions see Di Benedetto and co-workers (2014). 19, 21, 46 and 7 strips were tested for sea urchin, starfish, sea cucumber-derived and commercial membranes respectively. Samples were immersed in L-15 Leibovitz cell

culture medium throughout the mechanical test. They were subjected to elongations of 0.1 mm every 10 s until complete rupture. The force peaks generated at each elongation step were used to produce a stress-strain curve from which the mechanical parameters (stiffness, tensile strength and tensile strain) were calculated as follows:

Δ stress (MPa) = Δ F / CSA (Cross Section Area);

Δ strain = Δ l / l (sample starting length);

Stiffness (Young's Modulus; MPa) = Δ stress / Δ strain;

Tensile strength (MPa) = Maximum weight before rupture / CSA;

Tensile strain (%) = Extension / l (sample starting length) x 100.

### *2.6. In vitro tests*

Primary human dermal fibroblasts (hSDFs) derived from human epithelial biopsy were obtained as described in Coccè and co-workers (2016). Briefly, cells were cultured in minimum essential medium Eagle (EMEM) with Earles salts and $NaHCO_3$ (Sigma-Aldrich) supplemented with 10% fetal calf serum (Euroclone), 2 mM glutamine (cod. ECB3004D, Euroclone), antibiotic antimycotic solution 100 U/ml penicillin, 100 µg/ml streptomycin and 0.25 µg/ml amphotericin B (Sigma-Aldrich). Cells were seeded in 24x multiwells on EDCMs as well as on reassembled (fibrillar) bovine collagen membranes (BCMs), on bovine skin-derived soluble collagen (Sigma-Aldrich) and on plastic as controls, the last two being the commonly used controls for *in vitro* tests. 300 µl of bovine-skin derived soluble collagen (Sigma-Aldrich) was added to each well, left for 15 min and subsequently removed and left air-dry for at least 2 hours before use. This same soluble collagen was used to produce BCMs: 8 volumes of collagen mixed with 1 volume of 10x PBS and 1 volume of 0.1 M NaOH were added in each well and left to dry overnight at 37°C before use. *In vitro* tests lasted 4 days.

#### *2.6.1. Cell counting*

Cells seeded on the different substrates were fixed in 4% paraformaldehyde in PBS, stained with 0.1% methylene blue and carefully washed with filtered $dH_2O$. Photographs of five representative areas for each well were taken under a LEICA MZ75 stereomicroscope provided with a Leica EC3 Camera and Leica Application Suite LAS EZ Software (Version 1.8.0). Cell counting was independently performed from digital images by two different operators. Once absence of statistically significant differences between operators was verified (*t*-test), mean values were considered. The mean cell

number of each well was normalised against the mean cell number of the control (plastic) wells and expressed as a percentage. Each treatment (=substrate) was repeated in duplicates or triplicates. Experiments were repeated five times (rounds).

*2.6.2. Cell morphology and cell-substrate adhesion/interaction analysis*

SEM and immunofluorescence (IF) techniques were performed to analyse cell morphology as well as cell-substrate adhesion and interactions. For SEM analyses cell seeded substrates were fixed after 4 days in 2% glutaraldehyde in 0.1 M sodium cacodylate buffer for 2 hours (4°C) and then processed as previously described (see paragraph 2.5.1). Samples were observed under a scanning electron microscope (LEO-1430, Zeiss, Oberkochen, Germany). IF specific stainings were performed to reveal cytoskeletal F-actin organisation and both stress fibre and focal adhesion presence. After 4 days in culture, cells were fixed in 4% paraformaldehyde and permeabilised with 0.1% Triton X-100 in PBS for 30 min at RT. Cells were subsequently blocked with 10% normal goat serum in PBS for 1 hour and incubated with mouse monoclonal Anti-Vinculin antibody (1:500, Sigma-Aldrich) overnight at 4°C. Then, cells were incubated with FITC (fluorescein isothiocyanate) conjugated goat anti-mouse secondary antibody (1:250, Millipore) and Actin-stain 555 phalloidin (100 nM, Cytoskeleton) for 1 hour. Nuclei were counterstained with Fluoroshield with DAPI (4,6-diamine-2-phenylindole dihydrochloride, Sigma-Aldrich). Samples were then examined under a Leica TCS SP2 Laser Scanning Confocal microscope (Leica Microsystems).

### *2.7. Statistical analyses*

For mechanical tests non-parametric Kruskal-Wallis test, Tukey's test and Dunn's Multiple Comparison test were used to analyse stiffness, tensile strength and tensile strain of both EDCMs and commercial membranes (GraphPad Software). For *in vitro* tests Generalised Linear Model (GLM) was used to analyse the effect of both substrate type and round on cell number with Bonferroni *post-hoc* test (SPSS 15.0 Version Software). In both cases, differences were considered significant at the $P<0.05$ level (see Results).

## *3. Results*

### *3.1. Echinoderm-derived collagen extraction*

The extraction protocols optimised for the different echinoderm tissues (*i.e.* sea urchin peristomial membrane, starfish aboral arm wall and sea cucumber body wall) allowed us

to obtain highly concentrated collagen fibril suspensions. No fibril aggregates, cell debris and calcium carbonate residues were detected from both light and electron microscopy observations, thus they were considered suitable for the production of two-dimensional membranes (Fig. 2). Sea urchin-derived collagen was extracted from both animals collected in the wild and from commercial activities (e.g. waste from restaurants) but since ultrastructural, mechanical and *in vitro* analyses showed almost identical results (data not shown) they were pooled together.

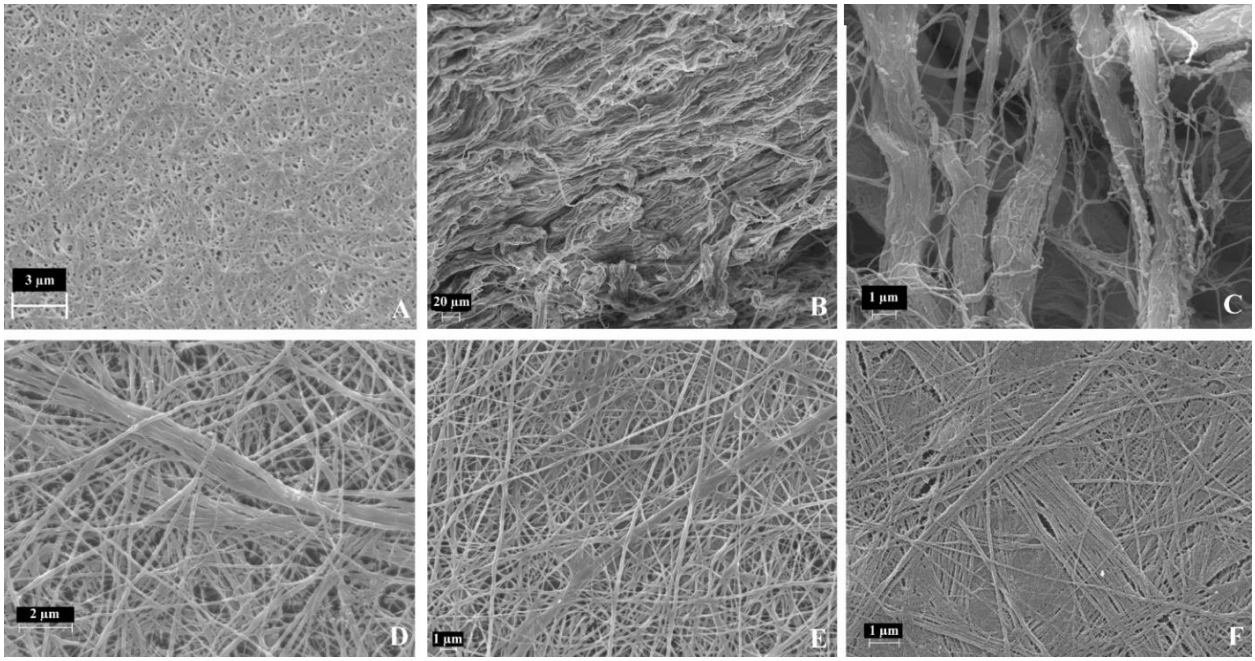


**Fig. 2.** SEM. *Collagen network of the different membranes*. It is possible to observe the comparable homogeneous and random distribution of collagen fibrils, the low superficial porosity and the absence of debris of the three EDCMs, the comparable fibril network of the reassembled (fibrillar) bovine collagen membrane (BCM) and the more oriented collagen fibril bundles of the commercial membrane. A) BCM. B) Commercial membrane. C) Commercial membrane detail on the collagen fibril bundles showing the high superficial porosity of the collagen network. D) Sea urchin-derived collagen membrane. E) Starfish-derived collagen membrane. F) Sea cucumber-derived collagen membrane.

### *3.2. Ultrastructural characterisation of collagen fibrils and membranes*

Table 1 summarises the mean fibril D-period for each type of collagen membrane. As shown in Fig. 3, in all three echinoderm collagen types GAGs were present regularly distributed along the whole fibril, strictly according to the D-patterning. As for TEM analyses, also SEM observations confirmed the “cleanliness” of the echinoderm-derived collagen suspensions since no debris and undissociated fibres were detected (Fig. 2). Data on fibril ultrastructural features and on membrane average mesh size and thickness are reported in Table 1. SEM analyses showed that in both EDCMs and BCMs, collagen

fibrils were randomly distributed on the well plastic surface, without a clearly organised pattern and creating a highly dense collagen network (Fig. 2). Differently, commercial membranes showed thick fibril/fibre bundles interspersed in a loose thin fibril network and displayed a more oriented distribution (Fig. 2B and C). Fig. 4 shows at a macroscopical level (stereomicroscopy) an example of commercial bovine collagen membrane and an example of EDCM (sea urchin-derived collagen membrane).

**Table 1.** *Ultrastructural features of collagen fibrils and membranes.* Data shown as mean ± SD and/or ranges. [a] Tricarico *et al.* (2012); [b] Di Benedetto *et al.* (2014).

| | **Commercial membrane (CM)** | **Sea urchin *P. lividus*** | **Starfish *E. sepositus*** | **Sea cucumber *H. tubulosa*** |
|---|---|---|---|---|
| **Mean fibril D-period (nm) ± SD** | - | 62.7 ± 2.8 | 63 ± 4.7 | 66 ± 1.6 |
| **Fibril D-period range (nm)** | - | 60 - 66 [a] | 60 - 70 | 61.4 - 68.9 |
| **Diameter range (nm)** | 70 - 3640 (fibrils and fibres) | 25 - 300 [b] (fibrils) | 37 - 362 (fibrils) | 36 - 520 (fibrils) |
| **Mean length (µm) ± SD** | - | 208 ± 93.3 | 337.7 ± 106.8 | 233 ± 115.8 |
| **Average mesh size (µm)** | >> 2 | < 2 [b] | < 2 | < 2 |
| **Membrane thickness range (µm)** | 316 - 390 | 9 - 14 | 9 - 15 | 10 - 11 |

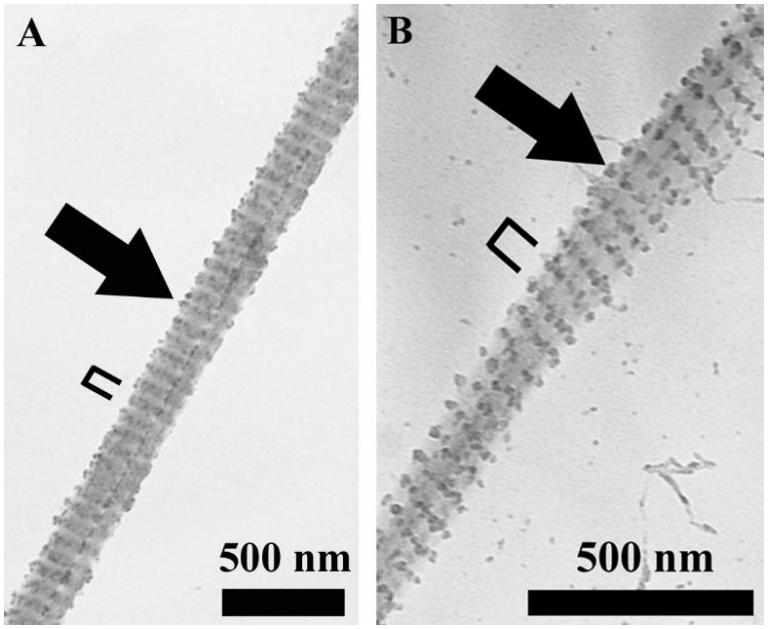


**Fig. 3.** TEM. *GAG distribution (arrows) on echinoderm collagen fibril surface according to the D-patterning (square brackets)*. A) Starfish-derived collagen fibril. B) Sea

◀ cucumber-derived collagen fibril. For GAG decoration on sea urchin-derived collagen fibril see Figure 2 in Di Benedetto *et al.* (2014).

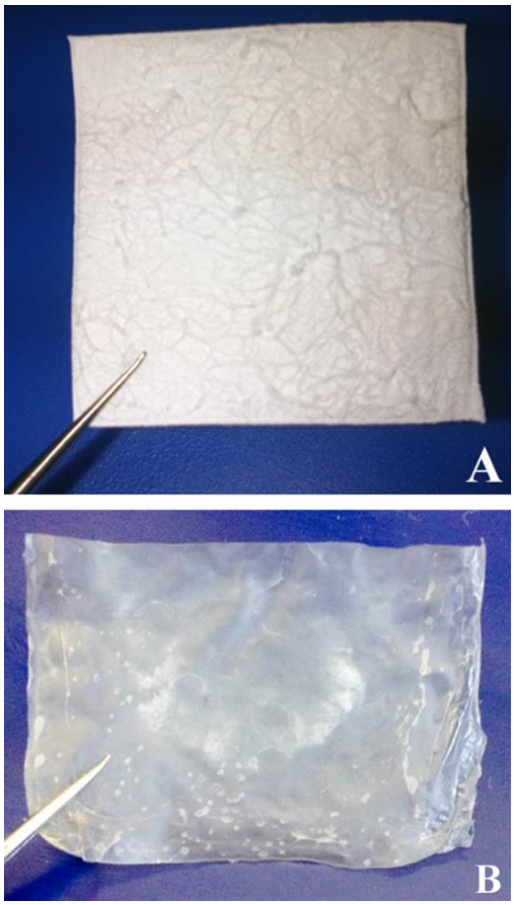


**Fig. 4.** Stereomicroscopy. *Examples of the collagen membranes*. A) Commercial membrane currently available for clinical purposes. B) Sea urchin-derived collagen membrane after the cross-linking protocol.

### *3.3. Mechanical characterisation of echinoderm-derived and commercial collagen membranes*

Stiffness (or Young's Modulus), tensile strength and tensile strain were evaluated in order to have a complete overview and comparison among the EDCM and commercial membrane mechanical features in physiological conditions (*i.e.* immersed in a fluid biochemically and osmotically similar to that present in human tissues). Both EDCM stiffness (Fig. 5) and tensile strength (Fig. 6) were significantly higher (~ 20 folds) than those of commercial membrane, which, on the contrary, showed higher tensile strain comparing to EDCMs. Sea urchin membrane stiffness (see also Di Benedetto *et al.*, 2014) was similar to that of both starfish and sea cucumber membranes ($P>0.05$; Dunn's Multiple Comparison Test), whereas sea cucumber membrane stiffness was significantly higher than that of starfish membrane ($P<0.001$; Dunn's Multiple Comparison Test). Both sea urchin and sea cucumber membrane stiffness was significantly higher than that of

commercial membrane (P<0.01 and P<0.001 respectively; Dunn's Multiple Comparison Test), whereas starfish membrane stiffness was statistically similar to commercial membrane values (P>0.05; Dunn's Multiple Comparison Test). Echinoderm membrane tensile strength was statistically similar among each type of collagen (P>0.05; Dunn's Multiple Comparison Test) and significantly higher than that of commercial membrane (P<0.01 sea urchin, P<0.001 starfish and sea cucumber; Dunn's Multiple Comparison Test). Commercial membrane mean tensile strain ± SD (62.12% ±14.43) was higher than that of EDCMs (sea urchin: 32.81% ±5.77 (see also Di Benedetto *et al.*, 2014); starfish: 49.48%±20.89; sea cucumber: 27.96%±9.89).

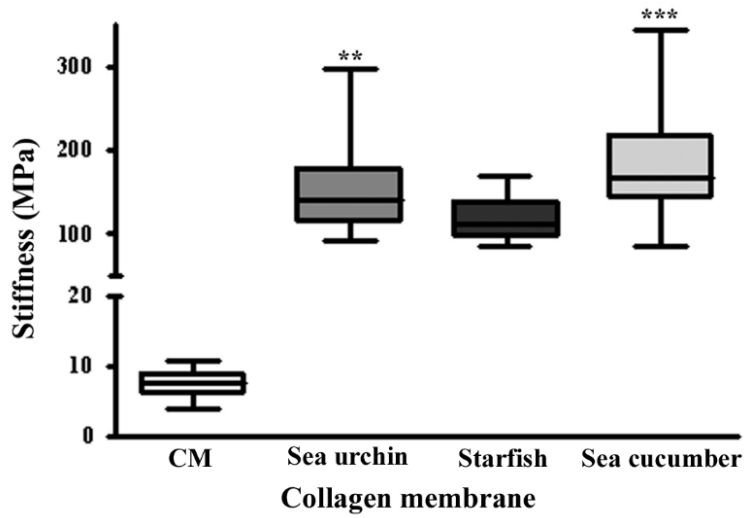


**Fig. 5.** *Box plot of stiffness (or Young's Modulus) of commercial membranes and EDCMs*. CM, commercial membrane (n = 7); sea urchin-derived collagen membrane (n = 19); starfish-derived collagen membrane (n = 21); sea cucumber-derived collagen membrane (n = 47). ** P<0.01, *** P<0.001 *vs* commercial membrane (Dunn's Multiple Comparison Test).

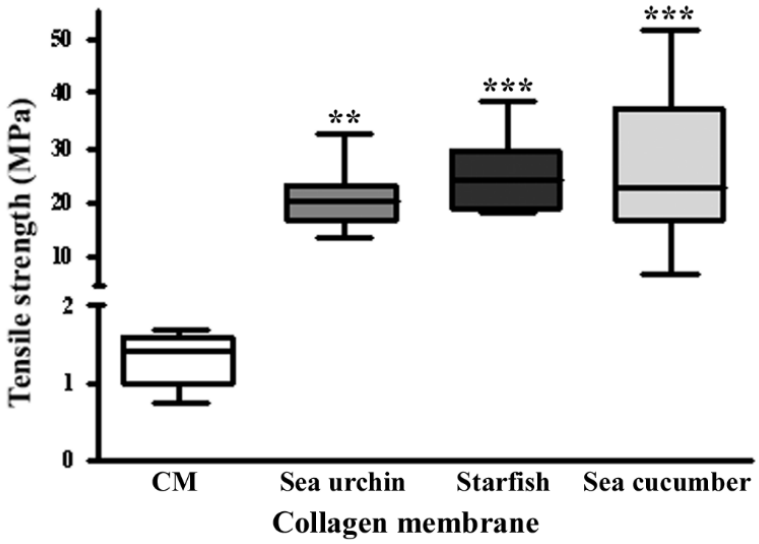

◀ **Fig. 6.** *Box plot of tensile strength of commercial membranes and EDCMs*. CM, commercial membrane (n = 7); sea urchin-derived collagen membrane (n = 19); starfish-derived collagen membrane (n = 21); sea cucumber-derived collagen membrane (n = 47). ** P<0.01, *** P<0.001 *vs* commercial membrane (Dunn's Multiple Comparison Test).

### *3.4. Cell counting*

The Generalised Linear Model (GLM) was used to evaluate the effect of substrate type, experimental round and their interaction on the number of seeded cells. Cell growth was significantly affected by both factors (P<0.001) but not by their interaction (P=0.079). This means that, during the same experimental round, changing the substrate, cells grew differently, and that, with the same substrate, cell grew differently in different experimental rounds depending on the specific condition of each experimental round. However, the statistical evaluation of the interaction between substrate type and experimental round indicates the substrate performance (from the most favourable to the least one in relation to the cell growth) did not significantly change in the different experimental rounds. Data on cell counting are reported in Fig. 7 and Table A (Appendices). Cell number on sea urchin-derived collagen was significantly higher than that on the other echinoderm-derived substrates (starfish P<0.001 and sea cucumber P<0.022) but was comparable to the control (plastic, 100%) and was also statistically similar to soluble bovine-skin collagen substrate (P>0.05); however, hSDFs were less numerous than on BCMs, even if only in one round. Cell percentage on starfish and sea cucumber-derived membranes was comparable (P>0.05) but significantly lower than all the other substrate types (P<0.05).

Moreover, hSDFs were seeded once also on aligned type I collagen fibrils (AlignCol®Matrix, Sigma-Aldrich) and the percentage of cells (normalised against the plastic) resulted comparable (81.63%±8.13) to that of cells seeded on EDCMs.

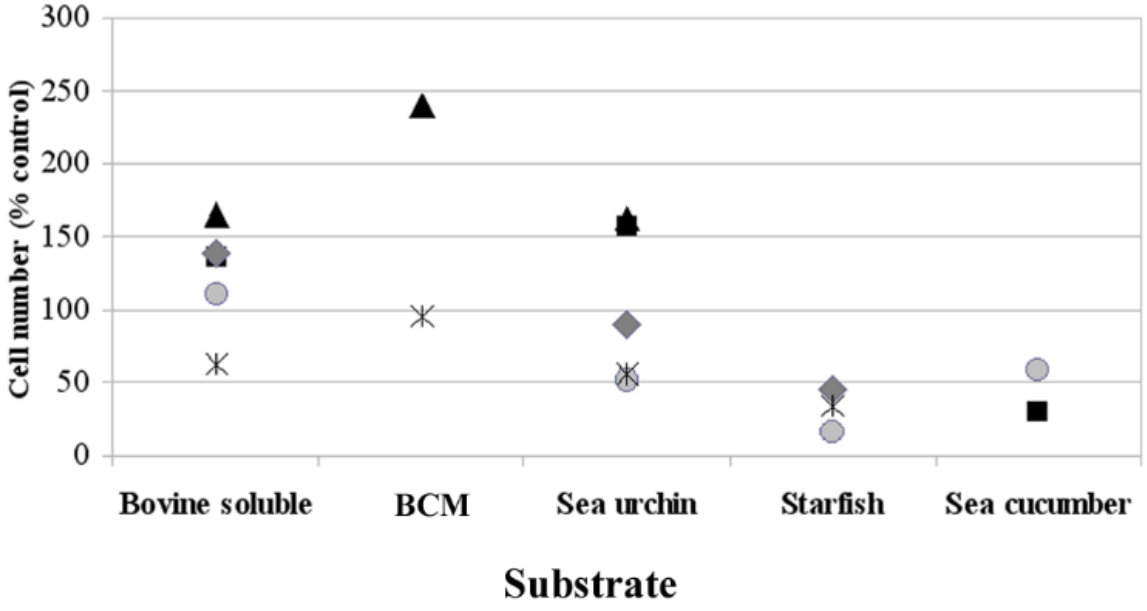


**Fig. 7.** *Cell counting after 4 days of culture of human skin-derived fibroblasts seeded on bovine skin-derived soluble collagen, reassembled (fibrillar) bovine collagen membranes (BCMs) and EDCMs normalised against the plastic control (100%)*. Data shown as mean values of 2-4 replicates (see Table A in Appendices for mean values ± SD for each round). Black square: first round; grey diamond: second round; grey circle: third round; black triangle: fourth round; asterisk: fifth round.

### *3.5. Cell morphology and cell-substrate adhesion/interactions*

Overall, hSDFs seeded on fibrillar substrates, namely EDCMs and reassembled bovine collagen membranes (BCMs; Fig. 8C) presented a more elongated shape in comparison to those on "flat" substrates, as plastic and soluble bovine collagen, where they showed a highly flattened "sun-like" morphology (Fig. 8). Considering cell-substrate interactions (Fig. 9), fibroblasts seeded on both EDCMs and BCMs similarly displayed a low number of short filopodial processes, which strongly localised only at the main cell attachment points (usually two), whereas cells on "flat" substrates (plastic and soluble bovine collagen) showed a higher number of numerous, long and thin filopodial processes, widespread on the whole cell surface. Immunofluorescence microscopy (IF) confirmed the different cell morphology already observed by SEM analyses and enabled visualisation of cytoskeletal organisation (phalloidin), particularly stress fibres, contractile actin bundles fundamental for cell adhesion. Fibroblasts seeded on fibrillar substrates (namely EDCMs and BCMs) showed less stress fibres and less numerous focal adhesion plaques (vinculin) comparing to those on "flat" substrates. Fig. 10 shows two representative examples (plastic and sea cucumber-derived membrane) of the aforementioned differences.

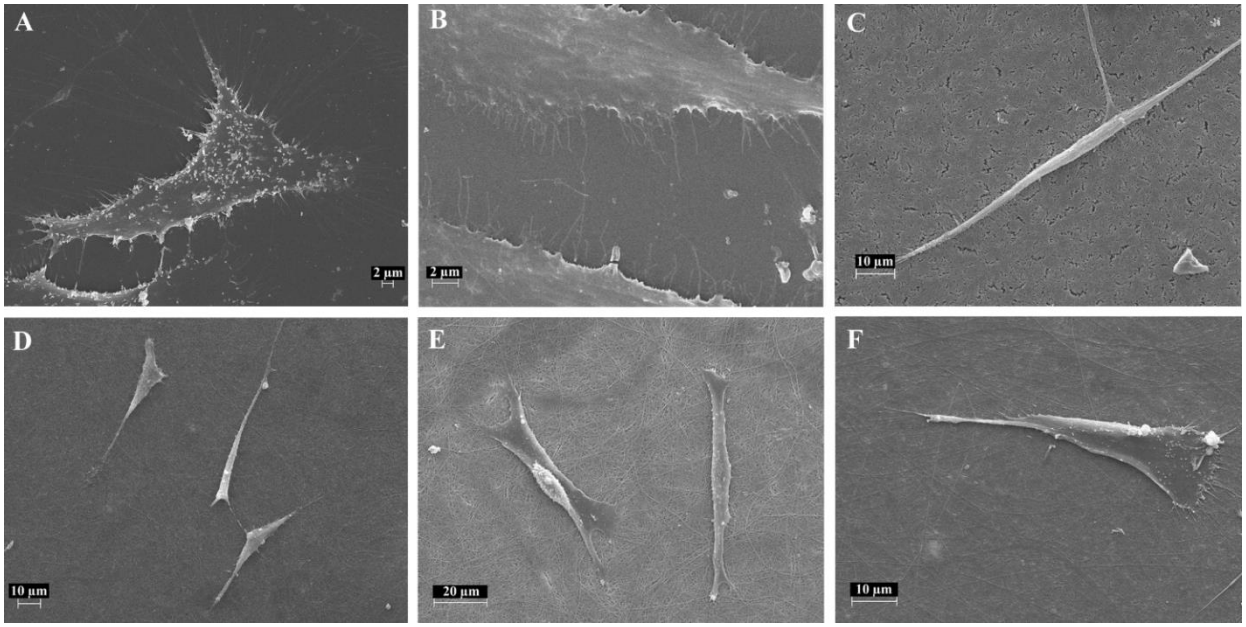


**Fig. 8.** SEM. *Morphology and shape of hSDFs seeded on different collagen membranes and on plastic*. hSDFs seeded on fibrillar collagen membranes present a more elongated shape than those seeded on "flat" substrates. A) Plastic (control). B) Bovine skin-derived soluble collagen. C) Reassembled (fibrillar) bovine collagen membrane (BCM). D) Sea urchin-derived collagen membrane. E) Starfish-derived collagen membrane. F) Sea cucumber-derived collagen membrane.

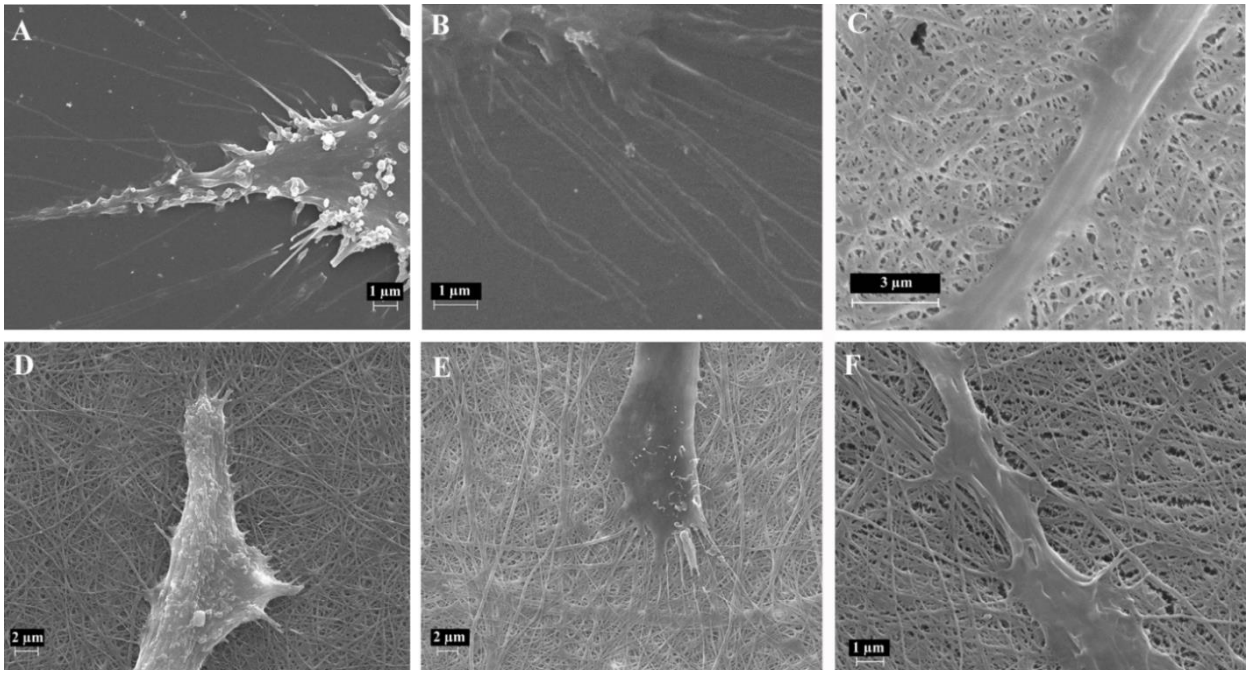


**Fig. 9.** SEM. *Details on the filopodial processes of hSDFs seeded on different collagen membranes and on plastic*. hSDFs seeded on fibrillar collagens present less numerous and shorter filopodial processes than those seeded on "flat" substrates. A) Plastic (control). B) Bovine skin-derived soluble collagen. C) Reassembled (fibrillar) bovine collagen membrane (BCM). D) Sea urchin-derived collagen membrane. E) Starfish-derived collagen membrane. F) Sea cucumber-derived collagen membrane.

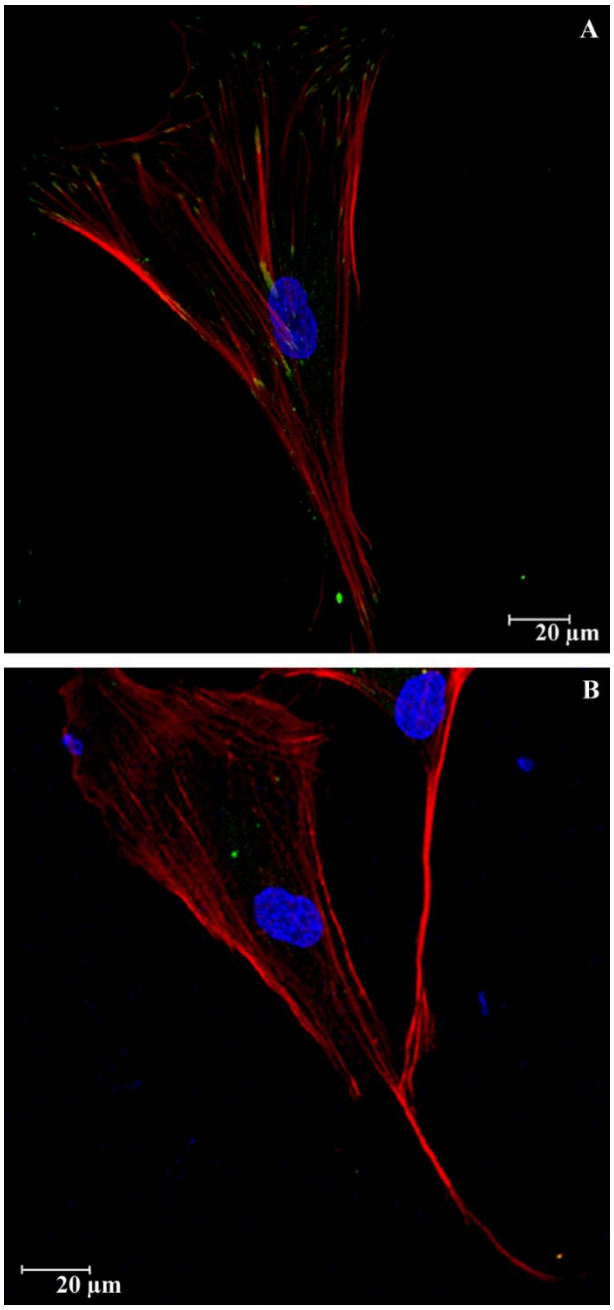


**Fig. 10.** IF. *Representative images of the morphology, cytoskeletal (F-actin) organisation and focal adhesion plaque pattern of hSDFs seeded on "flat" substrate (A) and fibrillar substrate (B)*. Cell nuclei are labelled in blue (DAPI), stress fibres in red (phalloidin) and focal adhesion plaques in green (vinculin). hSDFs seeded on fibrillar substrate present less numerous stress fibres and less visible focal adhesion plaques in comparison to those seeded on "flat" substrate.

### *4. Discussion*

Marine collagen is one of the most promising biomaterials for a wide range of different applications (Silva *et al.*, 2014; Silvipriya *et al.*, 2015). New biotechnology with a low environmental impact are nowadays widely encouraged since the large public attention and sensibility to both human health and eco-sustainable nature exploitation have highly

increased in the last few decades. Many marine animals are currently investigated and used to extract collagen (Nagai and Suzuki, 2000; Nagai *et al.*, 2000; Uriarte-Montoya *et al.*, 2010; Addad *et al.*, 2011; Pang *et al.*, 2013). Echinoderms especially can be valid "blue" and alternative sources of collagen to the currently used mammalian ones. Indeed, as previously described by Di Benedetto and co-workers (2014), fibrillar collagen can be easily extracted from echinoderm MCTs and the high plasticity of their collagen fibril cohesive forces/cross-linking (Wilkie, 2005) is probably one of the reasons for the relative ease with which collagen fibrils can be isolated.

In the present work we optimised different extraction protocols to efficiently obtain clean, relatively pure and highly concentrated native collagen fibril suspensions from three echinoderm MCTs/ species, which differ in the overall collagen fibril and fibre organisation and in the skeletal element presence (Fig. 1). Starfish aboral arm wall and partly sea urchin peristomial membrane show highly packed fibrils/fibres and conspicuous calcareous ossicles, whereas sea cucumber body wall displays loosely packed and homogeneously widespread fibrils as well as small calcareous spicules. This can partially explain why fibril extraction is easily obtained by mild non-denaturing methods (such as PBS) for sea cucumber, whereas stronger treatments (disulphide bonds disruption) are necessary for both sea urchin and starfish. Despite these differences, the fibrillar conformation and integrity were maintained throughout the extraction protocols, an important feature for the subsequent employment in scaffolding. Indeed, it is well documented that the reassembling of mammalian solubilised collagen (by simple pH/temperature variation or electrospinning) produces fibrillar structures which are only partially similar to the native conformation in terms of both mechanical and structural properties (Zeugolis *et al.*, 2008; Chung *et al.*, 2010). Also collagens from other marine sources, e.g. fish, jellyfish and sponges, are currently extracted in their acid-soluble form, thus losing their native conformation (Nagai and Suzuki, 2000; Addad *et al.*, 2011; Barros *et al.*, 2014).

Fibril mean diameter and D-period were similar among the three types of echinoderm sources and comparable also to those reported for other MCTs (Barbaglio *et al.*, 2015), other marine animals (Heinemann *et al.*, 2007) and mammalian type I collagen (Gelse *et al.*, 2003; Wilkie, 2005; Fang and Holl, 2013). Glycosaminoglycan (GAG) presence along the fibril surface is fundamental to maintain fibril integrity (Tricarico *et al.*, 2012). Moreover, GAGs are important for cell migration, adhesion, proliferation and differentiation (Pieper *et al.*, 2000) both *in vitro* (e.g. cell culture) and *in vivo* (e.g.

morphogenesis and wound healing) and are often added to mammalian collagen scaffolds to improve their performances in tissue engineering applications (Haugh *et al.*, 2011). Therefore, obtaining a native fibrillar collagen already provided with GAG decoration is one of the advantages of EDCMs.

The average superficial porosity of EDCMs was much smaller than the size of human cells. Therefore, they are likely to be efficient as cell barrier for biomedical applications where a proper division between two anatomical compartments is requested, such as Guided Tissue Regeneration (GTR). In GTR these barriers help the healing process avoiding mixture of adjacent regenerating tissues and are useful to prevent post-surgical tissue adhesions (Tsai *et al.*, 2005). These latter are widespread and serious medical problems, not only for the patient health (Diamond and Freeman, 2001) but also from an economic point of view (Wilson *et al.*, 2002). Commercial bovine collagen membranes are currently used for this kind of purposes (Fig. 4). However, their porosity is much higher and their network is less homogeneous than those of EDCMs (Table 1; Fig. 2), thus suggesting these latter are likely to display a more efficient barrier-effect. EDCM limited thickness, combined with high mechanical resistance, can be further advantages since this biomaterial simultaneously provides handleability during surgery, reduced steric hindrance in the wound and post-surgery resistance to avoid dehiscence occurrence: the higher the tensile strength and the resistance to uni-axial tension (Young's Modulus) the better the biomaterial can support stresses before rupture. The mechanical resistance of commercial membranes (Fig. 5 and 6), which display a much higher thickness, or reported for bovine-derived collagen membranes cross-linked with EDC/NHS (~30 MPa; Grover *et al.*, 2012) is much lower compared to EDCMs, thus suggesting the potential utility of echinoderm collagens, especially in mechanically demanding tissue engineering applications. Lower values of EDCM tensile strain (relative elongation) than those recorded for commercial membranes further support the previous statement. Moreover, the possibility to produce much thinner membranes is an obvious advantage also from a practical point of view since a lower amount of fresh material is necessary. Having highlighted the advantages of EDCMs, is there a favoured echinoderm/MCT collagen source for the proposed application? Despite the comparable ultrastructural characteristics and mechanical performances (with sea cucumber membranes displaying slightly higher values), the three different EDCMs showed partially different results in the *in vitro* tests with human skin-derived fibroblasts. We previously demonstrated that sea urchin-derived membranes are not toxic for mammalian cells: horse mesenchymal stem

cells seeded on these substrates were viable and even able to actively proliferate in long-term period (21 days), although they showed an initial transitory “drop” (day 4) and a slight delay compared to controls (Di Benedetto *et al.*, 2014).

In this work we used human adult fibroblasts because this cytotype is the most suitable in view of GTR applications and because it was largely used to test also different marine-derived collagen substrates, such as from jellyfish (Song *et al.*, 2006; Addad *et al.*, 2011). Cells seeded on EDCMs and BCMs (both regarded as fibrillar substrates) were similar in terms of morphology, cytoskeletal organisation and substrate adhesion pattern, thus suggesting the absence of any anomalous cell behaviour due to the echinoderm-derived collagen. Interestingly, they presented a more elongated shape, less and shorter filopodial processes in comparison with those seeded on “flat” substrates (bovine skin-derived soluble collagen and plastic), possibly indicating a reduced substrate adhesion, a feature that can be advantageous in “cell barrier” for GTR applications. Nevertheless, cell numbers recorded after 4 days were different on the three EDCMs: sea urchin membranes displayed similar values to bovine collagen substrates and to plastic control, whereas both starfish and sea cucumber membranes showed a lower number. Whether this is only a transient and temporary cell behaviour, as we previously observed for sea urchin membranes (Di Benedetto *et al.*, 2014) or it is a toxic effect must be investigated by further long-term analyses. In general, our findings underline also that the standard controls usually employed for this kind of *in vitro* tests (soluble collagen and plastic) are not truly reliable to test biocompatibility of fibrillar substrates, as they display a different structure/geometry (“flat” *vs* fibrillar), a parameter strongly influencing cell behaviour and response (Murphy *et al.*, 2012). From a socio-economical perspective, sea urchins, and partially starfish, might display a major advantage if compared to sea cucumbers. In the former, collagen can be reliably obtained as food industry by-product without affecting natural populations. In starfish, high amount of eco-friendly collagen could be obtained from those ecologically “dangerous” species regularly subjected to massive control campaigns (e.g. the coral feeder crown-of-thorn *Acanthaster planci*; Fraser *et al.*, 2000; Mendonça *et al.*, 2010; Baird *et al.*, 2013). Sea cucumbers, from both fishery and aquaculture (Toral-Granda *et al.*, 2008; Purcell *et al.*, 2013; Yokoyama, 2013), have the undoubted advantage of the amount of collagen obtainable from a single animal but are over exploited as source of food, especially in the Asian cuisine and, therefore, they could not be conveniently used as by-product. Thus, in terms of ecosustainability sea urchins and starfish should be preferred to sea cucumbers. However, considering a possible

industrial scale-up, at present sea urchin employment seems more promising and feasible. The increased market demand and the simultaneous decline of sea urchin wild populations all over the world are making aquaculture a fundamental alternative to sea urchin fishery (Carboni *et al.*, 2012; Parisi *et al.*, 2012). The possibility to valorise sea urchin by-product is likely to further promote the development of this mariculture sector. Moreover, sea urchin farming in (environmentally sustainable) integrated multi-trophic aquacultures (IMTA) will also ensure social acceptance and additional economic advantages (Schuenhoff *et al.*, 2003; Barrington *et al.*, 2009).

## *5. Conclusions*

Echinoderm MCTs can be considered eco-sustainable sources of fibrillar collagen for biomedical applications. The possibility to rapidly produce valuable collagen membranes suitable for specific clinical purposes makes these marine invertebrates highly interesting in terms of both research and applied studies. We propose this “blue” biomaterial derived from marine invertebrates, especially from sea urchins, as a promising alternative to the nowadays mammalian-derived collagen biomaterials. Further *in vitro* and *in vivo* studies are necessary to more deeply evaluate EDCM exploitability, including permeability, biodegradability and immunogenicity, all of these being key features to validate new biomaterials for human clinical applications (Chung *et al.*, 1990).

## *6. Appendices*

**Table A.** *Mean cell number (from two to four wells/replicates) ± SD on the different substrates normalised against the corresponding plastic control well mean values for each of the five rounds and estimated marginal mean ± SE of cells on each type of substrate for the corresponding rounds (normalised as just described).* Not all the different substrates were present in each round due to starting material availability.

| | Bovine skin-derived soluble collagen substrate | Reassembled (fibrillar) bovine collagen membrane (BCM) | Sea urchin-derived collagen membrane | Starfish-derived collagen membrane | Sea cucumber-derived collagen membrane |
|---|---|---|---|---|---|
| **Round 1** | 136.19 ± 18.58 | - | 156.17 ± 16.50 | - | 29.73 ± 2.16 |
| **Round 2** | 139.73 ± 18.62 | - | 90.60 ± 7.67 | 45.66 ± 9.75 | - |
| **Round 3** | 109.97 ± 10.71 | - | 51.41 ± 6.33 | 16.61 ± 4.70 | 58.17 ± 15.93 |
| **Round 4** | 165.21 ± 85.48 | 240.17 ± 148.25 | 161.97 ± 13.31 | - | - |
| **Round 5** | 62.51 ± 9.18 | 96.07 ± 18.13 | 55.29 ± 3.94 | 34.60 ± 5.82 | - |
| **Estimated Marginal Mean ± SE** | 122.73 ± 10.33 | 168.12 ± 14.91 | 103.09 ± 8.44 | 32.29 ± 13.55 | 43.95 ± 17.83 |

## *7. Supplementary Materials*

### *7.1. Extended Materials and Methods*

#### *7.1.1. Animal collection and maintenance*

Adult specimens of *E. sepositus* (diameter ~ 10-20 cm), *P. lividus* (variable size) and *H. tubulosa* (variable size) were collected by scuba divers at depth of 5-8 meters in the Marine Protected Area of Portofino (Paraggi, GE, Italy). They were immediately transported to our laboratory at the University of Milan. Sea urchins were immediately dissected and the oral halves were stored at -20°C until use for collagen extraction, whereas starfish and sea cucumbers were put in aerated 50 L glass tanks with a closed system of artificial sea water (ASW; 37‰ salinity) prepared mixing a commercial aquarium salt (Instant Ocean®) with partially deionised water at 17°C. In order to guarantee optimal stabling conditions, specimens were exposed to 8 hours/day of light, salinity and temperature were checked daily, whereas nitrites and nitrates concentrations, pH, and other ASW parameters were measured weekly. Animals were left to acclimatise few weeks before dissecting them for collagen. Starfish and sea cucumbers used for collagen extraction were dissected and the aboral body walls and the whole body walls respectively were stored at -20°C until use. Starfish and sea cucumbers were fed once a week with pieces of cuttlefish and pellets respectively.

# 4) GENERAL CONCLUSIONS AND PERSPECTIVES

Echinoderms have always caught the interest of scientists in particular for their striking regenerative abilities and their peculiar dynamic connective tissues, two of their most amazing physiological adaptations. Although studies have been performed on both topics still a lot needs to be clarified. Can studies on echinoderm regeneration shed light on the regenerative process events and reveal the “secrets” of an effective regeneration? Can biomaterials derived from echinoderm connective tissues be useful for regenerative medicine applications? In this research we aimed to contribute answering these questions and showed that echinoderms can be valid models to study biological processes, such as regeneration, as well as explore the potential of marine resources/materials for different human applications.

### *4.1. Echinoderm regeneration*

The starfish *Echinaster sepositus* and the brittle star *Amphiura filiformis* were used to investigate and describe arm regeneration after traumatic amputation from both tissue/cellular and molecular perspectives. After having defined the main histological events occurring during arm regeneration, we focused our attention on two fundamental aspects: the role of the connective tissue (particularly collagen) and the involvement of immune system during the first repair phase.

Our findings showed that starfish regenerative process can be subdivided in three main phases similarly to that of brittle star (Biressi *et al.*, 2010): a) the repair phase, characterised by quick emergency reaction and wound healing (re-epithelialisation); b) the early regenerative phase, characterised by the first signs of differentiation; and c) the advanced regenerative phase, during which the proper morphogenesis occurs. Regeneration in starfish follows the distalisation-intercalation model (Agata *et al.*, 2003, 2007) described also for brittle star arm regeneration (Czarkwiani *et al.*, 2016) but, comparing to this latter, it is accomplished in a longer period (Dupont and Thorndyke, 2006). In both cases the regenerative process leads to the formation of completely differentiated and functional new arms, event that is not clearly occurring in adult mammals after amputation of whole body parts.

As far as the connective tissue is concerned, we showed that during regeneration fibrillar collagen deposition and organisation occur earlier in brittle star in comparison to starfish and in both echinoderm models the fibrillar extracellular matrix (ECM) deposition is

delayed in comparison to mammals and no over-deposition of collagen (fibrosis) is detectable, these aspects being fundamental to allow the subsequent effective tissue re-growth. We identified a total of 10 new ECM-related genes and we performed for the first time *in situ* hybridisation on *E. sepositus* regenerating samples. Molecular results suggested that different tissues are involved in ECM deposition/remodelling in diverse regenerative phases and the regenerating epidermis plays a key role in collagen biosynthesis in both experimental models.

The post-traumatic immune response was initially investigated by evaluating the presence and distribution of a TNF-α-like molecule, which is one of the key player of the repair phase in mammals. We showed that this molecule is present in brittle star and its distribution is comparable to that of mammal wound healing. Moreover, we identified 2 new genes (fibrinogen-like in starfish and ficolin in brittle star) that seem involved in echinoderm immediate reaction to injury.

Overall, our findings showed that quick emergency reaction and re-epithelialisation, delayed ECM fibrillar organisation and absence of fibrosis are some of the “secrets” of effective repair of severe damages and subsequent regeneration in comparison to animals that are less or not at all capable of regenerating whole body parts after injury. Moreover, we showed that echinoderms can be used as valid models to investigate and compare immune system involvement during the repair phase.

Taking into account that the gene regulation of arm regeneration in starfish is still an almost unexplored field, the next steps will be to obtain high-throughput molecular screening (transcriptomes) of regenerating tissues at different stages. This will provide new tools to investigate in detail echinoderm regeneration and will give further insights into the evolution of the molecular mechanisms underlining this fascinating phenomenon both within the echinoderm phylum and along the deuterostomian lineage.

### *4.2. Echinoderm biotechnological potential*

The dynamic connective tissues of echinoderms are well known for their importance in many life aspects. Together with their biological importance, they can also be regarded as potential source of material, mainly fibrillar collagen, for regenerative medicine applications, such as Guided Tissue Regeneration (GTR). Indeed, marine-derived materials are nowadays highly demanded as alternative products to mammalian-derived materials, even more considering they can be obtained from eco-friendly sources, e.g. food industry wastes.

Using as representatives of the echinoderm classes the starfish *Echinaster sepositus*, the sea urchin *Paracentrotus lividus* and the sea cucumber *Holothuria tubulosa*, we showed that, after extraction protocol optimisation, we obtained homogeneous fibrillar collagen suspensions that were used to produce thinner, more compact and more resistant two-dimensional membranes (EDCMs) than mammal-derived commercial ones, all advantages for GTR applications. *In vitro* tests with human skin-derived fibroblasts suggested among the different echinoderm sources sea urchin-derived collagen membranes as the most promising ones.

The characterisation of EDCM biocompatibility and biodegradability *in vivo* will be necessary to evaluate their future use for human medical applications. Moreover, three-dimensional echinoderm-derived collagen scaffolds can be produced allowing us to expand the regenerative medicine applications for which marine collagen could be used as alternative to mammal-derived collagen, e.g. for skin substitutes or dermis regeneration. This could be done also taking into account information from *in vivo* studies on regenerating echinoderms. Indeed, for instance, re-epithelialisation described after injury in echinoderms could inspire the development of biomaterials of marine origin useful for quick and effective (e.g. against pathogens) skin reconstruction in humans. Finally, the improvement of starting material supply could be achieved establishing active collaborations with fishermen, food industries, farmers and institutions in order to start a promising pipeline “from the seas to the operating room” for the future production of a new eco-friendly marine-derived biomaterial.

### *4.3. A summary of the main outcomes of this research*

Overall, we showed that **echinoderms are valid models for both basic and applied research studies**. Indeed, they can be used to shed light on effective regeneration and uncover its “secrets” from both cellular/tissue and molecular perspectives. Comparisons of processes and mechanisms between animals that can so efficiently regenerate and those with limited regenerative abilities will help understanding key similarities and differences that in the future hopefully may be useful for regenerative medicine and to solve human medical problems, e.g. severe wounds or amputations. Moreover, we showed that echinoderm connective tissues are valuable and promising eco-friendly sources of fibrillar collagen that can be employed to produce marine-derived biomaterials (*i.e.* collagen membranes) for human biotechnological applications such as regenerative medicine, GTR or tissue engineering.

# 5) REFERENCES


Abrams EW and Andrew DJ (2002). Prolyl 4-hydroxylase alpha-related proteins in *Drosophila melanogaster*: tissue-specific embryonic expression of the 99F8-9 cluster. Mech Dev 112:165-171.

Addad S, Exposito JY, Faye C, Ricard-Blum S, Lethias C (2011). Isolation, Characterization and Biological Evaluation of Jellyfish Collagen for Use in Biomedical Applications. Mar Drugs 9:967-983. doi: 10.3390/md9060967.

Agata K, Saitoh Y, Nakajima E (2007). Unifying principles of regeneration I: epimorphosis *versus* morphallaxis. Dev Growth Differ 49:73-78.

Agata K, Tanaka T, Kobayash C, Kato K, Saitoh Y (2003). Intercalary Regeneration in Planarians. Developmental Dynamics 226:308-316.

Akimenko MA, Marì-Beffa M, Becerra J, Géraudie J (2003). Old Questions, New Tools, and Some Answers to the Mystery of Fin Regeneration. Developmental Dynamics 226:190-201.

Alberts B, Johnson A, Lewis J, Raff M, Roberts K, Walter P (2002). Molecular biology of the cell. Ath ed. New York: Garland Science 1065-1125.

Alitalo K, Kurkinen M, Vaheri A (1980). Extracellular matrix components synthetized by human amniotic epithelial cells in culture. Cell 19:1053-1062.

Baird AH, Pratchett MS, Hoey AS, Herdiana Y, Campbell SJ (2013). *Acanthaster planci* is a major cause of coral mortality in Indonesia. Coral Reefs 32:803-812. doi: 10.1007/s00338-013-1025-1.

Balser EJ (1998). Cloning by Ophiuroid Echinoderm Larvae. Biol Bull 194:187-193.

Bannister R, McGonnell IM, Graham A, Thorndyke MC, Beesley PW (2005). *Afuni*, a novel transforming growth factor-β gene is involved in arm regeneration by the brittle star *Amphiura filiformis*. Dev Genes Evol 215:393-401. doi: 10.1007/s00427-005-0487-8.

Barbaglio A, Tricarico S, Di Benedetto C, Fassini D, Lima AP, Ribeiro AR, Ribeiro CC, Sugni M, Bonasoro F, Wilkie IC, Barbosa M, Candia Carnevali MD (2013). The smart connective tissue of echinoderms: a materializing promise for biotech applications. Cahiers de Biologie marine 54:713-720.

Barbaglio A, Tricarico S, Ribeiro A, Di Benedetto C, Barbato M, Dessì D, Fugnanesi V, Magni S, Mosca F, Sugni M, Bonasoro F, Wilkie IC, Barbosa M, Candia Carnevali MD, (2015). Ultrastructural and biochemical characterization of mechanically adaptable collagenous structures in the edible sea urchin *Paracentrotus lividus*. Zoology 118:147-160. doi: 10.1016/j.zool.2014.10.003.

Barbaglio A, Tricarico S, Ribeiro A, Ribeiro C, Sugni M, Di Benedetto C, Wilkie IC, Barbosa M, Bonasoro F, Candia Carnevali MD (2012). The mechanically adaptive connective tissue of echinoderms: its potential for bio-innovation in applied technology

and ecology. Marine environmental research (Special Issue Marine Organisms) 76:108-113. doi: 10.1016/j.marenvres.2011.07.006.

Barnes RSK, Calow P, Olive PJW (1990). Invertebrati una nuova sintesi. Zanichelli Editore, Bologna, pp.173-184.

Barrington K, Chopin T, Robinson S (2009). Integrated multi-trophic aquaculture (IMTA) in marine temperate waters. In D. Soto (ed.). Integrated mariculture: a global review. FAO Fisheries and Aquaculture Technical Paper. Rome, FAO 529:7-46.

Barrios JV, Gaymer CF, Vasquez JA, Brokordt KB (2008). Effect of the degree of autotomy on feeding, growth, and reproductive capacity in the multi-armed sea star *Heliaster helianthus*. J Exp Mar Biol Ecol 361:21-27.

Barros AA, Aroso IM, Silva TH, Mano JF, Duarte ARC, Reis RL (2014). Water and Carbon Dioxide: Green Solvents for the Extraction of Collagen/Gelatin from Marine Sponges. ACS Sustainable Chem Eng 3:254-260. doi: 10.1021/sc500621z.

Barros CS, Franco SJ, Müller U (2011). Extracellular matrix: functions in the nervous system. Cold Spring Harb Perspect Biol 3:a005108.

Bateman PW and Fleming PA (2009). To cut a long tail short: a review of lizard caudal autotomy studies carried out over the last 20 years. Journal of Zoology 277:1-14.

Baumiller TK and Ausich WI (1996). Crinoid stalk flexibility: theoretical predictions and fossil stalk postures. Lethaia. 29:47-59. Oslo. ISSN 0024-1164.

Bely AE and Nyberg KG (2009). Evolution of animal regeneration: re-emergence of a field. Trends in Ecology and Evolution 25(3):161-170.

Ben Khadra Y, Ferrario C, Di Benedetto C, Said K, Bonasoro F, Candia Carnevali MD, Sugni M (2015a). Wound repair during arm regeneration in the red starfish *Echinaster sepositus*. Wound Repair and Regeneration 23:611-622. doi: 10.1111/wrr.12333.

Ben Khadra Y, Ferrario C, Di Benedetto C, Said K, Bonasoro F, Candia Carnevali MD, Sugni M (2015b). Re-growth, morphogenesis, and differentiation during starfish arm regeneration. Wound Repair and Regeneration 23:623-634. doi: 10.1111/wrr.12336.

Ben Khadra Y, Said K, Thorndyke M, Martinez P (2014). Homeobox Genes Expressed During Echinoderm Arm Regeneration. Biochem Genet 52:166-180.

Ben Khadra Y, Sugni M, Ferrario C, Bonasoro F, Varela Coelho A, Martinez P, Candia Carnevali MD. An integrated view of asteroid regeneration: tissues, cells and molecules. *In press* in Cell and Tissue Research. doi: 10.1007/s00441-017-2589-9.

Biressi A, Ting Z, Dupont S, Dahlberg C, Di Benedetto C, Bonasoro F, Thorndyke M, Candia Carnevali MD (2010). Wound-healing and arm regeneration in *Ophioderma longicaudum* and *Amphiura filiformis* (Ophiuroidea, Echinodermata): comparative morphogenesis and histogenesis. Zoomorphology 129:1-19.

Blankenship J and Benson S (1984). Collagen metabolism and spicule formation in sea urchin micromeres. Exp Cell Res 152:98-104.

Bock O and Mrowietz U (2002). Keloids. A fibroproliferative disorder of unknown etiology. Hautarzt 53:515.

Bonasoro F, Candia Carnevali MD, Moss C, Thorndyke MC (1998). Epimorphic *versus* morphallactic mechanisms in arm regeneration of crinoids and asteroids: pattern of cell proliferation differentiation and cell lineage. In Echinoderms: San Francisco (Mooi and Telford, eds.). Balkema, Rotterdam, The Netherland 13-18.

Bonasoro F, Candia Carnevali MD, Wilkie IC (1995). The peristomial membrane of regular sea-urchins: Functional morphology of the epidermis and coelomic lining in *Paracentrotus lividus* (Lamarck). Bollettino di Zoologia 62(2):121-135.

Bosch TCG (2007). Why polyps regenerate and we don't: Towards a cellular and molecular framework for *Hydra* regeneration. Developmental Biology 303:421-433.

Bradley JR (2008). TNF-mediated inflammatory disease. J Pathol 214:149-160.

Brockes JP and Kumar A (2002). Plasticity and reprogramming of differentiated cells in amphibian regeneration. Molecular Cell Biology 3:566-574.

Brockes JP and Kumar A (2008). Comparative aspects of animal regeneration. Annu Rev Cell Biol 24:525-549.

Brockes JP, Kumar A, Velloso CP (2001). Regeneration as an evolutionary variable. J Anat 199:3-11.

Buck II DV, Alam M, Kim JYS (2009). Injectable fillers for facial rejuvenation: a review. Journal of Plastic, Reconstructive and Aesthetic Surgery. 62:11-18. doi: 10.1016/j.bjps.2008.06.036.

Burnett WJ and McKenzie JD (1997). Subcuticular Bacteria from the Brittle Star *Ophiactis balli* (Echinodermata: Ophiuroidea) Represent a New Lineage of Extracellular Marine Symbionts in the α Subdivision of the Class *Proteobacteria*. Applied and Environmental Microbiology 63(5):1721-1724.

Burns G, Ortega-Martinez O, Dupont S, Thorndyke MC, Peck LS, Clark MS (2012). Intrinsic gene expression during regeneration in arm explants of *Amphiura filiformis.* Journal of Experimental Marine Biology and Ecology 413:106-112.

Burns G, Ortega-Martinez O, Thorndyke MC, Peck LS, Dupont S, Clark MS (2011). Dynamic gene expression profiles during arm regeneration in the brittle star *Amphiura filiformis.* Journal of Experimental Marine Biology and Ecology 407:315-322.

Byrne M (1994). Ophiuroidea. In: Microscopic Anatomy if Invertebrates. Volume 14: Echinodermata 247-343. Wiley-Liss, Inc.

Cabrera-Serrano A and García-Arrarás JE (2004). RGD-containing peptides inhibit regeneration in the sea cucumber *Holothuria glaberrima*. Dev Dyn 31:171-178.

Cameron RA, Samanta M, Yuan A, He D, Davidson E (2009). SpBase: the sea urchin database and web site. Nucleic Acids Research D750-754.

Campochiaro PA, Jerdan JA, Glaser BM (1986). The extracellular matrix of human retinal pigment epithelial cells *in vivo* and its synthesis *in vitro*. Invest Ophthalmol Vis Sci 27:1615-1621.

Candia Carnevali MD (2006). Regeneration in echinoderms: repair, regrowth, cloning. ISJ 3:64-76.

Candia Carnevali MD and Bonasoro F (2001a). Introduction to the Biology of Regeneration in Echinoderms. Microsc Res Tech 55:365-368.

Candia Carnevali MD and Bonasoro F (2001b). A microscopic overview of crinoid regeneration. Microsc Res Techniq 55:403-426.

Candia Carnevali MD and Burighel P (2010). Regeneration in Echinoderms and Ascidians. ELS. John Wiley and Sons Ltd, Chichester 2010.

Candia Carnevali MD, Bonasoro F, Lucca E, Thorndyke MC (1995). Pattern of cell proliferation in the early stages of arm regeneration in the feather star *Antedon mediterranea*. J Exp Zool 272:464-474.

Candia Carnevali MD, Bonasoro F, Trezzi M, Giardina A (1998). Nerve dependent myogenesis in arm regeneration of *Antedon mediterranea*. Echinoderm research (1998), (Candia Carnevali and Bonasoro eds.) Balkema Rotterdam 139-143.

Candia Carnevali MD, Bonasoro F, Welsch U, Thorndyke MC (1998). Arm regeneration and growth factors in crinoids. In: Mooi R, Telford M, editors. Echinoderms. San Francisco Rotterdam Balkema 145-150.

Candia Carnevali MD, Lucca E, Bonasoro F (1993). Mechanisms of arm regeneration in the feather star *Antedon mediterranea*: healing of wound and early stages of development. The Journal of Experimental Zoology 267:299-317.

Candia Carnevali MD, Thorndyke MC, Matranga V (2009). Regenerating echinoderms; a promise to understand stem cells potential. In: Rinkevich B, Matranga V, editors. Stem cells in marine organisms. Heidelberg: Springer 165-186.

Carboni S, Addis P, Cau A, Atack T (2012). Aquaculture Could Enhance Mediterranean Sea Urchin Fishery, Expand Supply. Global aquaculture advocate, Issue May/June 44-45.

Castellucci V, Pinsker H, Kupfermann I, Kandel ER (1970). Neuronal Mechanisms of Habituation and Dishabituation of the Gill-Withdrawal Reflex in *Aplysia*. Science 167(3926):1745-1748.

Chen CP and Lawrence JM (1986). The Ultrastructure of the Plumula of the Tooth of *Lytechinus variegatus* (Echinodermata: Echinoidea). Acta Zoologica 67:33-41.

Chia F-S and Koss R (1994). Echinodermata. In: Harrison FW, Chia FS, editors. Microscopic Anatomy of Invertebrates. Wiley-Liss, 169-245.

Chia F-S and Xing J (1996). Echinoderm coelomocytes. Zoological Studies 35(4):231-254.

Chung KH, Bhadriraju K, Spurlin TA, Cook RF, Plant AL (2010). Nanomechanical properties of thin films of type I collagen fibrils. Langmuir 26:3629-3636. doi: 10.1021/la903073v.

Chung KM, Salkin LM, Stein MD, Freedma AL (1990). Clinical Evaluation of a Biodegradable Collagen Membrane in Guided Tissue Regeneration. Journal of Periodontology 61(12):732-736. doi: 10.1902/jop.1990.61.12.732.

Clark RA (1988). Overview and general considerations of wound repair. In: Clark RAF, Henson PM (eds.) The molecular and cellular biology of wound repair. Plenum, New York, 3-23.

Clark RAF (2001). Fibrin and wound healing. Annals of the New York Academy of Sciences 355-367.

Clark MS and Souster T (2012). Slow arm regeneration in the Antarctic brittle star *Ophiura crassa* (Echinodermata, Ophiuroidea). Aquatic Biol 16:105-113.

Clouse RM, Linchangco Jr GV, Kerr AM, Reid RW, Janies DA (2015). Phylotranscriptomic analysis uncovers a wealth of tissue inhibitor of metalloproteinases variants in echinoderms. R Soc open sci 2:150377.

Coccè V, Vitale A, Colombo S, Bonomi A, Sisto F, Ciusani E, Alessandri G, Parati E, Brambilla P, Brambilla M, La Porta CAM, Pessina A (2016). Human skin-derived fibroblasts used as a “trojan horse” for drug delivery. Clinical and Experimental Dermatology 41(4):417-24. doi: 10.1111/ced.12811.

Conand C (2004). Present status of world sea cucumber resources and utilization: an international overview: 13-23. In: Advances in sea cucumber aquaculture and management. Lovatelli A, Conand C, Purcell S, Uthicke S, Hamel JF and Mercier A (eds). FAO Fisheries Technical Paper. Rome, FAO 463:425.

Czarkwiani A, Dylus DV, Oliveri P (2013). Expression of skeletogenic genes during arm regeneration in the brittle star *Amphiura filiformis*. Gene Expression Patterns 13:464-472.

Czarkwiani A, Ferrario C, Dylus DV, Sugni M, Oliveri P (2016). Skeletal regeneration in the brittle star *Amphiura filiformis*. Frontiers in Zoology 13:18.

Czirok A, Rongish B, Little C (2004). Extracellular matrix dynamics during vertebrate axis formation. Developmental Biology 268(1):111-122.

Dawydoff C (1901). Beiträge zur Kenntnis der Regenerationserscheinungen bei den Ophiuren. Z Wiss Zool 69:202-234.

Delroisse J, Ortega-Martinez O, Dupont S, Mallefet J, Flammang P (2015). *De novo* transcriptome of the European brittle star *Amphiura filiformis* pluteus larvae. Marine Genomics 23:109-121.

Delroisse J, Ullrich-Lüter E, Ortega-Martinez O, Dupont S, Arnone MI, Mallefet J, Flammang P (2014). High opsin diversity in a non-visual infaunal brittle star. BMC Genomics 15:1035.

Dembitsky VM, Gloriozova TA, Poroikov VV (2005). Novel antitumor agents: marine sponge alkaloids, their synthetic analogs and derivatives. Mini Rev Med Chem 5:319-336.

Diamond MP and Freeman ML (2001). Clinical implications of postsurgical adhesions. Hum Reprod Update 7:567-76.

Di Benedetto C, Barbaglio A, Martinello T, Alongi V, Fassini D, Cullorà E, Patruno M, Bonasoro F, Barbosa MA, Candia Carnevali MD, Sugni M (2014). Production, Characterization and Biocompatibility of Marine Collagen Matrices from an Alternative and Sustainable Source: The Sea Urchin *Paracentrotus lividus*. Marine Drugs 12:4912-4933. doi: 10.3390/md12094912.

Diegelmann RF and Evans MC (2004). Wound healing: an overview of acute, fibrotic and delayed healing. Front Bioscience 9:283-289.

Di Lullo G, Sweeney S, Korkko J, Ala-Kokko L, San Antonio J (2001). Mapping the Ligand-binding Sites and Disease-associated Mutations on the Most Abundant Protein in the Human, Type I Collagen. Journal of Biological Chemistry 277(6):4223-4231.

Djagny KB, Wang Z, Xu S (2010). Gelatin: A Valuable Protein for Food and Pharmaceutical Industries: Review. Critical Reviews in Food Science and Nutrition 41(6):481-492. doi: 10.1080/20014091091904.

Dolmatov IY and Ginanova TT (2001). Muscle regeneration in holothurians. Microsc Res Tech 55:452-463.

Dolmatov IY, Eliseikina MG, Bulgakov AA, Ginanova TT, Lamash NE, Korchagin VP (1996). Muscle regeneration in the holothurian *Stichopus japonicus*. Roux's Arch Dev Biol 205:486-493.

Dolmatov IY, Eliseikina MG, Ginanova TT (1995). Muscle repair in the holothurians *Eupentacta fraudatrix* is realized at the expense of transdifferentiation of the coelomic epithelium cells. Biology Bull 22:490-495.

Donia M and Hamann MT (2003). Marine natural products and their potential applications as antiinfective agents. The Lancet 3:338-348.

Drew AF, Liu H, Davidson JM, Daugherty CC, Degen JL (2001). Wound-healing defects in mice lacking fibrinogen. Blood 97(12):3691-3698.

Dubois P and Ameye L (2001). Regeneration of Spines and Pedicellariae in Echinoderms: A Review. Microscopy Research and Technique 55:427-437.

Dubois P and Ghyoot M (1995). Integumentary resorption and collagen synthesis during regression of headless pedicellariae in *Sphaerechinus granularis* (Echinodermata: Echinoidea). Cell Tissue Res 282:297-309.

Dubois P and Jangoux M (1990). Stereom morphogenesis and differentiation during regeneration of fractured adambulacral spines of *Asterias rubens* (Echinodermata, Asteroidea). Zoomorphology 109:263-272.

Ducati CC, Candia Carnevali MD, Barker MF (2004). Regenerative potential and fissiparity in the starfish *Coscinasterias muricata*. In: Heinzeller T, Nebelsick JH, editors. Echinoderms. Proceedings of the 11th International Echinoderm Conference, 2003 Oct 6-10; München: Taylor & Francis Group, London 113-118.

Dupont S and Thorndyke MC (2006). Growth or differentiation? Adaptive regeneration in the brittle star *Amphiura filiformis*. J Exp Biol 209(19):3873-3881.

Dylus DV, Blowes LM, Elphick MR, Oliveri P. Developmental transcriptome of the brittle star *Amphiura filiformis* provides insights on evolution of skeleton and GRN re-wiring in echinoderms. *Submitted* to Genome Biology and Evolution.

Eaves AA and Palmer AR (2003). Reproduction: Widespread cloning in echinoderm larvae. Nature 425:146.

Emson RH and Wilkie IC (1980). Fission and autotomy in echinoderms. Oceanogr Mar Biol Ann Rev 18:155-250.

Endean R (1966). The coelomocytes and coelomic fluids. In: Boolootian RA, editor. Physiology of Echinodermata. New York: Intersciences 1966.

Epel D (1978). Mechanisms of Activation of Sperm and Egg During Fertilization of Sea Urchin Gametes. Current Topics in Developmental Biology 12:185-246.

Etchevers HC, Vincent C, Le Douarin NM, Couly GF (2001). The cephalic neural crest provides pericytes and smooth muscle cells to all blood vessels of the face and forebrain. Development 128:1059-1068.

European Commission (2012). Blue Growth: Opportunities for marine and maritime sustainable growth. Communication from the Commission to the European Parliament, the Council, the European Economic and Social Committee and the Committee of the Regions. Luxembourg: Publications Office of the European Union, 2012; ISBN 978-92-79-25529-8. doi:10.2771/43949.

Exposito J and Lethias C (2013). Invertebrate and vertebrate collagens. In: Evolution of extracellular matrix, Mecham, Keeley, Chapter 3.

Exposito J, Valcourt U, Cluzel C, Lethias C (2010). The Fibrillar Collagen Family. IJMS 11(2):407-426.

Fallahi A, Kroll B, Warner LR, Oxford RJ, Irwin KM, Mercer LM, Shadle SE, Oxford JT (2005). Structural model of the amino pro-peptide of collagen XI α1 chain with similarity to the LNS domains. Protein Science 14:1526-1537.

Fang M and Holl MMB (2013). Variation in type I collagen fibril nanomorphology: the significance and origin. BoneKEy Reports. 2:394. doi:10.1038/bonekey.2013.128.

Ferrario C (2013). Arm-tip regeneration in the red starfish *Echinaster sepositus* (Echinodermata, Asteroidea) following traumatic amputation: morphological and ultrastructural analyses. Master Thesis. University of Milan.

Ferrario C, Czarkwiani A, Piovani L, Candia Carnevali MD, Sugni M and Oliveri P. Extracellular matrix gene expression patterns during arm regeneration in *Amphiura filiformis*. *In preparation* for Cell and Tissue Research.

Ferreira AM, Gentile P, Chiono V, Ciardelli G (2012). Collagen for bone tissue regeneration. Acta Biomaterialia 8:3191-3200.

Franco CF, Santos R, Coelho AV (2011). Proteome characterization of sea star coelomocytes-The innate immune effector cells of echinoderms. Proteomics 11:3587-3592.

Franco CF, Soares R, Pires E, Koci K, Almeida AM, Santos R, Coelho AV (2013). Understanding regeneration through proteomics. Proteomics 13(3):686-709.

Fraser N, Crawford B, Kusen J (2000). Best practices guide for crown-of-thorns clean-ups. Proyek Pesisir Special Publication. Coastal Resources Center Coastal Management Report 2225. Coastal Resources Center, University of Rhode Island, Narragansett, Rhode Island. 38 pages.

Fujita T (2002). Evolution of the lectin-complement pathway and its role in innate immunity. Nature Reviews 2:346-353.

Gage JD (1990). Skeletal growth bands in brittle stars: microstructure and significance as age markers. Journal of the Marine Biological Association of the United Kingdom 70(01): 209-224.

García-Arrarás JE and Dolmatov IY (2010). Echinoderms; potential model systems for studies on muscle regeneration. Curr Pharm Des 16(8):942-955.

García-Arrarás JE, Schenk C, Rodrigues-Ramirez R, Torres II, Valentin G, Candelaria AG (2006). Spherulocytes in the echinoderm *Holothuria glaberrima* and their involvement in intestinal regeneration. Dev Dyn 235:3259-3267.

Gelse K, Pöschl E, Aigner T (2003). Collagens-Structure, function, and biosynthesis. Adv. drug Deliv Rev 55:1531-1546. doi: 10.1016/j.addr.2003.08.002.

Gemberling M, Bailey TJ, Hyde DR, Poss KD (2013). The zebrafish as a model for complex tissue regeneration. Trends Genet 29(11): 611-620. doi: 10.1016/j.tig.2013.07.003.

Gilbert SF (2000). Developmental Biology. 6th edition. Sunderland (MA): Sinauer Associates, 2000.

Gillis JA, Modrell MS, Northcutt RG, Catania KC, Luer C, Baker CVH (2012). Electrosensory ampullary organs are derived from lateral line placodes in cartilaginous fishes. Development 139:3142-3146.

Glínski Z and Jarosz J (2000). Immune phenomena in echinoderms. Archivum Immunologiae et Therapiae Experimentalis 48:189-193.

Glowacki J and Mizuno S (2008). Collagen Scaffolds for Tissue Engineering. Biopolymers 89(5):338-344. doi: 10.1002/bip.20871.

Gomez d'Ayala G, Malinconico M, Laurienzo P (2008). Marine Derived Polysaccharides for Biomedical Applications: Chemical Modification Approaches. Molecules 13:2069-2106. doi: 10.3390/molecules13092069.

Gómez-Guillén MC, Giménez B, López-Caballero ME, MP Montero (2011). Functional and bioactive properties of collagen and gelatin from alternative sources: A review. Food Hydrocolloids 25:1813-1827. doi: 10.1016/j.foodhyd.2011.02.007.

González-Rosa JM, Martín V, Peralta M, Torres M, Mercader N (2011). Extensive scar formation and regression during heart regeneration after cryoinjury in zebrafish. Development 138:1663-1674.

Gorshkov AN, Blinova MI, Pinaev GP (2009). Ultrastructure of Coelomic Epithelium and Coelomocytes of the Starfish *Asterias rubens* L. in Norm and after Wounding. Cell Tissue Res 3(5):477-490.

Goss RJ (1969). Principles of regeneration. New York: Academic Press.

Grand A, Pratchett M, Rivera-Posada J (2014). The Immune Response of *Acanthaster planci* to Oxbile Injections and Antibiotic Treatment. J Mar Biol Article ID 769356. doi: org/10.1155/2014/769356.

Grant WT, Sussman MD, Balian G (1985). A disulfide-bonded short chain collagen synthesized by degenerative and calcifying zones of bovine growth plate cartilage. J Biol Chem 260:3798-3803.

Gray JS (1997). Marine biodiversity: patterns, threats and conservation needs. Biodiversity and Conservation 6:153-175.

Green H and Goldberg B (1965). Synthesis of collagen by mammalian cell lines of fibroblastic and nonfibroblstic origin. Pathology 53:1360-1365.

Greenberg SS (1989). Immunity and survival. New York: Human Sciences Press 19-34.

Grellner W, Georg T, Andwilske J (2000). Quantitative analysis of proinflammatory cytokines (IL-1beta, IL-6, TNF-alpha) in human skin wounds. Forensic Sci Int 113:251-264.

Gross PS, Al-Sharif WZ, Clow LA, Smith LC (1999). Echinoderm immunity and the evolution of the complement system. Developmental and Comparative Immunology 23:429-442.

Grover CN, Gwynne JH, Pugh N, Hamaia S, Farndale RW, Best SM, Cameron RE (2012). Crosslinking and composition influence the surface properties, mechanical stiffness and cell reactivity of collagen-based films. Acta Biomaterialia 8:3080-3090. doi: http://dx.doi.org/10.1016/j.actbio.2012.05.006.

Guadiz G, Sporn LA, Simpson-Haidaris PJ (1997). Thrombin cleavage independent deposition of fibrinogen in extracellular matrices. Blood 90:2644-2653.

Gupta S and Abu-Ghannam N (2011). Bioactive potential and possible health effects of edible brown seaweeds. Trends in Food Science and Technology 22:315-326.

Gurtner GC, Werner S, Barrandon Y, Longaker MT (2008). Wound repair and regeneration. Europe PMC 453(7193):314-321.

Guzmán EA, Johnson JD, Linley PA, Gunasekera SE, Wright AE (2011). A novel activity from an old compound: Manzamine A reduces the metastatic potential of AsPC-1 pancreatic cancer cells and sensitizes them to TRAIL-induced apoptosis. J New Anticancer Agents 29:777-785.

Haefner B (2003). Drugs from the Deep. Drug Discov Today 8:536-544.

Han M, Yang X, Lee J, Allan CH, Muneoka K (2008). Development and regeneration of the neonatal digit tip in mice. Dev Biol 315:125-135.

Haug T, Kjuul AK, Styrvold OB, Sandsdalen E, Olsen OM, Stensvag K (2002). Antibacterial activity in *Strongylocentrotus droebachiensis* (Echinoidea), *Cucumaria frondosa* (Holothuroidea), and *Asterias rubens* (Asteroidea). J Invertebr Pathol 81:94-102.

Haugh MG, Murphy CM, McKiernan RC, Altenbuchner C, O'Brien FJ (2011). Crosslinking and mechanical properties significantly influence cell attachment, proliferation, and migration within collagen glycosaminoglycan scaffolds. Tissue Eng Part A 17:1201-1208. doi: 10.1089/ten.tea.2010.0590.

Hayward PJ and Ryland JS (1990). Marine fauna of the British Isles and North West Europe. Volume 2. Molluscs to Chordates. Oxford University Press.

Heinemann S, Ehrlich H, Douglas T, Heinemann C, Worch H, Schatton W, Hanke T, (2007). Ultrastructural Studies on the Collagen of the Marine Sponge *Chondrosia reniformis* Nardo. Biomacromolecules 8:3452-3457.

Hernroth B, Farahani F, Brunborg G, Dupont S, Dejmek A, Sköld HN (2010). Possibility of mixed progenitor cells in sea star arm regeneration. J Exp Zool (Mol Dev Evol) 6:457-468.

Hodgkin AL and Katz B (1949). The effect of sodium ions on the electrical activity of the giant axon of the squid. J Physiol 108:37-77.

Holm K, Dupont S, Sköld HN, Stenius A, Thorndyke MC, Hernroth B (2008). Induced cell proliferation in putative haematopoietic tissues of the sea star, *Asterias rubens* (L.). J Exp Biol 211:2551-2558.

Hotchkiss FHC (2009). Arm stumps and regeneration models in Asteroidea (Echinodermata). Proc Biol Soc Wash 122(3):342-354.

Huet M (1975). Le rôle du système nerveux au cours de la régénération du bras chez une étoile de mer: *Asterina gibbosa*. J Embryol Exp Morph 33:535-552.

Huet M and Franquinet R (1981). Histofluorescence study and biochemical assay of catecholamines (Dopamine and Noradrenaline) during the course of arm-tip regeneration in the starfish, *Asterina gibbosa* (Echinodermata, Asteroidea). Histochemistry 72(1):149-154.

Hyman LH (1955). The Invertebrates, vol. IV. Echinodermata. New York: McGraw-Hill.

Ibrahim MM, Chen L, Bond JE, Medina MA, Ren L, Kokosis G, Selim AM, Levinson H (2015). Myofibroblasts contribute to but are not necessary for wound contraction. Laboratory Investigation 95:1429-1438.

Isaeva VV and Korenbaum ES (1990). Defense function of coelomocytes and immunity of echinoderms. Sov Mar Biol 15:353-363.

Iwanaga S and Lee BL (2005). Recent Advances in the Innate Immunity of Invertebrate Animals. Journal of Biochemistry and Molecular Biology 38(2):128-150.

Jaffe EA, Minick R, Adelman B, Necker CG, Nachman R (1976). Synthesis of basement membrane collagen by cultured human endothelial cells. The Journal of Experimental Medicine 144:209-225.

Janies DA, Witter Z, Linchangco GV, Foltz DW, Miller AK, Kerr AM, Jay J, Reid RW, Wray GA (2016). EchinoDB, an application for comparative transcriptomics of deeply-sampled clades of echinoderms. BMC Bioinformatics 17:48. doi: 10.1186/s12859-016-0883-2.

Jenkins ED, Yip M, Melman L, Frisella MM, Matthews BD (2010). Informed Consent: Cultural and Religious Issues Associated with the Use of Allogeneic and Xenogeneic Mesh Products. J Am Coll Surg 210(4):402-410. doi: 10.1016/j.jamcollsurg.2009.12.001.

Jha RK and Zi-rong X (2004). Biomedical Compounds from Marine organisms. Marine Drugs 2:123-146.

Kaack KE and Pomory CM (2011). Salinity effects on arm regeneration in *Luidia clathrata* (Echinodermata: Asteroidea). Mar Freshw Behavi Phy 44(6):359-374.

Kadler KE, Baldock C, Bella J, Boot-Handfort RP (2007). Collagens at a glance. Journal of Cell Science 120:1955-1958.

Karim AA and Bhat R (2008). Gelatin alternatives for the food industry: Recent developments, challenges and prospects. Trends in Food Science and Technology 19:644-656.

Karp RD and Coffaro KA (1982). Cellular Defense Systems of the Echinodermata. Phylogeny and Ontogeny 257-282.

Kew SJ, Gwynne JH, Enea D, Abu-Rub M, Pandit A, Zeugolis D, Brooks RA, Rushton N, Best SM, Cameron RE (2011). Regeneration and repair of tendon and ligament tissue using collagen fibre biomaterials. Acta Biomaterialia 7:3237-3247. doi: 10.1016/j.actbio.2011.06.002.

Kim I, Mogford JE, Witschi C, Nafissi M, Mustoe TA (2003). Inhibition of prolyl 4-hydroxylase reduces scar hypertrophy in a rabbit model of cutaneous scarring. Wound Repair and Regeneration 11:368-372.

Kimura S, Omura Y, Ishida M, Shirai H (1993). Molecular characterization of fibrillar collagen from the body wall of starfish *Asterias amurensis*. Comparative Biochemistry and Physiology Part B: Comparative Biochemistry 104(4):663-668.

King HD (1898). Regeneration in *Asterias vulgaris*. Wilhelm Roux Arch Entwicklungsmech Org 17:351-363.

King RS and Newmark PA (2012). The cell biology of regeneration. JCB: review 196(5):553-562.

Koh TJ and DiPietro LA (2011). Inflammation and wound healing: The role of the macrophage. Expert Rev Mol Med 13:e23. doi: 10.1017/S1462399411001943.

Koob J, Koob-Emunds M, Trotter J (1999). Cell-derived stiffening and plasticizing factors in sea cucumber (*Cucumaria frondosa*) dermis. The Journal of Experimental Biology 202:2291-2301.

Kuhn K (1987). The classical collagens: Types I, II and III. In Structure and Function of collagen types (Mayne R and Burgeson RE, eds.) 1-42 Academic Press, New York.

Lamash NE and Dolmatov IY (2013). Proteases from the Regenerating Gut of the Holothurian *Eupentacta fraudatrix*. PLOS ONE 8(3):e58433.

Laurens N, Koolwijk P, De Maat PM (2006). Fibrin structure and wound healing. Journal of Thrombosis and Haemostasis 4:932-939.

Lawrence JM (1992). Arm loss and regeneration in Asteroids (Echinodermata). In: Scalera-Liaci L, Canicatti C, editors. Echinoderm Research 1991, Balkema, Rottardam, 1992.

Leal M, Madeira C, Brandão C, Puga J, Calado R (2012). Bioprospecting of Marine Invertebrates for New Natural Products-A Chemical and Zoogeographical Perspective. Molecules 17(12):9842-9854.

Lee J, Cuddihy MJ, Kotov NA (2008). Three-Dimensional Cell Culture Matrices: State of the Art. Tissue Engineering: Part B 14(1):61-86. doi: 10.1089/teb.2007.0150.

Lee CH, Singla A, Lee Y (2001). Biomedical applications of collagen. Int J Pharm 221:1-22.

Leibovich SJ and Ross R (1975). The Role of the Macrophage in Wound Repair. A Study with Hydrocortisone and Antimacrophage Serum. American Journal of Pathology 78(1):71-99.

Liesi P, Kaakkola S, Dahl D, Vaheri A (1984). Laminin is induced in astrocytes of adult brain by injury. The EMBO Journal 3(3):683-686.

Martin P (1997). Wound healing-aiming for perfect skin regeneration. Science 276:75-81.

Mashanov VS and García-Arrarás JE (2011). Gut Regeneration in Holothurians: A Snapshot of Recent Developments. The Biological Bulletin 221:93-109.

Mashanov VS, Zueva OR, García-Arrarás JE (2013). Radial glial cells play a key role in echinoderm neural regeneration. BMC Biol 11:49.

Mashanov VS, Zueva OR, García-Arrarás JE (2014). Transcriptomic changes during regeneration of the central nervous system in an echinoderm. BMC Genomics 15:357.

Matranga V, Pinsino A, Celi M, Natoli A, Bonaventura R, Schöder HC, Müller WEG (2005). Monitoring Chemical and Physical Stress Using Sea Urchin Immune Cells. Progress in Molecular and Subcellular Biology Subseries Marine Molecular Biotechnology V. Matranga (Ed.), Echinodermata © Springer-Verlag Berlin Heidelberg, 2005.

Matsumura T (1974). Collagen fibrils of the sea cucumber, *Stichopus japonicus*: Purification and morphological study. Connect Tissue Res 2:117-125.

Matsushita M (2009). Ficolins: Complement-Activating Lectins Involved in Innate Immunity. J Innate Immun 2:24-32.

Mattson P (1976). Regeneration. Indianapolis: Bobbs-Merrill.

Mendonça VM, Al Jabri MM, Al Ajmi I, Al Muharrami M, Al Areimi M, Al Aghbari HA (2010). Persistent and Expanding Population Outbreaks of the Corallivorous Starfish *Acanthaster planci* in the Northwestern Indian Ocean: Are They Really a Consequence of Unsustainable Starfish Predator Removal through Overfishing in Coral Reefs, or a Response to a Changing Environment? Zoological Studies 49(1):108-123.

Milligan M (1946). Trichrome stain for formalin-fixed tissue. Am J Clin Pathol 10:184.

Miner JH and Yurchenco PD (2004). Laminin functions in tissue morphogenesis. Annu Rev Cell Dev Biol 20:255-84.

Mintz GR and Lennarz WJ (1982). Spicule formation by cultured embryonic cells from the sea urchin. Cell Diff 11:331-333.

Mladenov PV and Burke RD (1994). Echinodermata: asexual propagation. Adiyodi KG and Adyodi RG (eds.) Reproductive biology of invertebrates. Vol. VI part B. Asexual propagation and reproductive strategies. New Delhi. Oxford and Hill. 339-383.

Mladenov PV, Bisgrove B, Aostra S, Burke RD (1989). Mechanisms of arm-tip regeneration in the sea star *Leptasterias hexactis*. Roux Arch Dev Biol 198:19-28.

Mo J, Prévost SF, Blowes LM, Egertová M, Terrill NJ, Wang W, Elphick MR, Gupta HS (2016). Interfibrillar stiffening of echinoderm mutable collagenous tissue demonstrated at the nanoscale. PNAS 113(42):e6362-e6371. doi: 10.1073/pnas.1609341113.

Mora C, Tittensor D, Adl S, Simpson A, Worm B (2011). How Many Species Are There on Earth and in the Ocean? PLOS Biology 9(8):e1001127.

Morgan TH (1901). Regeneration. New York: Macmillan.

Morgulis S (1909). Regeneration in the brittle star *Ophiocoma pumila* with reference to the influence of the nervous system. Proc Am Acad Arts and Sci 44:655-659.

Moss C, Hunter J, Thorndyke MC (1998). Pattern of bromodeoxyuridine incorporation and neuropeptide immunoreactivity during arm regeneration in the starfish *Asterias rubens*. Phil Trans R Soc Lond B 353:421-436.

Motokawa T (2011). Mechanical Mutability in Connective Tissue of Starfish Body Wall. Biol Bull 221:280-289.

Mozzi D, Dolmatov IY, Bonasoro F, Carnevali MDC (2006). Visceral regeneration in the crinoid *Antedon mediterranea*: basic mechanisms, tissues and cells involved in gut regrowth. Cent Eur J Biol 1:609-635.

Murphy CM, Matsiko A, Haugh MG, Gleeson JP, O'Brien FJ (2012). Mesenchymal stem cell fate is regulated by the composition and mechanical properties of collagen-glycosaminoglycan scaffolds. J Mech Behav Biomed 11:53-62.

Nagai T and Suzuki N (2000). Isolation of collagen from fish waste material-skin, bone and fins. Food Chemistry 68:277-281.

Nagai T, Nagamori K, Yamashita E, Suzuki N (2002). Collagen of octopus *Callistoctopus arakawai* arm. International Journal of Food Science and Technology 37:285-289.

Nagai T, Worawattanamateekul W, Suzuki N, Nakamura T, Ito T, Fujiki K, Nakao M, Yano T (2000). Isolation and characterization of collagen from rhizostomous jellyfish (*Rhopilema asamushi*). Food Chemistry 70:205-208.

Nagai T, Yamashita E, Taniguchi K, Kanamori N, Suzuki N (2001). Isolation and characterization of collagen from the outer skin waste material of cuttlefish (*Sepia lycidas*). Food Chem 72:425-429.

Nissi R, Autio-Harmainen H, Marttila P, Sormunen R, Kivirikko KI (2001). Prolyl 4-hydroxylase isoenzymes I and II have different expression patterns in several human tissues. J Histochem Cytochem 49:1143-1153.

Nusbaum J and Oxner M (1915). Zur Restitution bei dem Seestern. Zool Anz 46.

Nye HLD, Cameron JA, Chernoff EAG, Stocum DL (2003). Regeneration of the Urodele Limb: A Review. Developmental Dynamics 226:280-294.

Ockelmann KW and Muus K (1978). The biology, ecology and behaviour of the bivalve *Mysella bidentata* (Montagu). Ophelia 17(1):1-93.

Oji T (2001). Fossil records of echinoderm regeneration with special regard to crinoids. Micr Res Tech 55:397-402.

Okazaki K (1960). Skeleton formation of sea urchin larvae. II. Organic matrix of the spicule. Embryologia 5:283-320.

Okazaki K and Inoué S (1976). Crystal properties of the larval sea urchin spicule. Develop Growth and Differ 18(4):413-434.

Ortiz-Pineda PA, Ramírez-Gómez F, Pérez-Ortiz J, González-Díaz S, Santiago-De Jesús F, Hernández-Pasos J, Del Valle-Avila C, Rojas-Cartagena C, Suárez-Castillo EC, Tossas K, Méndez-Merced AT, Roig-López JL, Ortiz-Zuazaga H, García-Arrarás JE (2009). Gene expression profiling of intestinal regeneration in the sea cucumber. BMC Genomics 10:262. doi:10.1186/1471-2164-10-262.

Özbek S, Balasubramanian PG, Chiquet-Ehrismann R, Tucker RP, Adams JC (2010). The Evolution of Extracellular Matrix. Molecular Biology of the Cell 21:4300-4305.

Pagliara P and Canicatti C (1993). Isolation of cytolytic granules from sea urchin amoebocytes. Eur J Cell Biol 60:179-184.

Pancer Z, Rast JP, Davidson EH (1999). Origins of immunity: transcription factors and homologues of effector genes of the vertebrate immune system expressed in sea urchin coelomocytes. Immunogenetics 49(9):773-86.

Pang S, Chang YP, Woo KK (2013). The Evaluation of the Suitability of Fish Wastes as a Source of Collagen. 2nd International Conference on Nutrition and Food Sciences IPCBEE Vol. 53 (2013) © (2013) IACSIT Press, Singapore. doi: 10.7763/IPCBEE. 2013. V53. 15.

Parenteau-Bareil R, Gauvin R, Berthod F (2010). Collagen-Based Biomaterials for Tissue Engineering Applications. Materials 3:1863-1887. doi: 10.3390/ma3031863.

Parisi G, Centoducati G, Gasco L, Gatta PP, Moretti VM, Piccolo G, Roncarati A, Terova G, Pais A (2012). Molluscs and echinoderms aquaculture: biological aspects, current status, technical progress and future perspectives for the most promising species in Italy. Italian Journal of Animal Science 11:e72. doi: 10.4081/ijas.2012.e72.

Parker MC, Ellis H, Moran BJ, Thompson JN, Wilson MS, Menzies D, McGuire A, Lower AM, Hawthorn RJS, O'Brien F, Buchan S, Crowe AM (2001). Postoperative Adhesions: Ten-Year Follow-Up of 12,584 Patients Undergoing Lower Abdominal Surgery. Dis Colon Rectum 44(6):822-829.

Pastar I, Stojadinovic O, Yin NC, Ramirez H, Nusbaum AG, Sawaya A, Patel SB, Khalid L, Isseroff RR, Tomic-Canic M (2014). Epithelialization in Wound Healing: A Comprehensive Review. Adv Wound Care (New Rochelle) 3(7):445-464.

Pawelec KM, Best SM, Cameron RE (2016). Collagen: a network for regenerative medicine. Journal of Materials Chemistry B 4:6484-6496.

Peacock EE (1984). Wound repair. In: Wound repair. Saunders, Philadelphia 38-55.

Pearse VB and Muscatine L (1971). Role of symbiotic algae (Zooxanthellae) in coral calcification. Biol Bull 141:350-363.

Pieper JS, van Wachem PB, van Luyn MJA, Brouwer LA, Hafmans T, Veerkamp JH, van Kuppevelt TH (2000). Attachment of glycosaminoglycans to collagenous matrices modulates the tissue response in rats. Biomaterials 21(16):1689-1699. doi: 10.1016/S0142-9612(00)00052-1.

Pinsino A, Thorndyke MC, Matranga V (2007). Coelomocytes and posttraumatic response in the common sea star *Asterias rubens*. Cell Stress Chaperon 12:331-341.

Pozzolini M, Scarfì S, Mussino F, Ferrando S, Gallus L, Giovine M (2015). Molecular Cloning, Characterization, and Expression Analysis of a Prolyl 4-Hydroxylase from the Marine Sponge *Chondrosia reniformis*. Mar Biotechnol 17:393-407.

Prockop DJ and Kivirikko KI (1995). Collagen: Molecular biology, diseases and potentials for therapy. Annu Rev Biochem 64:403-434.

Purcell SW, Mercier A, Conand C, Hamel JF, Toral-Granda MV, Lovatelli A, Uthicke S, (2013). Sea cucumber fisheries: global analysis of stocks, management measures and drivers of overfishing. Fish and Fisheries 14:34-59. doi: 10.1111/j.1467-2979.2011.00443.x.

Purushothaman S, Saxena S, Meghah V, Brahmendra Swamy CV, Ortega-Martinez O, Dupont S, Idris M (2015). Transcriptomic and proteomic analyses of *Amphiura filiformis* arm tissue-undergoing regeneration. Journal of Proteomics 112:113-124.

Quiñones JL, Rosa R, Ruiz DL, García-Arrarás JE (2002). Extracellular matrix remodelling and metalloproteinase involvement during intestine regeneration in the sea cucumber *Holothuria glaberrima*. Dev Biol 250(1):181-197.

Rahban SR and Garner WL (2003). Fibroproliferative scars. Clin Plast Surg 30:77.

Ramírez-Gómez F and García-Arrarás JE (2010). Echinoderm immunity. ISJ 7:211-220.

Ramírez-Gómez F, Aponte-Rivera F, Mendez Castaner L, García-Arrarás JE (2010). Changes in holothurian coelomocyte populations following immune stimulation with different molecular patterns. Fish Shellfish Immunol 29:175-185.

Ramírez-Gómez F, Ortiz-Pineda PA, Rivera Cardona G, García-Arrarás JE (2009). LPS-induced genes in intestinal tissue of the sea cucumber *Holothuria glaberrima*. PLOS ONE 4:e6178.

Ramírez-Gómez F, Ortiz-Pineda PA, Rojas Cartagena C, Suarez-Castillo EC, García-Arrarás JE (2008). Immune-related genes associated with intestinal tissue in the sea cucumber *Holothuria glaberrima*. Immunogenetics 60:57-71.

Rao KV, Donia MS, Peng J, Garcia EP, Alonso D, Martinez A, Medina M, Franzblau SG, Tekwani BL, Khan SI, Wahyuono S, Willett KL, Hamann MT (2006). Manzamine B and E and Ircinal: A Related Alkaloids from an Indonesian *Acanthostrongylophora* Sponge and Their Activity against Infectious, Tropical Parasitic, and Alzheimer's Diseases. J Nat Prod 69(7):1034-1040.

Rast JP, Smith LC, Loza-Coll M, Hibino T, Litman GW (2006). Genomic Insights into the Immune System of the Sea Urchin. Science 314(5801):952-956.

Reddien PW and Sánchez Alvarado A (2004). Fundamentals of planarian regeneration. Annual Review of Cell and Developmental Biology 20:725-757.

Reinisch CL and Bang FB (1971). Cell recognition: reactions of the sea star (*Asterias vulgaris*) to the injection of amoebocytes of sea urchin (*Arbacia punctulata*). Cell Immunol 2:496-503.

Ribeiro AR, Barbaglio A, Di Benedetto C, Ribeiro CC, Wilkie IC, Carnevali MDC, Barbosa MA (2011). New Insights into Mutable Collagenous Tissue: Correlations between the Microstructure and Mechanical State of a Sea-Urchin Ligament. PLOS ONE 6:e24822.

Ribeiro AR, Barbaglio A, Oliveira MJ, Ribeiro CC, Wilkie IC, Candia Carnevali MD, Barbosa MA (2012). Matrix metalloproteinases in a sea urchin ligament with adaptable mechanical properties. PLOS ONE 7:e49016.

Ricard-Blum S (2011). The collagen family. Cold Spring Harb Perspect Biol 3:a004978.

Riedl R (1991). Fauna e flora del Mediterraneo. Franco Muzzio Editore, Padova 543-560.

Ruszczak Z (2003). Effect of collagen matrices on dermal wound healing. Advanced Drug Delivery Reviews 55:1595-1611. doi: 10.1016/j.addr.2003.08.003.

Sahithi B, Ansari SK, Hameeda SK, Sahithya G, Durga Prasad M, Yogitha L (2013). A review on collagen based drug delivery systems. Indian Journal of Research in Pharmacy and Biotechnology 1(3):461-468.

Saló E and Baguñá J (2002). Regeneration in planarians and other worms: New findings, new tools, and new perspectives. J Exp Zool 292(6):528-39.

Saló E, Abril JF, Adell T, Cebrià F, Eckelt K, Fernàndez-Taboada E, Handberg-Thorager M, Iglesias M, Molina MD, Rodrìguea-Esteban G (2009). Planarian regeneration: achievements and future directions after 20 years of research. Int J Dev Biol 53:1317-1327. doi: 10.1387/ijdb.072414es.

Sánchez Alvarado A (2000). Regeneration in the metazoans: why does it happen? BioEssays 22:578-590.

Sánchez Alvarado A and Tsonis PA (2006). Bridging the regeneration gap: genetic insights from diverse animal models. Nature Reviews Genetics 7:873-884.

San Miguel-Ruiz JE and García-Arrarás JE (2007). Common cellular events occur during wound healing and organ regeneration in the sea cucumber *Holothuria glaberrima*. BMC Dev Biol 7:115.

Satoh A, Hirata A, Makanae A (2012). Collagen reconstitution is inversely correlated with induction of limb regeneration in *Ambystoma mexicanum*. Zoolog Sci 29(3):191-197.

Schapiro J (1914). Regenerationserscheinungen verschiedener Seesternarten. Arch Entw'mech Organ 38.

Schram JB, McClintock JB, Angus RA, Lawrence JM (2011). Regenerative capacity and biochemical composition of the sea star *Luidia clathrata* (Say) (Echinodermata: Asteroidea) under conditions of near-future ocean acidification. J Exp Mar Biol Ecol 407(2):266-274.

Schuenhoff A, Shpigelb M, Lupatschb I, Ashkenazi A, Msuya FE, Neori A (2003). A semi-recirculating, integrated system for the culture of fish and seaweed. Aquaculture 221:167-181. doi: 10.1016/S0044-8486(02)00527-6.

Schuppan D, Schmid M, Somasundaram R, Ackermann R, Ruehl M, Nakamura T, Riecken E-O (1998). Collagens in the liver extracellular matrix bind hepatocyte growth factor. Gastroenterology 114(1):139-152.

Sea Urchin Genome Sequencing Consortium (2006). The genome of the sea urchin *Strongylocentrotus purpuratus*. Science 314(5801):941-952.

Shibata TF, Oji T, Akasaka K, Agata K (2010). Staging of Regeneration Process of an Arm of the Feather Star *Oxycomanthus japonicus* Focusing on the Oral-Aboral Boundary. Dev Dyn 239:2947-2961.

Shimomura O, Johnson FH, Saiga Y (1962). Extraction, purification and properties of aequorin, a bioluminescent protein from the luminous hydromedusan, *Aequorea*. J Cell Comp Physiol 59:223-239.

Short K, Wiradjaja F, Smyth I (2007). Let's Stick Together: The Role of the Fras1 and Frem Proteins in Epidermal Adhesion. IUBMB Life 59(7):427-435.

Shoulders M and Raines R (2009). Collagen Structure and Stability. Annu Rev Biochem 78(1):929-958.

Shultz GS, Ladwig G, Wysocki A (2005). Extracellular matrix: review of its roles in acute and chronic wounds. World Wide Wounds.

Silva TH, Moreira-Silva J, Marques ALP, Domingues A, Bayon Y, Reis RL (2014). Marine Origin Collagens and Its Potential Applications. Marine Drugs 12:5881-5901. doi: 10.3390/md12125881.

Silvipriya KS, Kumar KK, Bhat AR, Kumar BD, John A, lakshmanan P (2015). Collagen: Animal Sources and Biomedical Application. Journal of Applied Pharmaceutical Science 5(03):123-127. doi: 10.7324/JAPS.2015.50322.

Singer AJ and Clark RAF (1999). Cutaneous wound healing. The New England Journal of Medicine 341:738-746.

Sivamani RK, Garcia MS, Isseroff RR (2007). Wound re-epithelialization: modulating keratinocyte migration in wound healing. Front Biosci 12:2849-2868.

Smith AB (1990). Biomineralization in echinoderms. Carter JG, editor. Skeletal Biomineralization: Patterns, Processes and Evolutionary Trends. New York: Van Nostrand Reinhold 413-443.

Smith VJ (1981). The echinoderms. In NA Ratcliffe, AF Rowley, eds. Invertebrate blood cells. London: Academic Press 513-562.

Smith LC, Ghosh C, Buckley KM, Clow LA, Dheilly NM, Haug T, Henson JH, Li C, Lun CM, Majeske AJ, Matranga V, Nair SV, Rast JP, Raftos DA, Roth M, Sacchi S, Schrankel CS, Stensvåg K (2010). Echinoderm immunity. Invertebrate Immunity, edited by Kenneth Söderhäll © 2010 Landes Bioscience and Springer Science+Business Media.

Song E, Yeon Kim S, Chun T, Byun HY, Lee YM (2006). Collagen scaffolds derived from a marine source and their biocompatibility. Biomaterials 27:2951-2961. doi: 10.1016/j.biomaterials.2006.01.015.

Sticker SA (1985). The ultrastructure and formation of the calcareous ossicles in the body wall of the sea cucumber *Leptosynapta clarki* (Echinodermata, Holothuroidea). Zoomorphology 105:209-222.

Stocum DL (2006). Regenerative biology and medicine. San Diego: Elsevier/Academic Press.

Storer TI, Usinger RL, Stebbins RC, Nybakken JW (1982). Zoologia. Zanichelli Editore, Bologna 26:707-727.

Sugni M, Di Benedetto C, Alongi V, Barbaglio A, Bonfanti C, Messina G, Martinello T, Patruno M, Candia Carnevali MD (2013). Echinodermi e biomimetica: potenzialità applicative di matrici collagene. Proceedings of the LXXIV Congresso Nazionale dell'Unione Zoologica Italiana. Modena. 30 settembre-3 ottobre.

Sugni M, Fassini D, Barbaglio A, Biressi A, Di Benedetto C, Tricarico S, Bonasoro F, Wilkie IC, Candia Carnevali MD (2014). Comparing dynamic connective tissue in echinoderms and sponges: morphological and mechanical aspects and environmental sensitivity. Marine Environmental Research 93:123-132.

Sugni M, Mozzi D, Barbaglio A, Bonasoro F, Candia Carnevali MD (2007). Endocrine disrupting compounds and echinoderms: new ecotoxicological sentinels for the marine ecosystem. Ecotoxicology 16(1):95-108.

Sun L, Chen M, Yang H, Wang T, Liu B, Shu C, Gardiner DM (2011). Large scale gene expression profiling during intestine and body wall regeneration in the sea cucumber *Apostichopus japonicus*. Comp Biochem Physiol D 6(2):195-205. doi: 10.1016/j.cbd.2011.03.002.

Swatschek D, Schatton W, Kellermann J, Müller WEG, Kreuter J (2002). Marine sponge collagen: isolation, characterization and effects on the skin parameters surface-pH, moisture and sebum. European Journal of Pharmaceutics and Biopharmaceutics 53:107-113.

Takehana Y, Yamada A, Tamori M, Motokawa T (2014). Softenin, a Novel Protein That Softens the Connective Tissue of Sea Cucumbers through Inhibiting Interaction between Collagen Fibrils. PLOS ONE 9(1):e85644.

Tal H, Moses O, Kozlovsky A, Nemcovsky C (2012). Bioresorbable Collagen Membranes for Guided Bone Regeneration, Bone Regeneration. Prof. Haim Tal (Ed.), ISBN: 978-953-51-0487-2. InTech.

Tamori M (2006). Tensilin-like stiffening protein from *Holothuria leucospilota* does not induce the stiffest state of catch connective tissue. Journal of Experimental Biology 209(9):1594-1602.

Tanaka EM and Reddien PW (2011). The cellular basis for animal regeneration. Dev Cell 21:172-185.

Tang S, Yang W, Mao X (2007). Agarose/collagen composite scaffold as an anti-adhesive sheet. Biomed Mater 2:S129-S134. doi: 10.1088/1748-6041/2/3/S09.

Tata JR (1993). Gene expression during metamorphosis: an ideal model for post-embryonic development. Bioessays 15(4):239-248.

Thorndyke MC and Candia Carnevali MD (2001). Regeneration neurohormones and growth factors in echinoderms. Can J Zool 79(7):1171-1208.

Thorndyke MC, Chen WC, Beesley PW, Patruno M (2001). Molecular approach to echinoderm regeneration. Microsc Res Tech 55:474-485.

Thorndyke MC, Chen WC, Moss C, Candia Carnevali MD, Bonasoro F (1999). Regeneration in Echinoderms: cellular and molecular aspects. Echinoderm Research 1999. Candia Carnevali MD and Bonasoro F (eds.). Balkema. Rotterdam 159-164.

Thorndyke MC, Patruno M, Dewael Y, Dupont S, Mallefet J (2003). Regeneration in the ophiuroid *Amphiura filiformis*: cell biology, physiology and luminescence. In: Féral J-P, David B (eds.) Echinoderm Research 2001, Swets and Zeitlinger, Lisse 193-199.

Thouveny Y and Tassava RA (1988). Regeneration through phylogenesis. In Cellular and Molecular Basis of Regeneration: from Invertebrates to Humans (eds Ferretti P, Geraudie J) 9-44. Chichester: John Wiley & Sons.

Tipper J, Lyons-Levy G, Atkinson M, Trotter J (2003). Purification, characterization and cloning of tensilin, the collagen-fibril binding and tissue-stiffening factor from *Cucumaria frondosa* dermis. Matrix Biol 21:625-635.

Tonnesen MG, Feng X, Clark RAF (2000). Angiogenesis in Wound Healing. JID Symposium Proceedings 5:40-46.

Toral-Granda V, Lovatelli A, Vasconcellos M (2008). Sea cucumbers: A global review of fisheries and trade. FAO fisheries and aquaculture technical paper 516. ISBN 978-92-5-106079-7.

Tortonese E (1965). Fauna d'Italia Vol. 6: Echinodermata. Ed. Calderoni Bologna.

Toshinori H, Nobuhiko M, Yoko U, Mitsumasa O, Hisato K (2004). FGF2 triggers iris-derived lens regeneration in newt eye. Mech Develop 121:519-526.

Tredget EF, Nedelec B, Scott PG, Ghahary A (1997). Hypertrophic scars, keloids and contractures: the cellular and molecular basis for therapy. Surg Clin North Am 77:701-730.

Tricarico S, Barbaglio A, Burlini N, Del Giacco L, Ghilardi A, Sugni M, Di Benedetto C, Bonasoro F, Wilkie IC, Candia Carnevali MD (2012). New insights into the mutable collagenous tissue of *Paracentrotus lividus*: preliminary results. Zoosymposia 7:279-285.

Trotter J, Lyons-Levy G, Chino K, Koob T, Keene D, Atkinson M (1999). Collagen fibril aggregation-inhibitor from sea cucumber dermis. Matrix Biology 18(6):569-578.

Trotter JA, Thurmond FA, Koob TJ (1994). Molecular structure and functional morphology of echinoderm collagen fibrils. Cell Tissue Res 275:451-458.

Tsai S-W, Fang J-F, Yang C-L, Chen J-H, Su L-T, Jan S-H (2005). Preparation and Evaluation of a Hyaluronate-collagen Film for Preventing Post-Surgical Adhesion. The Journal of International Medical Research 33:68-76.

Tsonis PA (2000). Regeneration in Vertebrates. Dev Biol 221:273-284.

Uriarte-Montoya MH, Arias-Moscoso JL, Plascencia-Jatomea M, Santacruz-Ortega H, Rouzaud-Sández O, Cardenas-Lopez JL, Marquez-Rios E, Ezquerra-Brauer JM (2010). Jumbo squid (*Dosidicus gigas*) mantle collagen: extraction, characterization, and potential application in the preparation of chitosan-collagen biofilms. Bioresource Technology 101:4212-4219. doi: 10.1016/j.biortech.2010.01.008.

Uthicke S, Schaffelke B, Byrne M. (2009). A boom-bust phylum? Ecological and evolutionary consequences of density variations in echinoderms. Ecological monographs 79(1):3-24.

Veijola J, Koivunen P, Annunen P, Pihlajaniemi T, Kivirikko KI (1994). Cloning, baculovirus expression, and characterization of the alpha subunit of prolyl 4-hydroxylase from the nematode *Caenorhabditis elegans*. This alpha subunit forms an active alpha beta dimer with the human protein disulfide isomerase/beta subunit. J Biol Chem 269(43):26746-26753.

Vickery MC, Vickery MS, Amsler CD, Mc Clintock JB (2001). Regeneration in echinoderm larvae. Microsc Res Tech 55(6):364-373.

Viehweg J, Naumann W, Olsson R (1998). Secretory Radial Glia in the Ectoneural System of the Sea Star *Asterias rubens* (Echinodermata). Acta Zoologica 79:119-131.

Villamor A, Espluga R, Becerro MA (2010). Feeding habits of the common sea star *Echinaster sepositus* and its ecological implications on Mediterranean shallow rocky bottoms. XVI Simposio Ibérico de Estudios de Biologia Marina. Alicante, Spain.

Werner S and Grose R (2003). Regulation of wound healing by growth factors and cytokines. Physiol Rev 83:835.

Whittaker CA, Bergeron KF, Whittle J, Brandhorst BP, Burke RD, Hynes RO (2006). The echinoderm adhesome. Developmental Biology 300:252-266.

Wilgus TA (2008). Immune cells in the healing skin wound: Influential players at each stage of repair. Pharmacological Research 58(2):112-116.

Wilkie IC (1996). Mutable collagenous tissues: extracellular matrix as mechanoeffector. In Echinoderm Studies Vol. 5 (ed. Jangoux M and Lawrence JM):61-102. Balkema Rotterdam.

Wilkie IC (2001). Autotomy as a prelude to regeneration in echinoderms. Micr Res Tech 55:369-396.

Wilkie IC (2005). Mutable collagenous tissue: overview and perspectives. In: Matranga V, editor. Echinodermata. Progress in molecular and subcellular biology. Marine molecular biotechnology. Berlin: Springer 5:221-250.

Wilkie IC, Candia Carnevali MD, Andrietti F (1994). Microarchitecture and mechanics of the sea urchin peristomial membrane. Bollettino di Zoologia 61:39-51.

Wilkie IC, Candia Carnevali MD, Trotter JA (2004). Mutable collagenous tissue: recent progress and an evolutionary perspective. Heinzeller T and Nebelsick J (eds.). Proc 11th Int Echinoderm Conf Munich, 2003.

Wilkie IC, Fassini D, Cullorà E, Barbaglio A, Tricarico S, Sugni M, Del Giacco L, Candia Carnevali MD (2015). Mechanical Properties of the Compass Depressors of the Sea-Urchin *Paracentrotus lividus* (Echinodermata, Echinoidea) and the Effects of Enzymes, Neurotransmitters and Synthetic Tensilin-Like Protein. PLOS ONE 10(3):e0120339.

Wilson MS, Menzies D, Knight A, Crowe AM (2002). Demonstrating the clinical and cost effectiveness of adhesion reduction strategies. Colorectal Dis 4:355-360.

WoRMS Editorial Board (2016). World Register of Marine Species. Available from http://www.marinespecies.org at VLIZ. Accessed 2016-12-05. doi:10.14284/170.

Xu X and Doolittle RF (1990). Presence of a vertebrate fibrinogen-like sequence in an echinoderm. Proc Natl Acad Sci USA 87:2097-2101.

Yamada A, Tamori M, Iketani T, Oiwa K, Motokawa T (2010). A novel stiffening factor inducing the stiffest state of holothurian catch connective tissue. Journal of Experimental Biology 213(20):3416-3422.

Yamamoto K, Igawa K, Sugimoto K, Yoshizawa Y, Yanagiguchi K, Ikeda T, Yamada S, Hayashi Y (2014). Biological safety of fish (Tilapia) collagen. Biomed Res Int Article ID 630757. doi: 10.1155/2014/630757.

Yang CR (2012). Enhanced physicochemical properties of collagen by using EDC/NHS-crosslinking. Bull Mater Sci 35:913-918.

Yokoyama H (2013). Growth and food source of the sea cucumber *Apostichopus japonicus* cultured below fish cages - Potential for integrated multi-trophic aquaculture. Aquaculture 372-375, 28-38. doi: http://dx.doi.org/10.1016/j.aquaculture.2012.10.022.

Yun S (2014). The role of extracellular matrix in planarian regeneration. PhD thesis (University of Hong Kong).

Zeleny C (1903). A study of the rate of regeneration of the arms in the brittle-star, *Ophioglypha lacertosa*. Biol Bull 6(1):12-17.

Zeugolis DI, Khew ST, Yew ESY, Ekaputra AK, Tong YW, Yung LYL, Hutmacher DW, Sheppard C, Raghunath M (2008). Electro-spinning of pure collagen nano-fibres- Just an expensive way to make gelatin? Biomaterials 29:2293-2305. doi: 10.1016/j.biomaterials.2008.02.009.

Zhang G and Cohn MJ (2006). Hagfish and lancelet fibrillar collagens reveal that type II collagen-based cartilage evolved in stem vertebrates. PNAS 103:16829-16833.

## *Acknowledgements*

After three years of PhD, after both happy and difficult moments, it is so beautiful to think at this time I lived between Lurate, Milan and London (and in many other countries I visited to attend incredible conferences ;)) and at how many people helped me to reach this final goal I hope is just the beginning of a long adventure in science and biology. This PhD was not just a life of work (one of the most amazing ones I have to say;)) but also a school of life: the shy student I was became a more confident woman and student with the strong will of exploring our beautiful world with the curiosity typical of all people of science.
I will repeat “thank you” so many times I’m sure I will be quite boring ;) but I’m convinced that these two simple words enclose my deepest gratitude going to all the people who supported me during these years of work and not only! And I want to apologise right now if I’m forgetting someone.
First, I would like to thank my supervisor Prof. M. Daniela Candia Carnevali for giving me the possibility to work on our beloved echinoderms in her lab during the years of my master degree and my PhD and for sharing with me her huge knowledge.
The biggest thank you is reserved to my co-tutor Dr. Michela Sugni: you were and are my guide and my constant support. I learned so much from you from so many different points of view. We shared both happy and difficult moments and believe me when I tell you that your never ending enthusiasm for what you do and all you did for me will be never forgotten!
All my gratitude goes to my “foreign” supervisor at University College London, Dr. Paola Oliveri: I was so lucky to meet not only a great and enthusiastic scientist with a huge passion for her work but also (and above all) a great person who gave me a lot. You patiently introduced me to the fascinating world of the molecular biology and I enjoyed it so much! I really hope our collaboration will last for a long time!
Another big thank you to Prof. Caterina La Porta for kindly introducing me to the “cell culture world” and cheer me with her constant enthusiasm and her thousand ideas.
A special and deep thank you to Dr. Francesco Bonasoro, the man who has always an answer to all my questions! Your quiet and constant presence and your encyclopaedic knowledge were and are a great support, a precious landmark and an amazing source of inspiration.
Another huge thank you to the wonderful PhD students I was so lucky to meet during these years and who shared with me, for few months or almost a year, laboratory work and not only: Yousra Ben Khadra, Anna Czarkwiani, David Dylus, Angela Duque-Alarcon and Libero Petrone. I learned a lot from all of you and you kindly supported me in many ways, from “Baci di Dama” and chocolate brownies to orange juices ;) A special thank you to Yousra and Anna: without you I would have never done all I did in these three years and it was a pleasure and a joy to live and work with you! I wish you the best of luck!
During my period of PhD in London at UCL I was so lucky to meet two groups of great people I would like to thank: thanks to all the people of Dr. Paola Oliveri’s and Prof. Max Telford’s labs, especially Wendy Hart, Fraser Simpson, Dr. Anne Zakrzewski, Helen Robertson, Johannes Girstmair, Steven Müller, Alun Jones, Jack Taylor, Prudence Liu,

Patrick Toolan-Kerr, Virinder Reen and Danila Voronov. You helped me a lot in many ways, maybe you did not even realise how ;)
For their help with microscopy protocols and the hours with me (sometimes funny and sometimes sad ;)) at the microscopes many thanks to Miriam Ascagni, Dr. Nadia Santo and Laura Madaschi at University of Milan and to Mark Turmaine at University College London.
Thanks to my old and new colleagues of the 1st floor tower A at the Department of Biosciences (University of Milan): Dr. Cristiano Di Benedetto, Renato Bacchetta, Dr. Alice Barbaglio, Dr. Silvia Mercurio and Dr. Dario Fassini for their continuous support and for sharing with me their huge knowledge in different fields. A special thanks to Cristiano and Renato. Cristiano, you are the most patient teacher I have ever met: you taught me how to work in the lab, the importance of looking always for new questions and try to find the answers and you shared with me your passion for microscopy that is now one of my passions too! Renato, you are simply and beautifully an example not only of how to work but also and especially of how to live: your never ending kindness will be never forgotten!
Thanks to the Sven Lovén Centre in Kristineberg (Sweden) for the help with the collection of experimental brittle stars and the Marine Protected Area of Portofino (Italy) and the Marine Protected Area of Bergeggi Island (Italy) for the permission to collect experimental starfish, sea urchins and sea cucumbers. A deep thanks to the scuba divers who helped with the collection of the animals, especially Dr. Cristiano Di Benedetto, Dr. Dario Fassini, Livio Leggio and Marco Di Lorenzo. Many thanks also to the restaurants around our university that kindly provided sea urchin wastes to extract collagen.
Thanks to all the students I was so lucky to follow during these years: Alessandra Aleotti, Arianna Daviddi, Silvia Guatelli, Livio Leggio, Laura Piovani, Pasquale Puglisi, Andrea Spalletti, Greta Valoti and the new entries Beatrice Cambiaghi, Alessandra Moreni, Francesco Rusconi and Marika Tassara. Thanks to you I understood the importance of sharing expertise, create a good work (and not only;)) environment in the lab and how much I enjoy teaching something I really like. Thanks also for all the coffees I did not drink and all the sweets I actually ate!
Many thanks to all the people of different universities who helped me in different ways, for reagents, materials, instruments and protocols without which I could not have done part of my thesis, in particular Renato Bacchetta, Prof. José E. García-Arrarás, Prof. Graziella Messina, Dr. Roberta Pennati, Dr. Graziano Colombo, Dr. Elena Canciani, Dr. Simona Masiero, Dr. Maria Enrica Pasini, Dr. Giuliana Rossi, Dr. Giorgio Scarì, Dr. Roberta Leone, Silvia Colombo, Mariarosa Gioria, Luca Guidetti, Silvia Colombo, Bianca Galliani, Silvia Messinetti, Dr. Anna Ghilardi, Maria Chiara Lionetti, Griselle Valentin, Dr. Anoop Kumar, Dr. Andrew Gillis, Liisa Blowes, Dr. Dean Semmens and Dr. Avi Lerner.
The deepest gratitude to Dr. Paolo Tremolada who helped me with the statistical analyses of Chapter 5 and to Prof. Iain C. Wilkie for mechanical equipment use.
A big thank you to the two referees Prof. Maurice Elphick (Queen Mary University of London) and Prof. Emili Saló (University of Barcelona) whose comments helped me improving this manuscript.

During these three years I met many interesting people working on echinoderms and not only during conferences or summer schools: I want to thank all of you for sharing with me your knowledge and your enthusiasm for echinoderms and science in general!
A huge thanks to the other PhD students of the XXIX Cycle with whom I shared both happy and difficult situations ;) from lessons to PhD thesis writing. We will do it! And thanks also to our secretary, Margherita Russo, who was our lighthouse in the darkness of the PhD bureaucracy.
A special thanks goes to a person I met at the end of my PhD, Dr. Maria Flora Mangano, who in literally three days helped me a lot not only for my work but also for my life, re-giving me self-confidence and precious pearls of wisdom I will never forget.
Thank you to my old and new friends, in particular all the beautiful girls of the Alpha group and thanks to Alessandra, Camilla, Elena, Monica, Roberta, Valentina and Veronica for always being with me, to laugh together, fight together, complain together, live together!
A great thank you to my guys of the ‘98: your enthusiasm and your constant support were really important and precious to me, especially when I was away.
And last but not least, the biggest and most heartfelt thank you goes to all my family, my rock and my happiness! Without you, your help, your support and your love nothing of this would have been possible. A special thanks to my beautiful little cousins Serena and Anna: never lose your curiosity of children for all things around you!
And hoping that science will be my future, again a huge thank you to you all!

*Cinzia*